# From Externally Controlled to Autonomous DNA Molecular Motors

Thesis submitted in partial fulfillment

of the requirements for the degree of

“DOCTOR OF PHILOSOPHY”

By

**Brevirios Shhade**

Submitted to the Senate of Ben-Gurion

University of the Negev

November 2024

Beer-Sheva

This work was carried out under the supervision of Prof. Eyal Nir

In the Chemistry Department

Faculty of Natural Sciences

# Abstract

Developing bioinspired, fast, processive, and reliable synthetic molecular machines remains a significant challenge, as current synthetic nanomotors often underperform compared to biological counterparts. My research advances DNA based externally controlled and autonomous linear and rotary molecular motors through innovative design and optimization. The thesis contains three parts, the manufacturing of micrometer long origami track for linear externally controlled bipedal motors, the design and manufacturing of origami-base externally controlled rotary motors, and a detailed proposal of a bipedal autonomous operational mechanism that can be implemented in the rotary motor.

First, I engineered a 955 nm-long DNA origami track composed of six addressable rectangular origami monomers. High hexamer production yield and purity was achieved by optimizing the 'sticky ends' technique using a novel computer algorithm that generates proper sticky ends sequences, and by optimizing the origami preparation procedures, including fine-tuning of the ionic conditions to minimize unintended origami hybridization that disrupts hexamer production.

Second, I designed and fabricated a DNA origami rotary motor that offers an 'infinite' track, made of two origami discs that are connected by single-stranded swivel elements that allow free rotation but prevents rotor dissociation upon operational error. The rotor is powered by two externally controlled bipedal walker systems and is monitored using defocused light-scattering from an attached gold nanorod, enabling high-resolution azimuthal angle characterization. We demonstrate the performance of eight full rotations, amounting to 96 microfluidics-based externally controlled steps. Main innovations include iterative *in-silico* design of stable and planar origami discs that properly hold the propulsion mechanism and the gold nanorod, as well as detailed optimization of the preparation procedure.

Finally, I proposed a detailed design of an autonomous propulsion mechanism that is chemically driven, capable of sustained processive operation (does not 'burn the bridge'), is bidirectional, and fast. This novel mechanism is fueled by carefully designed metastable DNA hairpins, directionality and leg coordination is provided by strategically

positioned a catalyst strand that associates the rear leg with the hairpin fuel, facilitating leg lifting. Through meticulous design optimizations and kinetic simulations, the system demonstrates high *in-silico* stepping yields of ~99% with stepping times below 3 minutes ,subject to model assumptions. This novel mechanism can be implemented into our rotary motor.

Collectively, I believe that my work significantly advances our ability to produce high-performing synthetic molecular DNA motors, including advance towards the 'Holy grail' of truly autonomous operation. Finally, in each of these projects I learned that there is still 'plenty of room at the bottom'.

# Acknowledgments

First and foremost, I would like to express my deepest gratitude to my supervisor, Professor Eyal Nir, for his unwavering support both scientifically and personally. His vast knowledge of DNA and physical chemistry has been invaluable to my research. No matter the hour—even at 3 a.m.—he was always available to answer my calls and provide guidance.

I am also profoundly grateful to my colleagues, Dinesh Khara and Mary Popov, for their assistance during the early days of my doctoral journey. They taught me how to navigate the chemical laboratory and introduced me to our laboratory methodologies.

My sincere thanks go to my colleague and friend, Haggai Shapira. Our friendship dates back to our undergraduate days, and among countless things, I have learned from him the importance of challenging the status quo. Without his expertise and passion, the rotor project would not have come to fruition.

I would like to extend my appreciation to Samrat Basak for teaching me not only how to speak English more fluently but also for his guidance in proper buffer and material preparations. Special thanks to Ofer Perel and Meitar Uralevitch for their friendship and support both inside and outside the lab.

I am indebted to those outside our lab who have contributed to my research. I thank Thomas Gering for his insights into advanced DNA origami design, Massimo Kube for his instructions on Cryo-TEM, and Christopher Maffeo for his assistance with the MrDNA simulation package installation.

Lastly, I would like to express my heartfelt gratitude to my family for their unconditional support. They have always been there for me, nurturing my love for curiosity and knowledge.

# Table of Contests

# List of Figures

# List of Tables

# Chapter 1: Introduction

## 1.1 Biological Motors

Biological molecular motors, composed of proteins, play major roles in many biological processes and are characterized by their remarkably high chemical yield and speed. Bipedal walkers, such as kinesin, can perform hundreds of steps at a rate of hundreds of steps per second before dissociating from the microtubule track. Similarly, rotary motors such as F1-ATPase and bacterial flagellum can rotate at rates of ten to thousands of rotations per second, and millions of times before they cease to operate [1-6] (Figure1.1). Unlike bipedal motors that depart from the track in the event of operational error, the rotating element in rotary motors are permanently locked to the motor frame, preventing departure while allowing free rotations, solving the problem of processivity.

**Inspired by this feature, I present here my contribution for the development of DNA origami-based interlocked rotary motors.**

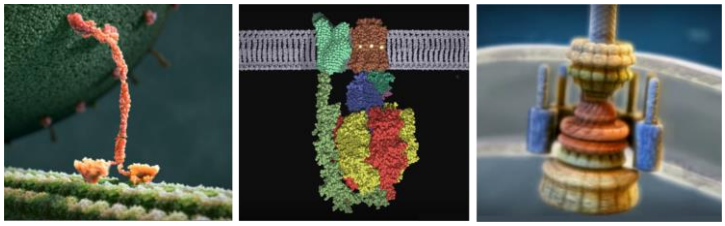

**Figure 1.1: Illustrations of Biological Motors.** From left to right: bipedal kinesin, F1-ATPase, and bacterial flagellum rotary motors. Biological rotary motors are typically much more processive than bipedal walkers.

Biological molecular motors have several notable characteristics. By consuming energy, they progress **directionally** (or bidirectionally [2]), that is, beyond Brownian motion. There is **no irreversible chemical change** to the biological motors themselves during operation, that is, they function as enzymes) [5, 6]. They can perform many cycles of operation in their lifetime, defined as **processivity** [1]. Finally, biological motors are **autonomous**, meaning they do not require external intervention to function.

**Artificial molecular motors typically do not meet all these characteristics. For example, some DNA molecular motors are not autonomous and are controlled externally** [7-9] **and DNA molecular walkers may change the track on which they stride** [5, 10-12]**.**

## 1.2 Building Artificial Nanomachines with DNA

The design and fabrication of synthetic molecular machines and motors presents significant challenges. Developing methods to organize nano-constructs into a functioning molecular machine with specific structure and topology is essential. The molecular complex must exhibit robustness while maintaining flexibility at designated sites, and an effective propulsion mechanism to power the machine should be integrated into the system. The DNA molecule is likely one of the most attractive self-assembled building blocks for the construction of artificial nanomachines. First, Watson-Crick base pairing is highly predictable and specific. Second, the information embedded in the DNA nucleic acid sequence dictates the structural dynamics of DNA complexes in a well-understood and typically predictable manner, allowing for the rational bottom-up design of both static and dynamic structures. Third, the convenient automatic synthesis of DNA oligonucleotides makes them affordable, and the DNA molecule can be modified by a variety of other molecules rather easily. **In this thesis, we leverage the structural and dynamical properties of DNA to design and build synthetic molecular motors.**

## 1.3 Structural DNA

The X-ray crystallography work of Rosalind Franklin and Maurice Wilkins [13, 14], combined with the theoretical contributions of Francis Crick and James Watson [15], revealed the three-dimensional structure of DNA, highlighting the crucial link between structure and function in structural biology. Understanding a biomolecule's shape, such as that of a protein, provides insights into its function. For example, flexible regions may act as hinges, and uniquely shaped pockets can serve as active sites. Crick and Watson's double helix model suggested a mechanism for DNA replication[15, 16], which was later confirmed. This structural knowledge not only explains biological functions but also provides the foundation for DNA nanotechnology. By utilizing DNA's structure, scientists can design and engineer artificial nanoscale structures and devices that mimic biological creations and even extend beyond them. **In this work, two DNA constructs are produced to serve as DNA origami tracks for our motors: the first is a hexamer built from six origami tiles, and the second is a rotor structure made from two multilayered origami discs.**

### 1.3.1 DNA Nanotechnology

Traditionally, DNA has been primarily associated with its role in storing and transmitting genetic information. However, in the 1980s, Nadrian Seeman's pioneering work redefined its function by proposing that DNA could also serve as a fundamental building material [17]. Seeman demonstrated that by leveraging the principles of Watson-Crick base pairing [15] and utilizing Holliday junctions—formed by four DNA duplex arms [18]—DNA could be engineered into a variety of complex structures. These structures, connected through single-stranded extensions known as sticky ends, allowed the motifs to interlock much like Lego pieces (Figure 1.2A). DNA strands could hybridize in an antiparallel fashion to form rigid structural motifs (Figure 1.2B) [19-21], such as Seeman's concept of DNA double crossover (DX) tiles, which employed multiple Holliday junctions between two double helices [20], significantly enhancing structural complexity and flexibility. This approach enabled researchers to utilize a small set of basic motifs to design and construct increasingly sophisticated structures, including two-dimensional junctions [22-27], three-dimensional frameworks [19-21, 28-31], spatially organized molecular assemblies [32], systems for encapsulating single molecules [33], and biological sensors [34]. These innovations marked the birth of DNA nanotechnology and revolutionized the field of nanoscience.

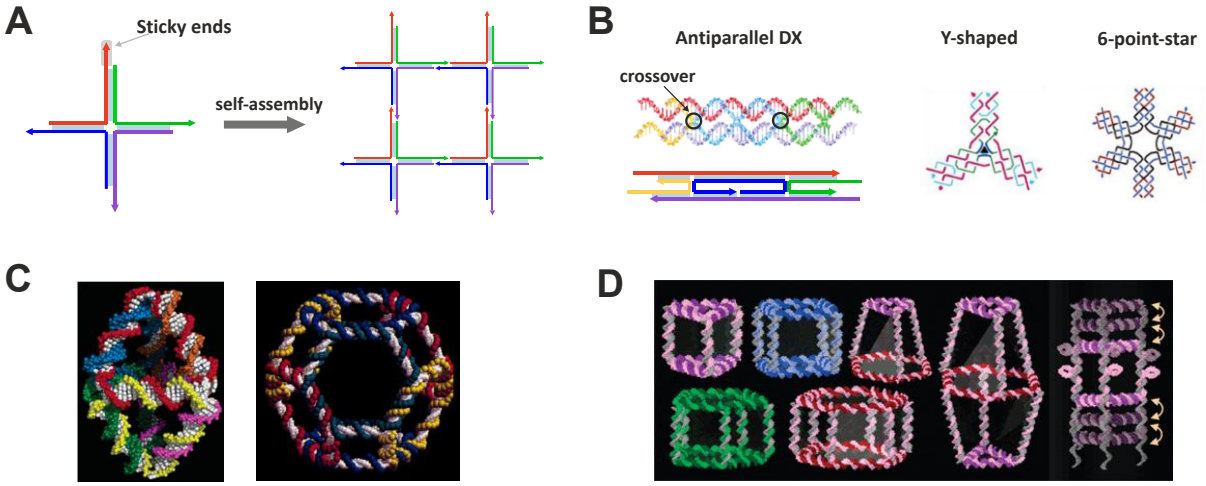


**Figure 1.2: DNA nanotechnology based on branched junctions.** (A) A DNA four-way junction with self-complementary single stranded sticky ends. (B) motifs based on the double-crossover (DX) structures. (C) A self-assembled DNA bipyramid (left) [28], an octahedron constructed from a long DNA strand and five smaller strands(right) [21]. (D) A face-centered approach to build prismatic cage.

### 1.3.2 DNA Origami

Constructing larger DNA structures presents significant challenges, including the complexity of design, the necessity for multiple purification processes, and the requirement to elongate DNA strands via ligation. These challenges generally constrain the creation of structures to sizes below approximately 50 nanometers [35]. To overcome these obstacles, Paul Rothemund introduced an innovative approach for designing DNA nanostructures, known as DNA origami [36]. This technique was inspired by William Shih's octahedral DNA structure [37], and Nadrian Seeman's double crossover tiles [20]. With this technique a single strand **DNA 'scaffold'** (7300-8200 bases in length) is folded into the desired shape by 100-200 short (15-60 bases lengths) complementary **DNA 'staple'** strands, together creating multiple double helices linked periodically by Holliday-junction-like crossovers and is typically achieved in a one-pot annealing reaction (Figure 1.3A). The DNA origami technique has since become widely adopted and has been further refined to create three-dimensional [38-41] and curved structures [42] of diverse shapes (Figure 1.3B). Additionally, computational tools like caDNAno [43], oxDNA [44] and mrDNA [45] have been developed to assist researchers in designing their own DNA origami structures. The high spatial accuracy and addressability of DNA origami have enabled development of dynamic DNA devices, such as a 3D DNA box with a controllable lid [46], DNA origami actuator [47], and others [48, 49], expanding the capabilities of the nanotechnology field (Figure 1.3C)

**One limitation, however, is that the size of DNA origami structures is determined by the length of the scaffold sequence, typically a 7-8k bp M13 scaffold, limiting the length of origami-made walkers' track. I am dealing with this problem here.**

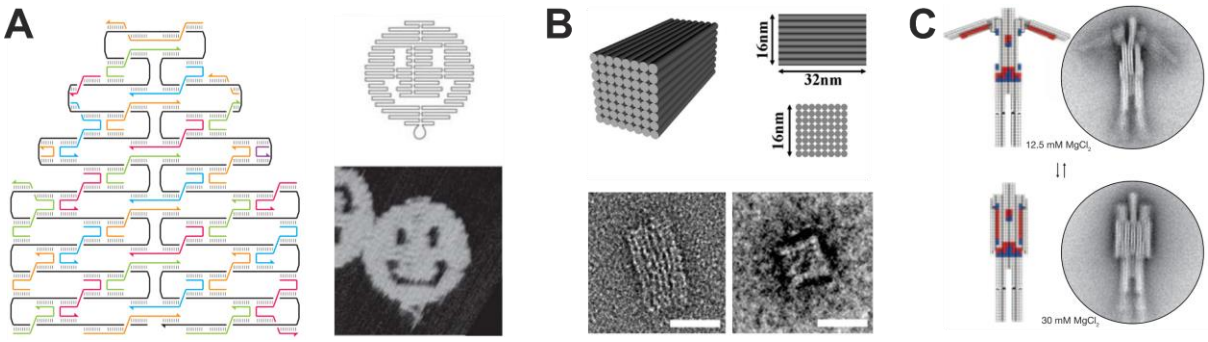


**Figure 1.3: Scaffolded DNA Origami.** (A) Demonstration of a long genomic DNA strand folded with the help of small staple strands, each consisting of 20-60 nucleotides [36]. (B) square lattice DNA origami [43]. (C) Dynamic DNA origami device [49].

### 1.3.3 Methods for Higher-Order Structures

The construction of larger DNA origami structures is fundamentally constrained by the length of the DNA scaffold molecule. While longer scaffolds—such as those with sizes of 20k [50], 30k [51], and 50k [52] nucleotides—have been employed, these scaffolds typically exhibit reduced purity. This reduction in purity often leads to lower yields of correctly folded origami structures, additionally these scaffolds have limited commercial availability. One strategy to circumvent the size limitation involves the polymerization of identical origami units into linear and other two-dimensional structures. Through this method, researchers have successfully constructed structures composed of hundreds of monomer units [38, 53-58] (Figure 1.4A). **However, a significant drawback of this approach is the uncontrollable polymerization of the origami monomers. Furthermore, because the monomers are completely identical, this method offers limited addressability and diversity in the resulting construct.**

To address these limitations, a more sophisticated approach, in principle akin to a Lego-like assembly, has been proposed. This method involves the use of diverse origami building blocks, each designed with unique connectivity. These blocks are prepared and prefunctionalized separately, allowing them to be joined together to create structures of almost any desired architecture and size [36, 59-73]. Typically, the assembly of these structures has been achieved through the hybridization of **'sticky ends'** [36, 59, 74, 60-63], **blunt-end stacking** interactions of helices [64-67], or a combination of both techniques [68-72]. The sticky ends sequences and the positions of the blunt ends generally

determine the addressability and reaction hierarchy, which can be further enhanced by complementary origami shapes (Figure 1.4B) [64, 68-70].

Despite the conceptual elegance of this approach, the practical assembly efficiencies of structures composed of different origami units often remain suboptimal (see my short review of this issue, **Sheheade et al.** [75]). For instance, using the sticky-ends method, researchers have achieved dimer yields ranging from 80% to 90% [74, 60, 61], while octamer yields were limited to just 63% [62]. These values reflect an 80% [74] to 95% [62] attachment reaction yield for each monomer added to the structure. When using only or predominately stacking interactions, the total yields for constructing tetramers, pentamers, octamers, and nonamers were 44% [64], 24%-74% [64, 67, 69], 46% [67], and 35%-41% [67, 70], respectively, with per-monomer yields ranging from 70% [69] to 92% [67]. In a noteworthy study by Tikhomirov et al., 2x2, 4x4, and 8x8 origami arrays, composed of 4, 16, and 64 unique origami tiles (Figure 1.4C), were assembled using stacking interactions and short sticky ends (1 or 2 nucleotides in length) through hierarchical assembly, the total yields achieved were 93%, 48%, and 1.8%, respectively [72]. The authors suggest that the weak stacking interactions facilitate rearrangements that enabled the building blocks to escape kinetic traps during assembly in a complex reaction mixture.

An alternative approach to constructing higher-order structures involves the use of one-pot annealing with custom-made orthogonal scaffolds to produce pentamers. While this method offers a simplified assembly process with strong bonding, it also introduces challenges, such as the need for precise equimolar concentrations of scaffolds and increased production costs proportional to the number of different scaffolds [76].

**Here I present a long DNA origami track composed of six monomer tiles, developed using an improved sticky ends method that addresses issues of connectivity yield. This track is intended to serve as a platform for the unidirectional movement of linear bipedal walkers.**

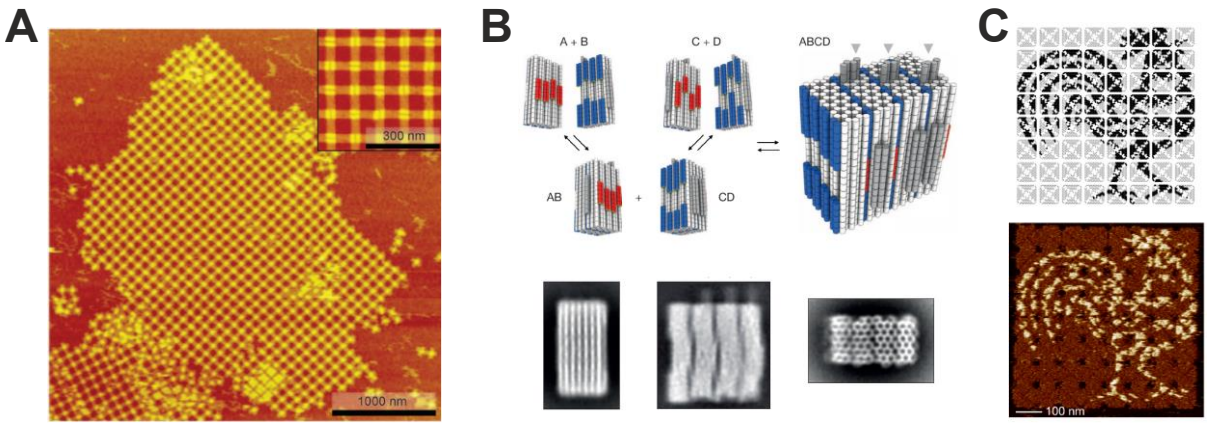


**Figure 1.4: Higher-order structures.** (A) Uncontrolled crystalline two-dimensional DNA-origami arrays [53]. (B) Device assembled by blunt ends and shape-complementary 3D components [51]. (C) Arbitrary pattern made from 64 unique origami tiles [72].

## 1.4 Dynamic DNA

DNA has long been recognized for its versatility in constructing virtually any desired shape at the nanoscale. Traditionally, however, these structures have remained static, retaining their form once assembled. Yet DNA is not confined to static configurations; it can be engineered to create dynamic systems that evolve and respond over time.

**In this section, I delve into the core mechanisms underlying the development of time-responsive DNA systems and introduce various tools and strategies that were employed in the development of the proposed autonomous DNA rotary motor**.

### 1.4.1 DNA Hybridization

DNA hybridization, the process in which complementary single-stranded DNA (ssDNA) sequences pair to form double-stranded DNA (dsDNA) via Watson-Crick base pairing (A-T, G-C), plays a vital role in both biology and DNA nanotechnology. In biology, hybridization is fundamental to numerous cellular processes. In nanotechnology, it is used to drive DNA self-assembly, enabling the creation of rationally designed nanoscale structures and machines.

The thermodynamics of DNA hybridization have been extensively characterized using techniques such as spectrophotometric and viscometric analysis of thermal melt curves. DNA duplex stability is influenced by the sequence-dependent interactions, that is hydrogen bonds of complementary base pairs and the hydrophobic stacking of bases

[77, 78]. Predictive models for DNA melting temperature (Tm) — the temperature above it less than 50% base pairs are formed — rely on a two-state nearest-neighbor approach, which estimates the stability of a base pair based on the identity of neighboring nucleotides [77]. The Tm of a DNA duplex is calculated by summing the free energy contributions of all adjacent base pairs, with additional considerations for the stabilities at the duplex ends [77, 78]. This method has been experimentally parameterized [79-86] and is effective in predicting melting temperatures across various buffer conditions.

While the thermodynamics of DNA hybridization are well understood, the kinetics of the process remain less clear. DNA hybridization kinetics are sequence-dependent, but direct observation of hybridization pathways has proven difficult [87-90]. Early studies [91-93], later supported by molecular dynamics simulations [94-96], proposed that hybridization proceeds through a slow bimolecular nucleation step, where about three base pairs form, followed by rapid zippering of the remaining base pairs to complete the duplex. The stability of the nucleating interactions, which depends on the DNA sequence, largely governs the activation energy and overall hybridization rate. Furthermore, secondary structures can significantly influence hybridization kinetics by reducing the availability or stability of nucleating interactions, as these structures must first be denatured before hybridization can proceed [97-99]. Several algorithms have been developed to predict sequence-dependent hybridization rates, with the most successful prediction being methods that consider the availability of nucleation based on secondary structure [98, 100], along with repetitive nucleation sites [101].

### 1.4.2 Strand Displacement

**Proximal Toehold:** Toehold-mediated strand-displacement reactions are a critical mechanism in DNA nanotechnology, enabling precise control over molecular dynamics. The key function of a toehold is to accelerate the rate of strand displacement by increasing the frequency of branch migration events. This process is illustrated in Figure 1.5A, where the incumbent strand is displaced from the substrate strand by an invader strand. The invader ultimately forms a new duplex with the substrate strand. The toehold, denoted as the single-stranded extension in red, serves as the starting point for the displacement reaction by providing an initial binding site for the invader strand. The reaction progresses through multiple intermediate stages of branch migration until the incumbent strand is fully displaced, forming the final duplex.

The experimentally measured forward reaction rates as a function of toehold length generally qualitatively align with expectations [102, 103]. For short toeholds, the likelihood of the invader strand remaining attached long enough to displace the incumbent strand is low, primarily due to the high thermal dissociation rate and repeated returns of the branch point to the toehold-proximal end of the substrate. With longer toeholds, the rate of dissociation decreases, allowing for successful displacement as the branch point completes its path along the substrate. As a result, the overall rate constantly increases with toehold length before reaching saturation at sufficiently long toeholds of about 7 bases [103].

**Remote Toehold:** Several modified motifs have been developed to improve or adjust the properties of strand displacement reactions. Among these, Genot et al. introduced the concept of a remote toehold as an improvement over the traditional proximal toehold used in DNA strand displacement reactions [104]. Unlike the proximal design, where the toehold is directly adjacent to the displacement domain, the remote toehold separates these domains by inserting a spacer (Figure 1.5B). This modification was introduced to gain greater control over the kinetics of strand displacement, allowing fine-tuning by adjusting the length and nature of the spacer. By utilizing remote toeholds, these researchers demonstrated the ability to modulate strand displacement rates over several orders of magnitude, providing a more versatile approach for controlling hybridization

reactions, offering significant advantages for constructing more complex, efficient, and adaptable DNA-based systems.

**Associative Toehold:** Another modification, developed by Xi Chen et. al, introduced an alternative strategy for toehold-mediated strand displacement, known as associative toehold activation [105]. Traditional toehold methods rely on predefined, hardwired connections between toeholds and branch migration domains, which limit the flexibility and adaptability of DNA circuits. To address this limitation, Chen proposed linking the toehold and branch migration domain via hybridization during the circuit's execution, rather than during synthesis (Figure 1.5C). To accelerate this motif, Chen employed coaxial stacking to stabilize the three-way junction. The key advantage of these new motifs is the enhanced flexibility and modularity of DNA circuits, as demonstrated through processes like toehold switching and the creation of a simple self-replicator, significantly expanding the design potential for complex, autonomous DNA-based systems.

**My work harnesses proximal (regular), remote, and associative toehold mediated strand displacement, along with their kinetics modification to create externally controlled and autonomous propulsion mechanisms.**

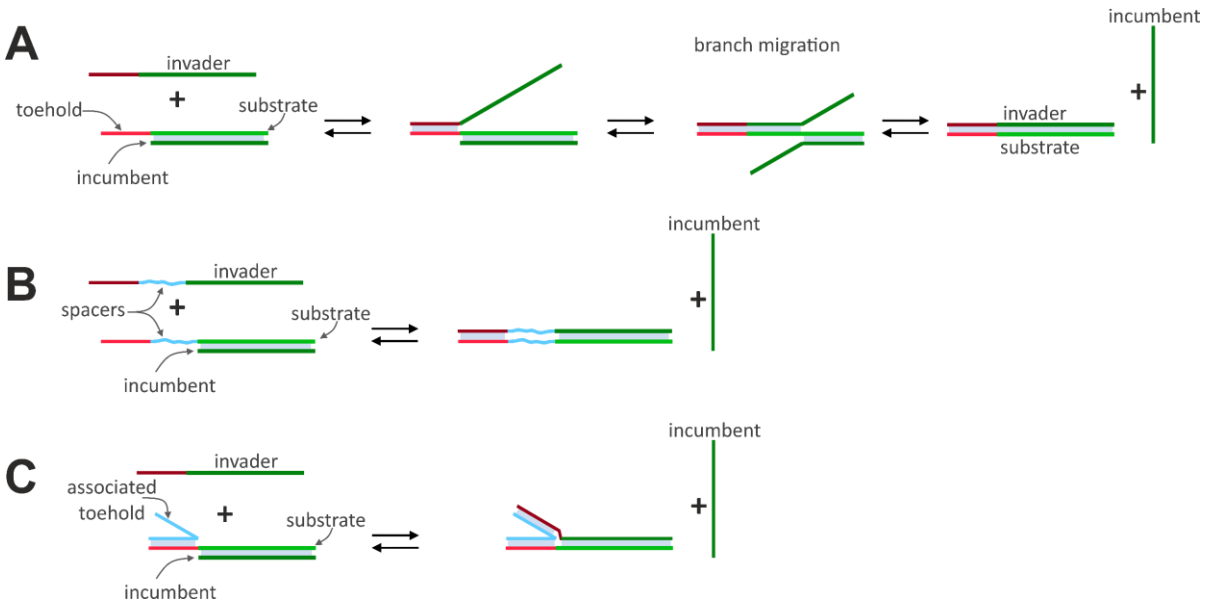


**Figure 1.5: Strand Displacement.** (A) Describes the process of displacement initiated by a proximal toehold [95, 96]. (B) Illustration of the remote toehold motif [104]. (C) Illustration of the associative toehold motif [105]

### 1.4.3 Mismatch Creation and Elimination

**Mismatch Creation:** The previously section discussed method of controlling DNA strand displacement rate through manipulation of toehold length and position. In contrast, Machinek et al., introduced an alternative approach that achieves kinetic control by creating mismatched base-pairs at specific locations within the displacement domain [106]. While variations in toehold length primarily influence both the reaction rate and the thermodynamic stability of the system, this new approach offers greater flexibility by decoupling kinetics from thermodynamics. By strategically placing a mismatch, the researchers were able to precisely tune the reaction rate over three orders of magnitude without significantly affecting the free-energy change associated with the reaction.

The study revealed that the position of the mismatch within the displacement domain has a substantial impact on the kinetics of strand displacement. Mismatches closer to the toehold (proximal mismatches) present a greater barrier to displacement, significantly slowing down the reaction. In contrast, mismatches located further from the toehold (distal mismatches) have a much smaller effect on the reaction rate. This precise control of kinetics as a function of mismatch location enables greater flexibility in designing DNA systems for applications requiring fine-tuned temporal control, such as in molecular computing and dynamic nanodevices.

**Mismatch Elimination:** An opposite motif to that of Machinek et al. was developed by Haley et al., enabling enhanced thermodynamic driving in DNA strand displacement systems by eliminating mismatches within the initial DNA duplex [107]. Their approach specifically involves eliminating mismatches at carefully chosen positions, which act as hidden thermodynamic drivers, allowing for fine-tuning of reaction kinetics while avoiding the typical trade-off between increased reaction yields and unwanted leak reactions. Their experiments showed that mismatches positioned close to the toehold (early in the displacement process) have the most substantial effect on increasing the reaction rate, by up to two orders of magnitude compared to a mismatch-free system. The key advantage of this new motif is its ability to decouple the rate of the overall forward reaction from the thermodynamic stability of the product, making it ideal for engineering non-equilibrium systems that require catalytic control without the risk of leak reaction.

**Mismatch creation and elimination are harnessed in this thesis to optimize the in-silico performance of the proposed autonomous propulsion mechanism developed here.**

### 1.4.4 DNA Hairpins

DNA hairpin structures have been instrumental in the development of dynamic DNA systems, particularly as metastable DNA fuel for DNA machines, enabling catalytic hybridization and dehybridization reactions [108-110] and dictating reaction hierarchy [111]. The pioneering work by Turberfield et al. [108] demonstrated such a system, where a single-stranded DNA catalyst accelerates the reaction between a metastable hairpin-like loop complex and a complementary single strand (Figure 1.6A). The catalyst employs toehold-mediated strand displacement to open the loop complex, removing the steric hindrance and permitting the reaction to proceed.

**Importantly, the catalyst is released unchanged after the reaction, ready to catalyze subsequent cycles.** Building upon this design, Seelig et al. [109] enhanced the stability of the metastable fuel, extending its lifetime to a scale of weeks. This improvement was achieved by incorporating the complementary strand into the loop of a second hairpin complex (Figure 1.6B). In this refined system, the intermediate process involves a four-way branch migration, in contrast to the three-way migration of the initial design, thereby increasing the robustness and control of the processes. Subsequently, Green et al. [112, 113] modified the system by integrating the loop domain into a classic hairpin structure rather than the more complex assembly introduced before. This simplification improved both the efficiency and practicality of the system. Further details of this design are discussed in Section 4.2.

Hairpins have been utilized for other applications such as in hybridization polymerization systems that exploit hidden toeholds within short loop domains. Notable examples include the "hairpin chain reaction" see Figure 1.6C [114], "catalytic hairpin assembly" [110] , and even polymerization motors [115].

**The fuel developed for the autonomous propulsion mechanism in this thesis was inspired by Green's design of metastable hairpins and by the design of the loop implemented in the hairpin chain reaction.**

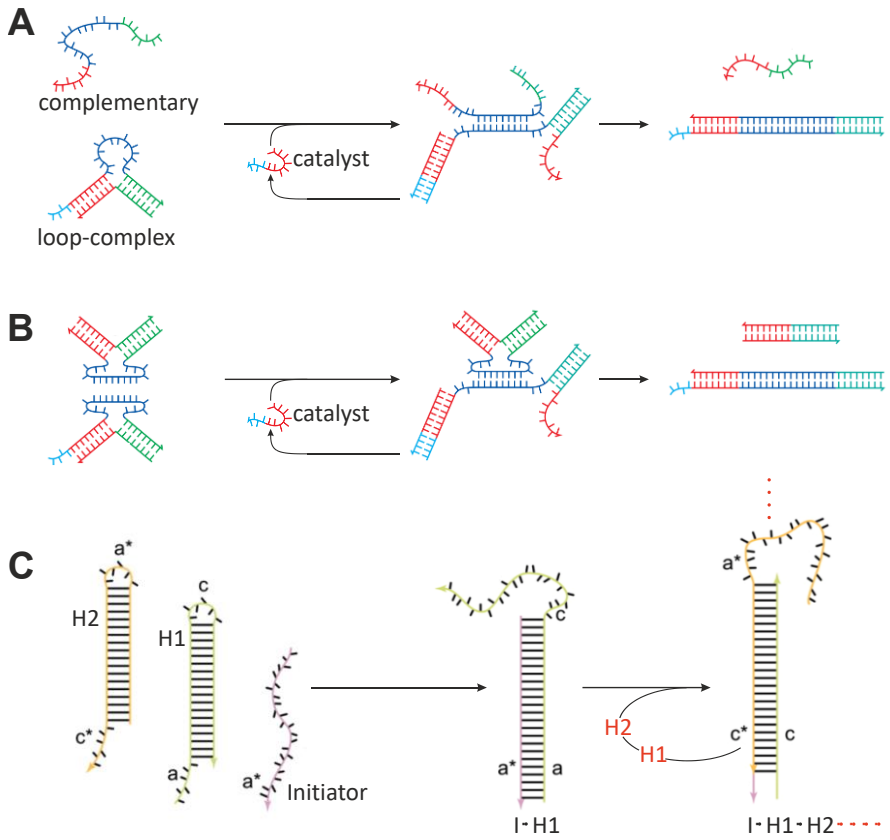


**Figure 1.6: Various DNA hairpin systems.** (A) DNA fuel for free running nanomachines [108]. (B) Catalyzed relaxation of metastable DNA fuel [109] . (C) Triggered amplification via hybridization chain reaction [104].

### 1.4.5 Reaction Leakage

Leakage in DNA dynamic nanotechnology refers to the dynamical production of unintended output, compromising the system performance. Leakage can be divided too extrinsic and intrinsic [116]. Extrinsic leakage is typically due to chemical impurities, defective oligonucleotides, or malformed network components, which can be minimized through careful manufacturing and processing of the DNA elements [117, 118]. Intrinsic leakage, on the other hand, stems from the inherent design of the network. A typical example for such leakage, is catalytic reaction networks, in which even with perfectly synthesized components and in the absence of an intended toehold, the interaction between fuel and substrate can still take place [119]. One of the primary mechanisms enabling intrinsic leakage is the thermal fluctuation at the ends or nicks of the DNA strands, known as **fraying**. This spontaneous dissociation of terminal base pairs increases the probability of nucleation between fuel and substrate, leading to leakage reaction [116].

**Bases Mutual Availability:** Olson et al. introduced a metric called mutual availability [116], which provides a quantitative tool for predicting leakage rates. Higher mutual availability correlates with a greater likelihood of nucleation between the fuel and the substrate, and consequently, a higher leakage rate. Total mutual availability is defined as the integral of the availability-level over all pairwise (complementary) bases between two strands, whereas bases in single unstructured strands have the highest availability and those hidden within a stable duplex have the least. This measure has been shown by these researchers to provide approximately 80% accuracy in predicting leakage rates.

**Leakage Reduction Techniques:** Intrinsic leakage reduction techniques include careful sequence and domain design, such as the use of GC pairs at fraying locations [119], optimized reaction conditions [120], clamping domains [121, 122], sequestration of domains in hairpin structures [111], incorporation of mismatches [123], and novel domain-level redundancy [124].

**Bases mutual availability was utilized here to predict and reduce various leakage pathways in the proposed autonomous propulsion mechanism, thereby enhancing the performance and validity of our design.**

## 1.5 DNA Motors

### 1.5.1 Propulsion Mechanism Challenges

A typical macroscopic automobile engine translates its pistons reciprocate motion to unidirectional camshaft rotation, thereby propelling the vehicle forward in a specific direction along a frictional surface. This transformation from macroscopic shuttle-like movement to unidirectional motion is primarily facilitated by inertia. Inertia becomes insignificant compared to thermal fluctuations at the molecular nanoscale, thus nanoscopic motors cannot relay on inertia. At this smaller scale, to sustain movement, a molecular walker must maintain some kind of continuous contact with the track; otherwise, the motor will permanently disassembled. Achieving an efficient propulsion mechanism, therefore, requires tight coupling between the energy source turnover and the stepping mechanism. Directionality at the nanoscale is typically achieved through

symmetry-breaking, energy dissipation, and, particularly for two-footed motors, leg-coordination.

Various synthetic propulsion mechanisms for operating DNA molecular motors are described in the following section, highlighting modes of operation and providing general characteristics.

### 1.5.2 Externally Controlled

A major class of DNA artificial motors are track-walking types, where the **“walker”** transfers between specific binding sites on a track. The pioneering examples of such DNA motors were developed by the research groups of Niles Pierce and Nadrian Seeman in 2004. Both groups created bipedal DNA walkers utilizing somewhat similar propulsion mechanisms. These motors comprised two single-stranded **"legs",** connected to each other either by a duplex (Figure 1.7A) [7], or by a triple crossover molecule [8].

**Notably, these bipedal motors do not undergo irreversible chemical changes, allowing them to be operated bidirectionally, and in principle, perform unlimited number of steps.**

The tracks for these walkers consisted of rigid structures with periodic spacing for single-stranded extensions, often referred to as **"footholds".** The motor was placed at a particular position on the track by coupling strands, often referred to as **"fuel"** strands. Each fuel strand complemented the sequence of one specific leg and one specific foothold. The fuel strands also featured an additional single-stranded domain that functioned as a **"toehold"** for invader strand called **"anti-fuel"**, that is fully or partially complementary to the corresponding fuel, and its interaction with the fuel results in fuel removal and leg lifting. Thus, to achieve walking, these motors require sequential external introduction of command fuel and antifuel strands. The source of energy to operate this mechanism comes from the increased number of base pairs formed by the hybridization of the fuel and the antifuel strands, forming a product often called "**waste**".

**The Problem of Two Fuel Binding Events:** These and others [125], first-generation externally controlled motors, although impressive and inspirational, suffer from two fundamental general problems. The first major problem is the **irreversible consecutive**

**binding of two fuels** of the same sequence, one to the leg and the other to the foothold (instead of one fuel connecting the leg and the foothold, Figure 1.7B), **forming a trap-state**, and **resulting in walker dissociate** upon the introduction of the consecutive antifuel [111, 9].

To completely avoid this trap state, our group previously developed **fuel before antifuel strategy (FBAF,** Figure 1.7C). In this approach, the corresponding consecutive fuel is introduced while both legs are still placed on the corresponding footholds (T1 and T2). The fuel (F3) then binds the corresponding foothold (T3), followed by a washing of redundant fuels (F3), for example, **using microfluidics device**. At this stage, the fuels (F3) cannot bind the corresponding leg (L1), since it is blocked by the previous fuel (F1), thus avoiding the trap-state effect. Introducing antifuel strands (AF1) partially lifts the leg (L1) by design, and the remaining portion can then thermally dissociate along with the unavoidable transient interaction between AF1 and the placed fuel (F3) [126].

**Removing Redundant and Used Strands using Microfluidics:** A second problem is the accumulation of redundant out-of-phase fuels and antifuels command strands in the solution. Redundant antifuels detach the walker from the track, and out-of-phase fuels may ordered the bipedal motor to walk in the wrong direction [111, 9]. To overcome this problem, our group developed a microfluidics device (in collaboration with the group of Doron Gerber [127, 128]) that enables convenient, accurate and reliable computer controlled delivery of strands to motors that are immobilized on a glass coverslip inside the microfluidics device (Figure 1.7D) [9]. Importantly, this device also enables straightforward, near-complete removal of redundant and used fuel and antifuel strands from the motor solution environment.

**The FBAF propulsion mechanism, together with our development of microfluidics-based washing scheme, enables rapid reactions with high concentrations of fuels and antifuel strands while avoiding the trap state. Using these techniques our group demonstrated two new motors.**

**The first, a bipedal linear motor that performed 48 walking steps back-and-forth on a single origami tile, which amounts to almost 580 nanometers traveled by the**

**walker (96 consecutive chemical reactions with ~98% yield per reaction, Basak et al., manuscript in preparation).**

**The second, a double bipedal origami-based rotary motor that achieved 8 full rotations, corresponding to 96 motor steps, which includes the ability to recover from dissociations (Shapira and Sheheade, manuscript in preparation). I will show here my contribution for the latter.**

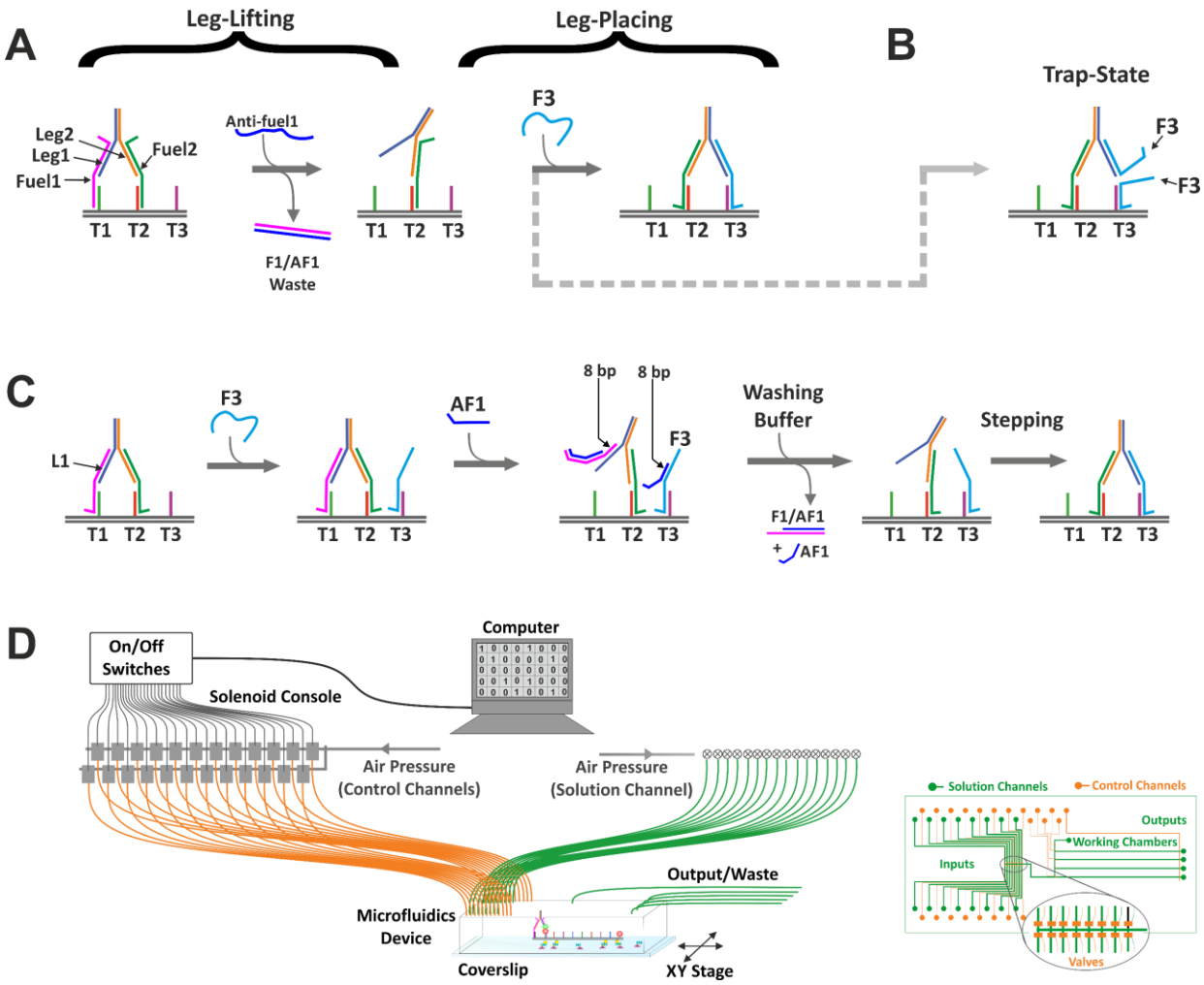


**Figure 1.7: Enhancing the performance of the externally controlled bipedal walker.** (A) antifuel before fuel strategy, which can lead to correct stepping but also to (B) a trap state where two fuel molecules bind, inhibiting movement. (C) Fuel before antifuel strategy (FBAF) ,that utilizes half-length antifuel that enables trap state free operation [126]. (D) Immobilized and washed motors within a microfluidic system [9].

### 1.5.3 Burnt-Bridge

An alternative operational method is the burnt-bridge mechanism, where the motor achieves directionality by rendering the traversed track unusable, typically through chemical modification. For instance, a single-legged DNA motor moves along a series of footholds by performing a sequence of toehold-mediated strand displacement reactions (Figure 1.8A) [5]. This mechanism relies on creating a free toehold domain on the motor strand. This is achieved by cleaving the foothold strand close to its top, but only when the motor strand is bound, allowing the top fragment of the foothold to thermally dissociate. The exposed motor top then acts as a toehold, enabling the current foothold to be replaced by the next foothold along the track through toehold-mediated strand displacement reaction, effectively moving the motor forward. The cleavage is performed by an external ATP-based nicking enzyme, Nt.BbvCI, which cuts a single strand of a duplex at a specific recognition sequence and provides energy to the motor. By destroying the track behind, the motor gains directionality, favoring forward movement rather than diffusing backward, where fewer base pairs can form.

This type of motor, and similar designs [10, 11], as well as those that gain directionality through physical coverage (Figure 1.8B) [12, 129], adopt the strategy of **"burning the bridge behind"** to ensure forward motion, thus, rendering them none-reusable and these motors cannot be consider as enzymes.

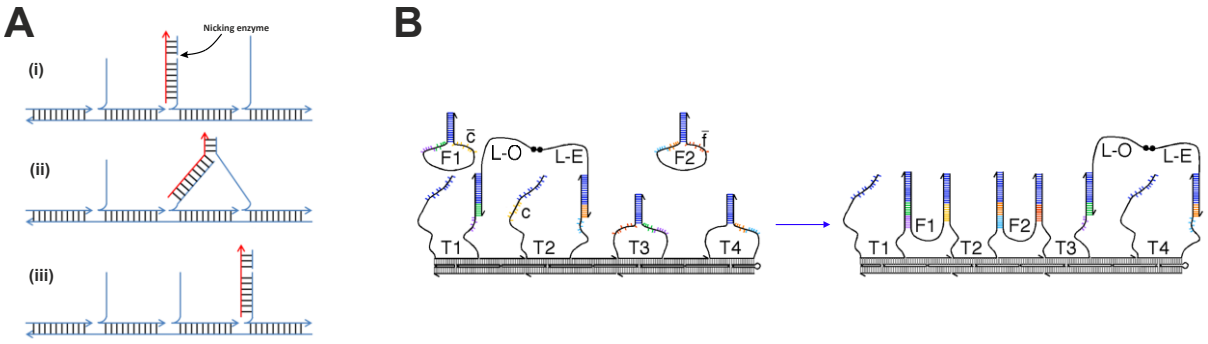


**Figure 1.8: Burnt-bridge motors.** (A) Single-legged DNA motor powered by cutting the foothold via nicking enzyme [5]. (B) Bipedal DNA motor with coordinated legs that gain directionality by covering the rear footholds [12].

### 1.5.4 Autonomous Operation

Early DNA based externally controlled motors required the sequential addition of command - energy providing – strands to facilitate movement, meaning they couldn't progress independently. A key feature of an effective motor is its ability to operate autonomously, moving forward without needing externally timed chemical additions or other interventions. For this autonomous operation to take place, each additional operation of the motor (i.e., a walking step) must depend on the successful completion of the previous operation, ensuring a continuous sequence of events and movement. Yin and collaborators introduced the first autonomous motor, capable of transporting six nucleotides along a track through cycles involving alternating endonuclease cuts and subsequent ligation [10]. However, the usage of biological ATP driven enzyme renders this motor only semi-artificial, and the core operational mechanism is based on biology and not a ground-up artificial design.

**Holy-Grail: The Autonomous, Directional, non-Burnt-Bridge, Artificial DNA Motor**

A more modular approach to that of Yin, which can be operated without the use of biological enzymes, was introduced by **Green and colleagues** [113]**.** They developed an autonomous DNA motor with two identical feet connected by a duplex, capable of walking autonomously along a single-stranded DNA track featuring repeating foot-binding domains. A detailed discussion of this motor, along with advancements made by Haley, NEC, from the same group [130], is provided in Section 4.2. The motors' directionality is determined by an asymmetric track, with foot lifting initiated through competition for limited space on the single stranded track. This motor has successfully lifted its feet via DNA hybridization of two metastable hairpins serving as fuel for the motor [113].

**In contrast to burnt-bridges designs, this motor preserves its track as it moves along it, thus the motor can be considered autonomous, directional, non-burnt-bridge, artificial DNA motor, and by that, in principle, mimicking all the features of biological molecular motors. However, Green's walker demonstrates only 1.5 steps, largely due to lack of long, rigid single-stranded DNA tracks, as well as other faults.**

**The autonomous propulsion mechanism proposed in this thesis is inspired by Greens' approach and should be considered an autonomous, directional, non-burnt-bridge, processive, fully artificial DNA motor.**

## 1.6 Thesis Goal

The primary goal of this thesis is to advance the field of DNA nanotechnology by developing high performance DNA-based molecular motors, both linear and rotary, and to lay the groundwork for autonomous propulsion mechanisms. The research focuses on overcoming existing limitations in molecular motor design, motor and track assembly, and motor operation to achieve sustained, directional movement at the nanoscale.

**Aim 1: Construction of a hexamer DNA origami track**

**I will develop an improved assembly procedure for high-quality, high-yield, addressable DNA origami construct made of six origami monomer that will serve as a track for externally controlled linear bipedal walkers.**

Specifically, the origami track, approximately 955 nm long and 50 nm wide, will be constructed from six addressable rectangular monomers connected via an improved sticky ends procedure. Critical optimizations were implemented to achieve a high-quality track assembly with 98% purity and high production yield. These include refining the sticky end technique, optimizing origami preparation procedures, fine-tuning salt conditions to minimize aggregation, and designing sticky end sequences to reduce unintended hybridization events using novel computer algorithm called NuCraft. Additionally, a smaller origami structure (~1000 bp) attached to the bipedal walker is introduced, labeled with replaceable fluorescent markers for precise single-molecule tracking.

**Aim 2: To develop externally controlled DNA origami rotary motor**

**I will present my contribution to the development of high-performance origami-based rotary motor that is powered by bipedal walkers, and capable of sustained rotation without permanent dissociation, while ensuring precise monitoring of its rotational behavior.**

Specifically, the rotary motor consists of two origami discs connected by a single-stranded swivel element that allows free rotation but prevents rotor dissociation. Powered by two sets of externally controlled bipedal walkers, the motor's rotational behavior is monitored using defocused light scattered from a photostable gold nanorod

attached to the upper disc, a technique that enables monitoring rotation at high-azimuthal resolution. A key feature is the design of the planer origami discs that avoid twisting, disc dimerization and aggregation. For that purpose, I employ iterative in silico MrDNA simulations, employ the interlocked scaffolds technique and improve edge passivation. Optimization of the preparation procedures, including origami folding, origami interaction and gold nanorod attachment are presented.

**Aim 3: In-silico design and validation of autonomous propulsion mechanisms**

**Design of an artificial DNA fuel-driven, autonomous, non-burnt-bridge, bidirectional and processive propulsion mechanism. The proposed mechanism was iteratively developed and tested using kinetic simulations that were semi-empirically parametrized.**

Specifically, I designed autonomous propulsion mechanisms that can be integrated into a stator-shaft construct, exemplified here with our DNA-origami rotary motor developed in Aim-2. The proposed system leverages a catalyst that associates the fuel with the rear leg to facilitate leg lifting operation and addresses limitations of previous designs by usage of modified fuel-hairpins, simplifying coordination mechanism while avoiding leakage and trap states.

Basic and more detailed schematics of the propulsion mechanism reaction pathways are provided, highlighting strategies and tricks to maximize performance while minimizing leakage reactions. Kinetics simulations with variable parameters were conducted to test and fine-tune the system, demonstrating 99% stepping yield at a rate of 3 minutes per step, subject to model assumptions.

**Author Contributions**

**Project 1 - Long Track for Bipedal Walker:** This research was a collaborative effort involving significant contributions from several individuals**, but the overall project was led by me.** I was primarily responsible for designing the DNA origami structures, developing the experimental protocols, and performing data analysis. Dr. Mary Popov, a senior researcher, played a crucial role in synthesizing the samples and conducting most of the measurements. The TIRF microscopy experiments were conducted by Dr. Samrat Basak, and the worm-like chain analysis software was developed by Dr. Haggai Shapira. For the origami-based fluorescence rod experiments, I designed the origami structures, and Mr. Ofir Perel and Dr. Samrat Basak were responsible for conducting the experiments and measurements.

**Project 2 - DNA Origami Rotary Motor:** This project was conducted in collaboration with group member Dr. Haggai Shapira. I was responsible for all rotor-related design, including the in-silico iterative efforts to achieve planar origami disc, while the synthesis of the rotor was carried out in close collaboration. Additionally, Dr. Shapira was fully responsible for the development, execution, and monitoring of the externally controlled walking measurements.

**Project 3 - Autonomous Propulsion Mechanism:** The entire project was conducted by me.

**Existing and expected publications:**

1. A paper describing origami tiles dimerization, with me being the leading first author, was published in SMALL (sheheade et al. [75]).
2. Another manuscript, describing the fabrication of the origami hexamer, also with me as the leading first author is under preparation.
3. A manuscript describing the nonautonomous rotor, with me as a second name, is under preparation.
4. A manuscript describing the proposed autonomous rotor, with me the leading first author, is under preparation.

# Chapter 2: Hexamer DNA origami track

## 2.1 Motivation

One of the lab's main goals over the years has been to develop high-processive and fast bipedal linear motors, and the walker's performance has been improved by 3-4 orders of magnitude of the last 13 years. To date, our bipedal walker (introduced at Section 1.5.2) was striding on a single origami unit of the length 90 nm [131] or 150 nm [9] (and in one case, walking between two connected origami units of 180 nm total length [60]). However, the lab's current walker can stride over almost 1000 nm, thus, to demonstrate unidirectional long-distance walking it is necessary to fabricate a specific and addressable origami-based track at sufficient yield, purity, structural stiffness and length.

## 2.2 Previous Work

An adequate track for our purpose should possess structural stiffness and produced with sufficient yield and purity. The track should include repetitive and identical sets of footholds staples but should also be addressable to allow dictating specific track length and allow distinguishing between starting and ending points. This can be achieved by joining separately prepared origami units with different addressability that allows determining specific lengths and specific start and end points. Therefore, the sticky ends origami attachment method is suitable for these requirements. However, the current sticky end technique has insufficient yield (Sheheade et al. [75], see Section 1.3.3).

Our group have studied the kinetics and thermodynamics of origami dimerization, initially by Liber et al. [61, 60], who compared the 'sticky ends' and the 'weaving welding' techniques and demonstrate that a bipedal walker can successfully move between the origami tiles. To understand the factors that limits dimerization, Liber primarily utilized single molecule fluorescence, to determining origami dimerization and dimer dissociation rates, and the dependency of these rates and of dimer stability on buffers ionic content (concentrations and type, i.e. Na+ and Mg+2) and on the length and quantity of the sticky ends. However, the origami dimerization yield in this work was limited to 86%.

Building on this research during my undergraduate studies, I expanded the investigation by utilizing Atomic Force Spectroscopy (AFM) and gel analysis to study various aspects of origami attachment mechanisms. **This work led to identifying the two main limiting factors in dimerization, and enabled their resolution, achieving 99% dimerization yield (sheheade et al** [75]**).**

**Inadequate purification**: Insufficient purification of excess sticky ends and poly-T edge strands after annealing, as was the case with a single round of PEG purification, led to the formation of incorrect structures and a decrease in product purity (Figure 2.1A). This issue was partially mitigated by using two or more rounds of PEG purification.

**Homodimerization via blunt ends:** We showed that rectangle origami monomers extensively interact nonspecifically through blunt-ends interaction of the sticky-ends origami edges to form homodimers and larger structures. These interactions block the interaction between the correct monomers. Specifically, more than half of the monomers formed unwanted homodimers and larger structures during the thermal annealing (conducted at 12 mM $Mg^{2+}$ buffer, Figure 2.1C). Furthermore, we found that this interaction is influenced by salt concentration and salt type, as well as the length and quantity of the sticky end staples. Runing the annealing products in a gel containing 100 mM NaCl and utilizing longer but fewer sticky end strands facilitated the dissociation of most of the unwanted homodimers into their monomeric form (see Figure 2.1B). Reacting the gel-extracted monomers to form the designated heterodimers resulted in significantly increased product yield (depend on sticky-ends design, 98.5-99.6%).

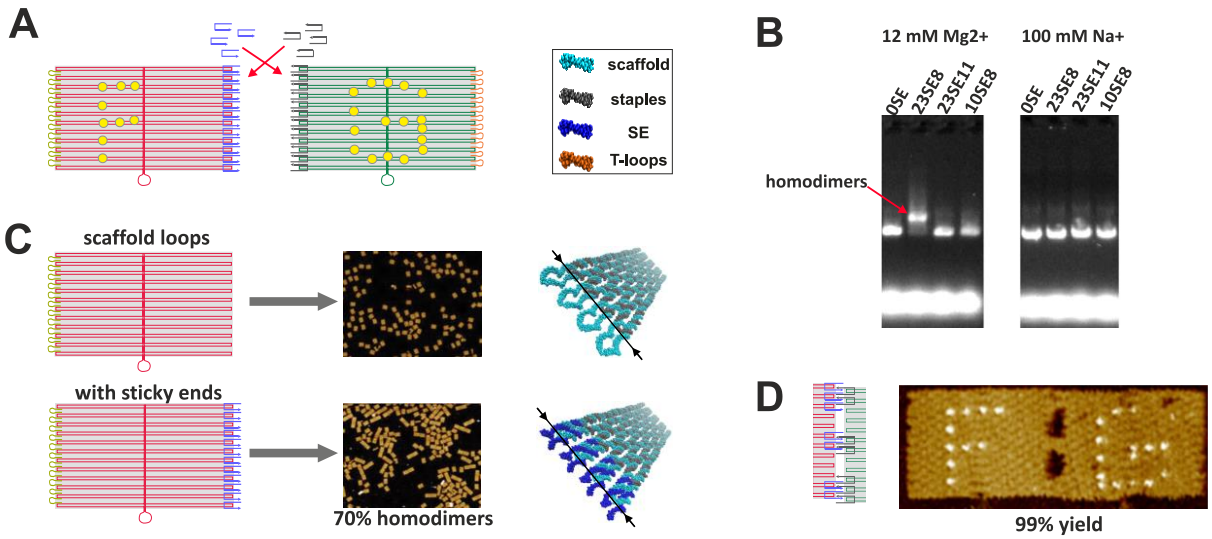


**Figure 2.1: Identifying and solving sticky ends yield limitations.** (A) Adding sticky ends to an edge induces non-specific interactions at that edge, caused by blunt ends located near the edge. (B) Several options can reduce this interaction, such as increasing the length of the sticky ends (11nt vs. 8nt), reducing the number of sticky ends (10 vs. 23), or changing the salt to a monovalent salt (Na+ vs. Mg2+). (C) A typical PEG cleaning procedure results in residual sticky ends strands, which react and block reaction sites when monomers are mixed. (D) combining the best cleaning method, gel extraction, with optimized salt and sticky ends produces near-perfect yields [75].

## 2.3 Hexamer Track

While our previously achieved high dimer reaction yield is adequate for the intended hexamer track, scaling the connectivity introduces additional challenges that must be addressed. Direct mixing of all monomers would lead to increased nonspecific interactions due to the higher number of sticky end edges, which react nonspecifically via blunt-end interactions. Furthermore, gel purification of each monomer is time-consuming, and the technical inaccuracies makes precise equimolar mixing difficult to achieve, reducing the overall production yield and purity. As the number of sticky ends in the system increases, the sequence design of these sticky ends requires more attention. The following sections will describe the strategies employed to overcome these challenges.

### 2.3.1 Origami Monomer Design and Attachment Principle

The origami monomers were based on the Rothemund square lattice rectangle origami [36], but to allow longer track for the same number of origami units, were redesigned to be longer and narrower in comparison to the original rectangle (~50X155 nm, Figure 2.2A) that was also twist corrected. For detailed origami monomers design and preparation

procedures see Appendix A: Origami tile's section. The sticky ends sequences were generated using a computer algorithm tool I developed, called 'NuCraft'.

**The NuCraft algorithm:** The NuCraft algorithm produces a pseudo-random sequence for the sticky ends while ensuring that no unintended segment hybridization occurs beyond a user-defined order, which, in this work, was set to a maximum of 6 base pairs. In other words, aside from the planned interactions, no sticky end segment should be able to hybridize at 6 nucleotides or more (see detailed algorithm in Appendix C.1).

In some cases, when AFM recognition of the monomer's location and orientation in trimers and hexamers was required, monomers were imprinted with 'A' to 'F' letters using the 'dumbbell staple' technique [36]. The scaffolds and main staples of all six monomers were identical, and the origami monomer's edges consists of eight scaffold loops. Attachment of adjacent origami units was achieved through hybridization of three sets of orthogonal sticky ends strands (SE-1, SE-2 and SE-3) that were designed to hybridize with the scaffold loops during the thermal annealing process such that SE-1 attach origami-A to origami-B (A/B) and D/F, SE-2 attach B/C and E/F, and SE-3 attached C/D (Figure 2.2A). The overhanging 'sticky ends' segments were of 11 nucleobases length, and upon hybridization, formed a total of 15X11 base-pairs (strands directionality dictates that one set of sticky ends segments were negated, and the origami units were slightly shifted in respect to each other).

The edge tiles, origami-A and origami-F were prepared with eight polythymine (poly-T) overhanging strands designed to hybridize with the origami left-side and right-side scaffold loops, respectively. To enable single-molecule fluorescence imaging, origami-A and origami-F were introduced during the annealing with ATTO-647N fluorophore labeled strand, that hybridized with six elongated staples located about 20 nm away from the origami peripheral edges, and to enabled coverslip immobilization, origami A and F were introduced with five biotinylated staples, with the biotin facing downward.

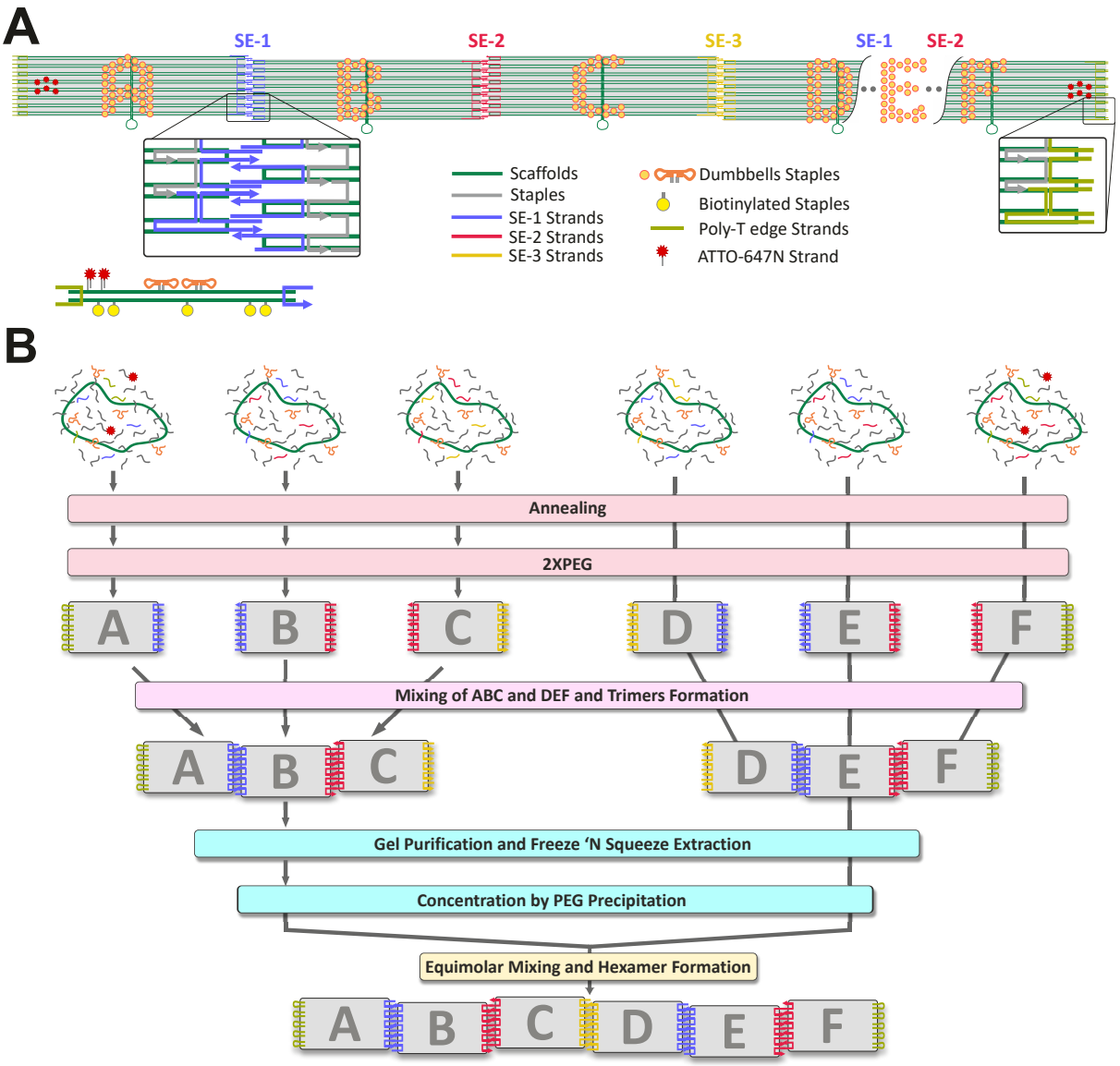


**Figure 2.2: Origami hexamer design and hexamerization procedure.** (A) Schematics of the hexamer upper view and origami-A side view. Shown are scaffolds (green), staples (gray), three sets of sticky end strands (SE-1, SE-2 and SE-3; blue, red, yellow, respectively), dumbbell staples (orange), poly-T loop strands (olive), and biotinylated staples (yellow circles). Insets show closeups of the staples, sticky ends, poly-T overhangs and scaffolds design and hybridization strategy. (B) Schematics of the hexamer preparation procedure. The six monomers are separately thermally annealed, and PEG purified twice. Monomers A, B and C and monomers D, E and F are mixed to form trimers ABC and DEF. The trimers are gel purified, extracted from the gel using Freeze 'N Squeeze and concentrated by PEG precipitation. Equimolar concentrations of the trimers are mixed to form the target hexamer.

### 2.3.2 Detailed Hexamer Fabrication Procedure

To examine and monitor the hexamer fabrication process, the origami products were analyzed using agarose gel chromatography at various steps, including after thermal annealing, PEG purification, and trimerization and hexamirization reactions steps. The

importance of the buffer's ionic content is demonstrated in Figure 2.3. All six different origami units, sampled after the thermal annealing and after PEG purification, were analyzed using gel containing 12 mM $MgCl_2$ (**Gel12**) and gel containing 100 mM NaCl + 2 mM $MgCl_2$ (**Gel102**) (Figure 2.3A, C and 2.3B, D, respectively). The origami pellets formed in the second PEG round were dissolved using buffers that match the intended gel (**B12, B102**).

For NuCraft-generated sticky ends, strong monomers bands were clearly observed for all six monomers before and after PEG purification in Gel102, homodimers and larger structures bands were mostly absent (Figure 2.3A, B). In comparison, Gel12 shows mixed results, with significantly more nonspecific homodimers that could restrict reaction between correct origami monomers. This finding is supported by AFM measurements demonstrating similar trends based on salt concentration (see Appendix D.2). Thus, these results support the usage of a low ionic buffer in the preparation and purification steps after annealing.

Furthermore, for randomly generated sticky ends, in contrast to NuCraft-generated sequences, there was either complete absence or weak monomers bands, with most of the origami contracts remaining in the (gel) well when using Gel12. This indicates extensive formation of nonspecific homo-structures that, due to their size, did not migrate (Figure 2.3C). Low ionic buffers can mitigate the unwanted homo-oligomerization effect (Figure 2.3D), however, homodimerization was still present as was the case for origami-C and origami-F (Figure 2.3D, lane11,14). Therefore, using low ionic buffers and NuCraft optimized sticky end sequences to minimize random cross interactions was found to be highly beneficial.

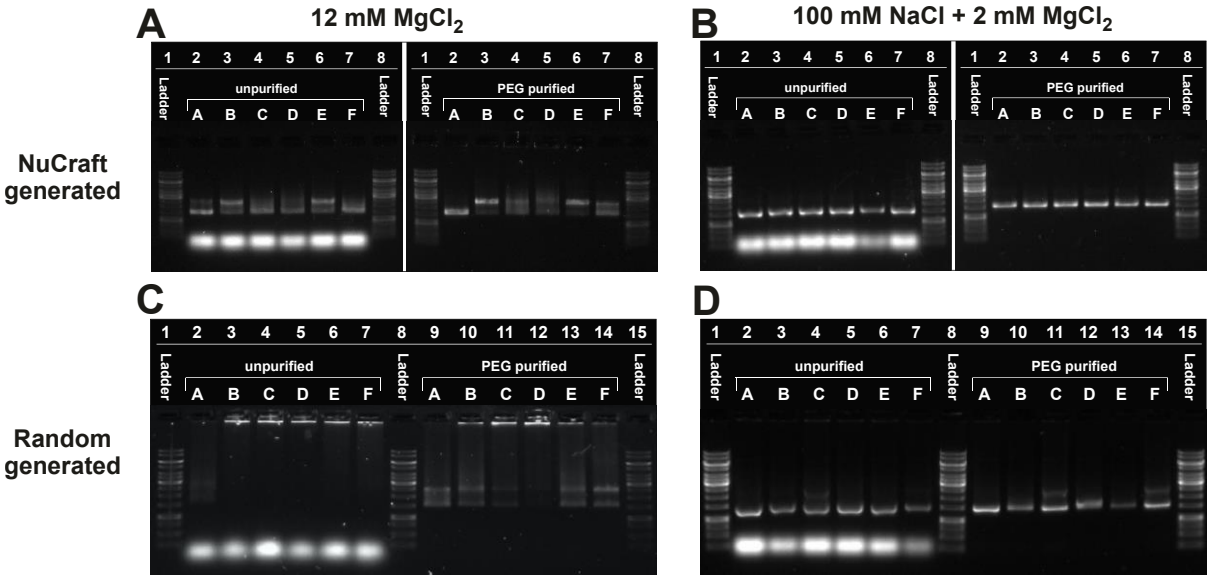


**Figure 2.3: Evidence for aggregation depending on buffer and sequence.** (A) Gel12, NuCraft generated sticky ends: Agarose gel containing 12 mM $MgCl_2$. Shown are all six monomers analyzed after the thermal annealing process (unpurified, left side) and after PEG purification (right side). The pellet formed in the second PEG purification round was dissolved in B102 buffer. 1kb ladder (Lanes 1,8), origami-A to F is lanes 2 to 7, respectively. (B) Gel12: Same as (A), but the gel contained 100mM NaCl +2 mM $MgCl_2$ and the pellet formed in the PEG purification was dissolved using buffer containing the corresponding salt. (C), (D) respectively like (A), (B), but the sticky ends sequence was generated randomly. All Gels are 0.6% agarose, 1x TAE buffer.

Figure 2.4A shows a chromatogram of Gel102 used for purifying the ABC and DEF trimers containing NuCraft optimized sticky ends sequences. To prevent lane overloading, each trimer sample was divided into three lanes. Analysis of the band intensity profile (e.g., for trimer DEF, Figure 2.4A, right panel) reveals, alongside the predominant trimer band (95%), small quantities of monomers and dimers. If not removed, these may interfere with the subsequent hexamerization reaction and reduce product purity. This demonstrates the importance of employing size-dependent gel purification over PEG purification, which cannot remove these structures.

Figure 2.4B displays Gel102 with reintroduction of the trimers extracted from the gel shown in Figure 2.4A and of the final hexamer product. Hexamers and trimers bands are clearly observed in the respective lanes. The bands intensity profile of the hexamer lane shows, in addition to a minor trimer population (<2%), a smeared slow band (~31%). Based on AFM images of the product sample (Figure 2.4C, all data are shown in Appendix D.4) and manual counting of hexamers and trimers, shows a 92% hexamer yield suggests

that the gel's slow band likely represents correct structures that experience delayed migrating into the gel.

In contrast, when sticky ends sequences were randomly generated (Figure 2.4D, E), gel analysis showed high amount of trimer aggregation (Figure 2.4D). However, the process maintained a high hexamer-to-trimer ratio (Figure 2.4E), further demonstrating the procedure's ability to remove impurities and emphasizing the necessity for optimized sequences to enhance the total yield of the process.

A straightforward in-silico analysis of all the system sticky ends, without spatial geometry considerations and only counting sequential base pairings (not considering mismatches and gapped interactions), reveals a threefold decrease in 5-nt segment counts and none at 6-nt or above for NuCraft sequences (Figure 2.4F). This may explain the difference in trimer quality when using random generated sticky ends in comparison to NuCraft generation.

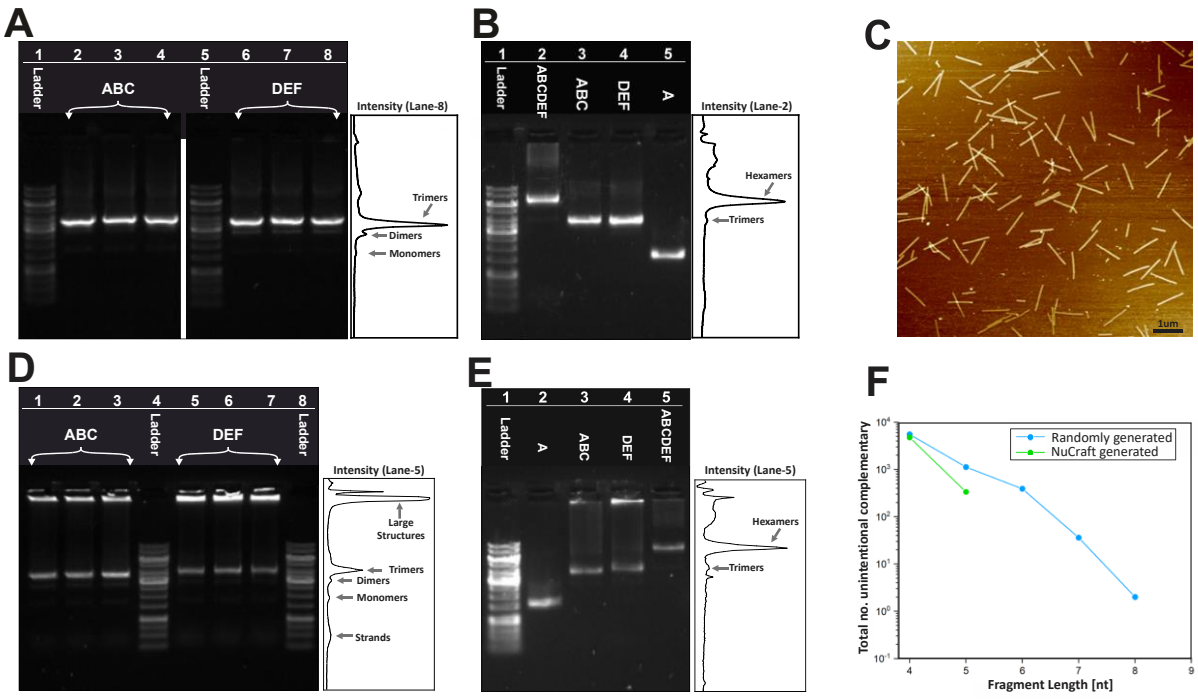


**Figure 2.4: Gel and AFM of trimers and hexamers with different sticky ends sequences.** (A) Gel102, NuCraft generated sticky ends, used for trimers purification. 1kb ladder (lanes 1 and 5), ABC and DEF trimers (lanes 2, 3 and 4 and lanes 6, 7 and 8, respectively). In addition to the prominent trimers bands structures that slowly migrated out of the wells and minor monomers and dimers bands (total ~ 7%) can also be seen (intensity profile of lane 8, right panel). (B) Analytical gel102, show the formation and purity of the final hexamer product. 1kb ladder (lane 1), final hexamer product (lane 2) ABC and DEF trimers purified by gel102 shown in A. (lanes 3

and 4, respectively) and origami-A (lane 5). Excluding slow-migrating structures, hexamers were ~98% and excess trimers were ~2% (intensity profile of lane 5, right panel). (C) AFM images of the final product. (D), (E) respectively like (A), (B), but the sticky ends sequence was generated randomly. (F) in silico analysis of the sticky ends sequences unintentional complementary count at each fragment length.

### 2.3.3 Analysis of Origami Hexamer Lengths and Stiffness

The length and stiffness of the hexamer tracks were estimated using AFM and single molecule florescence imaging (see details Appendix B.4), and by fitting to worm-like chain (WLC) model. Analysis of AFM images of several seemingly straight hexamers yield end-to-end distance of ~ 950 ± 10nm (Figure 2.5A and Appendix D.3), in a very good agreement with the theoretical value (955 nm, based on 2809 base-pairs(bp) multiplied by the literature 0.34 nm/bp value). Visual inspection of the AFM images show that some hexamers were bend, and some were buckled and partially flipped upside down (Appendix D.5). Bending or buckling was not more prominent around the monomers attachments sites, indicating that the sticky ends provide mechanical stability similar to that of the origami core. The origami interaction with the AFM mica may cause the hexamer to behave differently than in single molecule coverslip immobilization.

To estimate the track length and stiffness in conditions that are more relevant for single molecule experiments, the hexamers were introduced into a microfluidics-based flow chamber identical to the one previously used for operating bipedal motor based on a single origami [9]. The hexamer tracks were immobilized on the chamber coverslip surface using biotin-avidin interaction and imaged using total internal reflection (TIRF, Figure 2.5C, for details, see Appendix B.4). The distances between pairs of nearby fluorescence spots, emitted from two groups of six fluorophores, each group located ~21 nm away from the track peripheral edges (Figure 2.2A), were estimated by fitting a mathematical model consisting of a pair of 2D Gaussians, and the resulting spot-to-spot distances were accumulated in a distance distribution histogram (Figure 2.5D). About 90±2% of the total fluorescence spots located at two nearby Gaussians spots, were attributed to hexamers, while the remaining single spots were attributed to the presence of trimers (Figure 2.5E, Appendix D.1). The histogram was fitted using a worm-like chain model[132] (after removing cases of single imaged spots corresponding to tetramers), that contained two free parameters, contour lengths and persistence length (Lc, Lp,

representing the length of the track and the track stiffness, respectively). Fitting the histogram acquired from samples measured at B102 (Figure 2.5D), yields Lc=793 nm and Lp=1171 nm. Considering that the fluorophores were ~21 nm away from the hexamer edges, the entire hexamer counter length was calculated to be Lc=829. The fact that almost all the spots show two distinguished fluorescence spots with spots distance distribution well fitted with WLC model, demonstrate that the hexamer track structural integrity and stiffness are adequate for operating bipedal motors, and in conditions suitable for single molecule tracking experiments.

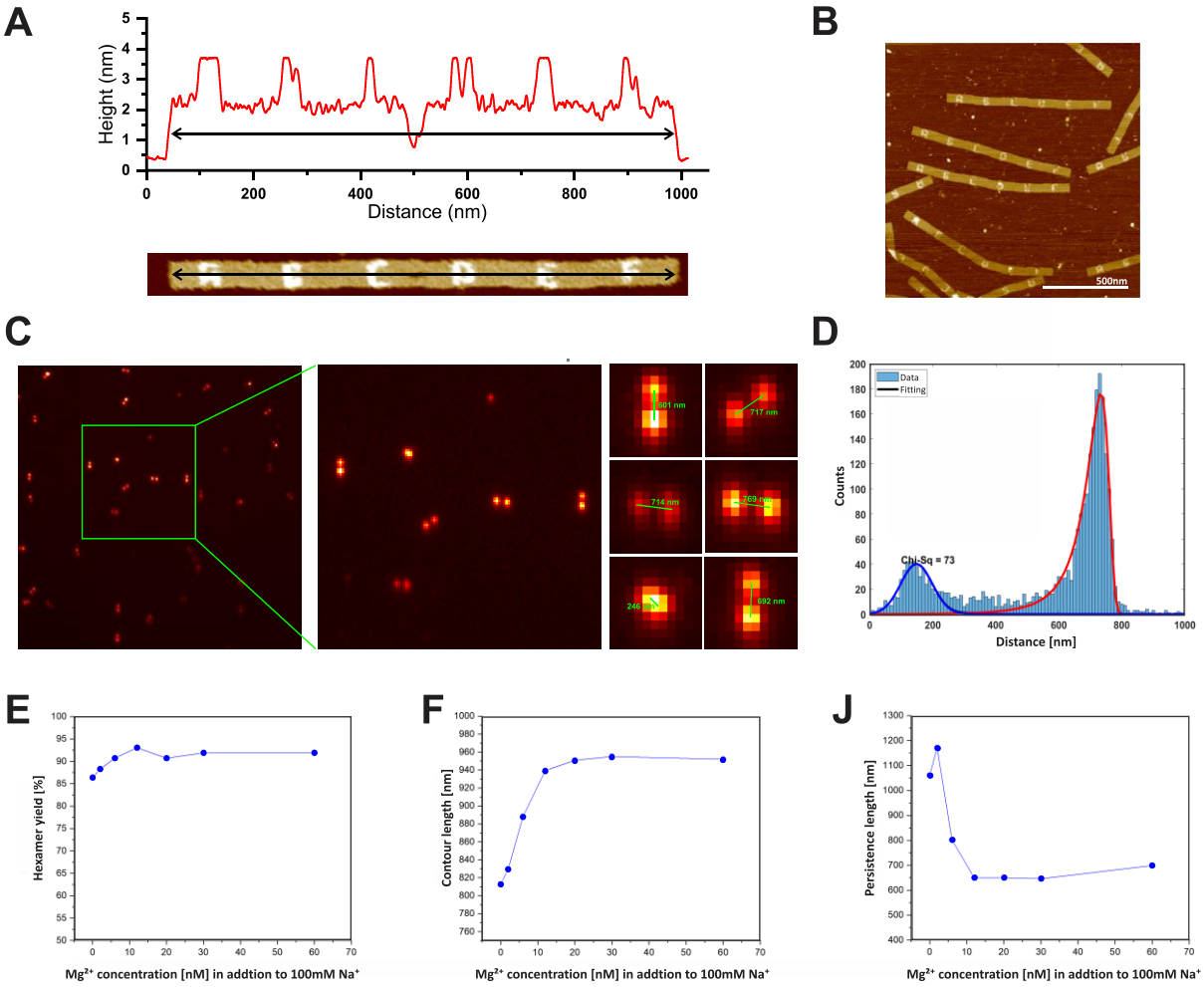


**Figure 2.5: Characterization of hexamer properties employing AFM and TIRF imaging.** (A) AFM hexamer z-profile analysis, where height peaks corresponded to letter dumbbells. (B) AFM imaging of hexamer samples with letter, scale bar 500nm. (C) TIRF microscopy reveals ATTO 647N-labeled tracks near both edges, tethered to a slide coverslip through biotin-avidin interaction, featuring distinctive pairs of bright dots. Inset in C. provides a zoomed-in view of the labeled tracks. (D) Histogram displays length distribution from MATLAB-based analysis. A narrow Gaussian distribution (~740 nm average distance between dot pairs) signifies high-quality tracks with consistent attachment to the coverslip, crucial for efficient motor movement. (E) attributing the short distance spots, to trimers, and longer distances for hexamer, integral of the two different

fitted curves, result in average hexamer yield, over different salts, 90±2%. (F) The contour length peaks at approximately 950 nm with the escalating salt conditions, specifically at 100 mM NaCl+20 mM $MgCl_2$. (J) The dependence of persistence length on salt concentration unveils a decrease in stiffness as the concentration of magnesium salt increases.

To assess the length of the track and its stiffness in different environments, the hexamer construct were incubated at various salt concentrations and then immobilized within the microfluidics chamber, maintaining a consistent salt throughout. The histograms display the length distributions (see Appendix D.1). Worm-like chain analysis reveals a contour length of approximately 813 nm at 100 mM NaCl, with an increase in contour length observed as the concentration of $MgCl_2$ is raised. The contour length reached a final value of 952 ± 2 nm at 100 mM NaCl and 20–60 mM $MgCl_2$ (Figure 2.5F), in agreement with the hexamer length measured by AFM on a mica surface. It appears that the introduction and increasing concentration of magnesium ions caused the crossovers (Holiday junctions) to shift from an open-X conformation to a stacked-X conformation [133].

Additionally, the persistence length, which reflects the level of hexamer bending and fluctuation, was calculated. At 100 mM NaCl, the persistence length was Lp=1061 nm. With the increase in concentration of $MgCl_2$, the persistence length dropped to 699 nm at 100 mM NaCl and 60 mM $MgCl_2$ (Figure 2.5F). Apparently, increased magnesium concentration increases origami length [134] but decreases its stiffness.

## 2.4 Origami-Based Fluorescent Rod for Bipedal Walker

The lab's current linear bipedal walker is investigated using single molecule FRET spectroscopy, which allows the identification of only 2-3 different steps, and the organic fluorophores tend to bleach rather quickly. To enable continuous monitoring of the walker over all steps and the entire length of the hexamer, I have developed a fluorescently labeled origami-based rod that contains up to 12 fluorophores that can be refurnished by toehold mediated strand displacement. With this scheme, the position of the fluorescence rod can be monitored for the entire hexamer length and for all steps, including identification of operation failure at all steps.

### 2.4.1 Design of the Rod-Like Origami

The rod-like DNA origami was designed to have 13 helices of 26 nm length, arranged at honeycomb lattice conformation (13 nm effective diameter, Figure 2.6). The structure was made of 1033 base long scaffold that was folded using 30 short complementary staples. Twelve of these strands were elongated by a segment that allows hybridization with fluorescently labeled strands. Each of these strands contains a toehold segment that allows removal of the fluorescently labeled strand for the purpose of fluorophores refreshment.

### 2.4.2 Assembling the Rod-Walker-Track Complex

Assembling the origami rod with the walker and the track needs to be carried out in steps, one-pot reaction would result in very low yields due to excess walker binding site strands. The hexamer tracks, pre-prepared with the bipedal walker (without the origami-rod) positioned on origami-A, are introduced into the microfluidics device, followed by washing to remove any residual binding strands, followed by introduction of the rod-origami (see Figure 2.6C). To avoid interaction with excess connecting strands from the rod side, the rod-origami was designed to hybridize with the walker via its scaffold (for which there are no excess, via interaction of 30 bases overhangs). Preliminary results indicate that this design scheme works sufficiently well (see Figure 2.6E). Fluorescently labeled rods were introduced into the microfluidics, interact with the walker over 4 hours, followed by washing steps that did not remove the rod. Further, toehold mediated strands

displacement reaction that dissociates the legs, removed 96% of the total rods, indicating the successful assembly of the entire linear rod-loaded bipedal motor.

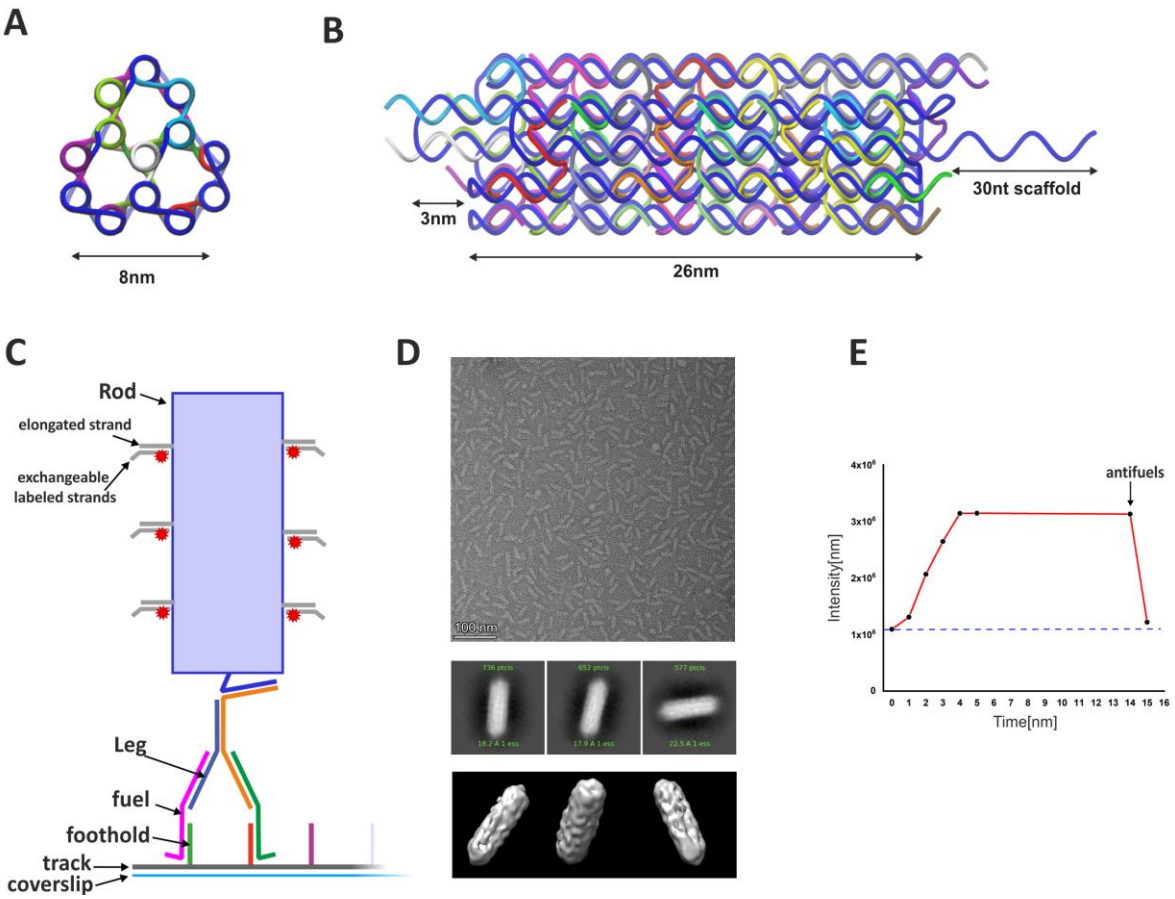


**Figure 2.6: Rod design, synthesis, and connection.** (A) Top view of the rod design. (B) Top view of the rod design. (C) Schematic of the rod connected to the walker located at the beginning of the track. (D) Top: negative staining TEM image of many rods after annealing. Middle: first 3 classes from 2D classification of many negative staining TEM images. Bottom: 3 points of views on the 3D construction based on 2D classification. (E) Ensemble TERF red on red signal, shows signal.

## 2.5 Summary of Aim-1

In this part of the research, I successfully developed a long DNA origami track, constructed from six addressable rectangular monomers, which were linked using sticky end staples that were optimized by our novel computer algorithm that minimize cross interactions. The primary objective of this effort was to fabricate origami track that is suitable for unidirectional walking of the bipedal walkers over a micrometer distance.

Unlike my initial work, where extensive gel extraction that was utilized to remove excess staples and that could obstruct reaction sites, the current method uses high-quality PEG purification for the monomers. Gel extraction was then utilized for the trimers to ensure the removal of incorrect origami structures, including residual high-order structures, excess dimers and leftover monomers resulted from imperfect equimolar mixing. Consequently, the formation of the hexamer, achieved by combining two trimers, was only susceptible to minor contamination resulting from imperfect mixing.

Characterization of the hexamer was conducted using AFM and gel electrophoresis, and further validation was performed under conditions more closely aligned with the intended walker experiments using fluorescence microscopy. Additionally, the stiffness of the DNA origami structures was fine-tuned by adjusting magnesium ion concentrations, which influenced the crossover conformations. Higher magnesium concentrations were found to increase flexibility and contour length, while lower concentrations increased the rigidity and straightness of the structures.

A rod-like DNA origami structure was also developed to house fluorophore-modified strands. This rod demonstrated successful connection and disconnection from the track, a critical feature achieved by attaching to the walker using scaffold extensions rather than staple elongation. This work lays the foundation for future more detailed investigations of the bipedal motor by allowing tracking the walker during all steps, and not only in the track edges, as is the case with our previous walker [126], hopefully advancing our understanding of motor failures.

# Chapter 3: DNA Origami Rotary Motor

## 3.1 Motivation

The motivation for this project arises from the need to advance the development of autonomous motors capable of sustained, unidirectional movement. Here a structure has been developed to provides an "infinite" track with precise, continuous monitoring capabilities and an error self-healing mechanism. By initially employing a well-established, externally controlled bipedal walker, the complexities of autonomous motor can be sidestepped. This approach allows focus on refining the motor's structural design and enhancing the monitoring systems, essential steps toward achieving a fully autonomous motor which I promote in Aim-3.

## 3.2 Design of the Rotor

### 3.2.1 General Design

The rotor's design consists of two separately prepared origami discs (bottom and top discs) that are connected to each other through hybridization of the two swivel elements (Figure 3.1). A key important point was that the swivel that locked the two discs together by irreversible hybridization, but as a single-strand DNA axis, allows free rotation. Each disc is made of four layers of square-lattice origami [36, 39]. The two main (larger diameter) layers are designed to house a circular foothold track (bottom disc) and two bipedal walkers (upper disc). Two smaller concentric layers are designed to house a centrally positioned swivel and to maintain a gap of ~10 nm between the main layers to provide room for free operation of the bipedal propulsion mechanism. The discs are designed to be large enough (~90 nm in diameter) to house two sets of six different footholds spaced 12-nm apart (Figure 3.1C). The footholds are positioned far enough from the origami edges to prevent unwanted interactions with the coverslip surface. To prevent nonspecific interactions of the gold nanorod with the coverslip surface, the disc's diameter is designed to be large enough to house the 65-75 nm gold nanorod (peak scattering at ~640 nm) without bulging out of the discs. Because of their sizes (~15.5 Kbp), each of the discs are assembled (in a one-pot thermal annealing process) using two orthogonal scaffolds that interact according to the 'scaffold interlocking' principle

recently developed by Dietz and co-workers [76]. To minimize discs twists, bends, and overhanging edges that may interfere with the rotation, the discs were designed and simulated iteratively using MrDNA package [45].

The rotor synthesis procedures include disc monomers annealing, PEG purification of excess staples, disc attachment via the swivel, attachment of the gold nanorod, immobilization on the coverslip surface within the microfluidics working chamber,and finally, bipedal leg attachment to the footholds. Each step and combination of steps were optimized separately to achieve optimal fabrication procedure.

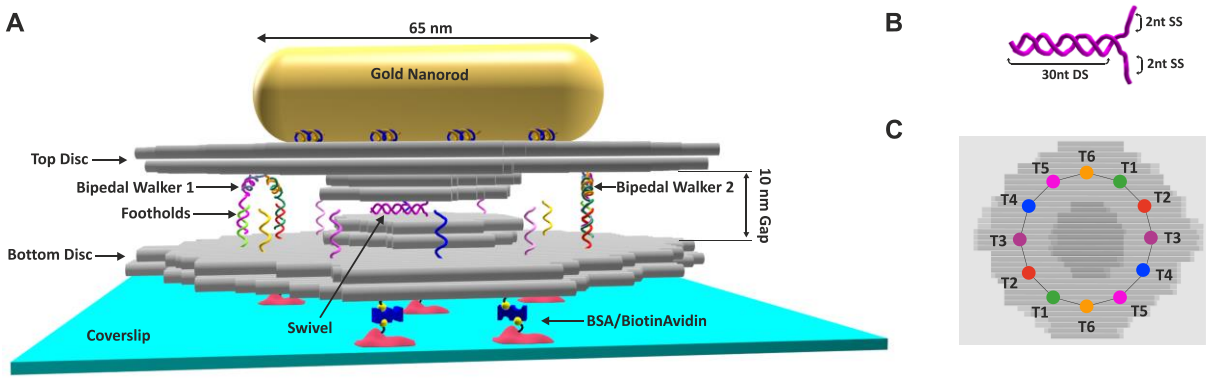


**Figure 3.1: Rotor design.** (A) Detailed rotor design. (B) Swivel consisting of 2 ss-DNA axes joined by a 30 base ds-DNA zipper connection. (C) Circular track foothold placement.

### 3.2.2 Origami Disc Twist Correction

In DNA origami mesh the spacings between crossovers that link a given helices pairs are constrained to be a multiplication of the periodicity of the double helix, which is approximately 10.5 base pairs/turn [42]. In practice, for square lattice origami, the crossovers between neighboring helix are taking place every 32 base pairs, and in a 16 base pairs phase with the crossovers to the other-side neighbor helix. The numbers of base-pairs between crossovers are not integer multiplication of 10.5 [36, 39] and therefore, non-corrected origami structures are typically somewhat globally twisted. In theory, a deletion (negation) of a single base every 64 bases should provide optimal correction for this problem. However, this is rarely the case, and many theoretically twist-corrected structures show some residual global twists [45]. Achieving flat non-twisted origami discs is necessary to avoid uneven height for the walker and unwanted steric interaction between the two rotating discs. Such residual twist may be corrected by fine tuning of the structures coupled with iterative *in silico* simulations (MrDNA [45]).

I have investigated several discs designs. The first design consisted of a single main layer and two smaller concentric layers (Figure 3.2A). However, with this approach, none of the correction and spacing patterns tested produced a flat structure, and the edges of the main layer were highly fluctuating above and under the origami plan, which may lead to undesired origami-edges/edges interactions.

Inspired by recent publications [135, 136], I tested an unorthodox structure consisting of multilayer DNA origami with perpendicular layers (Figure 3.2B). These structures have rather low crossovers density, and initial simulation show a significantly twisted structures with loose edges. In addition, this approach does not allow usage of two scaffolds (needed for achieving the desired disc size), and therefore, the approach was abandoned.

I, therefore, designed a multilayer structure, consisting of two large and two small regular layers (Figure 3.2C) that provide the necessary size, stiffness and avoid twists with base deletion every 32 bases. With this approach, to achieve the required disc size, we adapt a recently published method that allows incorporating two 'interlocking' orthogonal scaffolds to create a 15k base pairs structure in a one-pot annealing reaction procedure [76]. Using this approach, I iteratively designed the discs to achieve mostly flat structures with reasonably tight edges and high assembly yields.

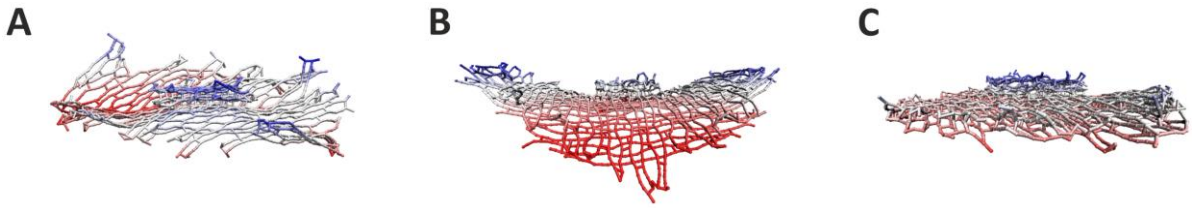


**Figure 3.2: MrDNA iterative simulation results.** (A) One main layer. (B) Two periodical main layers (C) Two regular main layers.

### 3.2.3 Interlocked Scaffolds

To achieve correct and high yield folding, I mostly followed the interlocking guidelines: 1) target length of the interlock is 100 bases, 2) interlocked regions should have a similar GC content, 3) the interlocking regions should not contain homogeneous sequences (Figure 3.3).

The two chosen scaffolds are the standard DNA origami scaffold, M13 bacteriophage genome p8064, and the custom created scaffold, cs4, which is almost completely orthogonal to the p8064, with a length of 7557 bases (all purchased from Tilibit Nanosystems, Germany). To avoid structural weakness in the sensitive internal concentric layers (the 4 smaller middle layers), where the two discs are in proximity, these internal layers were constructed from only one of the two scaffolds (p8064).

Each of the two scaffolds contains several internal homologous (or semi-homologous) sequences [76]. For example, p8064 contains two identical 42 base long identical sequences. In addition, the two scaffolds have 89-base and 107-base identical sequences. If not design properly, such homologous sequences may wrongly interact with undesired staples, resulting in placing of key components such as legs, footholds, swivel, gold-nanorod-attachments strands, and biotinylated staples in the wrong positions. To eliminate such wrong folding, I program an algorithm (using MATLAB) to locate all homologous sequences and design the discs such that the homologous sequences does not interact with key staples, and not more than 8 bases continuous interaction could take place with any of the other staples. In addition, the full lengths of the scaffolds were incorporated in the structure (no residual unstructured overhangs), to avoid unwanted interactions between the discs and between them and the surrounding coverslip bound avidin-biotin environment, restricting rotation.

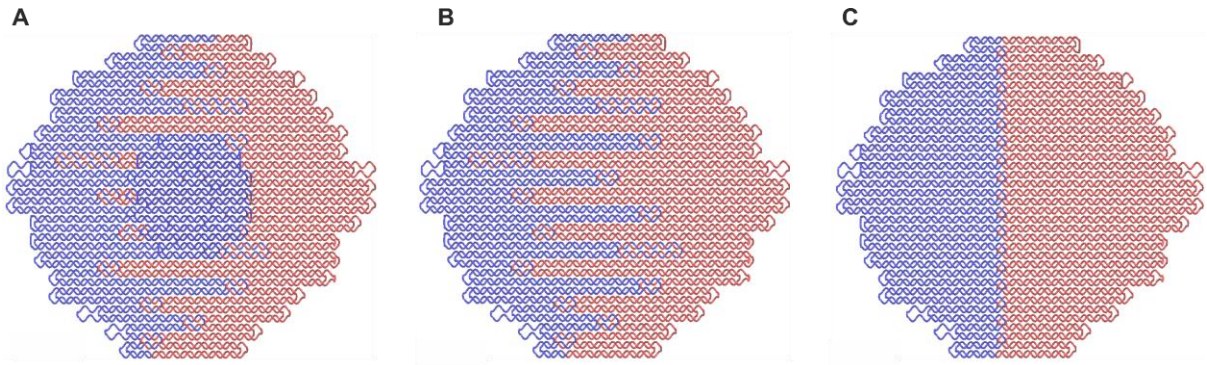


**Figure 3.3: Scaffolds routing top view.** (A) Actual interlock including the concentric layers. (B) Actual interlock omitting the concentric layers for visual reasons. (C) non interlocked scaffolds, omitting the concentric layers for visual reasons. The staples are not visible in the picture. The color blue and red indicate scaffold p8064, cs4 respectively.

### 3.2.4 Edge Passivation

Another challenge in designing DNA origami constructs concerns avoiding undesired origami aggregation. Such aggregation is often induced through blunt-end stacking interactions of the helix's edges, as I show in my research and Aim-1. Typically, an origami edge interface that contains six or more blunt ends, and that are structurally complementary to another six or more blunt ends edges, may unwantedly interact with each other, resulting in origami aggregation (or dimerization).

To reduce such aggregation, the edges should be sufficiently passivated. One technique for preventing aggregation is to design the edges such that they geometrically cannot fully align with each other (this is one of the reasons a round, rather than a rectangle, shape was chosen). In addition, the disc edges were designed with irregular pattern, further reducing the likelihood of shape matching stacking.

The second technique is to 'hide' the blunt ends by introducing edge staples that contain a poly-T or a poly-C overhang segments or loops. These segments hide the helices blunt-ends, interfering and reducing their interactions. Typically, poly-T is used, but because poly-A's and poly-T's were used to attached the gold nanorod, we used poly-C in the origami edges.

### 3.2.5 General Staples Strategy

To achieve structurally stable and high folding yields of origami constructs, several design principles should be met. Higher crossovers density and the presence of at least one continuous 16 bases long staple/scaffold interactions for each staple are recommended [137, 138]. The DNA staple strands are manufactured through solid-phase synthesis, in which the yield of full-length oligo decreases with increasing oligo length [139]. On the other hand, the staple should be long enough to allow maximum crossovers and at least one 16 bases continuous staple/scaffold interactions. Therefore, 48-64 base long staples were typically used [140].

For the square lattice 3D origami architecture, the basic cell unit is of 8 bases. For a helix that has four neighbors (as in the region of the disc where there are 4 layers) one needs to compromise between maximum crossovers and having at least one 16 base pairs

segments. I carefully designed these locations to maximize crossovers while maintaining at least one 16 base segments.

Another challenge was to design the origami such that the special elongated staples do not compromise structural stability (that can happen when the 16 base segments must be cut to two segments). Because most of the needed (most important) elongated staples (legs and footholds) are bulging from only one side of the discs (the inner layers), I designed the origami such that the 16 base segments are positioned in the outer layers and are not cut. In some places (e.g., elongated biotinylated strands) this was not possible, and staples were designed without 16 bases segments.

### 3.2.6 Footholds and Legs

In our lab, a linear bipedal walker propulsion system has been extensively optimized [141, 9]. We therefore choose to apply this system for the rotor with only minimal changes possible. Each foothold set should consist of at least 6 orthogonal footholds to avoid overreaching the neighboring foothold set [141]. The disc outer diameter is about 90 nm, the diameter of the smaller centric layers is about 30 nm, and the centric position circular foothold track has a diameter of 60 nm.

Arranging the track from two sets of 8 footholds at a 60 nm diameter will yield footholds distance of 11.7 nm which is the optimal distance according to our findings for a linear motor (~12 nm) [141]. However, the linear walker system was optimized with only 6 footholds per set, and we preferred not to add new unoptimized foothold sequences in the initial rotor design. Thus, the distance between the footholds in the rotor is 15.5±2 nm, which according to our findings, is almost as good as the 12 nm distance [141]. The diameter of the two sets of legs in the upper disc was designed to be 60 nm, to match the footholds track diameter.

### 3.2.7 Gold Nanorod Attachment

Methods for attachment of a gold nanoparticle to DNA origami has been extensively developed in the last 15 years. Typically, following modification the gold nanorod should be covered with hundreds of poly-T single stranded sequences, that are then attached to complementary poly-A elongated staples. Typically, the number of attachment sites (in our case, the number of poly-A sequences) is between 8 to 25 [142-144], with recommended length of 10 Adenine nucleotides [142]. A poly-A/poly-T helix of the length 10 transiently hybridize/dehybridize under our conditions (room temperature and ion concentrations), which enables rearrangement ('diffusion') of the gold nanorod to maximize the number of interactions. According to our design, such maximization happened when the gold nanorod is centrally positioned, minimizing the bulging of the rod outside of the rotor disc which is required to avoid rods contact with the biotin-avidin covered coverslip. The poly-A strands are arranged in 3 rows of the length 52 nm, an arrangement that encourages strong interaction and minimum bulging (see details in Figure E.5).

## 3.3 Optimized Synthesis of the Rotor

### 3.3.1 Disc Folding

The optimal folding conditions for the disc (15 mM [$Mg^{2+}$], 15min at 65°C then 1hr/1°C 60-44°C) were found using an approach based on a publication by the Dietz group [140]. Annealing temperature gradients, $MgCl_2$ concentrations, and staples/scaffolds ratios were screened (data not shown). An agarose gel chromatogram of a disc folded in optimized conditions is shown in Figure 3.4A (excess staples were removed by PEG-purification [140]). The monomer band is sharp, and the dimer band is relatively small. AFM image (Figure 3.4B) shows many correctly folded discs. These results indicate a clean and high yield folding reaction. Additionally, TEM image (Figure 3.4C) demonstrates that the desired flatness of the disc, important for free and controlled rotation, was indeed achieved. The most abundant class from the 2D classification of the cryo-TEM images show agreement with the theoretical design (Figure 3.4D). Additionally, 3D classification of the cryo-TEM images shows less than 4 nm out of plane twist (Figure 3.4E).

In the initial design, a significant population of discs was bound in pairs after the folding reaction, as explained in the following chapter (3.2.2), but this problem was corrected by rearranging a few poly-C edge staples in the disc's design.

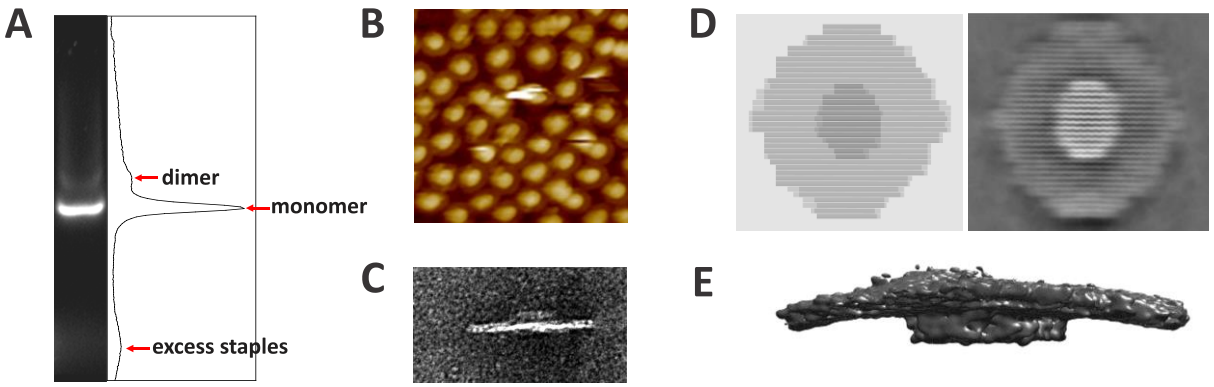


**Figure 3.4: Disc folding.** (A) Agarose gel electrophoresis chromatogram for disc. (B) AFM image of many discs. (C) Negative staining TEM image of single disc. (D) Left: theoretical top view of the disc in which each gray rectangle represents DNA helix. Right: most abundant class from 2D classification of cryo-TEM images. (E) side view of 3D cryo-TEM reconstruction.

### 3.3.2 Unwanted Disc Dimerization

The formation of undesirable origami dimers is a common problem for many origami constructs, and it is mainly caused by edge-to-edge interactions. The reasons for this dimerization can vary: 1) blunt end interactions (weak to medium strength), 2) random strand hybridization (weak to strong strength), 3) staple exchange, in which a staple segment from one monomer is thermally opened and connected to the same scaffold location in another monomer, resulting in staple bridging between two monomers (high strength), or any combination of the above mechanisms.

Figure 3.5A and B shows that the initial disc undesired dimerization is related to the cs4 scaffold region in the disc (right side of the origami structure). Using detailed AFM imaging (Figure 3.5C), the precise location of the unwanted interaction was identified (Figure 3.5D, black box). The design of this location was inspected, and it was discovered that three segments (yellow highlighted) from three separate staples (orange labeled) can potentially exchange. As a result, these three staples were replaced with staples that cannot undergo exchange (Figure 3.5D). The gel chromatogram in Figure 3.5F shows significant reduction in unwanted dimerization upon this correction.

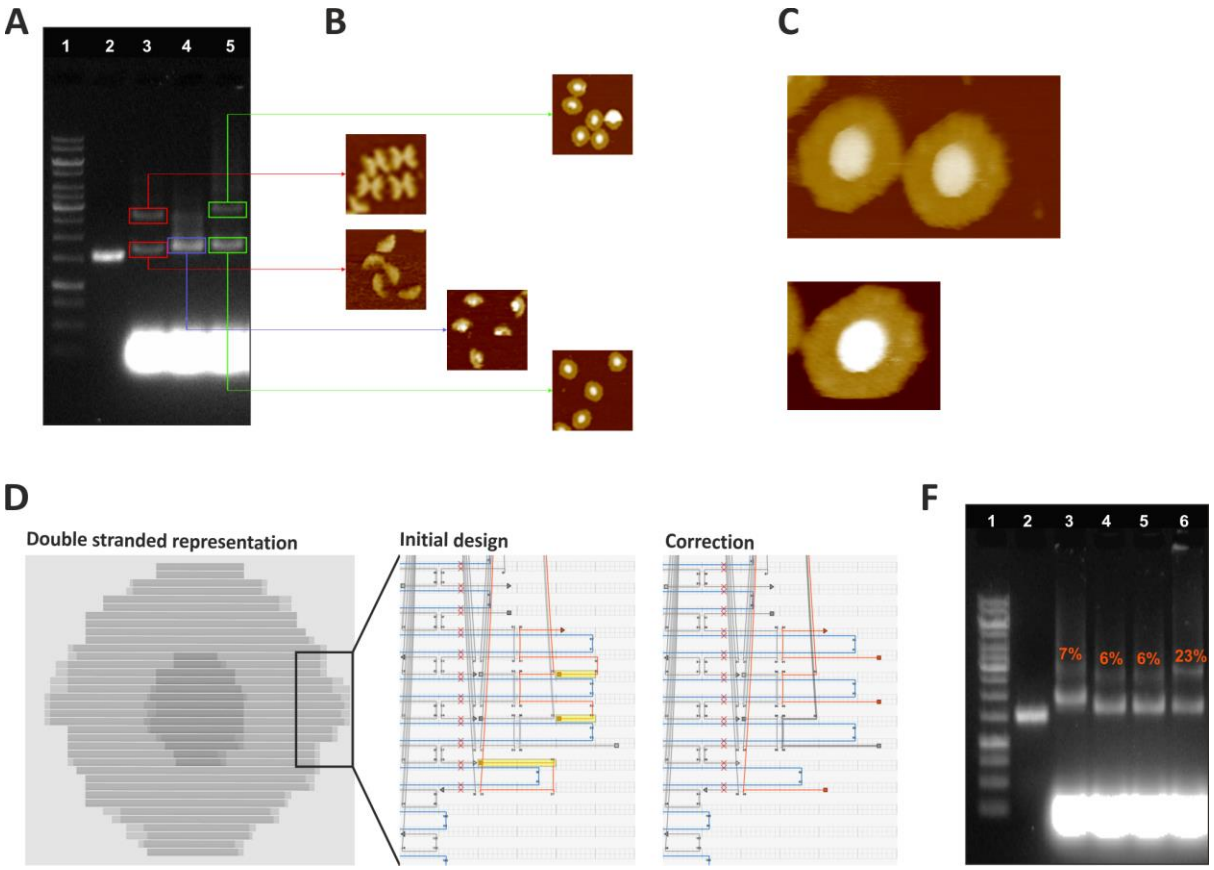


**Figure 3.5: Solving specific unwanted edge interaction.** (A) Gel chromatogram for different disc scaffold composition, lane1-1kb ladder, lane2-cs4 scaffold, lane3-Disc folding with only cs4 scaffold, lane4-disc folding with only p8064 scaffold, lane5-disc folding with both scaffolds. (B) Representative AFM pictures for indicated extracted band from Gel described in A, (C) More detailed AFM scan for the dimers. (D) Disc representation in which double stand is gray rectangle(left), problematic strands are highlighted in yellow(middle), correction design (right). (F) Gel chromogram for different edge composition, lane1-1kb ladder, lane2-cs4 scaffold, lane3-disc without all edge staples, lane4-disc without 3edge staples (orange labeled in initial design), lane5-disc including all staples according to correction, lane6-disc including all staples according to initial design, percentage with orange font indicates the percentages of disc in dimer(slow) band.

### 3.3.3 Origami Edge Staples Type

Origami passivation is usually done using poly thymine (poly-T) as such segment is more flexible than poly adenine (poly-A), and in the event of random undesired hybridization, the interaction will be weaker than if passivation is done with poly guanine (poly-G) or poly cytosine (poly-C). However, gold modification by salt aging is best achieve using poly-T stands, which means the capture site on top of the disc must be poly-A stands, which will naturally result in strong origami aggregation if the origami edges are passivated poly-T staples.

A recent paper [135] demonstrated possible solution for this problem, in which the researchers compromise on passivation by using poly-C. To ensure that this compromise is adequate for the disc, a gel comparison of poly-C and poly-T edges was conducted under various annealing conditions ($Mg^{2+}$ concentrations and annealing rates). As can be seen in the gel in Figure 3.6 poly-C origami aggregate more than the poly-T origami in some situations (18 mM [$Mg^{2+}$], 1hr/1°C), but for the most part the results look the same, and there was no significant difference at the previously chosen condition (15 mM [$Mg^{2+}$], 1hr/1°C annealing, chosen based on screening different set of conditions, data not shown). We, therefore, decided to continue working with poly-C edges, and poly-T/poly-A for the attachment of the gold nanorod.

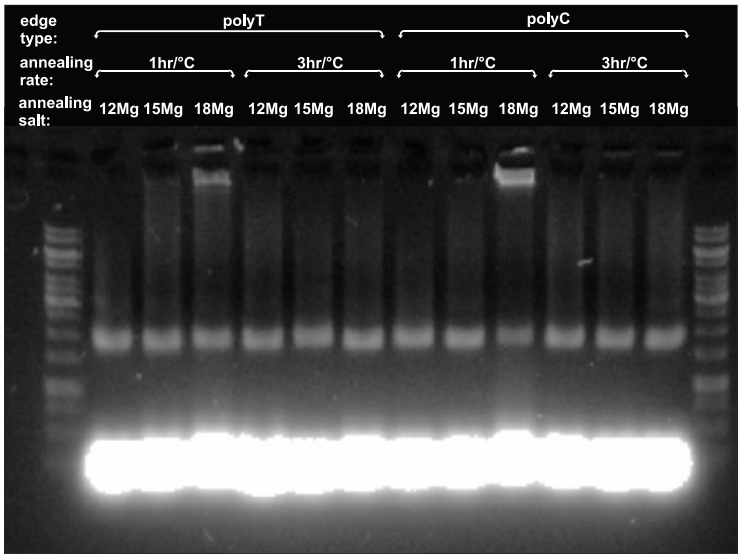


**Figure 3.6: Gel chromatogram for different edge passivation types.** The annealing window is 60-44°C, 12Mg means 12mM $Mg^{2+}$.

## 3.3.4 Stability of the Origami Disc

A typical experiment from preparation to measurement takes several days to one week. Thus, the disc must be structurally stable throughout this period. A typical magnesium concentration of 5-12 mM was sufficient to keep the structure stable [140]. Magnesium, on the other hand, promotes aggregation [75] that may interfere with the proper function of the motor (e.g., origami dimerization, disc dissociation, uneven distribution on microscope glass). Thus, reducing the magnesium and adding monovalent salts like sodium (NaCl) can reduce aggregation [75], but the structural integrity must be examined under these conditions.

To test the stability of the origami disc under different buffer conditions, the disc was incubated in different buffers ([$Mg^{2+}$], [$Na^{+}$], Tris or TAE, Figure 3.7). The results show that TAE based buffers stabilize the origami discs better than Tris based buffers, and a minimum of 100 mM NaCl and 2 mM magnesium (MgCl) was required to maintain stability. We therefore store the origami at 100 mM $Na^{+}$ and 6 mM $Mg^{2+}$ concentrations (B106, in TAE buffers), and measurements were conducted at 100 mM $Na^{+}$ and 2 mM $Mg^{2+}$ concentrations (B102, in TAE).

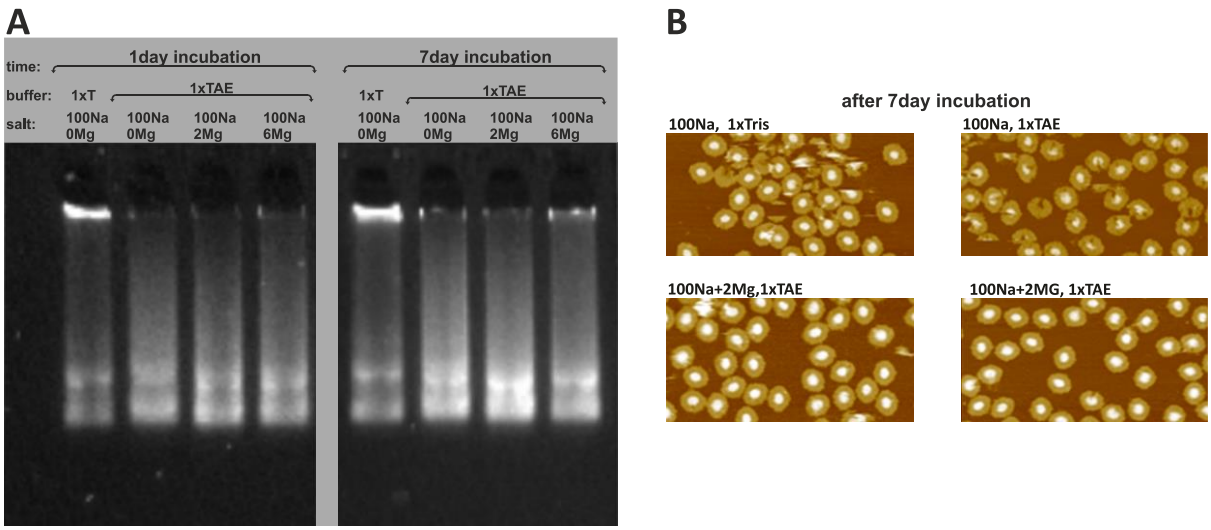


**Figure 3.7: Disc stability under different salts and buffers.** (A) Gel chromatogram for same mother material under different conditions. (B) Representative AFM pictures after 7 days of incubation.100Na means 100 mM $Na^{+}$,#Mg means #mM $Mg^{2+}$ , TAE composed of Tris base, acetic acid and EDTA.

## 3.3.5 Hybridization of the Bottom and Top Discs

To allow free rotation of the origami discs in respect to each other, the two discs were designed to be connected by a single strand DNA that allows free rotation around its covalent axis at room temperature (Figure 3.1B). In practice, this was achieved by using two partially complementary DNA strands, one attached to the bottom disc and the other to the top disc. Upon mixing of the two discs, the two strands hybridize in a parallel fashion (‘zipper’ orientation, Figure 3.1B), leaving two ssDNA segments where free rotation can take place.

The procedure of dimerization of large origami constructs through hybridization of a single pair of strands is not well established in the DNA origami literature, thus requires extensive optimization. I conducted a series of experiments that checked many of the

factors that may help or interfere with dimerization kinetics and the final dimerization yields, resulting in increased from 6% initial dimerization yields to ~80% for the optimized procedure detailed below. For simplification, only selected experimental and optimization procedures are described (data not shown).

All yields were calculated by dividing the intensity of dimer bands in gel by the total intensity of dimer and monomers bands. Reactions were carried out in 10 nM disc monomers concentrations, unless stated otherwise, and the typical reaction time was 20 hours. Each change that resulted in increased yields was adopted for the following optimization experiments unless stated otherwise.

**Salt type and concentrations:** According to my previous published research [75], a low ionic strength is required for a fast and high yield origami dimerization reactions. This rather counterintuitive results can be explained by the excess nonspecific interactions taking place in high salt concentrations that decrease DNA positive charge repulsion. Thus, the dimerization was optimized under 100 mM $Na^+$ and 2 mM $Mg^{2+}$, or 100 mM $Na^+$ and 6 mM $Mg^{2+}$ (B102 and B106).

**Temperature:** The disc dimerization yield increased by 166% when the reaction was conducted in 35°C, compared to room temperature. Apparently, the low ionic salt alone is insufficient to prevent all the nonspecific aggregations (which is essential, as explain in Aim-1). Typically, at about 40°C, origami structures tend to begin to disassembled, we therefore adapt 35°C for the disc attachment procedure.

**Excess staples purification method:** Typically, in the field, origami structures are prepared at 5-10 excess of staples over scaffolds (we used 10x, as is typical for 3D structures). This means that there are ~9x excess staples in the buffer after annealing, that may interfere with the following discs hybridization reaction. The excess free swivel strand elements may interact with the swivel strand, which is bound to the disc, blocking hybridization of the correct disc/swivel elements. Therefore, a proper purification of these excess strands was essential.

The disc origami mass is significantly higher than that of the free strands, thus PEG purification (centrifuge) should be able to properly remove the excess staples. Two PEG purification cycles were usually conducted for adequate purification, but because of the

sensitivity of the disc-swivel hybridization to the presence of excess swivel staples, initial PEG purification resulted in inadequate disc-swivel hybridization yields. We therefore adapted a protocol recently published by the Dietz group[140], where the volume of PEG solution relative to the sample solution was raised from the typical 1:1 to 10:1, resulting in a 2.5x increase in hybridization yields. The increased solution volume allows better strand/disc centrifugal separation.

**Spacer length:** The swivel elements were originally designed to each include a 2 T-bases segment (Figure 3.1B), that should provide adequate space between the bottom and the top disc inner surfaces (as well as swivel rotational flexibility). However, the origami disc surfaces are not completely flat, such that a total of 4 bases spacer may not be sufficient. Indeed, it was found that using an 8 bases spacer (4+4) resulted in substantially faster dimerization kinetics. The yield at 5 hours reaction time was 1.5x higher than that of the 4 bases spacer, although the final yield was only 10% higher. We therefore continue by using the 8 bases spacer swivel.

**Swivel excess in annealing:** To further decrease the concentration of the free swivel strands in the solution, we tested disc annealing in 3x excess swivel staples (instead of 10x), which resulted in an additional 10% increase in disc hybridization yields. This change is 'unorthodox' since the minimum recommended excess for strands is 5x (10x for important functional strands).

**Extra purification:** To check whether further swivel PEG purification will increase disc hybridization yields, we repeat the above experiments (for the 3x-swivel annealing procedure) using 4 rounds of PEG purification. Indeed, the yield increased by 3-5%, but we decided that such minor increase does not justify the additional efforts associated with 4 PEG purification rounds. Measurements of the concentrations of the residual swivel staples show that it does not influence more than 5% of the disc hybridization. Therefore, other time-consuming strand purification methods (e.g., HPLC, gel extraction) were not investigated.

**Longer swivels:** Our original swivel elements were designed to hybridize along 30 bases. We tested alternative swivel elements that were designed to hybridize along 40 bases,

but from reason that remain unknown, the hybridization yields dropped by about 20%. We therefore continue to work with the 30 bases swivels.

**Monomer disc concentrations:** Normally, the disc monomers concentrations in the mixture reaction were 10 nM. We tested hybridization at 40 nM monomers concentrations, and the results show 15% decreased yield. A higher order bands and a greater smearing appeared in the gel chromatogram (data not shown), indicating that high concentrations resulted in considerably higher aggregation, that in turn, reduced final yields. Although no fine tuning for concentration was conducted, several experiments conducted at 15 nM provide yields that were comparable to those obtained at 10 nM.

### 3.3.6 Synthesis of Gold Nanorods

We used gold nanorods to determine the upper disc orientation using a defocusing approach that uses red light (640 nm) scattered from the nanorod to detect the nanorod 3D orientation. The nanorod physical dimensions should be tuned to balance between two conflicting requirements: 1) good optical single to noise ratio, which can be achieved by high signal brightness that increased with the nanorod volume[144]. Additionally, the brightness is related to compliance between the illumination wavelength (640 nm diode laser) with the peak of the scattering coefficient spectrum that can be tuned by tuning the nanorods length to width ratio (aspect ratio). 2) preventing gold nanorods from interacting with the surroundings, which should be achieved by gold being smaller than the outer diameter of the disc (90 nm).

Initially, we used purchased nanorods (Nanopartz Inc, Colorado) however, due to inconsistency of the purchased nanorods and their tendency to aggregate during storing, I began bottom-up synthesis of gold nanorods according to published method [145]. The nanorods size were determined by software-based analysis (written by a lab coworker, Dr. Shapira Haggai, MATLAB) of TEM images (Figure 3.8A-C). This allowed systematic synthesis of different size and aspect ratios nanorods, followed by tests of the quality of the signal in the defocused optical setup (data not shown). These experiments revealed that gold nanorods of the length 80 nm and diameter of 40 nm are best matching our requirements [3]. The peak absorption of these nanorods is about 640 nm (Figure 3.8D),

and the 80 nm length is about the maximum rod length that does not bulge out of the upper disc.

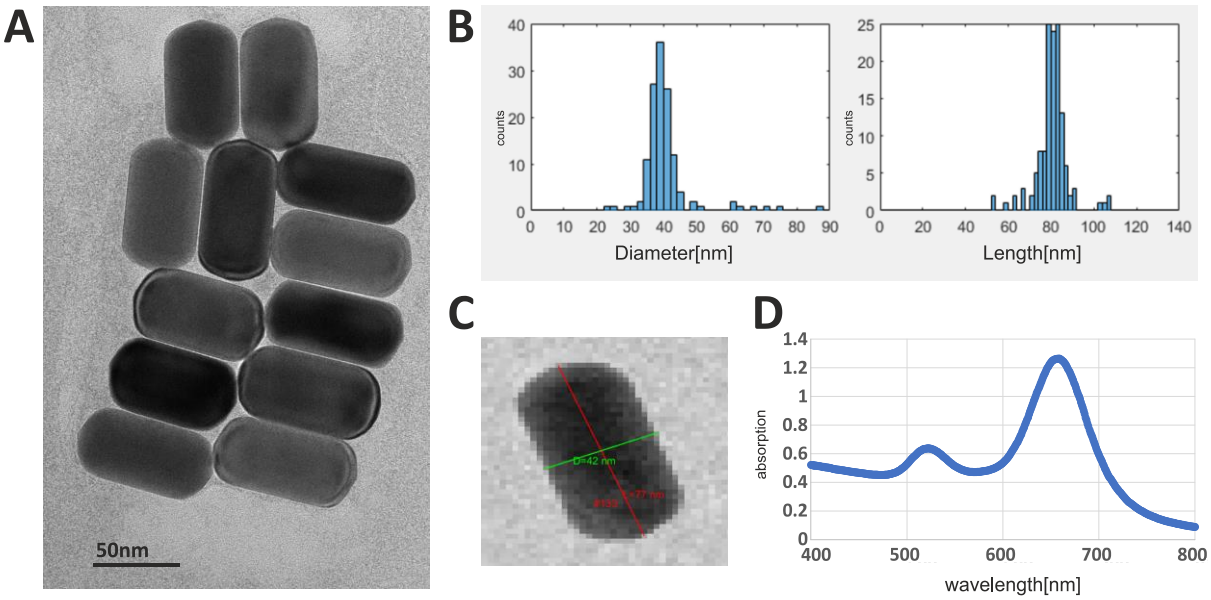


**Figure 3.8: Gold nanorod size analysis.** (A) An example of TEM picture for the optimal gold. (B) size distribution of the optimal gold for the rotor, $\bar{D} \cong 40nm$, $\bar{L} \cong 80nm$. (C) Long axis and short axis were found for each particle from the TEM images. (D) 40-80nm gold solution absorption spectrum.

### 3.3.7 Functionalization of Gold Nanorods

The gold nanorods were functionalized with thiolated ssDNA [146] using a salt-aging technique. Thiolated poly-T strands of length 21 were added to the nanorods, followed by titration of NaCl salt up to 1M concentration, which is added to minimize repulsion between DNA strands, boosting DNA attachment. Because salt can promote nanorods aggregation before they are properly covered with DNA, the salt is titrated gradually (Figure 3.9A) over 8 hours (12 hours for the entire procedure). To verify the success of the reaction, the NaCl concentration in the solution was raised to 2M. For proper DNA-gold reaction, the solution reddish color was maintained, disappearing of the color and formation of aggregates indicate improper covering of the nanorod. Further, the nanorods were examined using agarose gel electrophoresis. Properly covered negatively charged nanorods formed a clear band that successfully migrates in the gel (Figure 3.9C), while uncovered nanorods remained in the gel's well. Finally, TEM imaging of covered nanorod shows white color aura around the nanorods (Figure 3.9D), indicating successful poly-T attachment.

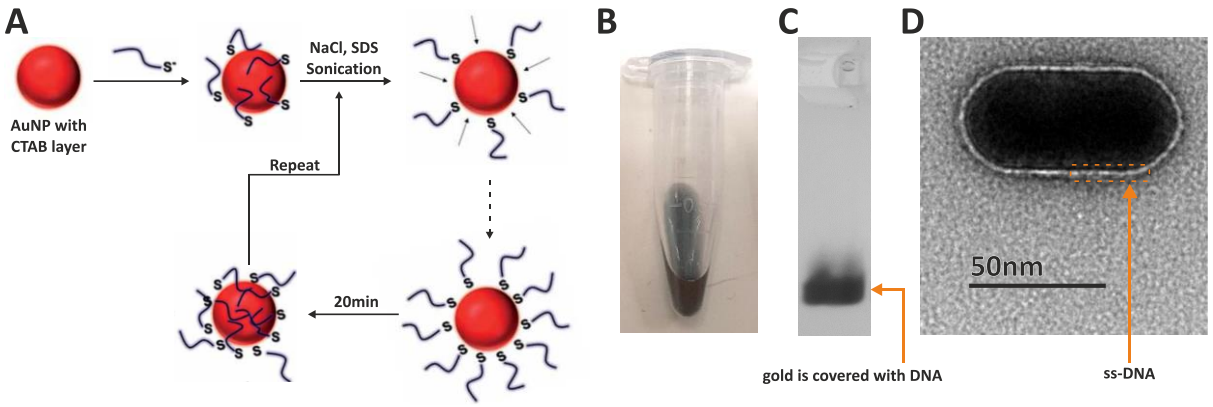


**Figure 3.9: Gold modification and verification.** (A) Typical salt ageing process schematics. (B) Solution of functionalized nanorods at 2M NaCl. (C) Agarose gel chromatogram of the functionalized nanorod, indicating negatively charged particles. (D) TEM image of a functionalized nanorod, with a cloud surrounding the nanorod, characteristic of a ss-DNA coverage.

### 3.3.8 Attachment of Gold Nanorods to the Disc Dimers

Attachment of the gold nanorods to the upper disc is taking place by hybridization of the poly$T_{21}$ nanorod-attached strands with 17 poly$A_{10}$ prepositioned (in the thermal annealing process) on top of the upper disc. Because of its size, a single nanorod may interact with more than a single disc. To avoid this problem, a 3-5x excess of nanorods were introduced. This reaction was followed by agarose gel purification of the entire motor, eliminating incomplete motors and excess gold nanorods (Figure 3.10B). TEM image of the complete rotor, extracted from gel, is shown in Figure 3.10C.

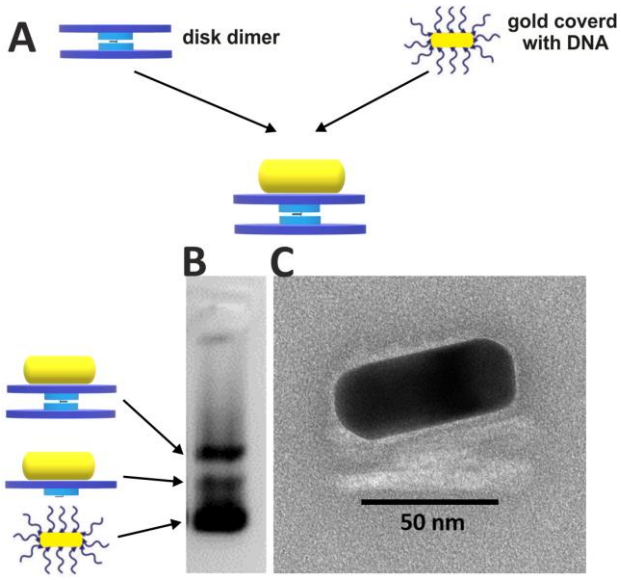


**Figure 3.10: Gold connection to origami.** (A) Schematics, (B) Gel shows the reaction products. (C) TEM image of the full rotor.

## 3.4 Monitoring Rotation via Defocused Light-Scattering Technique

To characterize the rotation of the rotary motors we have adapted and optimized an optical method that is based on scattering of polarized light from gold nanorods [3, 4, 135, 146], (large part of that was conducted by my collaborator, Dr. Shapira). This technique allows the three-dimensional nanorods orientations to be determined. A wide-field laser light beam (640 nm) scattered from 10-50 separate gold nanorods, were imaged by a EMCCD camera, yielding 10 to 50 separate time-dependent defocused shapes that report on nanorod orientations (Figure 3.11). The orientation of each nanorod was determined by comparing the defocused images to a pre-calculated table of thousands of theoretical images (a three-dimensional table with 144 different azimuthal angles, 20 different polar angles, and three different levels of defocusing) using a user-friendly MATLAB program developed by my colleague Dr. Shapira to perform real-time and post-acquisition analysis of motor rotation. The software performs automatic particle finding and tracking, calculates rotation time traces and conducts other important statistical analyses. The software runs on a GPU (CUDA, Nvidia) installed on the optical setup PC computer. The light scattered from the gold nanorods is typically ~5 orders of magnitude brighter than the fluorescence of typical organic fluorophores, and gold nanorods never blink or bleach [4]. The strong and stable flux of photons allows determination of the rotation of F1-ATPase with 1-5° azimuthal angle resolution at 10-μs temporal resolution [4], significantly higher resolutions than required for our rotary motors. The azimuthal angle time trace in Figure 3.11 (freely rotating gold nanorods attached to the surface) shows only 400 seconds (10-ms time resolution), but measurements can continue for days without any observed degradation in signal quality.

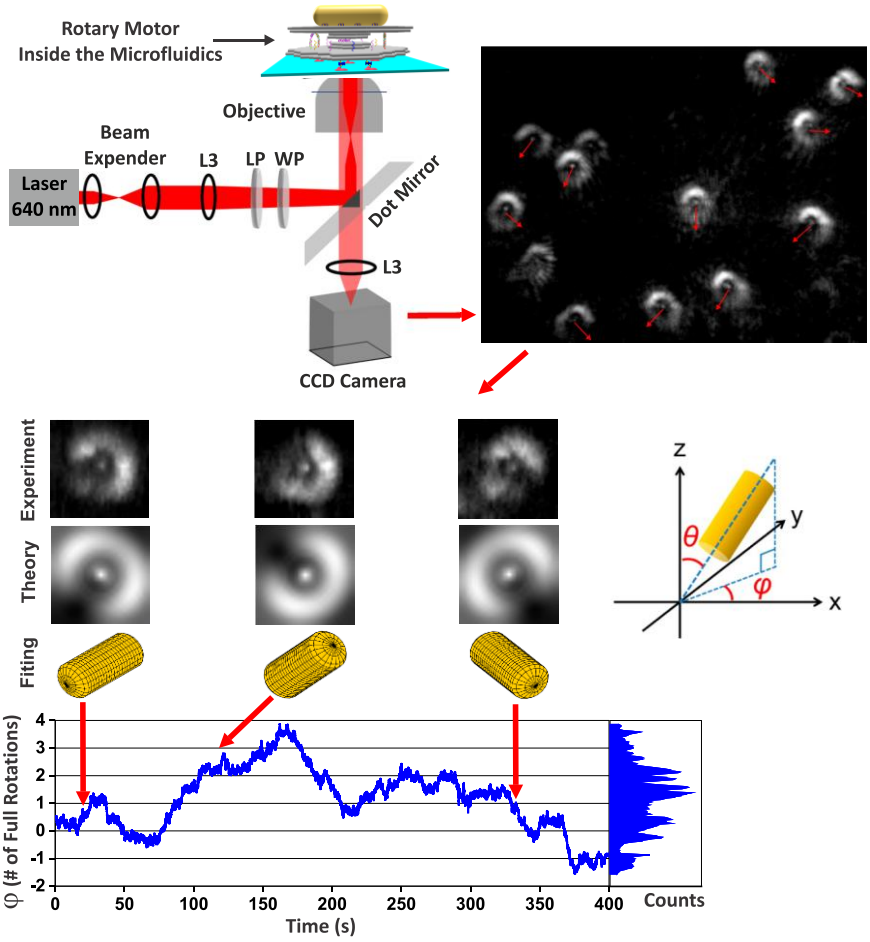


**Figure 3.11:** The gold nanorod monitored by the defocused light-scattering technique.

## 3.5 Externally Controlled Directional Rotation

To operate the rotary motor using the computer-controlled microfluidic device, a solution containing rotary motors coupled to nanorods was introduced into the microfluidics device's working chamber, allowing the motors to bind to the glass surface through biotin-avidin interactions. Under conditions of Brownian free rotation (swivel only), various motor behaviors were observed. Approximately 75% of the motors exhibited free rotation, while 25% displayed either semi-free rotation or complete immobility, that is when using a salt concentration of B102 (100 mM NaCl and 2 mM $MgCl_2$). Increasing the salt affected the fraction of motors in free rotation. For example, at 1000 mM NaCl (no magnesium), only 40% of the motors remained in free rotation mode. The angle distribution for the rotating rotors (those immobilized by fuel and freed by antifuel) often displayed non-uniform distribution. However, there were no major angle preferences, as the combined angle distribution was almost uniform (Figure 3.12A), indicating that the origami discs where 'smooth' enough and did not have significant unwanted, but specific, interactions.

Focusing on the rotors that responded to leg-foothold anchoring via 10 μM fuel, the immobilization rate showed varied results (Figure 3.12B). For instance, fuel-2 demonstrated a lifetime of 7 seconds for leg placing, approaching the rate observed for the linear bipedal walker with a 4 seconds lifetime [126], further supporting our conclusion that the origami discs do not significantly inhibit the reaction (although some reactions were somewhat slower, e.g., for fuel-1). Upon investigation, the slower reactions were mostly attributed to specific sequence issues rather than the corresponding foothold position within the rotor (data not shown). To accommodate these issues, the external operation timing was chosen to be typically of 10 minutes, although most reactions occurred much quicker.

Directional rotation was achieved using a bipedal walker operating under the FBAF mechanism. The process was Initiated by blocking the legs before adding the first two fuel molecules for the initial step to avoid trapped states. A full rotation, consisting of 12 consecutive steps, was successfully demonstrated (Figure 3.12D). Additionally, 75 steps were demonstrated (Figure 3.12C), including 5 recovery events, where all legs were lifted,

the swivel maintained the two discs together, and the motor recovered with the introduction of the next fuels.

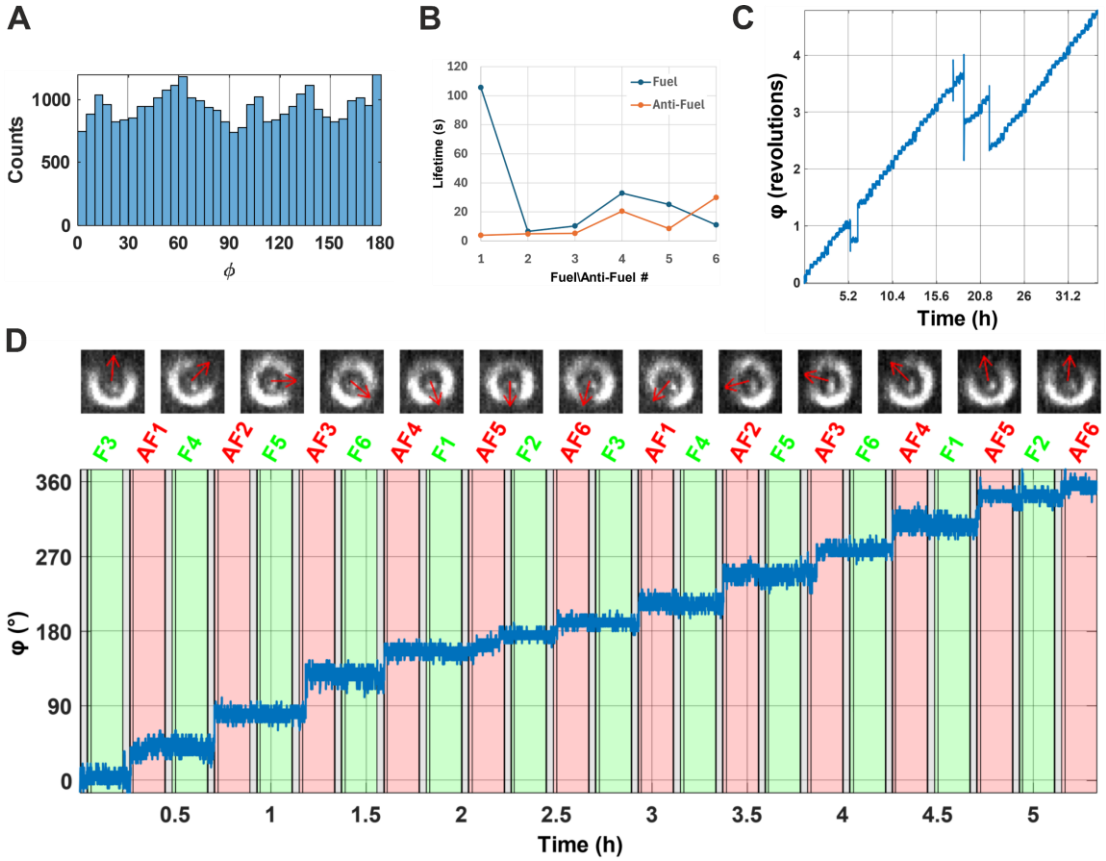


**Figure 3.12: Rotary motor behavior and directional rotation.** (A) Combined angle distributions relative to FH12 for motor that was responsive to fuels, the distributions from 54 motors collapsed to the limits of 180°. (B) First-order reaction lifetimes for each fuel and anti-fuel command. (C) Prolonged operation through recovery from dissociations from the track caused by chemical errors. (D) Twelve clockwise steps. Top: defocused images of the motor between each step. Bottom: Time trace of the rotation.

## 3.6 Summary of Aim-2

In this chapter, a robust and high-performance DNA origami rotary motor was developed, consisting of two origami discs and powered by two externally controlled bipedal walkers. The design focuses on enabling free rotation through a single-stranded swivel element, which allows the rotor to freely rotate without permanent dissociation, solving the problem of processivity. Key innovations include optimizing the design to avoid structural issues such as twisting, homo-dimerization, and aggregation, using advanced techniques like interlocked scaffolds, edge passivation, and iterative in silico simulations. The motor's rotational behavior is monitored through a defocused light-scattering technique, using gold nanorods attached to the upper disc to report on the motor's azimuthal angle with high resolution. I describe in details the extensive optimization of the motor's synthesis, including the preparation of the discs, the functionalization and attachment of gold nanorods, and the swivel hybridization process to ensure stable and effective operation. The rotor demonstrates directional rotation through up to 35 continuous steps, with the ability to recover from dissociations, showcasing its potential for future applications in DNA nanotechnology, particularly for the development of autonomous propulsion mechanisms as was conducted in Aim-3.

# Chapter 4: Autonomous Propulsion Mechanism

## 4.1 Motivation

To date, no synthetic autonomous molecular motor driven by chemical fuel, without the need for biological-enzymes, has not been capable of executing more than a single step[113]. The development of such a synthetic system that emulates the characteristics of biological motors is a highly sought-after goal in nanotechnology, with potential implications for biomedical applications and beyond. Achieving this complex objective necessitates an interdisciplinary approach that combines a broad range of tools and techniques. This not only requires access to existing knowledge but also fosters innovation, driving the discovery of novel tools and methods to extend and bridge the existing knowledge.

## 4.2 Previous Work

Green and colleagues [113] developed a pioneering bipedal autonomous DNA motor that represents a significant advancement toward achieving the goal I set for this research. Their motor (see Figure 4.1) operates on a single-stranded DNA (ssDNA) track composed of alternating domains, specifically a competition domain (marked green) and a binding domain (marked yellow). The motor itself is structured with two identical "feet" connected by a 16-base pair (bp) duplex, which forms the walker element. The feet are attached directly to the track at their 5’ ends through a flexible 4-thymine (4T) spacer. Each foot contains three distinct domains capable of binding to the track. These include (from the 5’ to the 3’ direction) a segment complementary to the track first ‘competition’ domain (called ‘foot heel’), followed by a segment that can bind the track ‘binding’ domain (called ‘foot arch’), and another segment complementary to the second competition domain (called ‘foot toe’).

The motor's coordination mechanism relies on its ability to bind to two consecutive foot-binding sites on the track. However, due to the track's configuration, only one foot can fully hybridize with the central competition domain at any given time. For a track oriented

from 5’ to 3’, the leading foot's toe and the trailing foot's heel compete to hybridize with the competition domain, which transiently exposes either the toe or the heel.

The motor's movement depends on the transient exposure of the toe and heel domains, which serve as toeholds for toehold-mediated strand displacement (TMSD). This process triggers the interaction and action of the DNA hairpin fuel. For movement along the track from 5’ to 3’, the fuel hairpin (H1) is designed to attach via its overhanging single strand to the exposed heel. This attachment leads to strand displacement between the fuel's stem and the loop domain within the foot, driving the lifting of the foot. An additional domain in the fuel's loop (shown in red), is now exposed, triggers fuel removal by the anti-fuel hairpin (H2), reactivating the foot and facilitating the reversibility of the mechanism. The anti-fuel hairpin, which is complementary to the fuel but lacks the overhang, displaces the fuel as waste via internal toehold-mediated strand displacement.

The two fuels preferentially interact with the trailing foot (left side foot) and lift it, providing directionality and internal synchronization. While either foot can be lifted thermodynamically due to their identical structure, the back foot is lifted more rapidly because of fuel directionality, kinetically favoring lifting the left foot. The directionality of the walker depends on whether the fuel (H1) interacts first with the heel or the toe segments (walking to the right, or to the left, respectively).

Once the foot is reactivated it can rebind the track in various ways. It may rebind in the same position, leading to an idle step, or in front of the stationary foot, resulting in a forward step.

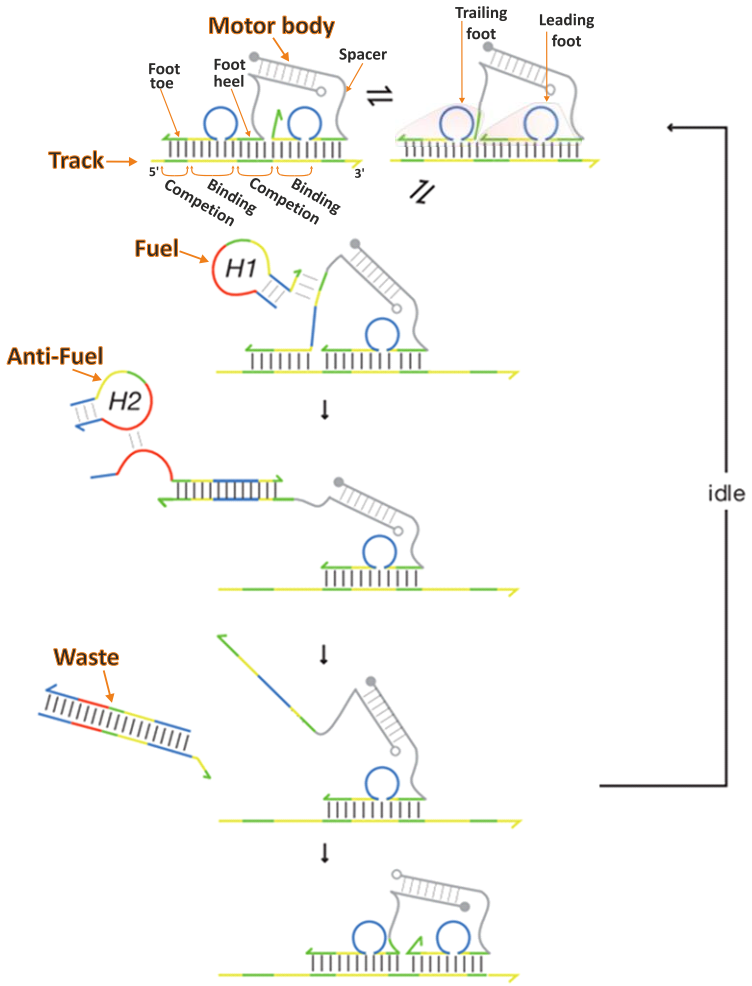


**Figure 4.1:** Hybridization-driven autonomous bipedal DNA walker, adapted from Green et al. [113].

In Green's initial work [113], only one forward step was demonstrated, as the track was too short to execute two or more steps. However, Subsequent studies [130, 147] reveals that a longer track of such design would be too structurally flexible, allowing walker-track interaction in the wrong positions that may result in motor stalling.

To address this issue, two solutions were attempted. The first, proposed by Shelley Wickham [147], involved using a “piece-wise” DNA origami track (Figure 4.2A). However, this method proved largely unusable for the walker, as the track assembly was of poor quality when prepared in a single pot annealing process due to a "super-stoichiometry effect". Additionally, the discontinuous nature of such tracks disrupted the fundamental mechanism of the motor, necessitating further design and try and error efforts [147].

In a second approach, Natalie Haley [130] utilized tightrope origami structures to stretch a track made of a long single-stranded DNA (Figure 4.2B). In addition to applying tension,

a mechanism modification was introduced, which included non-identical feet with two sets of fuel to reduce overstepping, and an addressable section at the start of the track that resulted in a successful initiation was demonstrated. However, the motor failed to exhibit experimentally significant forward movement along the track.

Both Wickham and Haley focused on an alternative fuel type based on Green's second work [148], which relies on a similar mechanism to lift the foot from the track (Figure 4.2C). In these designs, instead of using anti-fuel for fuel removal, a nicking enzyme cleaves the fuel, leaving the foot single-stranded and ready to rebind to the track, with a mismatch preventing track cleavage.

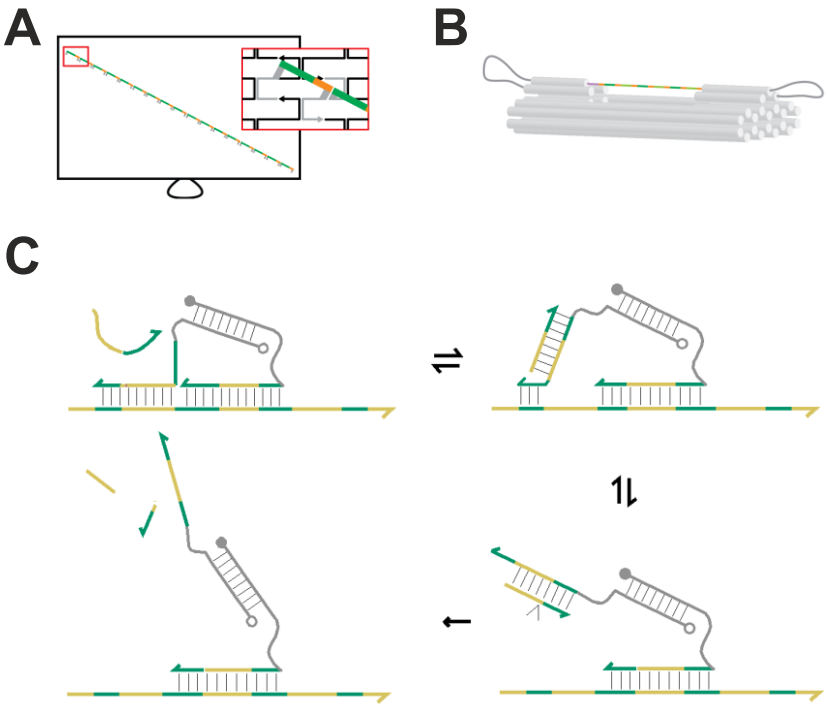


**Figure 4.2: Modifications for the autonomous bipedal motor.** (A) Piece-wise track on a 2D origami tile [147]. (B) Tightrope track on a 3D origami structure [130]. (C) Enzyme-driven variants of an autonomous bipedal DNA walker [148].

## 4.3 Design of the Mechanism

Previous works, primarily from the Turberfield group [148, 147, 130, 113], introduced a shared track and coordination mechanism, with the use of two fuels source, representing a significant advancement in the understanding and development of autonomous, directional, non-burnt-bridge molecular motors. However, while this innovation marked a significant breakthrough, it also exhibited limitations, particularly in its reliance on a continuous single-stranded DNA (ssDNA) track. This single stranded track, although

necessary for the foots coordination mechanism, posed a significant synthesis challenge.

In the previous chapter, I presented a rotor-based structure that offers a rigid base for the track and allows flexibility in the track design. The rotary discs design allows the incorporation of the gold nanorod that provides high-resolution tracking of the rotor position, and the rotor includes an error-correction mechanism significantly easing development and optimization of the rotor. In my opinion, our rotary structure provides a much more reliable platform on which we can develop autonomous walkers by addressing the shortcomings in the propulsion mechanism of previous approaches.

I believe that the propulsion mechanism proposed by Wickham could, in principle, be implemented in our rotary motor. For example, the track may be assembled post-annealing on the origami in a piecewise approach using block-unblocking method (based on the FBAF strategy and the microfluidics, see Section 1.5.2). However, issues related to the track internal junctions may hinder correct operation and it will not be easy to assemble a circular track because of differences in distances between consecutive footholds.

For these reasons, I have opted not to directly implement the exact mechanism from Turberfield's group works. Instead, the design developed in this thesis incorporates elements from it, such as the use of hairpins as fuel, while introducing key modifications. Specifically, I employed a different coordination mechanism that enables the walker to move along a track made of regular elongated footholds. This approach allows for the independent addressability of each foothold, and the design provides the capability to start, stop, and reverse direction using toehold-mediated strand displacement (TMSD) commands, independent of the fuel itself. These improvements address the limitations observed in previous designs, offering a more versatile and controllable molecular motor.

In my approach, special attention was given to rotor performance, defined as the product of motor forward speed (reaction rates) and stepping yields, that is, fast reaction with minimum leakage.

### 4.3.1 Design Guidelines

The goal of this artificial DNA motor design is to achieve the following intended features: chemically fueled, reversible, error-correcting capability, no usage of biological enzymes, and high performance. This motor is expected to operate autonomously while allowing external commands to control its start/stop functions or reverse its direction, independently of the fuel source.

**Key Design Principles:**

1. DNA hybridization as an energy source: The energy for motor operation is derived from DNA hybridization. This can be achieved using metastable hairpins inspired by the work of the Turberfield group.
2. Track rigidity: To ensure effective walking, the rigidity of the track must be significantly greater than that of the walker. This can be accomplished by using a DNA origami structure, a principle highlighted in Wang, Z. work [149].
3. Repetitive foothold sites: A track based on repetitive footholds, each designed to incorporated into the origami at a selected site, providing flexible and easy design.
4. Processivity through continuous contact: The motor should maintain continuous contact with the track to ensure processivity. This can be achieved via coordinated hand-over-hand bipedal walker mechanism.
5. Achieving directionality: Directionality requires breaking the symmetry, which in our design, can be geometrically accomplished by the origami structure, not the walker or the track which are symmetric. A strand placed in the origami behind the walker catalyzes the lifting of the rear leg.
6. Simplicity in design: While many design variations can accommodate the above concepts, simplicity is prioritized. If a simpler design meets (most of) the intended functionality, it is preferred.

Figure 4.3 illustrates a preliminary conceptual structure based on the above key design principles.

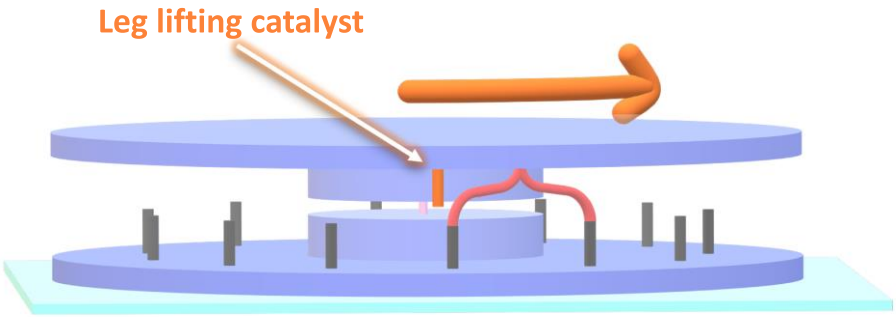


**Figure 4.3: Preliminary conceptual structure of the artificial DNA autonomous motor.** The bottom disc, acting as the stator, is fixed in place. Elongated footholds, represented in black, extend from the bottom disc and share the same sequence. A bipedal walker, shown in red, is attached to the upper segment. The strand positioned relative to the walker, marked in orange, acts as a catalyst for leg lifting. This catalyst breaks the symmetry, generating directional movement opposite to its position relative to the walker.

### 4.3.2 Basic Mechanism

Figure 4.4 shows the schematic of the basic operation of the proposed propulsion mechanism. The fuel hairpin (mark in green) transiently binds to the catalyst strand (mark in orange), which, in turn, transiently interact with the extension of the rear leg (mark in red, Figure 4.4.i and ii). The fuel hairpin initiates a strand displacement reaction, removing part of the leg from the foothold, and the remaining leg-foothold duplex dissociate thermally (Figure 4.4.ii and iii). The opening of the fuel hairpin loop accelerates interaction with the complementary anti-fuel hairpin, and together with the thermal dissociation of the fuel from the catalyst, removes the fuel hairpin from the system and generating fuel/anti-fuel waste (Figure 4.4.iv). Once these reactions are complete, the leg is free to react either with the same footholds, returning the rotor to the previous state, or, interact with the forward foothold, moving the rotor forward (Figure 4.4.i or v, respectively). In addition, we assume that there is some probability that once the trailing leg is removed from the trailing foothold, the fuel hairpin will be attracted to the leading foothold, and together with the catalyst that now can more easily reached and detach the leading leg-foothold complex, resulting in complete detachment and operational error (Figure 4.4.vi). In such cases, the rotor will be able to rotate freely, however, the swivel element will prevent rotor complete dissociation, the rotor will eventually rebind

somewhere along the track and continue operation despite the temporary error, as was the case for the nonautonomous rotor in Aim-2.

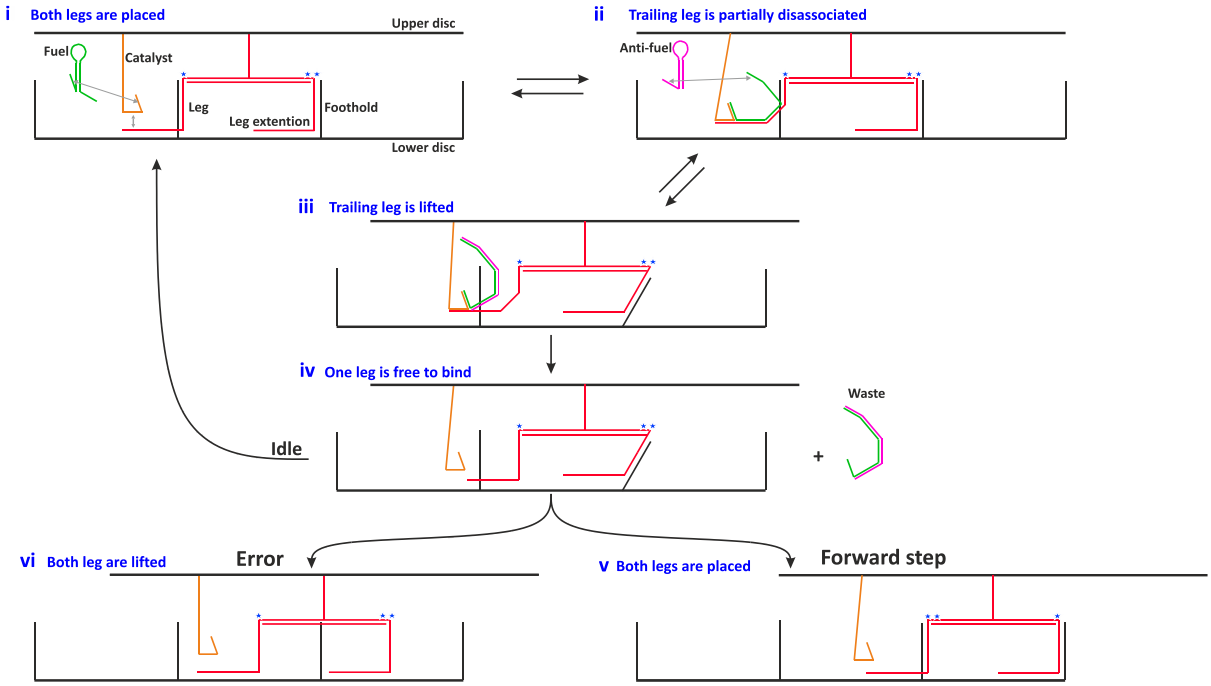


**Figure 4.4: Motor autonomous propulsion mechanism basics.** (i) Two identical legs are bound to adjacent foothold-binding sites extended from the lower DNA origami disc. The catalyst transiently binds to the fuel and to the leg extension, enabling the fuel hairpin to open, which leads to the dissociation of the leg-foothold portion via loop domain interaction, as shown in (ii). The fuel is then displaced by the anti-fuel hairpin (pink) to allow the foot to rebind to the track (iii). The leg can either reconnect at the same site or advance to the next foothold (v), providing directionality. However, if too much time elapses, the catalyst can trigger the release of the other leg, resulting in a lost-position error state (vi). One star and two blue stars are added for illustration purposes to differentiate between the two legs

### 4.3.3 Main Rationale of the Autonomous Operational Mechanism

I will now explain and discuss the basic rationale of the Autonomous Operational Mechanism.

1. Metastable hairpin pair as fuel: The fuel must be a single strand that binds either to the leg or the foothold to enable their separation via a toehold-mediated strand displacement mechanism. However, this becomes problematic if both the footholds and the legs exist as single strands when unbound, as they may interact with the fuel and anti-fuel in an uncontrolled manner, independent of the walking process. To prevent such interactions, their binding sites must be hidden from each other. The easiest way to achieve this requirement is hiding the fuels and anti-fuels binding sites in hairpins loops. This concept, previously demonstrated by the Turberfield group [112], ensures controlled interactions and prevents the unwanted spontaneous interaction of the fuel with the anti-fuel strands.
2. Usage of fuel strands to release the legs from the footholds: In principle, single-stranded fuels (whether placed in a loop or not) that are used for leg lifting can be implemented in two ways. First, the seemingly more direct strategy involves attaching the fuel to the foothold. In this case, until the anti-fuel activates, the leg only has one option—to connect to the foothold in the forward position, enhancing directional bias, as was demonstrated by Liu et al. [150], but using a biological enzyme. Without an enzyme, this strategy becomes too complicated and was not tested here. The second strategy, chosen here for reason of simplicity, involves connecting the fuel to the leg to facilitate leg lifting.
3. Coupling rear leg lifting with fuel turnover: The catalyst should act as an associative toehold, ensuring directionality and efficiency. The catalyst is located on the upper disc in a location that remains behind the walker and always closer to the trailing foothold-leg complex regardless of motor state, breaking the symmetry and providing directionality. The catalyst associates the fuel with the leg, allowing the fuel to be consumed only for the purpose of lifting the leg while remaining largely protected from interaction with the anti-fuel when free in the solution. The detailed design

needs to ensure that the catalyst does not reach the front leg while both legs are placed, maintaining the system's directional bias.

4. Toehold for anti-fuel and fuel length: In the original hairpin-based motor [113], the toehold that triggers anti-fuel activation was internal, located within the hairpin loop, and could only be activated when the loops open, a design that makes sense when the proper sequence of events take place. However, in our assessment, such an approach would not be optimal for our rotor. This is because it would require an approximately 22-base-long loop domain in the anti-fuel, which could, in principle, interact with the free foothold, partially or permanently blocking it (Figure 4.5A). Additionally, an equivalent interaction could occur between the fuel's loop and an unbound leg. To our knowledge, no studies have directly measured loop interaction with a single strand as a function of loop size. Therefore, we opted for a safer approach, limiting the loop length to between 6 and 9 bases (Figure 4.5B) which can be achieved by **making the toehold external** (sequence 'a'), and **utilizing partial fuel length** (sequence 'b1', a concept inspired by FBAF mechanism [126]).

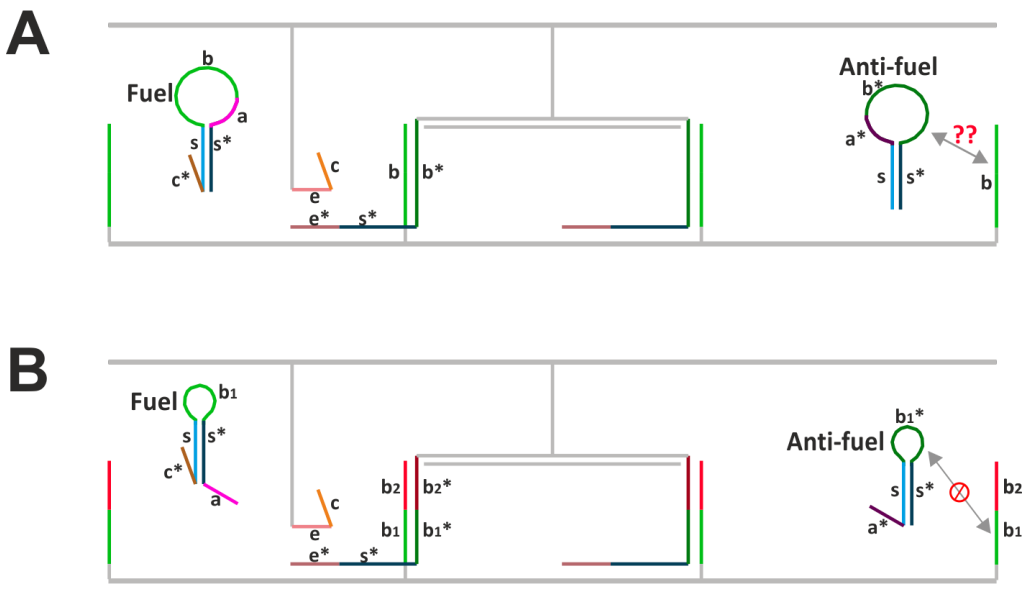


**Figure 4.5: Metastable fuel modification.** (A) The structure, if metastable hairpins implemented, for rotor topologies. Results in two interactions that can hinder functionality. First, the anti-fuel's loop can interact with the free foothold, potentially leading to permanent or partial blocking of the track. Similarly, the second interaction occurs when the fuel's loop interacts with the free leg. (B) Modified fuel system, with the toehold for the anti-fuel made external and the fuel section shortened by about half, which significantly decreases these interactions.

### 4.3.4 Introduction to the Main Challenges for the Mechanism's Performance

Several challenges must be addressed to ensure our mechanism operates correctly and efficiently. These challenges will be explored in detail in the following sections. Three key issues stand out:

1. A primary consideration is to avoid slow reactions, specifically, slow fuel-catalyst-leg initial interaction, which may slow the overall motor operation rate.
2. The second challenge involves achieving a high operational rate while maintaining a high stepping yield. Stepping yield is defined as the ratio between successful forward steps and error state probabilities. To maximize this ratio, it is crucial to ensure that the leg placing rate is significantly faster than the leg lifting rate.
3. Many leakage reactions can occur with varying degrees of probabilities and impact on the intended functionality, particularly fuel auto-depletion due to the presence of an external toehold. Additionally, uncontrolled leg lifting can disrupt coordinated walking.

To address these challenges, a comprehensive kinetic model is developed to fine-tune the propulsion mechanism by tuning the rates of the various reactions involved**,** ensuring motor performance.

### 4.3.5 Full Autonomous Model

The snapshots illustrated in Figure 4.4 represent some of the key states of the system, but numerous additional reaction pathways can also take place. For example, the sequence of transient reactions can vary, or the anti-fuel might bind to the fuel before the fuel interacts with the catalyst, among other possibilities.

To test and optimize our proposed model theoretically, it is necessary to account for all possible states and pathways, and to derive the expected kinetic equations over time. However, capturing the truly full dynamics is highly complex, particularly given that certain reaction rates depend on the position of the upper disc relative to the bottom disc. Therefore, several assumptions have been made to simplify the model, as outlined below.

**Model Assumptions:**

1. We assume that the fuel/anti-fuel complex does not react with the system, either because it exists in low concentrations or washed out by the microfluidics.
2. We assumed that, because of structural constraints, unbounded legs could not reach non-adjacent foothold and interact with it.
3. Reactions resulting from end fraying or other similar types of leakage are not considered in this model.
4. The catalyst cannot trigger leading-leg lifting when both legs of the walker are placed.
5. The movement of the upper disc is simplified. It cannot move when both legs are placed. When one leg is lifted, the disc can move to a centered position over the placed leg. If both legs are lifted, the disc moves to a free position.

These assumptions are further supported in the discussion below.

Note: The technical model was designed to simulate a single step, incorporating a cutoff mechanism. States where the front leg is placed forward are funneled into an unreactive, successful step state (labeled S14). Conversely, states where both legs are disconnected are directed into an unreactive, lost position state (labeled S37).

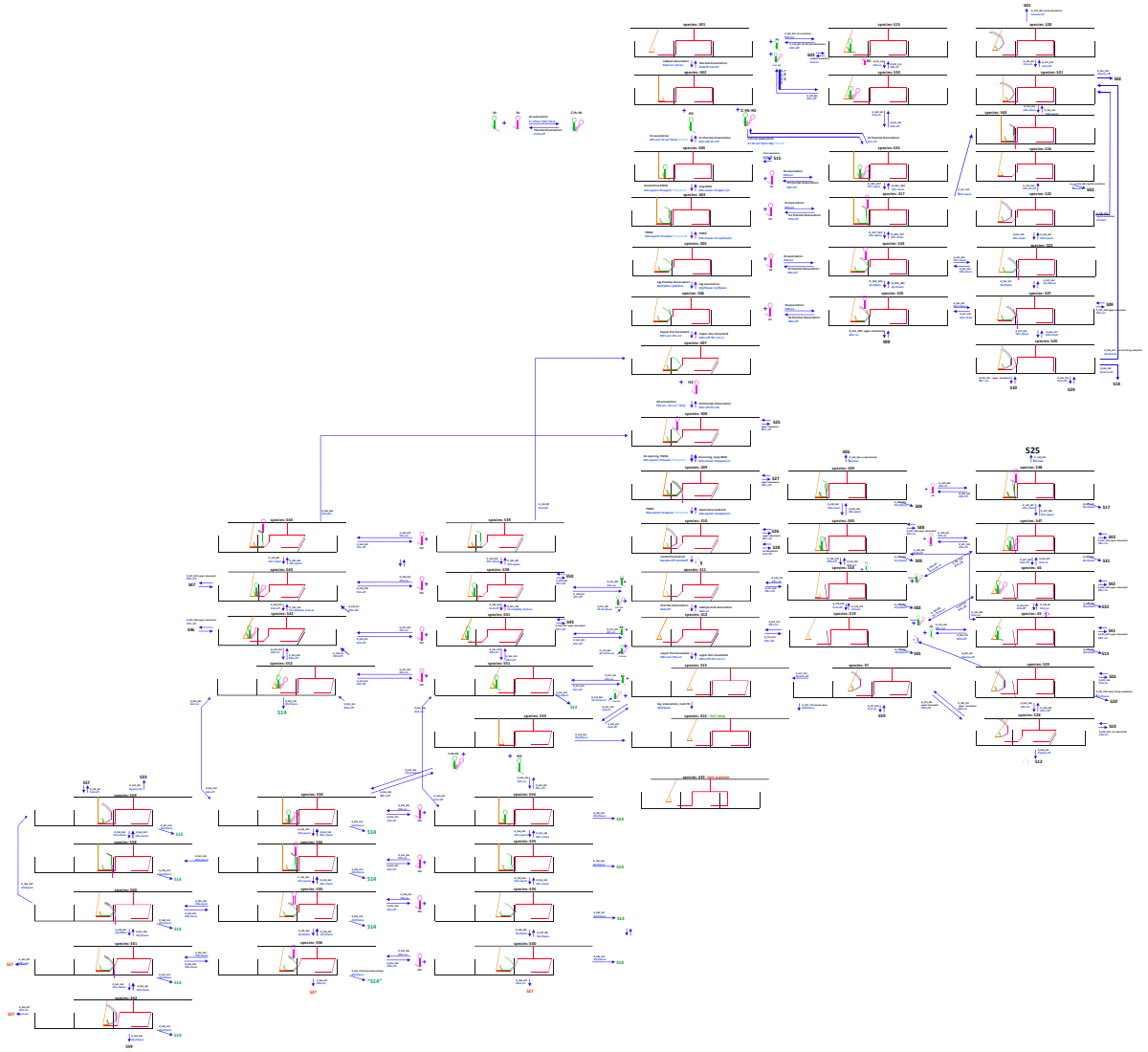

**Figure 4.6: Schematic representation of the model.** illustrating all pathways composed of different reaction sequences that lead to one of two outcomes: either a forward step (productive state) or a lost position (error state). Readers may zoom in for details. **Note: To clearly see the model details, please zoom in.**

### Model Dynamics and Pathways

Figure 4.6 show all the possible states and transitions. This model is essentially similar to the simple model shown in Figure 4.4, but includes all possible paths and sideway states. Detailed description of these reactions and the corresponding transitions parameters are provided in Section 4.5.1 and Appendix C.4. Ultimately, all pathways should converge into one of two outcomes: either a forward (productive) state or an error state. Given our reasonable assumptions, this model offers a balance between accuracy and computational feasibility, allowing for a manageable analysis of the system's dynamics without sacrificing essential details.

## 4.4 Design Optimizations

The design optimization process included two complementary tasks. In one task, I simulate the theoretical model presented in Figure 4.6 to test the influence of various parameters on motor performance. The second task involves addressing leakage pathways, which were excluded from the theoretical model for two reasons: to reduce the model's complexity, and, because leakage reactions are hard to parametrize (typically not well discussed in the literature). Accordingly, minimization of leakage reactions was relied on estimates based on the principle of reducing mutual availability [116].

These two optimization efforts are essential for achieving correct motor operation and high performance. However, addressing these two tasks at the same time can be challenging, as changes in one can influence the other. To simplify this complexity, the chosen optimization methods aim to limit cross-effects between the two tasks and within the same task, between different reactions. Nevertheless, this approach was not always feasible due to the inherent interdependencies between the pathways.

This section will first provide an overview of the leakage pathways, and the solutions implemented to address the more critical ones, followed by discussion of parameters optimization and kinetic simulation.

### 4.1.1 Leakage Pathways Overview

Although double-stranded segments and hairpin loop domains are usually assumed not to be able to react with invading strands, in practice, however, they may react due to edge fraying or loop exposure (more so for large loops). Accordingly, various types of leakage can occur within our propulsion system, each with different magnitudes and implications.

**One type of leakage** can occur when the anti-fuel loop interacts with footholds regardless of the position of the walker (see Figure 4.7A), rendering the footholds unavailable for proper interaction with the legs. This may be a critical issue, however it was minimized by limiting the hairpin loop sizes to a maximum of 9 bases.

**A second type of leakage** involves the fuel hairpin, which can open and block a free leg via three potential interaction pathways (Figure 4.7B). The first pathway, involved interaction of the loop with a free leg, was minimized by keeping the loop size small, as explained earlier. The second source of interaction comes from stem fraying at both ends and interacting with leg extension. Here, the last two bases at both edges of the stem, were designed to be G/C pairs, a design that according to mutual availability estimation, is supposed to significantly reduce this unwanted effect. Fortunately, however, unwanted effect cannot permanently halt the walker's movement, as the anti-fuel activates and displaces the fuel from the system, returning it to normal mode.

**A third type of leakage**, unrelated to the walker itself, is when the fuel reacts with the anti-fuel (Figure 4.7C), resulting in inefficient fuel consumption. Although this doesn't directly affect the walker's operation, it may necessitate a refresh supply of the fuel and anti-fuel strands. While metastable hairpins may be stable enough for our goals [112], the adjustment made to externalize the toehold significantly increased the leakage rate. This aspect is discussed in further detail in Section 4.4.2.

**Another potential leakage** occurs when the fuel interacts with a placed leg without the involvement of the catalyst (Figure 4.7D), leading to uncontrolled leg lifting. This situation may result in two legs being lifted simultaneously defined as operational error. This issue is addressed further in Section 4.4.3.

By identifying and addressing these leakages, the walker's efficiency and control were improved. Importantly, minimizing leakages is essential for the credibility of the kinetic model, as it initially assumed no leakage of the types mentioned above.

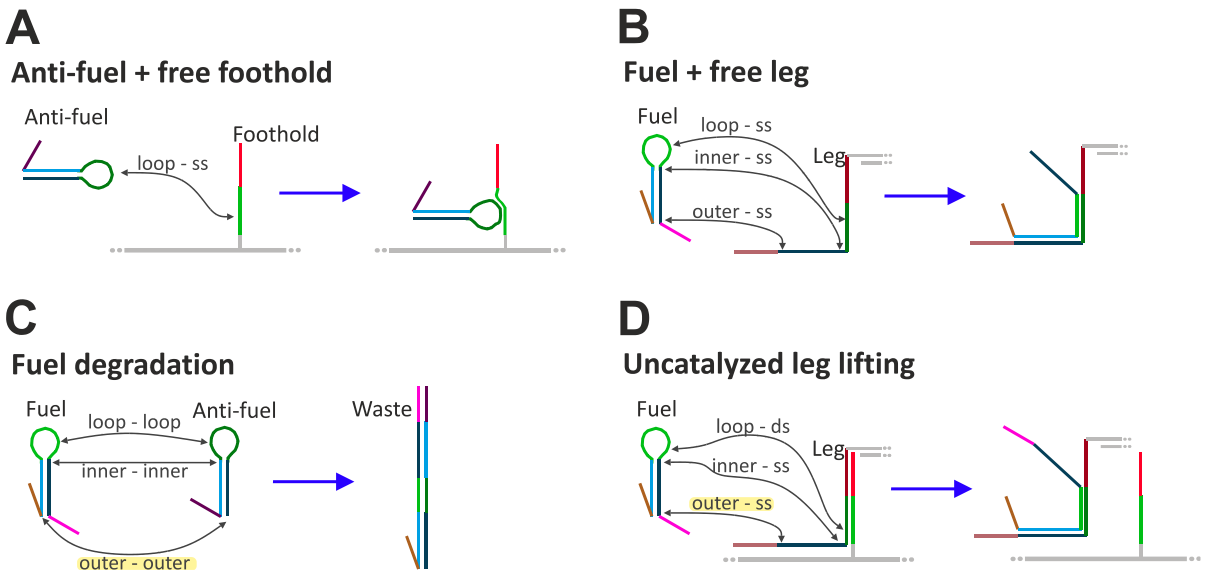


**Figure 4.7: Overview of leakage pathways.** Multiple leakage sources are present, all indicated by gray arrows, representing various interactions with differing levels of impact. The critical interactions, highlighted in yellow, have a significant effect on system behavior. (A) The anti-fuel's loop can interact with the complementary sequence in the foothold, potentially resulting in a semi-blocked foothold. (B) The fuel can interact with free footholds, causing delays or improper placement. (C) Fuel and anti-fuel may degrade independently of the walker, which requires correction as external toehold design amplify this leakage. (D) Fuel can activate without the catalyst, leading to uncontrolled leg lifting, which must be addressed to avoid an error state where both legs are lifted simultaneously.

### 4.4.2 Fuel Degradation

In earlier work by Green et al.[112], the spontaneous decay of the fuel complex was low, with half-life of about 6 hours (for loop=21nt, stem= 16nt), see Figure 4.8A. This indicates that leakage due to loop-loop (kissing) interactions and stem fraying was minimal and met our requirements.

However, repositioning the toehold to an external location (Figure 4.5B) would accelerate fuel-antifuel leakage due to spatial proximity. Data from Dabby NL thesis [151](Figure 4.8B) indicates a half-life of 26 minutes for slightly different reaction (overhangs was 16nt). To overcome this limitation, it was necessary to reduce the mutual availability. This was achieved by effectively implementing a clamp, where the first two bases on one side of the anti-fuel stem were mutated, and on the other side, they were removed (see Figure 4.8C).

As a result, 2-nt spacer is located between toehold and the branch migration domain facilitates the opening of the anti-fuel loop via remote toehold-mediated displacement reaction (Figure 4.8C). The kinetics of remote strand displacement with such a spacer length have not been previously measured to the best of our knowledge. Here, we estimate that the strand displacement rate would be approximately five times slower than without the spacer, based on measurements of similar systems with a one-side spacer remote toehold [152].

Despite the slower kinetics, this modification significantly reduces leakage. Based on estimates of mutual availability and fraying probabilities the leakage reaction is predicted to drop to around 3%. If this estimation holds, the leakage rate would be reduced by approximately 30 times, resulting in a fuel half-life of around 13 hours. The main reaction kinetics are slightly affected, but this slowdown is manageable and can be worked around through simulation-based optimization of other parameters.

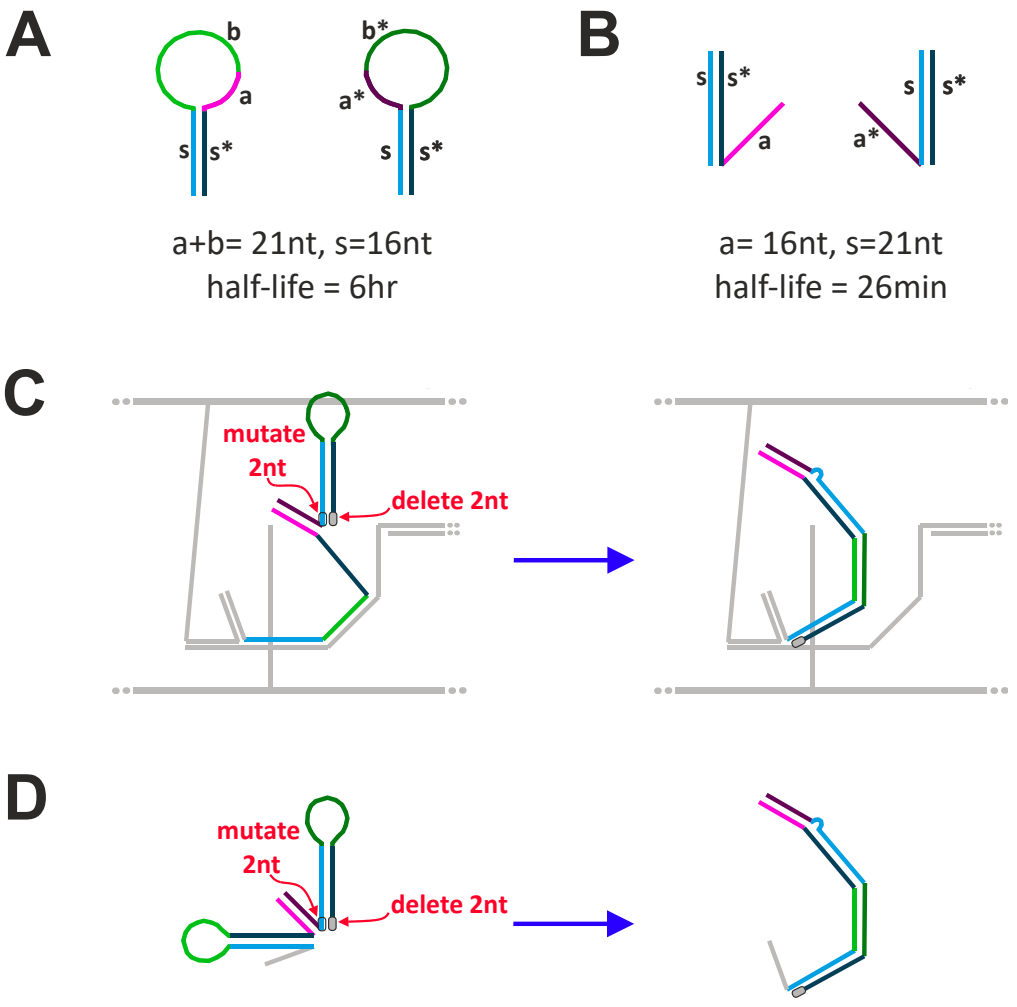

**Figure 4.8: Design for reducing fuel degradation.** (A) Metastable fuel hairpins degrade over several hours when they have a long stem, such as 16 nt (adapted from Green et al [112]. (B) Adding complementary overhang segments increases the decay rate to the range of tens of minutes (adapted from Dabby NL thesis [151]). (C) In the intended reaction, the anti-fuel displaces the fuel after activation with the leg. The modification, shown in red, makes the toehold slightly remote, slightly reducing the kinetics. (D) Leakage reaction involving the degradation of the fuel hairpin, unrelated to the walker. The modification, shown in red, slows the decay by approximately 30 times, extending the half-life to 13 hours.

### 4.4.3 Uncatalyzed Leg Lifting

In principle, there are three primary sources of uncatalyzed leg lifting (Figure 4.7D). The first source is related to the interaction between the loop of the fuel and the fraying end of the placed leg. This interaction is expected to have minimal impact due to the constrained nature of the loop. Additionally, the design includes guanine/cytosine (G/C) nucleotides at the last two bases, which further reduces fraying at this location.

The remaining two sources of leakage arise from the fraying of the fuel's stem at both edges. While the stem's edges are also designed with G/C pairs to minimize instability, additional attention must be given, especially to the outer fraying, as the loop structure stabilizes the inner fraying (as was confirmed through NUPACK tests, data not shown).

The overall leakage rate, referring to the rate of unintentional leg lifting, depends on the concentration of the fuel. For typical concentrations of around 10 μM, mutual availability estimates suggest that the half-life of the leakage process is approximately 1 hour. Although this rate is relatively slow, it is not ideal, as multiple uncontrolled leg-lifting events could occur during several hours of the intended motor operation. This could result in inconsistent walking behavior, including the possibility of both legs lifting simultaneously, leading to an error state.

To mitigate this effect, the primary source of leakage—outer stem fraying with extended leg, see Figure 4.9A—can be addressed using a leakage suppression technique developed by Yan S.A. et al. [153]. This method, known as 'inter-domain bridging,' is applicable in associative toehold-mediated strand displacement. It involves moving 1 or 2 bases from the invader (in this case, the extended leg) to the associated toehold (here, the catalyst), reducing strands mutual availability in the leakage pathway (Figure 4.9B). Based on mutual availability estimation, this technique is expected to reduce leakage by

a factor of 7 when 1 base is shifted to the catalyst, and by a factor of 30 when 2 bases are shifted.

However, this approach reduced the forward kinetics in two key aspects. The first aspect is that the population attempting fuel opening is halved due to the completion of the 1- or 2-base reaction before the hairpin opening can proceed (Appendix C.4, Figure C.1). The second aspect is that the thermal dissociation rate of the fuel hairpin from the catalyst becomes distinct from that of the waste molecule. When the fuel dissociates, it does so through two potential states: one where the 1- or 2-base reaction has not yet occurred, and the other after it has occurred (Appendix C.4, Figure C.2).

Given these considerations, I have decided to incorporate at least 1 base of inter-domain bridging into the system, as it reduces the probability of a single event of uncontrolled leg lifting to approximately half every 7 hours, which is satisfactory for the intended duration of operation. The decision to implement a 2-base inter-domain bridging approach is more complex and non-trivial. Therefore, both 1-base and 2-bases inter-domain bridging were included in the simulations, with the results and final decision presented in Section 4.5.4.

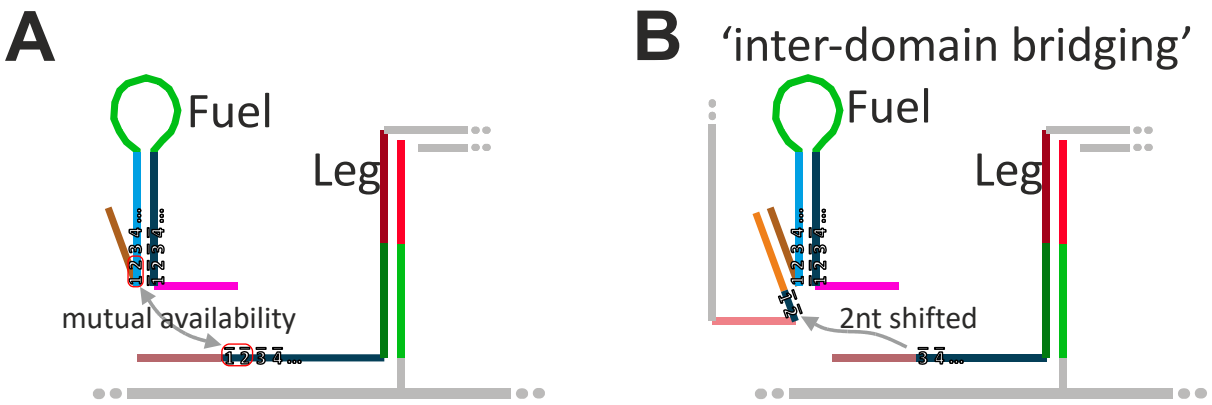


**Figure 4.9: Uncatalyzed leg lifting treatment.** (A) The main source of leakage, indicated by the arrow, arises from mutual availability caused by fraying at the stem edge. (B) The chosen solution involves moving 1–2 nucleotides (nt) from the leg extension to the catalyst. This adjustment breaks the mutual availability in the absence of the catalyst, thus suppressing leakage.

### 4.4.4 Main Pathways

In the kinetics model the pathways are represented by a set of differential equations, each corresponding to a specific chemical reaction within the model. The equations incorporate reaction rate constants and states population sizes (fractions of 1). The simulation starts with all motors populating the initial state where both legs are placed

on corresponding footholds, and states population propagate over time according to the given rates. The simulation reveals essential kinetic rates, including forward stepping rate and error rate.

To optimize the outcomes of these simulations, certain parameters can be adjusted. The first group of parameters are those that can be easily implemented experimentally. For example, the concentration of hairpins can be easily varied in the experiment, providing a straightforward method to influence the system's kinetics. Additionally, thermal dissociation rates can be tuned—albeit to a lesser extent—by altering the number of bases participating in each interaction of the various system elements (Figure 4.10). By allowing these parameters to vary within defined boundaries in optimization simulations, it was possible to identify parameters values that results in the most favorable kinetics. For detailed parameter ranges, refer to Appendix C.4.

The second group of adjustable parameters relates to the strand displacement rates. These rates can be modified by introducing or eliminating mismatches within the DNA strands. Adjusting the strand displacement rate offers a powerful means to tune the kinetics but requires careful consideration due to the intricacies involved. In the following section, the decisions made regarding the options for these parameters will be discussed, along with the implications for the system's performance.

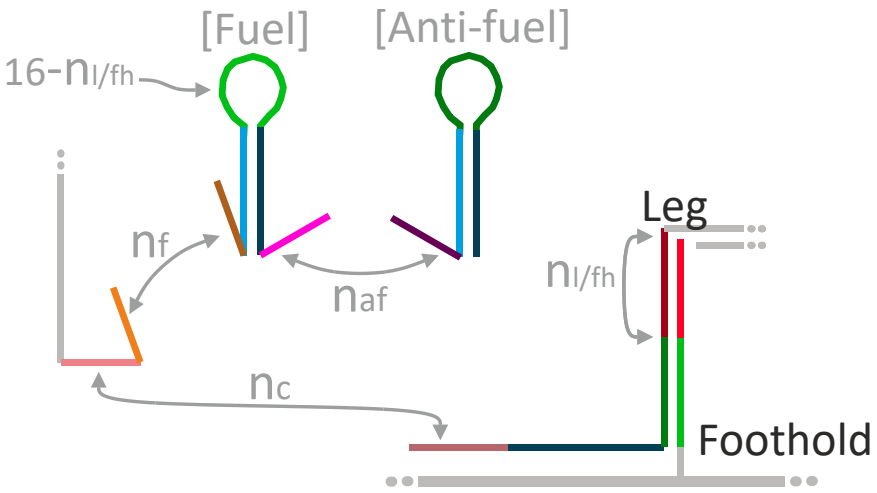


**Figure 4.10: Easily adjustable parameters.** The concentration of both hairpins can be set to any value by external control, independent of other aspects. Additionally, there are four different segments that can be adjusted, $\mathbf{n_c}$: catalyst–extended leg, $\mathbf{n_f}$: fuel–catalyst, $\mathbf{n_{af}}$: antifuel–fuel, $\mathbf{n_{l/fh}}$: portion leg–portion foothold. These parameters can be varied in simulations, and the optimized values can be set by adjusting the segment lengths.

### 4.4.5 Association Motif

The association motif, the segments that are responded to the interaction between the catalyst, the leg and the fuel, are arguably the main bottleneck in this reaction system. As was shown before [105], the displacement rate within such motif is approximately 0.3% of that observed for regular toehold-mediated reactions. To address this issue, the original study implemented two thymine bases spacer and adjusted the bases near the junction to promote co-axial stacking, thereby stabilizing the formed junction. This modification resulted in a fivefold increase in the displacement rate (Figure 4.11A).

Despite this improvement, the reaction rate remains too low, significantly limiting the overall optimization process. One might consider lengthening the binding site to enhance the effective concentration of the coexisting strands, thus reducing the bottleneck. However, while this strategy may increase the reaction rate, it also adversely affects the dissociation rate—a trade-off that was optimized using the kinetic simulations.

To optimize the association motif independently of other parameters, a combined motif is proposed here, that utilizes mismatch elimination in conjunction with associative toehold-mediated strand displacement (Figure 4.11B). To our knowledge, this combination has not been demonstrated before. The principle behind this method is that introducing a mismatch near the junction accelerates the displacement process, thereby shifting the reaction equilibrium forward.

Placing a mismatch at position 4 from the junction increases the displacement rate by approximately 45-fold [107]. However, this enhancement may increase leakage reactions, as the mismatch may promote edge fraying. To address this, three G/C base pairs at the edge provide sufficient closure, as confirmed by NUPACK simulations. If the mismatch were placed at position 3, the displacement rate would be even faster, but leakage could not be effectively suppressed. Such balanced design approach seeks to significantly improve the displacement rate while minimizing unwanted side reactions.

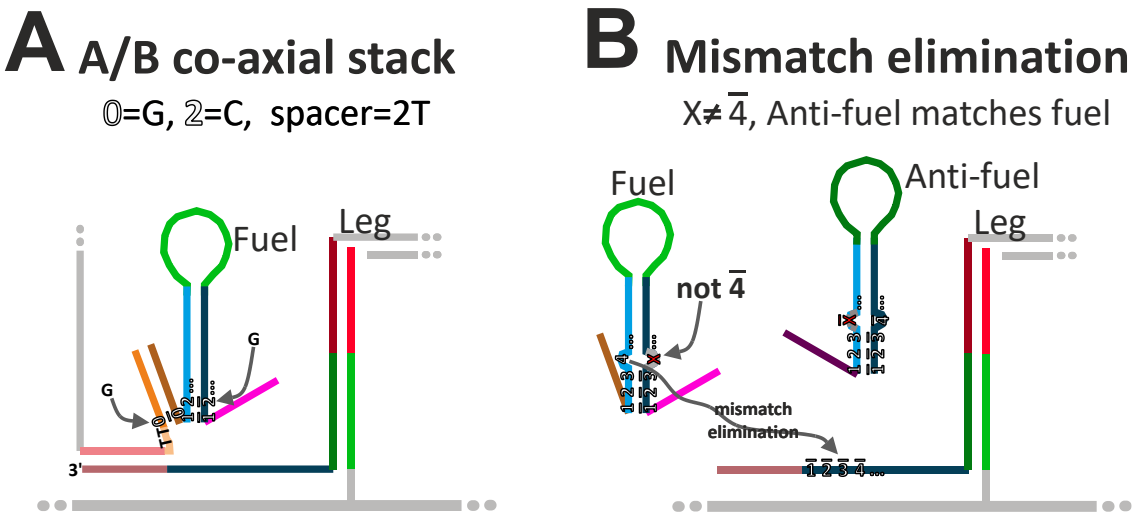


**Figure 4.11: Motifs for association reaction.** (A) Increasing the reaction rate by five times through the stabilization of a three-way junction using a technique called co-axial stacking [105]. This requires the addition of spacer and modification of specific bases to certain nucleotides, as shown. (B) Introducing a mismatch at position 4 in the fuel increases the forward displacement rate by 45 times. An additional mismatch was introduced in the anti-fuel, ensuring that the anti-fuel still matches the fuel, to avoid affecting the remaining displacement rates.

### 4.4.6 Other Displacement Rates

In contrast to the previously discussed limited association motifs, which demand an optimal forward boost (position 4, Figure 4.11), displacement reactions modification allow for more flexibility based on mismatch position. However, it is impractical to explore all possibilities due to computational constraints and diminishing returns from such extensive variation. Therefore, for simplicity reasons, we position the mismatch at position 4 (4 bases from the edge).

Displacement modifications can be introduced at position 4 from the inner edge of both the fuel and antifuel strands. While various configurations are theoretically possible, the most significant one is the forward "drive" adjustment (Figure 4.12A). This involves creating mismatches in both the fuel and antifuel strands, which promotes fuel and anti-fuel hairpins opening by slowing their closing process through proximal mismatch formation. This option was tested in simulations to assess whether it improves system performance. Alternative configurations, such as introducing mismatches only in the fuel strand while omitting them from the antifuel, were also considered. However, they tend to slow down the antifuel activation process, intuitively resulting in slower forward cycling

of the fuel. Simulations confirmed this intuition, suggesting that these alternatives are worse, therefore not discussed in further detail.

Another strand displacement reaction that can be modified is the displacement of the leg from the foothold via fuel loop domain (Figure 4.12B). One potential configuration called “drive”, involves introducing a mismatch at position number 4 in the foothold. This modification enhances the ability of the fuel's loop to open part of the foothold/leg connection through proximal elimination (Figure 4.12B). In the suggest configuration, the displacement of the fuel by the antifuel remains unaffected due to their matching sequences. This modification was included in the simulations to assess its viability. This proposed addition has a positive impact on leakage suppression, particularly by reducing interactions between the free foothold and the loop of the antifuel.

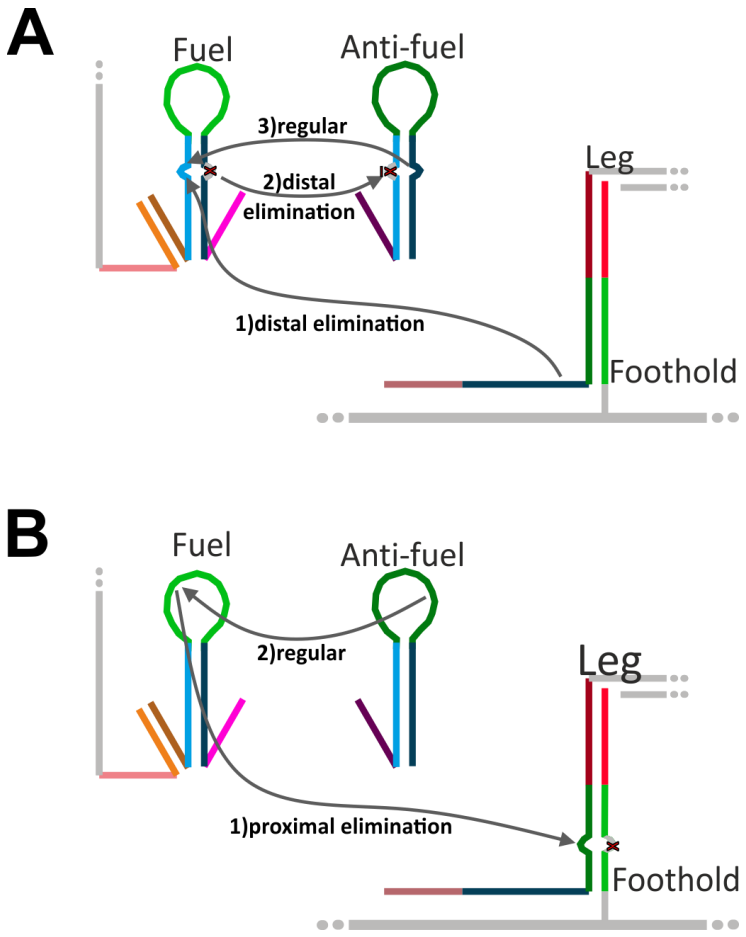


**Figure 4.12: Options for displacement modification.** (A) A viable option for altering position 4 from the inner side of the hairpins is introducing a mismatch in both the fuel and antifuel, providing additional drive for fuel cycling. (B) A viable option for altering position 4 from the bottom of the foothold/leg connection is promoting the hybridization of the fuel’s loop with the leg.

### 4.4.7 Optimization Summary

Several key optimizations were made to refine the basic mechanism, which include: 1) introducing G/C pairs at fraying locations, 2) mutating and deleting 2 nucleotides from the antifuel outer edge, 3) implementing coaxial stacking and positioning mismatch at the outer edge of the fuel hairpins, and 4) incorporating at least one nucleotide inter-domain bridge segment in the catalyst. These features were incorporated into the system and are illustrated in Figure 4.13A. These combined motifs are not expected to conflict with each other.

In addition to these optimizations, there are decisions for which the optimal approach remains undecided, as shown in Figure 4.13B (points 4 through 6), resulting in eight possible tuning options. Each of these options can be further refined by choosing the easily adjustable parameters, as indicated in point 7. The selection of the best parameter set was based on performance assessments derived from kinetic simulations, as discussed in the following section.

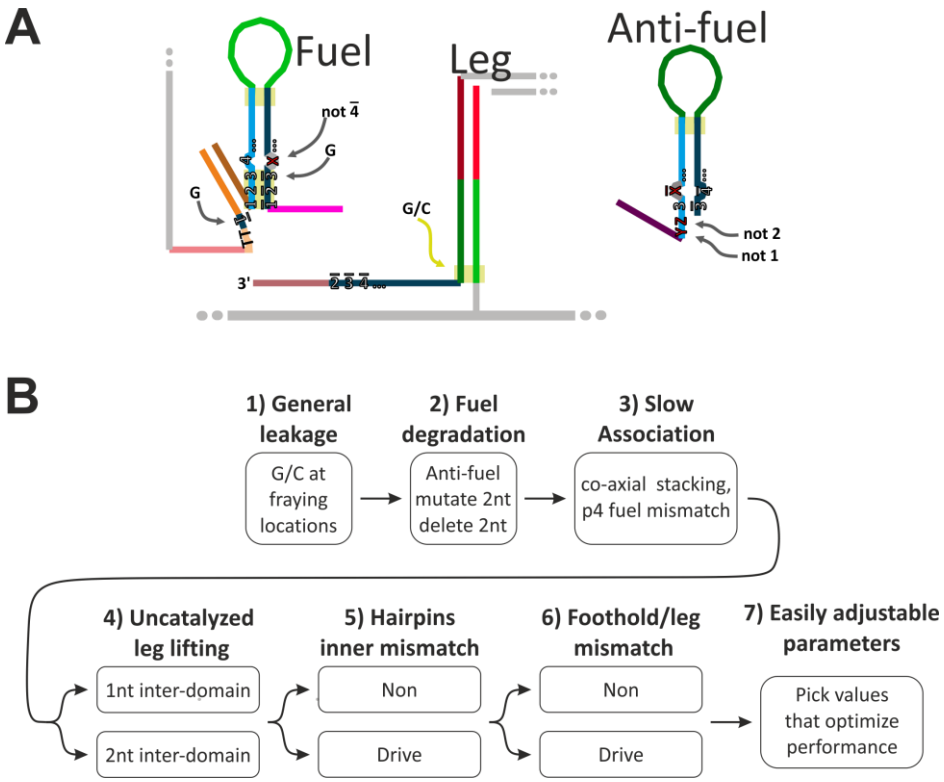


**Figure 4.13: Optimization decisions overview.** (A) The resulting combined motifs that have been decided upon. (B) Decision tree options: the first row represents the set optimizations, while the second row shows the decisions that will be determined through simulations.

## 4.5 Kinetics Simulation

Our simulations serve a dual purpose: they provide initial validation of the model's potential efficacy, and they allow fine parameters tuning by testing and optimizing various suggested motifs.

### 4.5.1 Parameters

For the simulation results to be credible, it is essential that the model accurately reflects the actual reactions and that the parameters used are both realistic and experimentally validated. However, achieving this level of accuracy presents several challenges. Experimental parameters reported in literature often vary significantly due to differences in measurement settings, such as variations in buffer or salt concentration, pH levels, or differences in strands purity. These conditions did not always align with the optimized settings required for our rotor system. Additionally, certain parameters, particularly those related to the geometry of the rotor, are either unavailable or were not determined experimentally, further complicating the simulation process.

To address this, I prioritized selecting parameters that best represent our experimental system. In instances where experimental values were unavailable, I tested the model using the most probable parameter value and using edge cases to explore potential outcomes and assess system robustness.

In the Appendix C.4, I have listed the different reaction types used in the model, along with their corresponding reaction rate constants. *Note:* H1 refers to the fuel hairpin, and H2 denotes the antifuel hairpin; these terms are used interchangeably throughout the text.

### 4.5.2 Time Course

The model was constructed based on the proposed design and implemented into COPASI software, version 4.42 (build 284) [154]. The process involved defining the species (states), reactions path and rates (parameters, Figure 4.14A). After setting the initial state as was discussed previously, a time course simulation was performed using the software (Figure 4.14B), allowing observation of the system's dynamics over time ( Figure 4.15). To evaluate the system performance the stepping forward rates (defined as

the time in which 0.66 of the initial population stepped forward) were multiplied by a stepping yield (in comparison to error level), see Figure 4.15. Finally, the system was optimized to achieve maximum performance for 12 consecutive steps, mimicking a full rotation (see the formula presented in Figure 4.15).

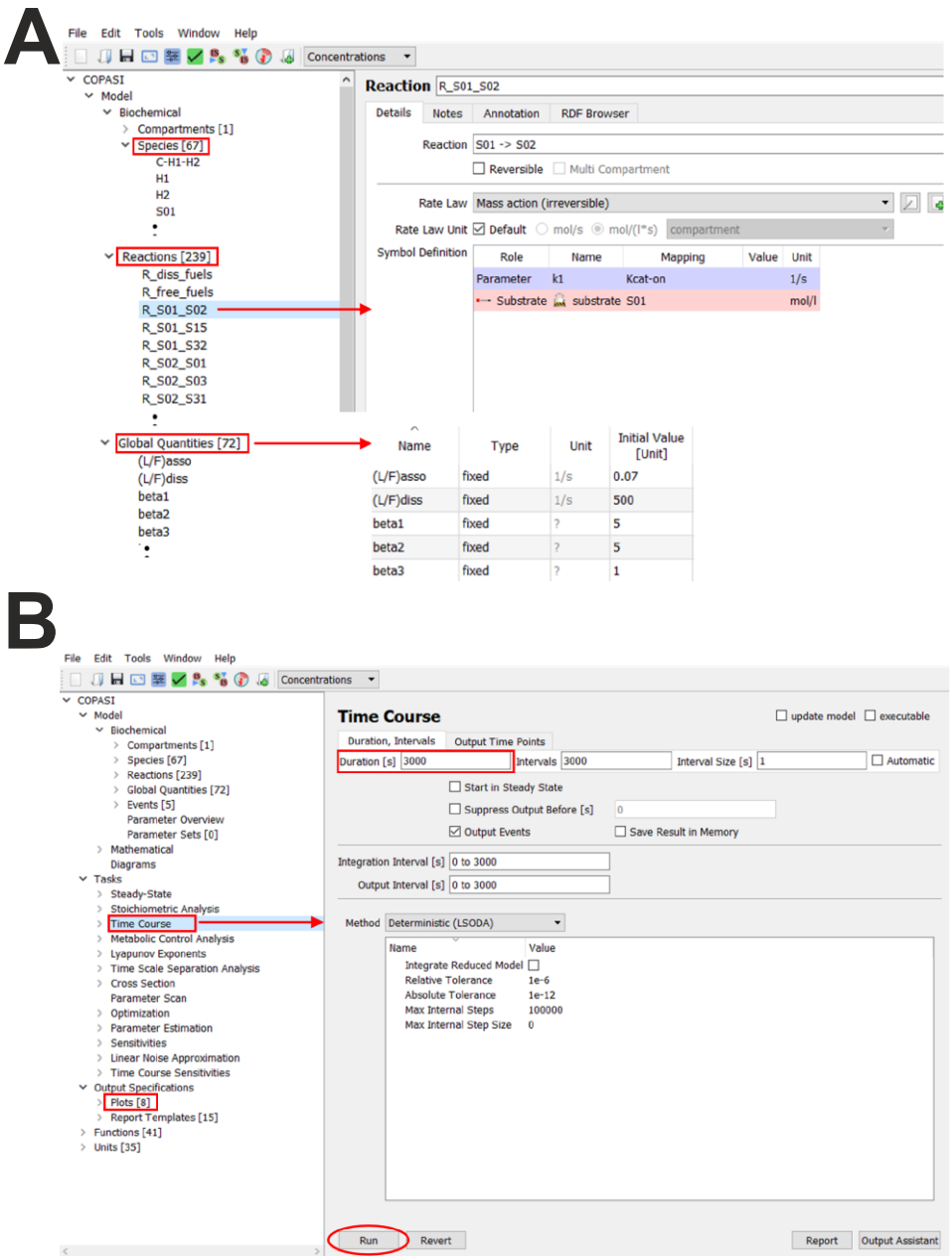


**Figure 4.14: COPASI workflow illustration.** (A) Model construction involves defining the species, the reactions between them, and setting the parameters. (B) In the time course tab, the typical simulation duration is set to 3000 seconds to account for the slowest reaction.

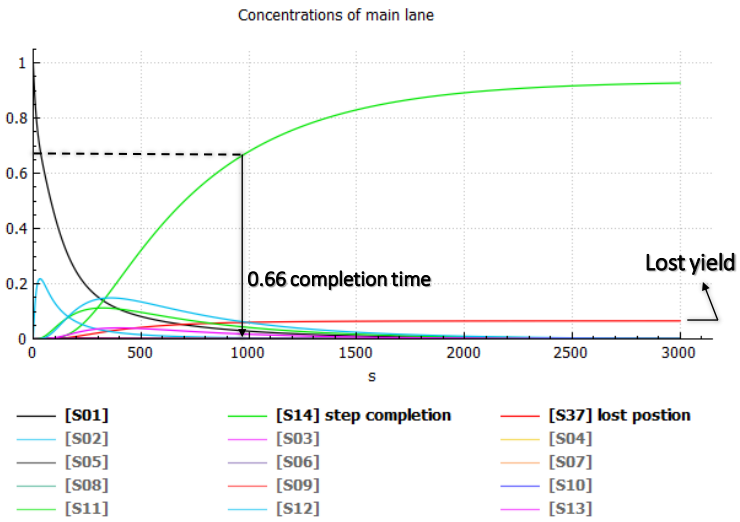


$$Performance = rate * yield^{12}$$

$$= \frac{1}{time_{0.66}} * (1 - lost\ yield)^{12}$$

**Figure 4.15: Time course for error-exaggerated setting.** The population changes as a function of simulation time are plotted. From this data, both the rate of forward leg placement and the error rate can be extracted, providing an evaluation of the system's performance.

## 4.5.3 Performance Optimization

For a specific set of parameters, performance was maximized by identifying the free variables within their possible ranges. This process was automated using the particle swarm multidimensional optimization method within COPASI software (Figure 4.16). To fully automate the parameter fine-tuning across all parameter sets, the Python package BasiCO [155] was used.

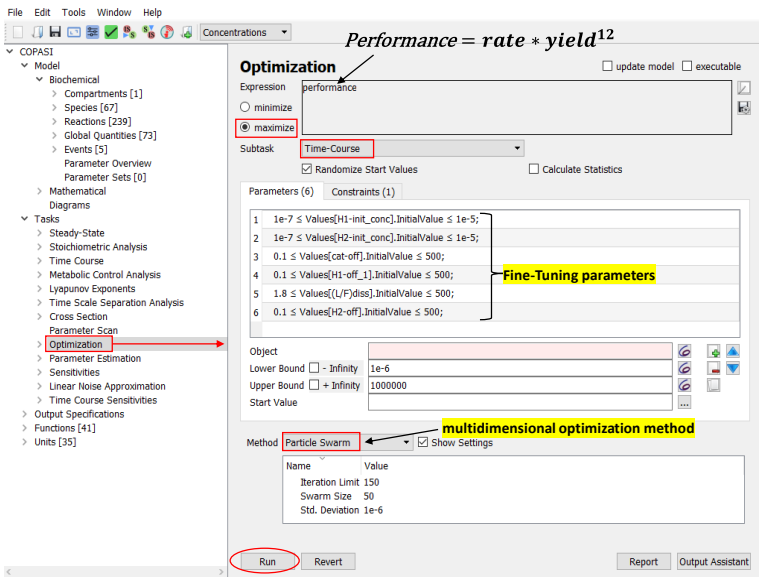


**Figure 4.16: COPASI multidimensional optimization.** The values of fine-tuning parameters that yield maximal performance can be identified using particle swarm optimization over time-course simulations.

### 4.5.4 Simulations Results

According to the simulation results, the model operates as intended, directing all populations into two key states: the correct forward step and the error state, see Figure 4.17. Additionally, the simulations show that most of the tested modification options produced favorable outcomes, delivering impressive performance. Specifically, the stepping yield exceeded 98% per step, and the stepping time was under 4 minutes (Figure 4.18).

Among the various modifications, **interdomain bridging** equal 1nt (see Section 4.4.3) proved better than 2nt option, demonstrating approximately 7% better performance while maintaining sufficient leakage reduction (Figure 4.18), making it the preferable choice. For the **inner mismatch modification** in hairpins (see Section 4.4.6, Figure 4.12A), the addition of the "drive" motif yielded a performance increase of about 25%, highlighting a clear advantage in including this feature. In the case of the **foothold/leg mismatch** (see Section 4.4.6, Figure 4.12B), the "drive" motif led to varying degrees of improvement, justifying its inclusion in the default optimization choice.

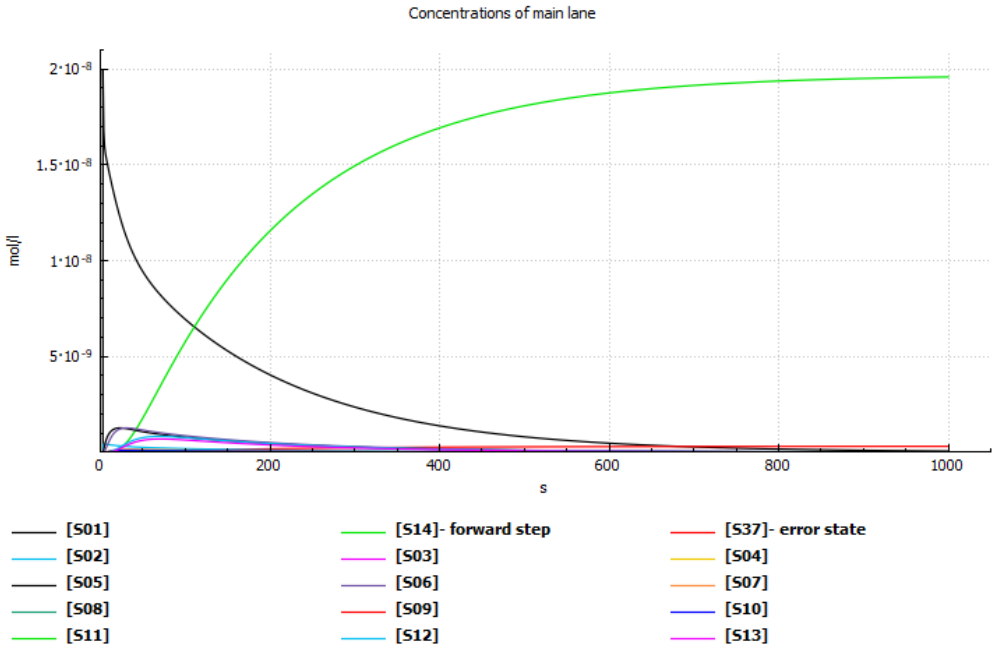


**Figure 4.17: Typical time course for the model.** The figure highlights selected states along the shortest path to the product, illustrating the decay of the initial state S01 and significant growth of state S14, representing forward stepping. Minimal growth is observed for the error state S37, while the intermediate states exhibit noticeable decay.

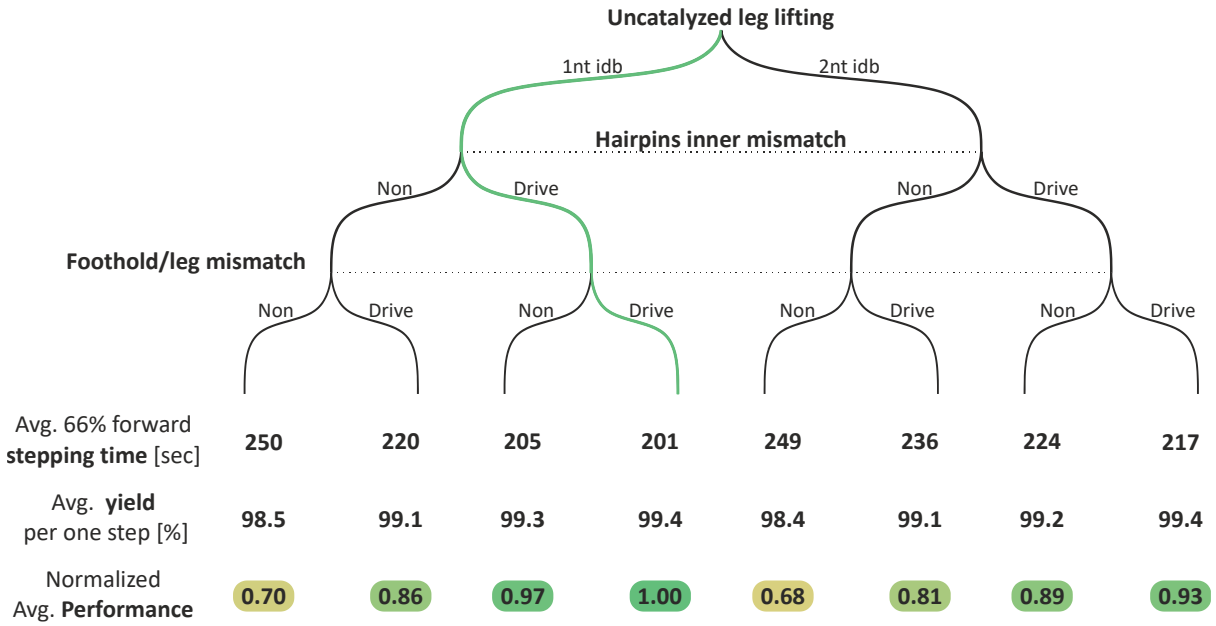


**Figure 4.18: Relevant Tuning Options.** This figure illustrates the various combinations of optimization motifs considered in the simulation, highlighting the impact of different tuning parameters such as interdomain bridging and mismatch motifs on system performance. The green route emphasizes the selected optimization pathway, representing the preferred set of tuning options.

Looking closely at the simulation results for the selected motif configuration (1nt, “drive”, “drive”), the following inputs and results were obtained:

| **Inputs** | | | | | | |
|---|---|---|---|---|---|---|
| $Rr1, Rr2\ [S^{-1}]$ | 0.2 | | 0.135 | 0.2 | | 0.135 |
| $H1on, H2on\ [M^{-1}S^{-1}]$ | $10^5$ | $2 \cdot 10^6$ | | $10^5$ | $2 \cdot 10^6$ | |
| $cat - on\ [S^{-1}]$ | 0.014 | | | 0.07 | | |
| **Results** | | | | | | |
| 66% stepping time $[S]$ | 291 | 254 | 260 | 154 | 120 | 128 |
| Yield per step [%] | 99.5 | 99.7 | 99.7 | 99.1 | 99.2 | 99.2 |
| Performance $* 10^3$ | 3.23 | 3.79 | 3.70 | 5.81 | 7.52 | 7.14 |
| | | | | | | |
| **Fine-tuned parameters** | | | | | | |
| $H1\ intial\ [\mu M]$ | 23.3 | 12.6 | 12.6 | 16.3 | 8.4 | 8.4 |
| $H2\ intial\ [\mu M]$ | 50.0 | 50.0 | 50.0 | 50.0 | 50.0 | 50.0 |
| $cat - off\ [S^{-1}]$ | 0.98 | 1.08 | 1.08 | 2.43 | 2.45 | 2.51 |
| $H1off \rightarrow n\ [nt]$ | 9.31 | 8.90 | 8.89 | 9.21 | 8.95 | 8.95 |
| $(L/F)diss\ [S^{-1}]$ | 0.17 | 0.28 | 0.32 | 0.12 | 0.24 | 0.27 |
| $H1off\ [S^{-1}]$ | 47.1 | 173.6 | 175.3 | 33.16 | 111.7 | 114.1 |
| **Results for exact segment lengths** $cat - off = 1.875\ S^{-1}(9nt) \mid n = 9nt \mid (L/F)diss = 0.1\ S^{-1}(10nt) \mid H1off = 31.25\ S^{-1}(8nt)$ | | | | | | |
| 66% stepping time $[S]$ | 317 | 289 | 298 | 156 | 144 | 154 |
| Yield per step [%] | 99.5 | 99.8 | 99.8 | 98.9 | 99.6 | 99.6 |
| Performance $* 10^3$ | 2.99 | 3.38 | 3.28 | 5.63 | 6.62 | 6.20 |

**Table 4.1:** Results for the option, 1nt IDB, drive, drive, depending on input variation.

Each column reflects a different set of input parameters, which were varied to assess the uncertainties in the input values. The most significant performance reduction was observed for the reduced catalyst activity (cat-on@20%, Figure C.2). Despite this, the overall system performance remained within acceptable limits, including in edge cases.

The fine-tuned parameters based on input variations showed an acceptable average variance of around 30%. When the thermal dissociation parameters were set to specific values corresponding to an exact segment length, the average performance dropped by approximately 10%. Interestingly, this decrease was primarily attributed to slower stepping times rather than a reduction in stepping yield, suggesting that system efficiency was preserved even under such conditions.

## 4.6 Construction Proposal

A mechanism that functions excellently but cannot be constructed holds little value. In this section, I propose a rotor preparation procedure, including integration of the propulsion mechanism into the rotor structure, and provide detailed descriptions of the system elements, segment length design, and motor initiation. Additionally, I highlight design options for achieving motor stopping, resuming and reversing functions.

### 4.6.1 Detailed Structure

**DNA direction and strands purification**

In my design, the strands 3'-5' direction of the strands can be completely reverse relative to what is presented here, however, with some limitations. Due to the technical aspects of DNA synthesis, which typically occurs in the solid phase from the 3' to 5' end, truncation at the 5' end can occur, compromising strand quality. This truncation can result in exposed bases that, according to the design, should be part of a double-stranded region, leading to variations in segment rigidity and potential misassembly. Additionally, these exposed bases could act as unintended toeholds for strand displacement, disrupting the intended reactions. To mitigate these effects, it is essential to use PAGE (polyacrylamide gel electrophoresis) purification for all mechanism's strands to minimize the impact of truncations. Despite its benefits, PAGE purification has limitations, as it is not effective at resolving single-base truncations due to separation

resolution constraints. To further minimize the effects of 5' end truncation, particularly in critical regions such as the end of the leg and the footholds, the sensitive ends are deliberately designed to be located at the 3' end. This choice dictates the directionality of the remaining strand (see Figure 4.19).

**Hairpin stem length**

Another crucial parameter in motor design is the hairpins stem. The stem length must be sufficient to ensure proper closure and stability of the hairpin, which directly influences the fuel's stability. The metastable hairpins used in the Greens work [112] demonstrate that a 16-nucleotide (nt) stem provides significantly more stability against uncatalyzed fuel decay compared to a 7-nt stem. Additionally, further work by Shaofei et al. [156] revealed that leakage reactions in hairpins predominantly result from edge effects, and a longer stem can limit these unwanted reactions. Specifically, stems 14 nt and longer exhibited minimal leakage in hybridization chain reactions. Based on these findings, a 16-nt stem length has been selected for the hairpins to ensure fuel stability and minimize leakage.

**Spacer design between legs**

A rigid spacer between the motor's legs is critical for consistent walking, as it prevents the legs from reaching non-adjacent footholds. The average distance between the footholds is 16 ± 3 nm, with each foothold capable of leaning about 4 nm from its base (based on typical strands length). To maintain controlled movement, the total spacer length between the legs should be less than 24mm (2 × 16 - 2 × 4). The proposed design includes two 18-nt double-stranded DNA spacers, corresponding to a distance of ~12 nm (2 × 18 × 0.34 nm per base pair), see Figure 4.19. Additionally, a total of 10 nt single-stranded spacers are introduced, amounting to up to 6 nm when fully stretched. This combined distance ensures that the leg can comfortably reach the nearby foothold without overextension to a further away foothold, optimizing the motor's walking mechanism.

**Vertical Spacing**

The vertical spacing in this design mirrors that of externally controlled bipedal walkers, where the leg/foothold length is set to 16 nt to ensure stability. The segment between the leg's spacer and the upper scaffold (disc) is 18 nt double-stranded segment. This total

vertical spacing accounts for the separation between the two discs structures, which is roughly 10 nm (four layers of origami). Single-stranded spacers are strategically implemented to provide flexibility, accommodate uniformity, and account for any inconsistencies in the distance between the relevant components.

**Catalyst Positioning**

For clockwise operation of the motor, the catalyst must be positioned relative to the walker in an anticlockwise direction. The catalyst is designed to be placed approximately 16 nm behind the walker's elongation point, and is supported by an additional strand, forming a total of 40 base pairs duplex. This geometry ensures that the active segment of the catalyst can reach the elongation point of the rear foothold. A longer may interfere with the forward leg extension that can be stretched backward towards the catalyst. For anticlockwise operation, the catalyst should be equivalently positioned 16 nm away on the opposite side.

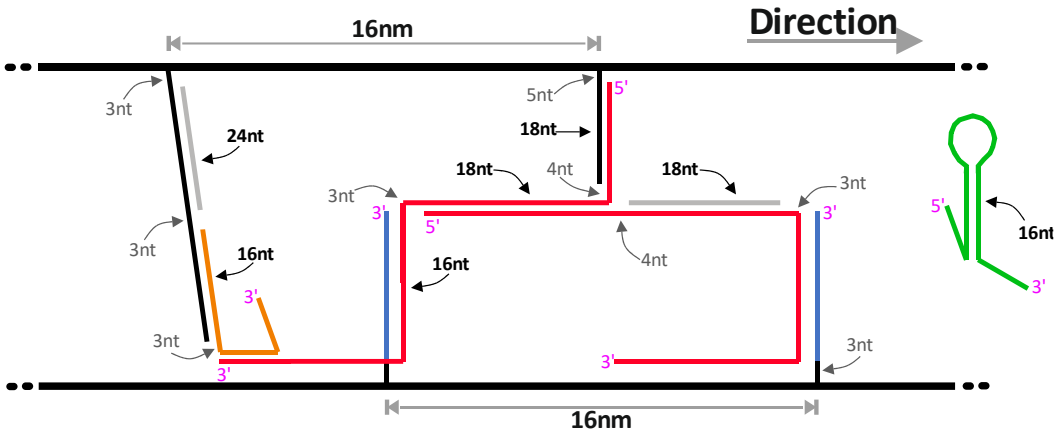


**Figure 4.19: Suggested detailed structure.** The legs are shown in red, footholds in blue, the catalyst strand in orange, and the black strands represent extensions from the origami. Black arrows indicate the double-stranded segments, while gray arrows highlight the single-stranded spacer segments.

## 4.6.2 Assembly and Initiation proposal

The assembly process for the rotor should be like the procedures used for externally controlled rotation system, with the primary difference being in the propulsion mechanism itself. Each disc is annealed separately, undergoing high-volume PEG purification to remove excess strands (especially the excess swivel strands). After purification, the discs should be mixed to dimerize via the swivel element. Once the

upper disc is connected to the gold nanorod, the entire assembly should be immobilized onto a coverslip.

Similar to external controlled rotary motor, here 12 footholds are elongated from the lower disc, at a 10x ratio to the scaffold in the annealing, to ensure proper attachment. The upper disc should be annealed with the remaining walking mechanism components: a walker elongation at 5x, the first leg at 10x, and the second leg at 15x. A leg blocker, applied at a 40x ratio, covers both legs to ensure control over the leg attachment to the track. A similar scheme is employed for the catalyst assembly (see Figure 4.20A). These increasing ratios are typical in DNA origami protocols to ensure complete assembly, compensating for inaccuracies in strand concentration and potential mixing errors.

After rotor immobilization into working chamber, a thorough washing step is crucial to remove any residual strands that were not cleaned during PEG purification. This is particularly important for excess leg and foothold strands, as they can potentially bind to anchored legs and footholds (after leg unblocking), thereby inhibiting the walking mechanism.

Following this washing step, an anti-leg blocker can be introduced at a high concentration (10 μM) to displace the leg blocker. The anti-leg blocker is designed to be half the length of the blocker to avoid permanent attachment to the footholds. Upon removal of the leg blocker, the legs are free to bind to a pair of adjacent footholds at random positions along the track. After an additional washing step and the introduction of the metastable hairpin fuel pair, the system is ready to start the walking operation. For more precise control over the movement start timing, the active part of the catalyst can be blocked during annealing. After fuel introduction, the anti-catalyst blocker can then initiate the system.

To achieve a precise starting position, unique addressable sequences need to be added to the upper section of each foothold. For specific leg-foot initial position, the system must reach a state where the legs are free to react while only two footholds are available for binding. Therefore, blocking the remaining footholds is necessary (It is generally easier to unblock two specific footholds than to block all except the desired two).

There are several strategies for removing the foothold blocker (that are added in the annealing) such as hairpin based anti-blocker, or half-length antiblocker that have

additional toehold for its removal, but here I chose a more elegant approach, illustrated in Figure 4.20B, involves the use of addressable handholds placed on the foothold. Here, a specific anti-foothold blocker interacts with the foothold blocker via handhold-mediated strand displacement [157], leading to the complete detachment of the desired blocker. Once the legs are released and fixed at the free positions, the remaining foothold blockers can be removed.

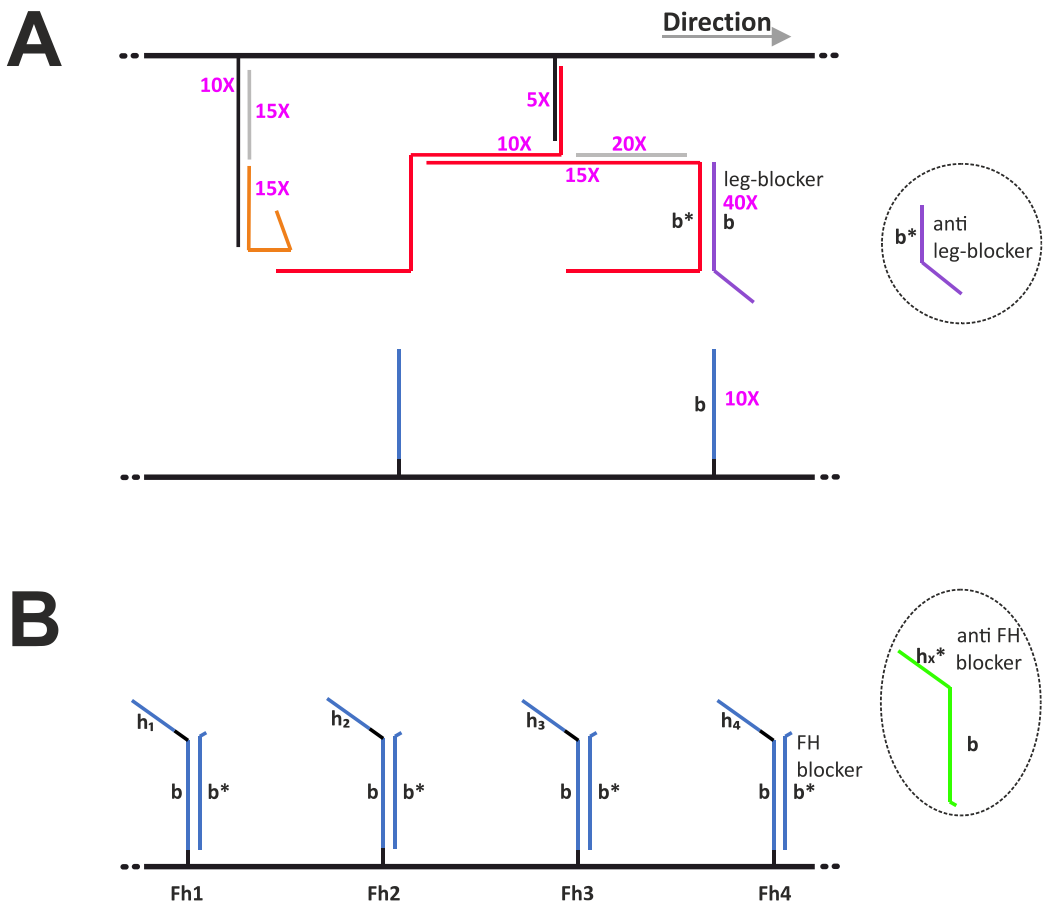


**Figure 4.20: Assembly and initiation.** (A) A hierarchical concentration strategy can be used during annealing to ensure complete assembly. After the swivel connection is formed, the leg blockers can be released using a half-length anti-blocker. (B) For specific initiation positions along the track, footholds need to be blocked during the annealing process. The removal of specific blockers can be achieved through handhold-mediated strand displacement.

### 4.6.3 Experimental Modification Options

While theoretical optimization aims to accurately predict experimental outcomes, in practice, many underlying assumptions may not hold true, leading to discrepancies between predicted and observed results. This necessitates experimental fine-tuning when the system does not function as expected in laboratory conditions. To facilitate this process, it is advantageous to adjust multiple parameters within the same experimental setup, thereby eliminating the need to reanneal the full structure of DNA origami - gold assemblies.

However, making all parameters adjustable is not necessarily optimal, as it can increase the complexity of both the structural design and the experimental procedures. Therefore, In this study, certain components—specifically, the legs and footholds of the molecular walker system—were designed to be unchangeable during the same experiment. On the other hand, other elements were made easily adjustable to allow for rapid optimization. For example, the parameters of the hairpin structures can be modified by washing the system and introducing different variants. Moreover, the ability to modify the catalyst is crucial. Its removal is necessary to reverse the walking direction by introducing a catalyst oriented in the opposite direction relative to the walker. Additionally, the catalyst's binding site structure can be altered to adjust its flexibility behavior by changing it's the spacer.

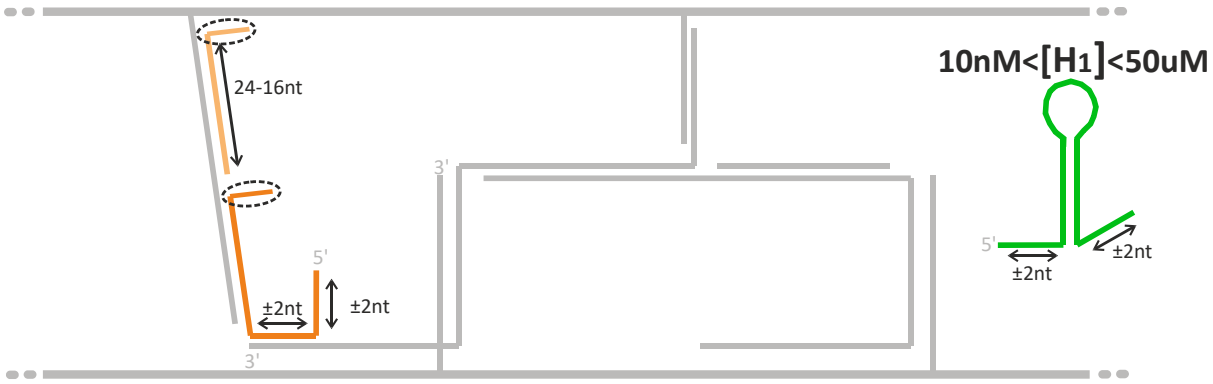


**Figure 4.21: Experimental modification options.** Both hairpins can be exchanged through washing, allowing for variations in concentration or segment length. Two toeholds are included for different parts of the catalyst to facilitate their exchange via regular toehold-mediated strand displacement (TMSD). The residual strand can be washed out, while the structure remains immobilized, and other variants can be introduced through washing in.

## 4.7 Specific Sequence Design

### 4.7.1 Requirements

Ensuring the optimal function of the propulsion mechanism requires careful attention to multiple sequence considerations. First, the sequences must include the specific chosen design motifs, such as coaxial stacking, mismatches, and G/C fraying.

Second, it is advantageous to design the sequences to be orthogonal to those used in DNA origami structures, including both scaffold and staple strands. This minimizes unintended interactions during the annealing process, reducing the risk of misassembly of the mechanism's strands. More critically, orthogonality between the strands involved in the mechanism itself is essential, particularly for active segments of the system, ensuring that these segments do not interact with one another, except where intended, enhances the assembly and the function of the propulsion mechanism.

Finally, sequences should be designed to minimize secondary structure formation in regions where it is unnecessary. Unintended secondary structures can lead to misassembly, and in active regions—such as footholds or toeholds—they may reduce kinetic rates, thus compromising the system's performance.

Balancing these requirements is non-trivial. The complexity increases with the length and number of sequences involved, necessitating iterative optimization to achieve the optimal design.

### 4.7.2 Methodology

To address these challenges, a method was developed here that balances the various considerations. Preliminary results have demonstrated its efficacy (data not shown).

**Tools utilized**

Modified versions of the computer algorithm 'Nucaft' tool, previously developed in Aim1, Section 2.3, were employed here. Nucraft is software that generates pseudo-random sequences while preventing unintended hybridization beyond a user-defined order of nucleotides. Several modifications were made to adapt the tool for specific tasks here:

1. Nucleotide position specification: The ability to demand specific nucleotides at specific positions along the sequence was added, allowing precise control over motif placement.
2. G/C content control: introduced the ability to dictate G/ C positions and to specify the percentage of C content.
3. Variable length checks: The tool was adjusted to allow different user-defined lengths for checks against initial sequences (origami scaffold and staples) and the sequences being generated (propulsion mechanism strands). Specifically, we set a length of 9 nucleotides for checks against origami sequences, and a length of 6 nucleotides for checks among the propulsion mechanism strands.
4. Sequential G bases adjustment: The default avoidance of sequential stretches of 4 G bases was adjusted to 3, further reducing the likelihood of G-quadruplex formation.
5. Automation of sequence generation: An automated process was coded to generate all required segments from a table of specifications, including the option to produce multiple variations of the same segment.

**Rationale for fragmentation**

It was decided here to fragment the strands into smaller segments based on their functional roles. For example, the first leg of the mechanism is divided into five segments: two double-stranded regions, a section that reacts with the foothold, an extension of the leg, a part that reacts with the catalyst (Figure 4.22). This fragmentation serves multiple purposes:

- Technical feasibility: Generating long sequences exponentially increases computational time and complexity. Smaller segments are more manageable.
- Requirement balancing: Different segments have different design requirements. Fragmentation allows us to apply specific constraints where needed.
- Improved G/C distribution: Smaller fragments facilitate better control over G/C base distribution along the sequence.

**Rationale for number of variations**

Despite these measures, the method is not entirely sufficient to eliminate all secondary structures. For example, unintended matches of 5-base sequences or 11-base segments with mismatches in the middle can still occur. To further reduce secondary structure formation, multiple variants of each segment were generated, and the best candidates were selected based on NUPACK analysis [158].

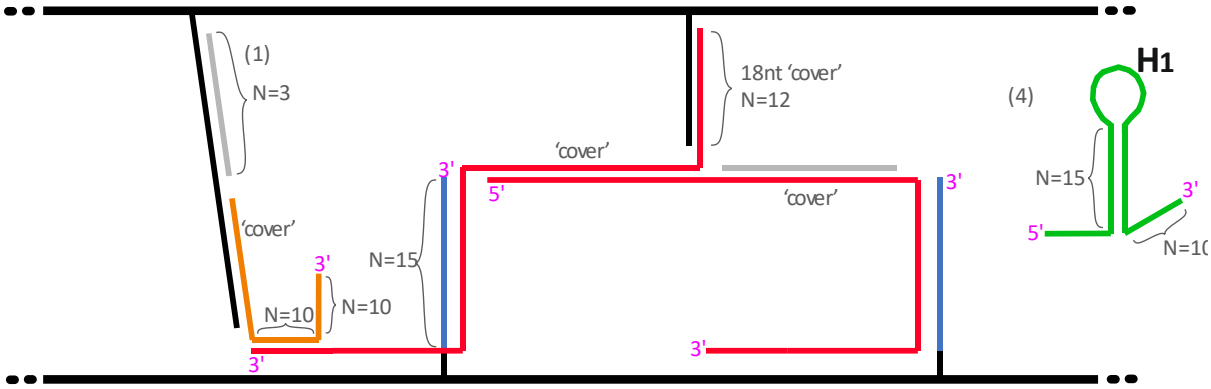


**Figure 4.22: Fragmented generation of the different sequences.** This figure showcases the different segments that were generated, with *N* representing the number of variants for each segment. The more sensitive a segment, the higher the value of *N*.

## 4.7.3 Protocol for sequence generation

The finalized protocol comprises the following steps:

**Step 1:** Sequence generation via Nucraft v2

- Generate all segments with sufficient variations to allow selection based on NUPACK results. The number of variations depends on the sensitivity of the region (Figure 4.22).

**Step 2:** Sequence Refinement Using NUPACK

1. Ranking individual segments: For each segment, rank the variations based on their free energy profiles, both for the segment itself and its complement. The best candidates exhibit minimal secondary structure.
2. Combination of segments: Create a list of all possible combinations using the top three variations from each fragment, aligned according to their positions in the strand.
3. Selection of optimal strands: Choose the best segments combinations based on NUPACK analysis, focusing on overall minimal secondary structures.

4. Cross-interaction check: Verify that the chosen strands do not have unintended interactions at active sites. If unintended cross-interactions are found, iterate the previous steps to refine the selection.

**Note on Protocol Limitations**

This protocol simplifies some requirements for the sake of practicality. It does not fully account for the implications of fragment combination. A more comprehensive optimization could involve automated weighted algorithms with embedded NUPACK code, but this is beyond the scope of the current work.

## 4.8 Summary of Aim-3

Building upon the foundation of our externally controlled rotor motor, I proceeded to design and in silico validate a simplified yet robust autonomous propulsion mechanism, representing a significant step toward creating synthetic, free of biological-enzymes, autonomous molecular motors driven by chemical fuel. The system developed utilizes a locked track and walker body—such as the rotary motor—along with a rear-leg catalyst for leg lifting. Additionally, advancements were made in metastable hairpin design to serve as the fuel for the propulsion mechanism. This system was modeled and optimized by modifying key parameters to increase stepping rates while reducing error rates. Kinetic simulations demonstrated stepping yields exceeding 99% and a stepping time of approximately three minutes per step, subject to model assumptions. Moreover, leakage pathways were minimized to ensure the accuracy and validity of the simulation results. Technical details were also proposed for proper walker construction, along with specific sequence designs, paving the way for the experimental realization of this motor.

# Chapter 5: Conclusions

Emulating the complexity of biological molecular motors with synthetic systems is a formidable challenge. This thesis has successfully advanced toward this goal by developing high-quality constructs and motor propulsion mechanisms through engineering new designs while carefully integrating structural, dynamical, and operational-conditions considerations.

By leveraging existing tools and knowledge in nanotechnology, as well as developing additional tools myself, I believe the aims of this thesis have been achieved. These accomplishments include fabrication of ~1 μm-long DNA origami track with high purity and a feasible preparation procedure, as well as the design and assembly of a robust origami-based bipedal rotary motor that contains a swivel that ensures rotation while maintaining processivity. The well-designed origami discs successfully incorporate the bipedal propulsion mechanism and seem not to interfere with its operation. Finally, using computer simulation I demonstrated a novel design for a fully synthetic, directional, non–burnt-bridge autonomous propulsion mechanism that can be implemented in our rotor.

While we have not yet fully bridged the gap with biological motors, this thesis offers a glimpse into the future of synthetic molecular machines. It highlights the vast potential for innovation at the nanoscale—a reminder that “there’s plenty of room at the bottom.”

# Appendix A: Origami Methods

## A.1 Annealing

### A.1.1 Tile

Assembly was performed separately for each of the six origami tiles in 50 µL 1× TAE annealing buffer (40 mM Tris, 20 mM acetic acid, 1 mM EDTA, 12 mM $MgCl_2$, pH 8.0). Thermal annealing procedure was as follows: samples were heated at 65 °C for 15 min, cooled to 40 °C at 1 °C/15 min, and cooled to 20 °C at 1 °C/10 min using a thermal cycler (Esco, SwiftMaxPro). The annealing solution contained 20 nM scaffold strands, 5-fold excess staples, and 10-fold excess sticky ends and poly-T overhangs strands, and in cases in which the origami was imprinted with 'A'-'F' letters, the 'dumbbell staples' were introduced also during the annealing process (5x excess).

### A.1.2 Disc

Assembly was performed separately for the top and bottom origami disc tiles in 50 µL of FOB15 annealing buffer (1x: 5 mM Tris, 1 mM EDTA, 5 mM NaCl, 15 mM $MgCl_2$, pH 8.0). The thermal annealing procedure was as follows: samples were heated at 65°C for 15 minutes, cooled from 60°C to 44°C at a rate of 1°C per hour, and then directly cooled to 25°C using a thermal cycler (Biorad). The annealing solution contained 20 nM of the two scaffolds, CS4 and P8064 (Tilibit Nanosystems), along with a 10-fold excess of staples (IDT) and a 3-fold excess of swivel strands.

## A.2 Purification

### A.2.1 PEG Precipitation - Tile

After annealing, monomers were purified from excess staples using polyethylene glycol (PEG) as a precipitating agent. Typically, the 50 µL of origami sample was mixed with 150 µL of the annealing buffer and 200 µL of PEG-buffer (10 mM Tris, pH 8.0, 1 mM EDTA, 15% (w/v) PEG-8000 and 500 mM NaCl) in an Eppendorf tube and mixed gently (achieving 250 mM NaCl and 3 mM $MgCl_2$ final concentrations). The mixture was centrifuged at 17800×g at 22 °C for 30 min. The supernatant was withdrawn carefully, and the pellet that was

typically sticks to the Eppendorf, was resuspended in 50 µL of 1xTAE buffer supplemented with 100 mM NaCl and 2 mM $MgCl_2$. This purification procedure was carried out once, yielding about 18-20 nM origami monomers concentration (corresponding to no more than 10% yield reduction).

### A.2.2 PEG Precipitation - Disc

After annealing, the discs were purified from excess staples using high-volume PEG precipitation. Typically, 50 µL of the origami sample was mixed with 450 µL of 106 buffer (1x TAE, 100 mM NaCl, 6 mM $MgCl_2$) and 500 µL of PEG buffer (10 mM Tris, pH 8.0, 1 mM EDTA, 15% (w/v) PEG-8000, and 500 mM NaCl) in an Eppendorf tube, and the mixture was gently mixed. The mixture was then centrifuged at 17,800×g at 25°C for 30 minutes. The supernatant was carefully withdrawn, and the pellet, which typically adhered to the Eppendorf tube, was resuspended in 500 µL of 106 buffer for a second round of PEG purification, similar to the first. After this, only 25 µL of 106 buffer was added to allow for precise dilution to 20 nM (with 106 buffer), following a Nanodrop (ThermoFisher Scientific) concentration measurement.

### A.2.3 Gel Extraction – Tile trimer

For all gel (analytical gel and the gel used to purify the trimers) the origami samples were loaded into wells of a 0.6% agarose gel prepared from SeaKem LE agarose with 1×TAE buffer containing 1x SYBR Safe stain (Invitrogen), supplemented with 100 mM NaCl and 2 mM $MgCl_2$ (gel102), and the running buffer was 1xTAE containing identical salts. The gel (10-cm length) was run for ~1.5 hours in an ice-cold water bath at 40 V. The trimer bands of interest were cut from the gel (typically 100-300 µL), extruded using 1 ml syringe equipped with a needle (Size: 18G, 1.5”), placed in the Freeze 'N Squeeze column and cooled at -20 °C for 10 min. The samples were then spun at 13000×g for 10 min at 20 °C and then transferred from the collection tubes to 1.5-ml Eppendorf tubes.

To increase the trimers concentration to about 10 nM, PEG precipitation was used as follows: Typically, 1×TE buffer (10 mM Tris, pH 8.0, 1 mM EDTA) containing 15% (w/v) PEG-8000 and 500 mM NaCl was added to the origami sample at equal volume to that extracted from the gel in an Eppendorf tube and mixed gently. The mixture was

centrifuged at 17800×g at 15 °C for 30 min. The supernatant was withdrawn carefully, and the pellet was resuspended in 15 µL of 1xTAE buffer supplemented with B102 buffer.

## A.3 Hybridization reactions

### A.3.1 Tile Trimerization

After PEG purification, 50 µL (~20 nM monomers concentrations) of each corresponding monomer (A, B and C, and D, E and F) were mixed with each other and gently stirred in a shaker (150 rpm) at room temperature for 60-120 min. resulting in ~7 nM trimers.

### A.3.2 Tile Hexamerization

After gel extraction of the trimers, the concentrations of the two trimer samples were carefully equilibrated to ensure a 1:1 mixing ratio. This was achieved using a Nanodrop spectrophotometer (ThermoFisher Scientific), adjusting each sample to approximately 5 nM in B102 buffer. Equal volumes (15 ill) of ABC and DEF trimers were then mixed in an Eppendorf tube and gently stirred on a shaker (120 rpm) at room temperature overnight to complete the hexamerization reaction.

### A.3.3 Disc Dimerization

Disk dimerization was achieved by mixing the bottom and top disk solutions in a 1:1 ratio and incubating them at 35°C with gentle shaking for at least 14 hours. The resulting solution was stored at room temperature.

### A.3.4 Nanorods Attachment

The rotor solution was adjusted to 10 nM, then mixed with the nanorod solution (~10 nM) in a 1:5 ratio, and incubated for at least 20 minutes.

# Appendix B: Microscopy

## B.1 Atomic Force Microscopy

For liquid-AFM imaging on a Cypher (Asylum Research), the samples were diluted (ratio 1/9) using buffer containing $MgCl_2$ (6 $MgCl_2$). The diluted samples were deposited onto freshly cleaved mica and left to adsorb for 5 min. The measurement was conducted under this liquid buffer and on an active anti-vibration table in liquid tapping mode using a HiRES-C14/AlBS probe (MikroMasch), typically at a scan rate of 3 min per 2x2 μM image size.

## B.2 Transmission Electron Microscope

Imaging was conducted using a Talos F200C TEM microscope (ThermoFisher Scientific) operating at 200 kV and equipped with a Ceta 16M CMOS camera. For sample preparation, 300-mesh copper grids (Ted Pella, Prod No. 01813-F) were glow discharged. Then, 2.5 μL of the sample was applied onto the grid, and after 1-minute, excess liquid was blotted off with filter paper. The grid was air-dried for 1 minute before applying 5 μL of 2% uranyl acetate (SPI CAS# 6159-44-0) as a negative stain for samples containing origami. Next, the grid was blotted again to remove excess uranyl acetate. Finally, the grid was air-dried before inserting into the microscope.

## B.3 Cryo-TEM

A ~200 nM DNA origami disc solution was applied to carbon-coated copper grids and frozen using a custom-built plunger. Imaging was conducted on a 300 kV FEI F30 Polara microscope equipped with a Gatan K2 direct detector and a Quantum GIF filter. Data collection was managed with SerialEM, and processing was completed using CryoSPARC and Relion.

## B.4 Total Internal Reflection Fluorescence

### B.4.1 Labeling

To enable single-molecule fluorescence imaging, origami-A and origami-F were designed with six staples located about 21 nm away from the origami peripheral edges that were

elongated by 21 bp sequences (5X excess). A complementary ssDNA sequence, pre-labeled with ATTO-647N fluorophore (ATTO-TECH) (7X excess). The ATTO-647N labeling was performed on HPLC-purified strand consisting of C6 dT internal amino modifier (IDT), and was purified again (HPLC, reverse-phase C18, Amersham Bioscience) in house.

### B.4.2 Immobilization

To enable coverslip immobilization, origami A+F were introduced with five biotinylated staples, with the biotin facing downward. The avidin-biotin based origami immobilization on the coverslip inside the microfluidics working chamber includes several steps, and between each different material introduction the chamber is washed using assembly buffer (AB, 10 mM Tris, 50 mM NaCl, pH 8.0). First, the working chamber was hydrated using assembly buffer and then biotinylated BSA (1 mg/mL, A8549, Sigma-Aldrich) was introduced with a constant flow rate (0.3 mm/min, which is 12 µl/min, achieved by tuning the channel back pressure to 10 psi) and incubated under a constant flow rate, inside the channel for 15 min followed by a 5-min rinsing with AB buffer. The NeutrAvidin (0.2 mg/mL, ImmunoPure NeutrAvidin Protein, Pierce) was introduced at the same rate as biotinylated BSA, and incubated under constant flow for 15-min followed by 5 min rinsing with AB buffer, completing the working chamber's coverslip surface modification step. The hexamer was dilution to 6 pM in measurement buffer (MB, 10mM Tris, 1mM EDTA, 3mM Trolox, 100 mM NaCl + X mM $MgCl_2$, pH 8.0), incubated for 15 minutes and followed by introduction into the working chamber in a continued flow (0.1 mm/min, which is 4 µl/min, achieved by tuning the channel back pressure to 3 psi) until the desired motor density was achieved, as was verified by live imaging. Finally, the excess origami was rinsed using MB.

### B.4.3 Measurement Setup

The single-molecule total Internal Reflection (smTIRF) experiments were carried out on a home-built optical setup. A 642 nm laser beam ( 1150205, CUBE, Coherent) was aligned into a single-mode fiber (Thorlabs, Newton, NJ) and was collimated, expanded by factor of 4.16X and then focused (achromatic lens 180 mm, Thorlabs AC508-180-A) off-axis on the back aperture of a high numerical aperture oil objective (NA 1.45, 100X, Olympus America) mounted on a commercial inverted microscope (IX71, Olympus America). The

laser intensity, measured before the objective, was 5 mW. The collected fluorescence was separated from the excitation light by a dichroic mirror (ZT532/638RPC, Chroma, Bellows Falls, VT), filtered (ZET 532/642 M, Chroma, Bellows Falls, VT), and the red channel of the emission path was filtered (by band-pass filter 731/137, Semrock, Rochester, NY) and focused on the EMCCD camera (IXON DU-897E, Andor, Belfast, UK) chip. The sample chamber was mounted tightly on the microscope table stage (IXSVL2, Olympus) using slide clips (IX-SCL, Olympus). The stage enabled convenience XY translocation of the sample chamber relative to the field of view so that different locations along the working chamber could be imaged. Fluorescence signal from the upper wall of the working chamber was avoided by illuminating only the first ~100 nm above the coverslip using TIRF.

# Appendix C: Algorithms and Equations

## C.1 Nucraft Generator V1 - Sticky Ends

**Overview**

The NuCraft Generator v1 is a software tool designed to generate a set of sequences for elongated sequences, such as sticky ends. The primary goal is to produce sequences that minimize unintended hybridizations while satisfying specific design constraints, including GC content and sequence uniqueness. The generator has an option for iterative algorithm for additional optimization steps.

**Inputs**

1. A file containing DNA sequences to unmatch against. This list may include all single-stranded sequences from existing origami structure, or it can include also all origami sequences.
2. The total number of new sequences required.
3. The length of each new sequence to be generated.
4. The desired GC content.
5. Maximum length parameters:
    - DBa: The segment length used for initial sequence generation and matching.
    - DBb: The segment length used during the optimization phase (typically DBa minus one).
6. The total number of iterations for the optimization algorithm.

7. The number of sequences to regenerate in each optimization cycle.

**Outputs**

A list of DNA sequences that meet the specified criteria.

**Sequence Generation Algorithm**

1. Prepare exclude List
2. Random sequence generation:
   - Generate a random (with weights for GC content requested) DNA sequence of length L.
3. Sequence Validation:
   - GC Content Verification: Confirm that the total number of G and C nucleotides conforms to the requested GC content.
   - Ensure the sequence does not contain any instances of four consecutive Gs or Cs to prevent the formation of G-quadruplexes.
   - Uniqueness check: compare all possible segments of length DBa within the sequence and its reverse complement against:
     i. The list prepared in step 1.
     ii. All previously accepted sequences.
     iii. The sequence itself (to avoid internal self-complementarity).

     Ensure no matching segments are found in these comparisons.
4. Iteration:
   - Repeat steps 2 and 3 until n unique sequences have been generated and validated.

**Optimization Algorithm**

The optimization phase is optional, and specific for wanted connectivity. It aims to further reduce unintended hybridizations among the generated sequences by refining their composition.

5. Assign Complementary Strands:
   - For each sequence generated in step 4, determine the complementary strands required for intended interactions for the needed connectivity.
6. Add these complementary sequences to the list of sequences for analysis.
7. Cross-Analysis at DBb:
   - Compare all possible segments of length DBb from each sequence in the list (including the original and complementary strands) against the reverse complements of all other sequences in the list.
   - Identify and count all instances where segments matches the reverse complements in other sequences.

- Subtract the number of intended hybridizations (as defined by the design of the DNA nanostructure) from the total number of matching segments to determine the number of unintended hybridizations.

8. Evolutionary Optimization:
   - Randomly select sequences from the list generated in step 4.
   - Regenerate these sequences by repeating the sequence generation and validation steps (steps 2 and 3).
   - Repeat the interaction assessment steps (steps 5 and 6) with the updated sequence list.
   - If the total number of unintended hybridizations decreases as a result of the regeneration, accept the new sequences.
   - If not, revert to the previous sequences.
9. Iteration:
   - Repeat the optimization cycle (steps 7 and 8) for a total of nop iterations or until no further reduction in unintended hybridizations is observed.

## C.2 Thermal Dissociation Rate Constant

The thermal dissociation rate is relevant for multiple parameters in the model, including cat-off, H1-off, H2-off, and (L/F) diss. This rate primarily depends on the GC content and the number of bases in the segment, with almost no effect from salt concentration. The relation used in this thesis is a fitted equation based on experimental data developed by Ralf Jungmann et al.[159].

$$\boldsymbol{K_{off} \approx 2K_{+}(n-N)S^{-(n-N)} = 2 * 10^{7}S^{-1} * (n-3) * 20^{-(n-3)}}$$

$$\boldsymbol{S = \frac{k+}{K-} = \exp\left(-\frac{\Delta G_{bp}}{K_B T}\right) = \exp(3) = 20}$$

| Segment length n [nt] | Rate constant $S^{-1}$ |
|---|---|
| 7 | 500 |
| 8 | 31.25 |
| 9 | 1.875 |
| 10 | 0.1 |
| 11 | 0.006 |

**Table C.1:** Relationship between segment length and its thermal dissociation rate.

## C.3 Strand Displacement Rate Constant

The displacement rate is largely insensitive to monovalent salt. D. W. Bo Broadwater et al. [160] developed the following relationship based on a one-dimensional random walk model, fitted with parameters obtained from the fission assay, which measured the first passage time.

$$\tau = \frac{1}{2K} n\left(n + \frac{2}{s} - 1\right), s = \frac{1}{30}, rate = \frac{1}{\tau}$$

| Segment length n [nt] | Mean first passage [ms] | Rate constant $S^{-1}$ |
|---|---|---|
| 24 | 68 | 14.55 |
| 16 | 40 | 24.15 |
| 12 | 35 | 34.02 |
| 8 | 18 | 54.08 |

**Table C.2:** Relationship between segment length and its strand displacement rate.

## C.4 Autonomous Mechanism Reaction Details

**Hairpins transient binding**

The bimolecular association rate constant used is, $Aon = 6.6 \cdot 10^8\ M^{-1} \cdot S^{-1}$. The initial concentration of the two hairpins is determined independently by the fine-tuned within the range of $10nM \leq [H_1] \leq 50\mu M$, $10nM \leq [H_2] \leq 50\mu M$. The resulting H1-H2 complex dissociates thermally, with the dissociation rate depending on segment length, which is also fine-tuned within the range of $0.1S^{-1}(10nt) \leq H_2 - off \leq 500S^{-1}(7nt)$, see Appendix C.2 for relation between rate and segment length used.

This reaction reaches equilibrium before interacting with the walker, as the hairpins are mixed externally and only introduced to the immobilized walkers after reaching equilibrium. To simulate this behavior, an additional parameter, multi = 1000, is applied to both reactions to ensure that equilibrium is achieved within 2 seconds. The initial population of the walker's state 1 is then introduced via an event at time = 3 seconds.

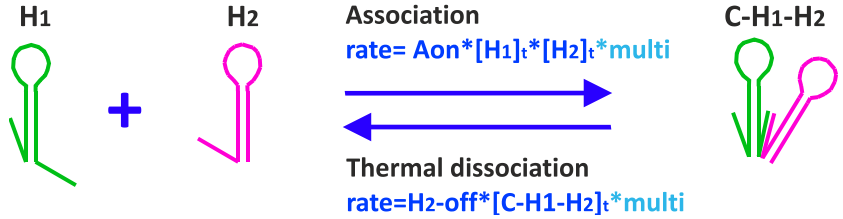


Figure C.3: Hairpins transient binding.

**Catalyst transient binding with leg extension**

The first species, 'S01', is set with the entire initial population at time t = 3 seconds, with a concentration of 20 nM. The exact concentration is not critical, as the molecule is fixed to the surface. The exact concentration can be used for normalization, allowing the percentage of each state to be calculated. The catalyst association constant is non-trivial, as it depends on the geometry of the structure attaching it to the upper disc. For the simulation, of $Kcat - on$ was assumed to be similar to that of leg placement during external controlled rotor walking, which is $0.07\,S^{-1}$. To account for worse-case scenarios, each test was also checked with a reduced value of $Kcat - on = 0.014\,S^{-1}$ (20% of the original rate).

For simplicity, the of $Kcat - off$ was set equal to the thermal dissociation rate, assuming no effect from the catalyst's fixation structure. This value was fine-tuned within the range of $0.1S^{-1}(10nt) \leq K_{cat} - off \leq 500S^{-1}(7nt)$.

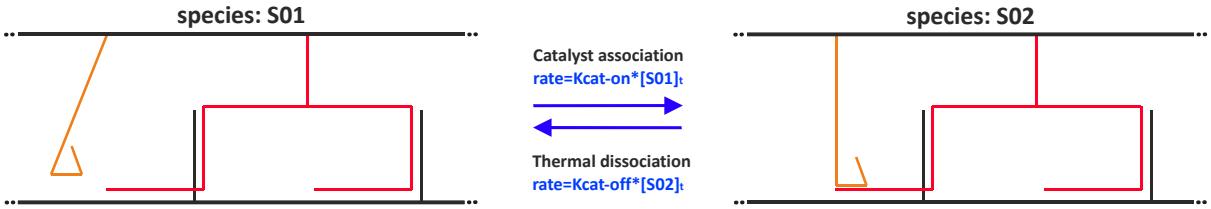

Figure C.4: Catalyst transient binding with leg extension.

**H1 transient binding with catalyst**

H1 association is considered a pseudo-first-order reaction because the walker is fixed to the surface, and the counts of hairpins is much higher, leading to the assumption that the hairpin concentration remains unaffected. This allows the hairpin concentration to be included in the reaction constant. When the sequences are free from secondary structure, as intended in the design, the association rate constant is typically measured to be in the range of $1 - 5 \cdot 10^6 M^{-1}S^{-1}$ (as reported by Hetel, S. et al.[101]). For our purposes, we used $H_1 - on = 2 \cdot 10^6 M^{-1}S^{-1}$. Additionally, tests were also conducted using $H_1 - on = 1 \cdot 10^5 M^{-1}S^{-1}$ to account for worse-case scenarios such as the influence of different salt concentrations, residual secondary structure, or interactions with the DNA origami.

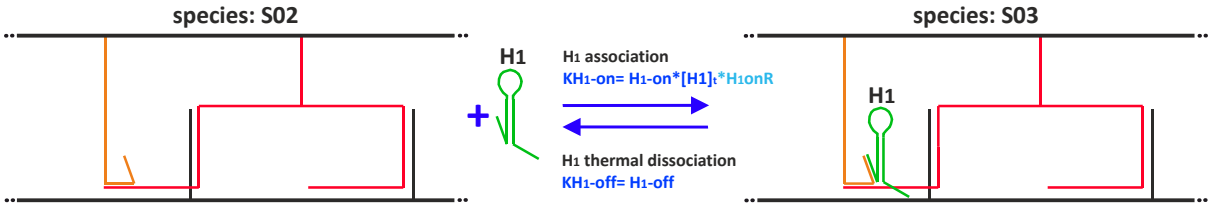

Figure C.5: H1 transient binding with catalyst.

Without the inter-domain bridging motif, the association rate ratio $H_1onR = 1$. However, with the bridging motif in place, the effective binding that allows further reaction is halved due to equal competition between reactions. This results in $H1onR = 0.5$, assuming fast equilibrium. This adjustment was made to avoid explicitly including this reaction in the full model.

Due to this competition, the thermal dissociation rate constant, $H_1 - off$, is also affected. For simplicity, it was assumed to be the weighted average of 0.5 × (dissociation rate for n bases) + 0.5 × (dissociation rate for n + idb bases), where idb represents the inter-domain bridging. The idb was tested for values of 1 and 2 bases.

For the case $idb = 1nt$, the length n, was fine-tuned within the range of $7nt \leq n \leq 10nt$ , for the case $idb = 2nt$, the length n, was fine-tuned within the range of $7nt \leq n \leq 9nt$.

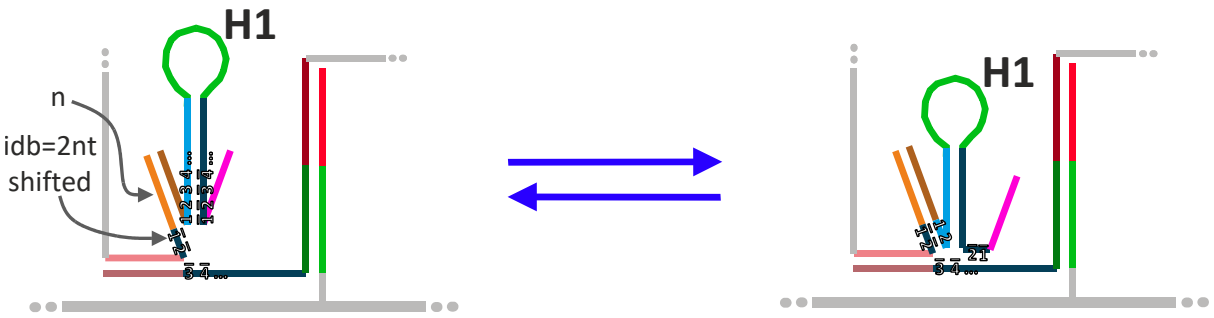

Figure C.6: Reaction Resulting from Implementing Interdomain Bridging Motif.

**H1 opening 1**

Assuming regular toehold-mediated strand displacement, the rate constant for strand displacement is $H1open1 = 24\ S^{-1}$, which corresponds to a displacement length of 16 nucleotides, based on the equation developed by Broadwater, DWB. et al. [160]. See Appendix C.3 for the equation used.

However, the associated toehold binding is slower, with a reduction ratio of $H1open1R = 0.015$, as reported by Xi Chen [105], when coaxial stacking is implemented, which is also a feature in the design here. Additionally, the displacement is influenced by the mismatch

elimination at position 4, which I estimate would boost the rate by a factor of 45, based on reports by Haley, NEC. et al. [107], resulting in a final value of $H1open1R = 0.675$.

As for the reverse reaction, which can be described as loop-mediated strand displacement, no direct data was found. Here, it is estimated to be approximately 5 times slower than the opening reaction, giving a value of $\beta_1 = 5$.

In the optional modification case where, inner hairpins have a mismatch at position 4 (see Section 4.4.6, Figure 4.12A), the mismatch affects the reversal reaction by creating a proximal mismatch. Thus, I estimate it slows the reaction rate constant by a factor of 10, based on reports by Machinek et al. [106], resulting in a final value of $\beta_1 = 50$.

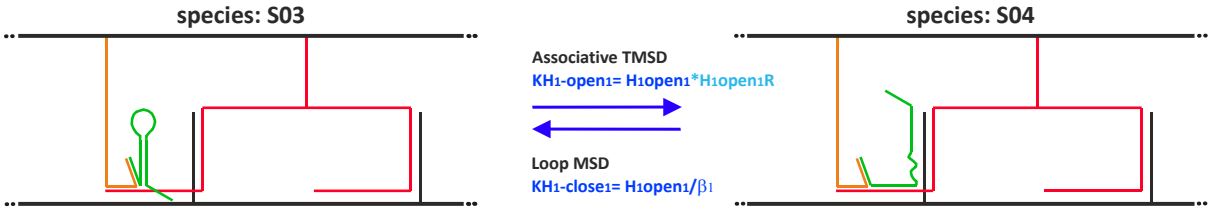

Figure C.7: First opening of H1.

**H1 opening 2**

The loop domain from H1 can displace a portion of the leg from the foothold. For an 8-nucleotide segment, the regular forward rate constant is $H1open2 = 54\ S^{-1}$ with ratio $H1open2R = 1$. While this length may vary slightly, such variations were not factored into the rate constant for simplicity.

The reverse reaction, without any modifications, should be equal to the unmodified forward rate, meaning $H1open2 = 54\ S^{-1}$, resulting in $\beta_3 = 1$.

In the optional modification case where, lower portion of leg/foothold have a mismatch at position 4 (see Section 4.4.6, Figure 4.12B), $H1open2R = 45$ (proximal mismatch elimination), $\beta_3 = 10$ (proximal mismatch creation).

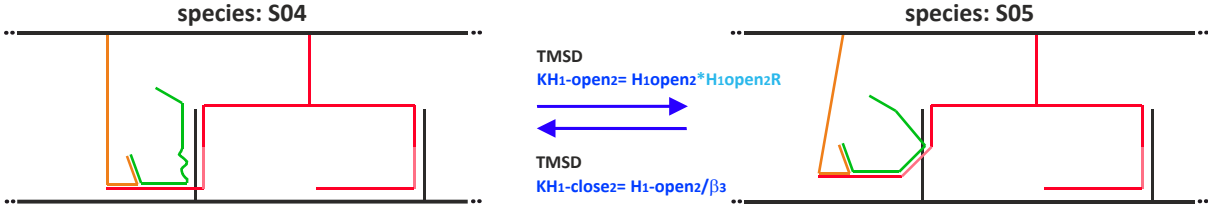

Figure C.8: second opening of H1.

**Leg thermal dissociation**

The remaining portion leg/foothold potion can be thermally dissociated, the exact length is pick by the fine tuning within the values $0.1S^{-1}(10nt) \leq (L/F)diss \leq 500S^{-1}(7nt)$.

The leg association rate constant was assumed to be $(L/F)asso = 0.07\ S^{-1}$, equal to leg placement for externally controlled rotor based bipedal walker.

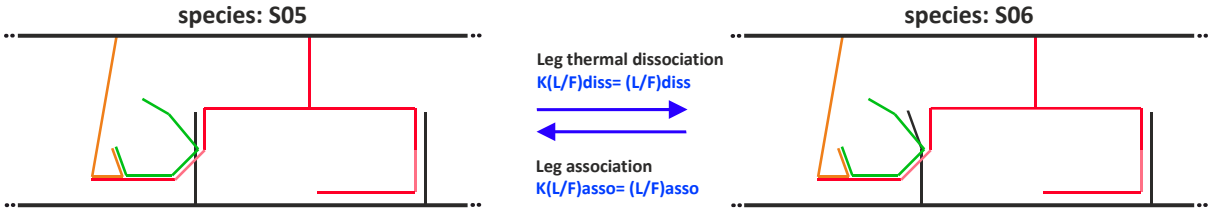


Figure C.9: Leg thermal dissociation.

**Upper rotor disc movement**

When one leg is fully detached from the foothold according to the model, the upper disc becomes free to move to a state where the lifted leg cannot reach the previous foothold. This state was defined to simplify the model; otherwise, it would be necessary to account for a larger number of angular states, each with different leg placement rates depending on the geometry.

To maintain this simplification, the bias parameter $\gamma_1$ was adjusted. Instead of reflecting the actual positional bias towards the forward position—which is about 20 times higher—value was set, $\gamma_1 = 1$ , to represent the actual probability of leg placement. This means that the leg placement rate when the leg is exactly above the foothold was considered equal to the experimentally measured externally controlled walking leg placement rate of $0.07\ S^{-1}$ . Leg placements from other positions were not accounted for, so the bias towards these positions is about 1, aligning with the actual rotor behavior.

The rate constant of movement out of positions is represented by Rr1-on, which was not measured directly in the externally controlled rotor system; instead, it was measured in combination with leg lifting via antifuel. Although the leg lifting rate itself was not measured independently, Rr1 can be estimated to be $0.2\ S^{-1}$. For worst-case scenarios, $\mathrm{Rr} = 0.135\ S^{-1}$. In the simulations, both values were tested.

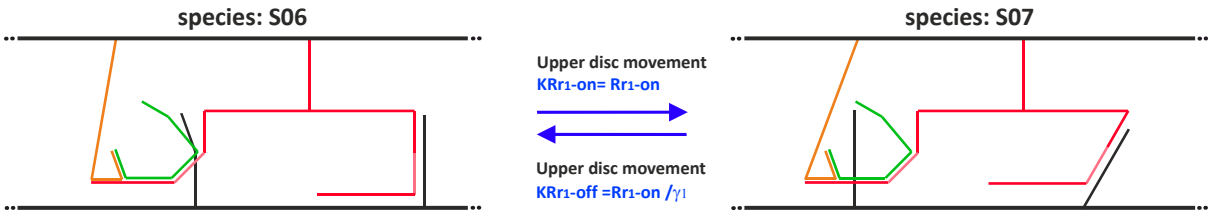

Figure C.10: Upper rotor disc movement.

**H2 transient binding with H1**

At any point, the second hairpin can transiently bind to H1, with the forward reaction following pseudo-first-order kinetics. The reaction constant for this process is $H_2 - on = H_1 - on$. All other parameters are described earlier.

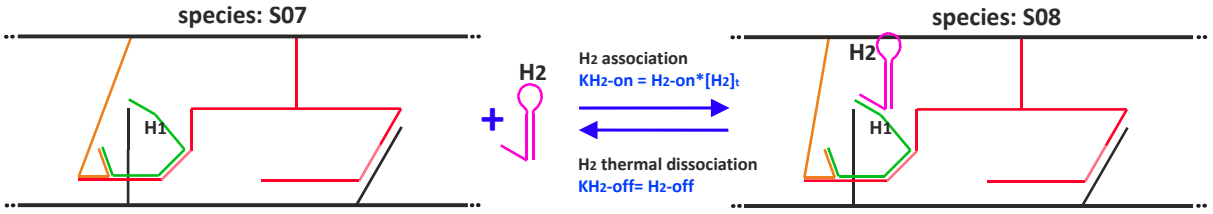

Figure C.11: H2 transient binding with H1.

**H2 opening 1**

Assuming regular toehold-mediated strand displacement, the rate constant for strand displacement is $H2open1 = 24\ S^{-1}$ $(H2open1R = 1)$, which corresponds to a displacement length of 16 nucleotides (stem's intended length).

However, the base case the forward reaction was modified to slight remote toehold, reducing the rate by $H2open1R = 0.2$ (see details motif in Section 4.4.2).

$\beta_2 = \beta_1 = 5$ for similar considerations. $\beta_2 = 50$, in the optional modification case where, inner hairpins have a mismatch at position 4 (see Section 4.4.6, Figure 4.12A).

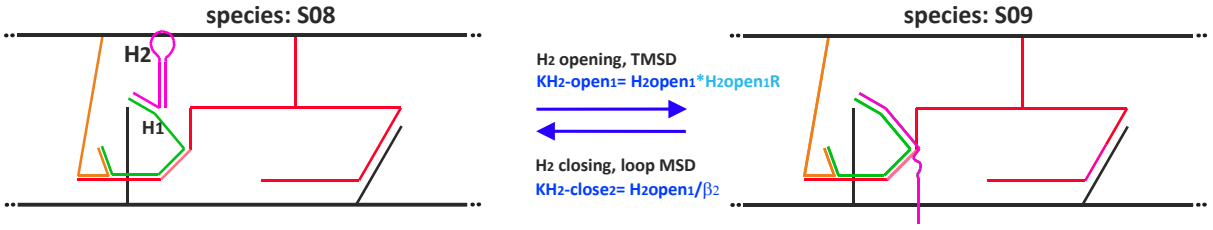

Figure C.12: First opening of H2.

## H2 opening 2

Assuming regular toehold-mediated strand displacement, the rate constant for strand displacement is $H2open2 = 14\ S^{-1}$ $(H2open2R = 1)$, which corresponds to a displacement length of 24 nucleotides (stem's intended length 16 + loop's intended length 8). The reversal reaction depends on the association motif, meaning $\beta_4 = \frac{1}{0.015} = 66$.

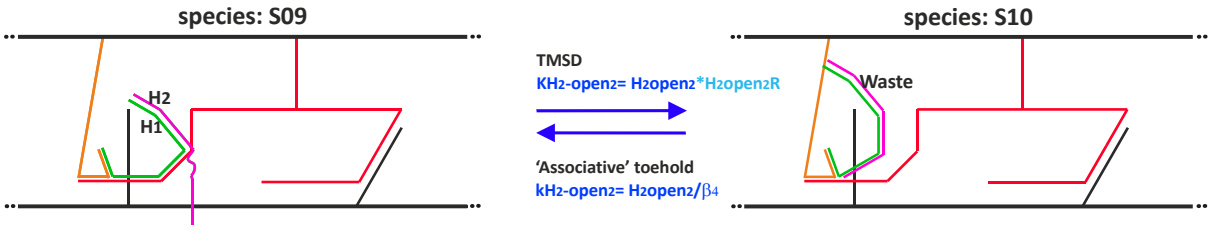


Figure C.13: Second opening of H2.

## Waste thermal dissociation

Due to the decision to delete the last two bases from H2 (see Section 4.4.2), the thermal dissociation of the waste complex now corresponds to the thermal dissociation of the segment with length n + idb (inter-domain bridging). Based on the model assumptions, the reversal reaction cannot occur.

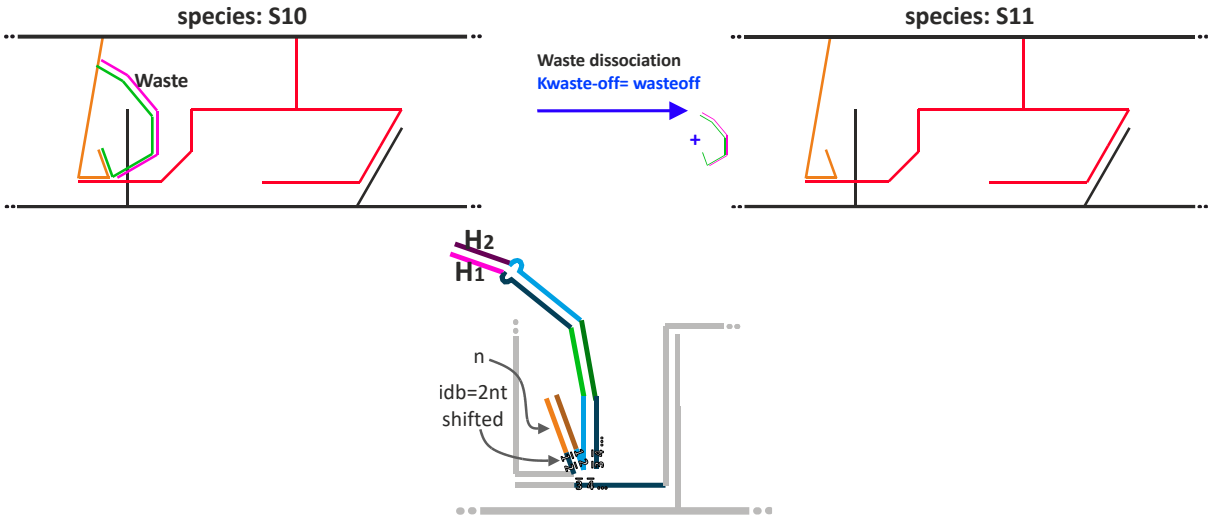


Figure C.14: Waste molecule thermal dissociation.

**Upper rotor disc movement**

The upper rotor can rotate from the 'middle' state into the forward position, with no bias toward either state, as $\gamma_2 = 1$, similar to the previously discussed $\gamma_1$, due to the model-defined states. For simplicity, the rate constant of this movement can be assumed to be equal to that of the previous movement, i.e., Rr2 = Rr1.

The placement of the leading leg here is equal to $(L/F)asso$, owing to the symmetry with the previously discussed leg placement.

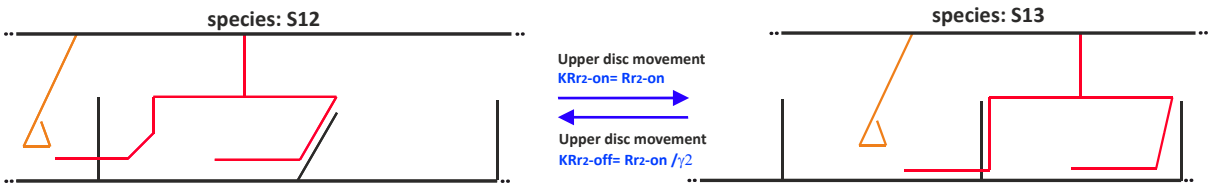

Figure C.15: Upper rotor disc movement.

# Appendix D: Additional Data

## D.1 Worm Like Chain Fitting - Hexamer

The middle population grew as magnesium concentration increased, which decreased the accuracy of the automatic model fitting. To improve the WLC fitting accuracy and lessen the middle peaks effect, either the minimum persistence length or the maximum contour length was restricted manually see Figure D.1. The yield calculated by the fitting is based on counts of spots, is converted to mass count (amount of trimer is hexamer structure), vie the equation, 2*x/(2*x+100%-x), x is hexamers counts yields.

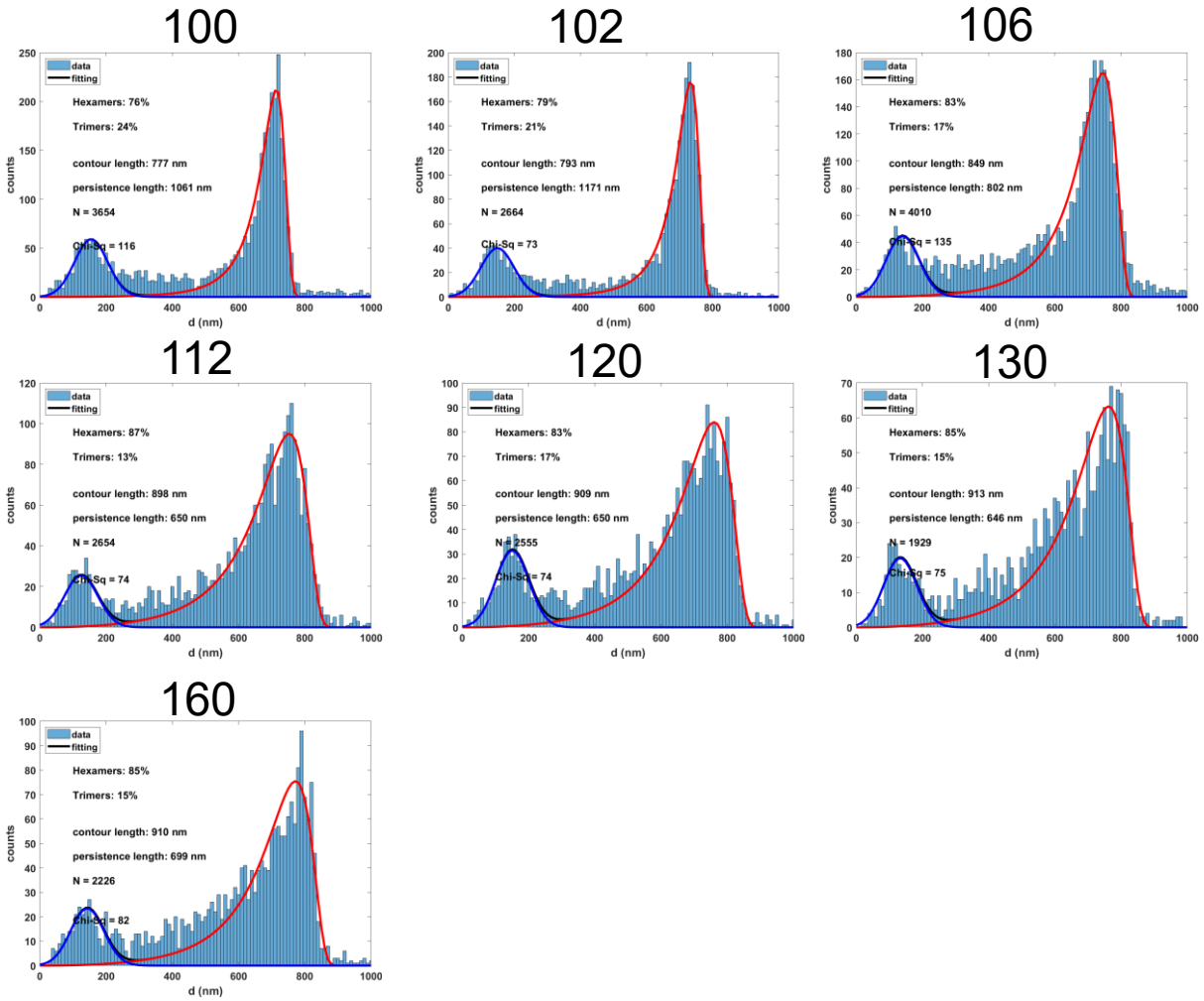


**Figure D.1: Worm-like chain fitting for the hexamer.** Length distribution histogram, based on the distances between dot pairs across different salt conditions. At each histogram shorter distances are attributed to trimers, while longer distances correspond to hexamers. "titile120" refers to 100 mM NaCl + 20 mM $MgCl_2$.

## D.2 Tiles Homodimerization

**Table D.1: Summary of non-monomeric yields.** (%is mass percentage)

| Monomer type | Sticky-end type | Salt [mM] $Mg^{2+}$ | Non-monomeric yields |
|---|---|---|---|
| F | Nucraft | Titration to 12 | 6.3% |
| F | Nucraft | 4 | 0.9% |
| F | Random | Titration to 12 | 41.7% |
| F | Random | 4 | 10.7% |
| B (lapeled P) | Nucraft | Titration to 12 | 23.2% |
| B (lapeled P) | Nucraft | 4 | 17.2% |
| B (lapeled P) | Random | Titration to 12 | 59.6% |
| B (lapeled P) | Random | 4 | 14.0% |

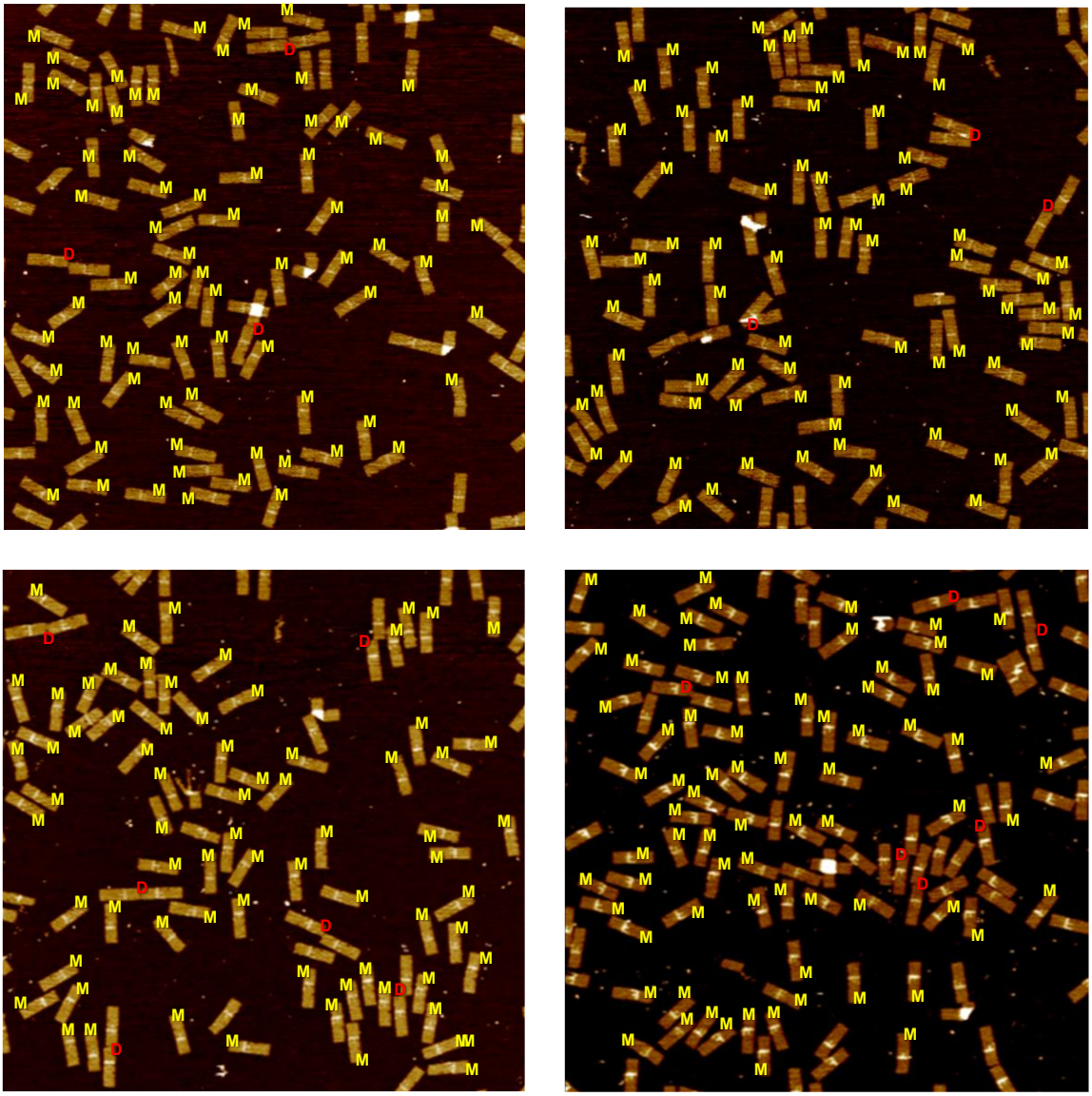

**Figure D.2: AFM images of F monomer after PEG purification.** At 4mM $Mg^{2+}$, randomly generated Sticky ends. The non-monomeric yield is 10.7% (units count is 336).

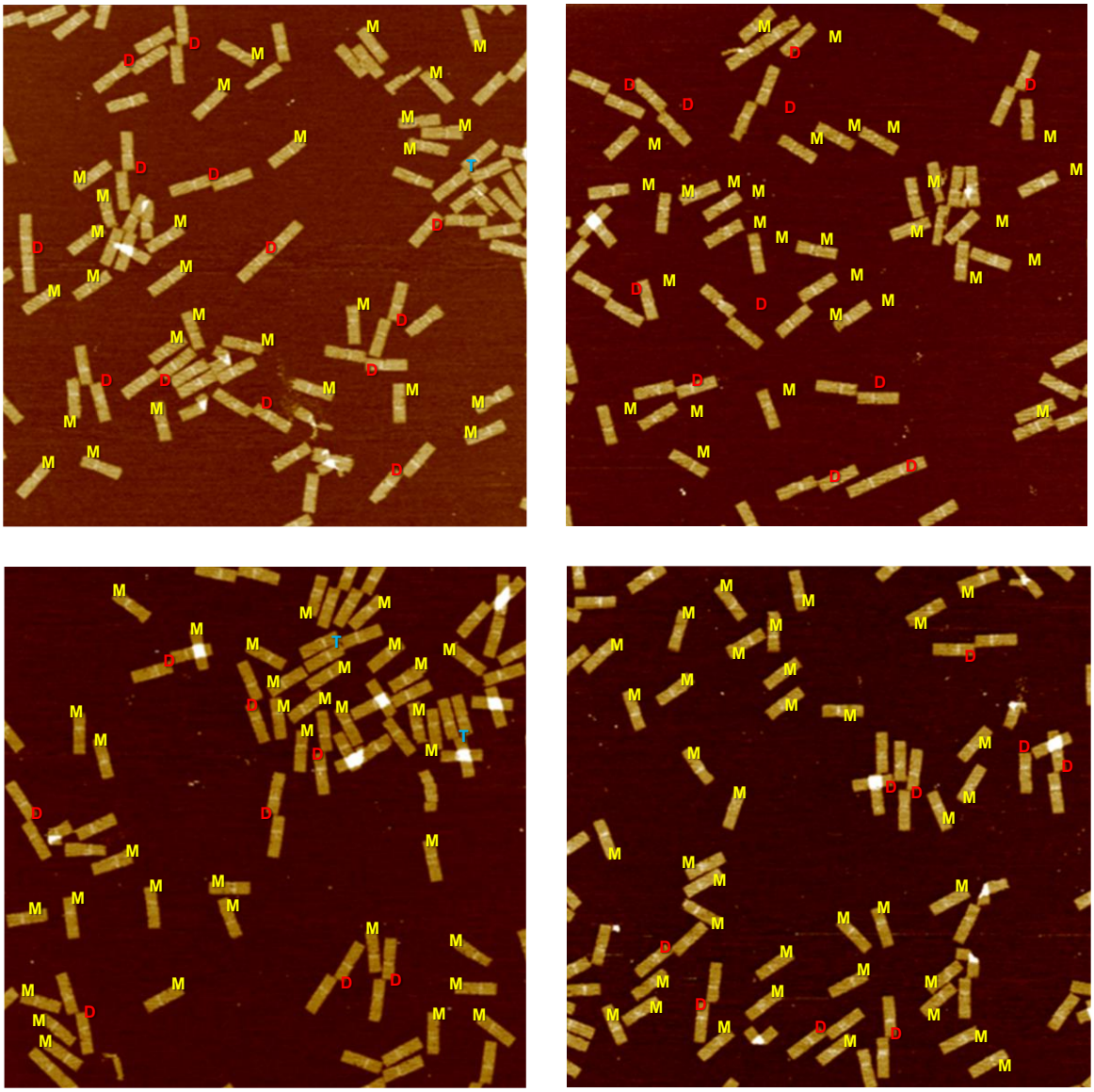

**Figure D.3: AFM images of F monomer after PEG purification.** Titration to 12mM $Mg^{2+}$, randomly generated Sticky ends. The non-monomeric yield is 41.7% (units count is 218).

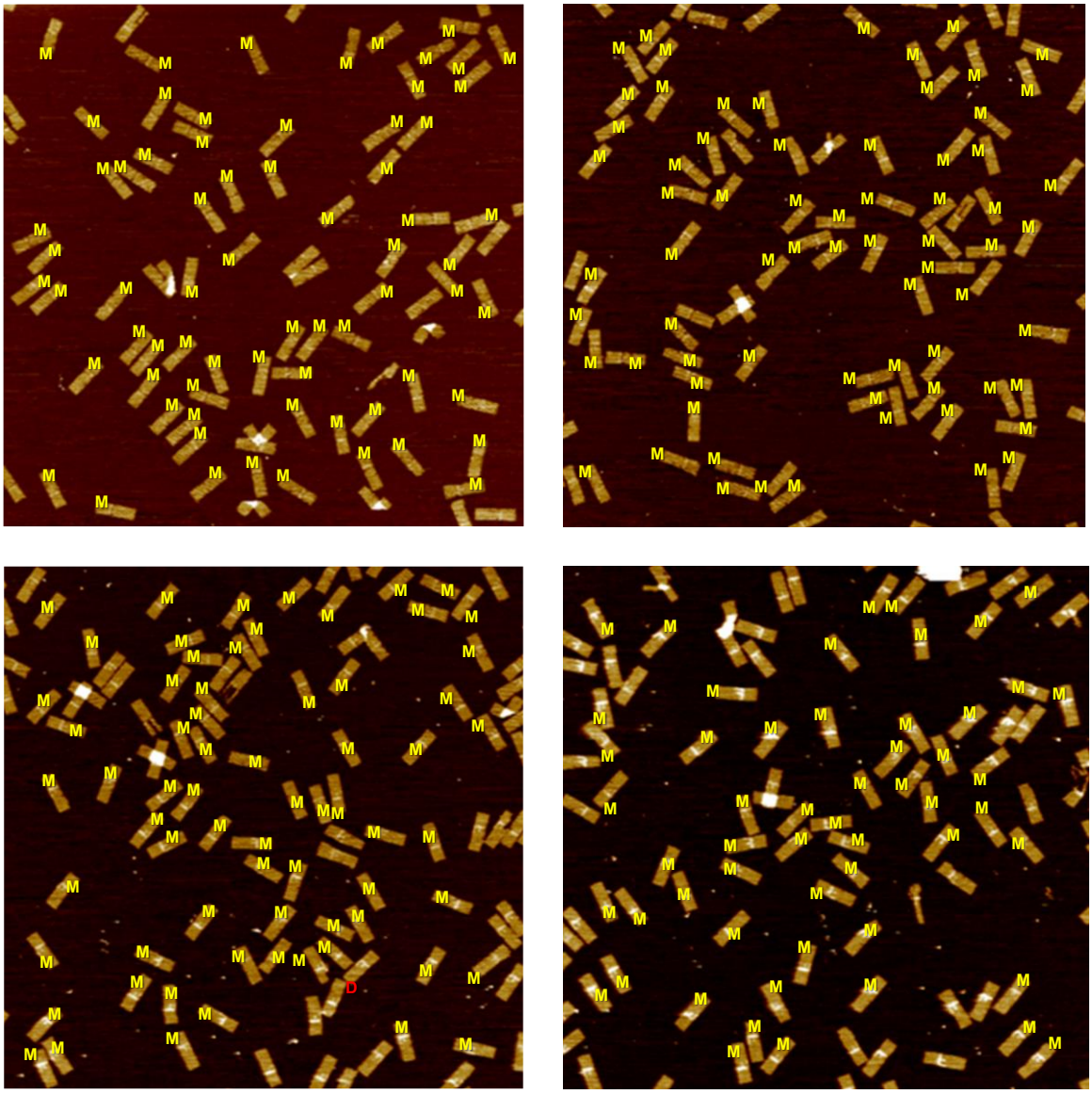

**Figure D.4: AFM images of F monomer after PEG purification.** At 4mM $Mg^{2+}$, Narcos generated Sticky ends. The non-monomeric yield is 0.9% (units count is 218).

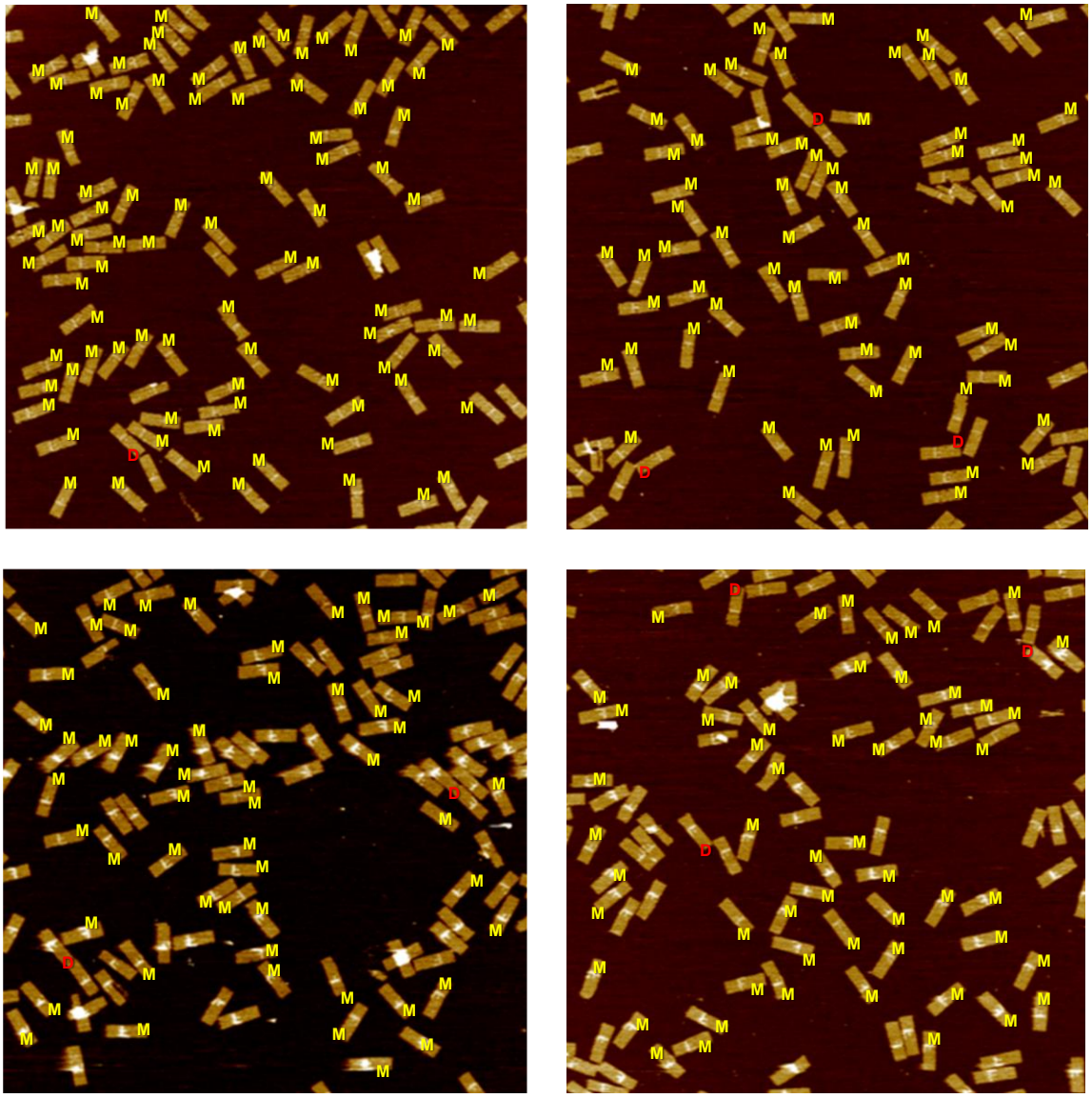

**Figure D.5: AFM images of F monomer after PEG purification.** Titration to 12mM $Mg^{2+}$, Narcos generated Sticky ends. The non-monomeric yield is 6.3% (units count is 285).

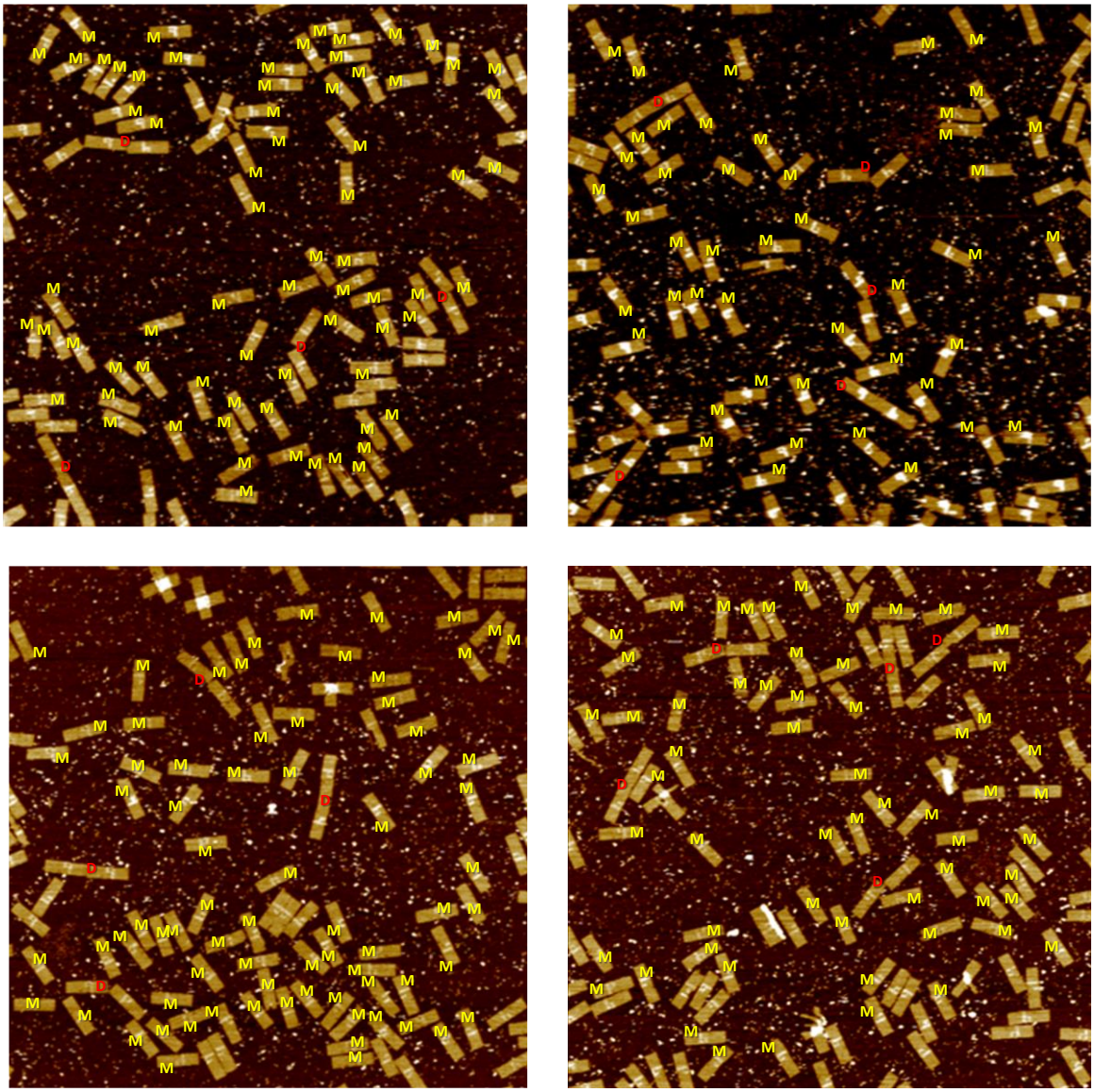

**Figure D.6: AFM images of B monomer after PEG purification.** At 4 mM $Mg^{2+}$, random generated Sticky ends. The non-monomeric yield is 14.0% (units count is 258).

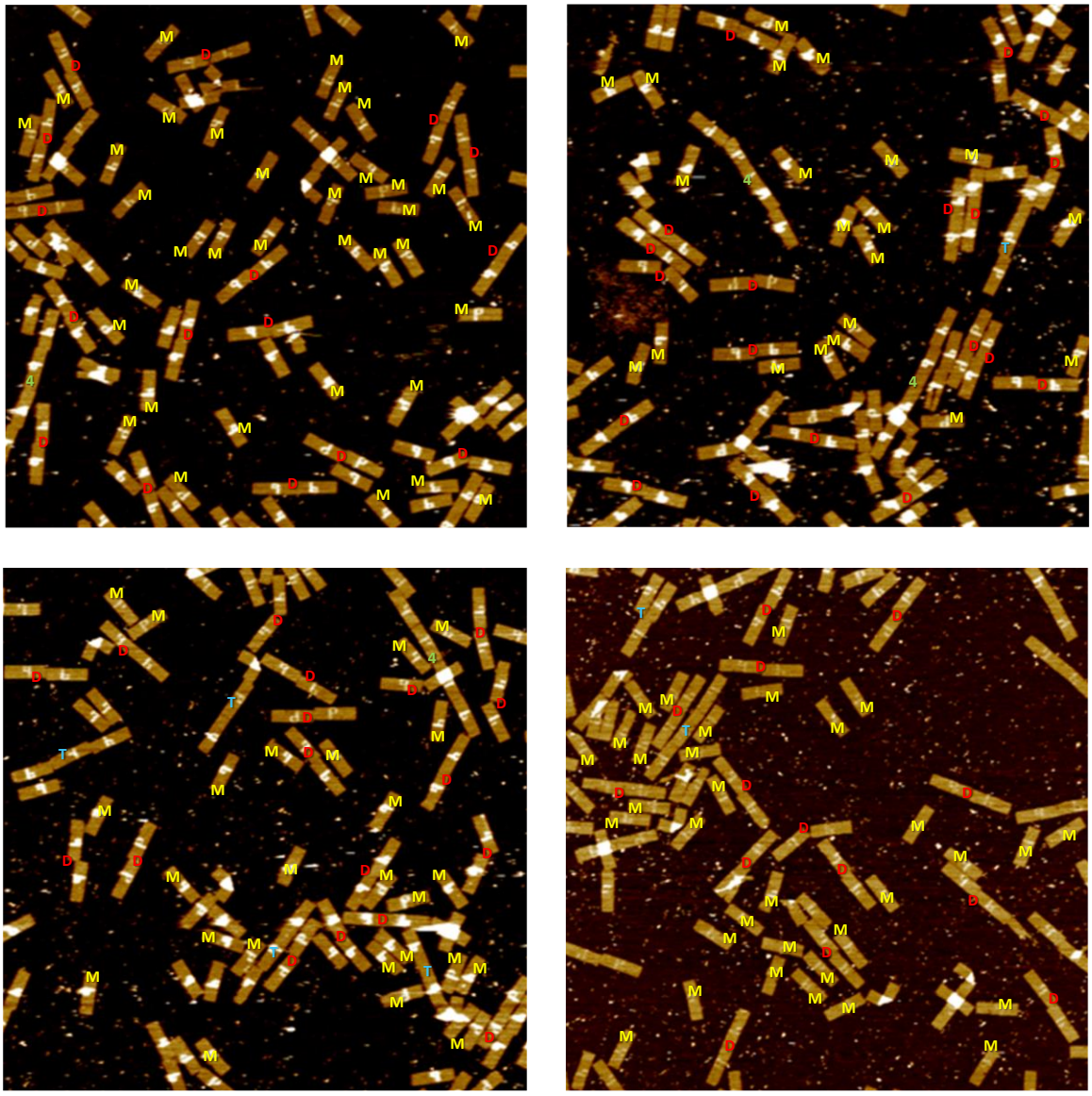

**Figure D.7: AFM images of B monomer after PEG purification**. Titration to 12mM $Mg^{2+}$, random generated Sticky ends. The non-monomeric yield is 59.6% (units count is 275).

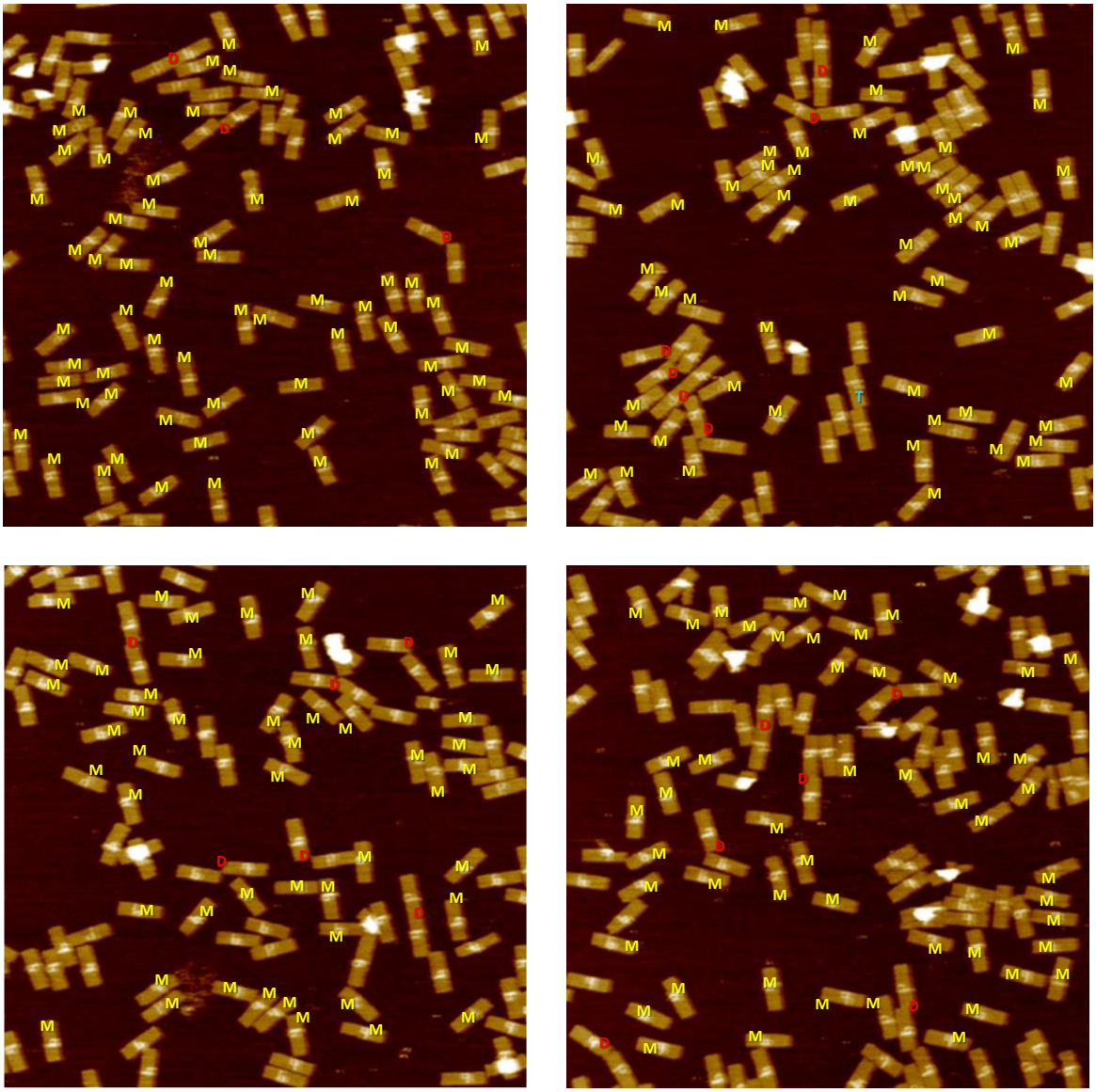

**Figure D.8: AFM images of B monomer after PEG purification.** 4mM $Mg^{2+}$, Narcos generated Sticky ends. The non-monomeric yield is 17.2% (units count is 262).

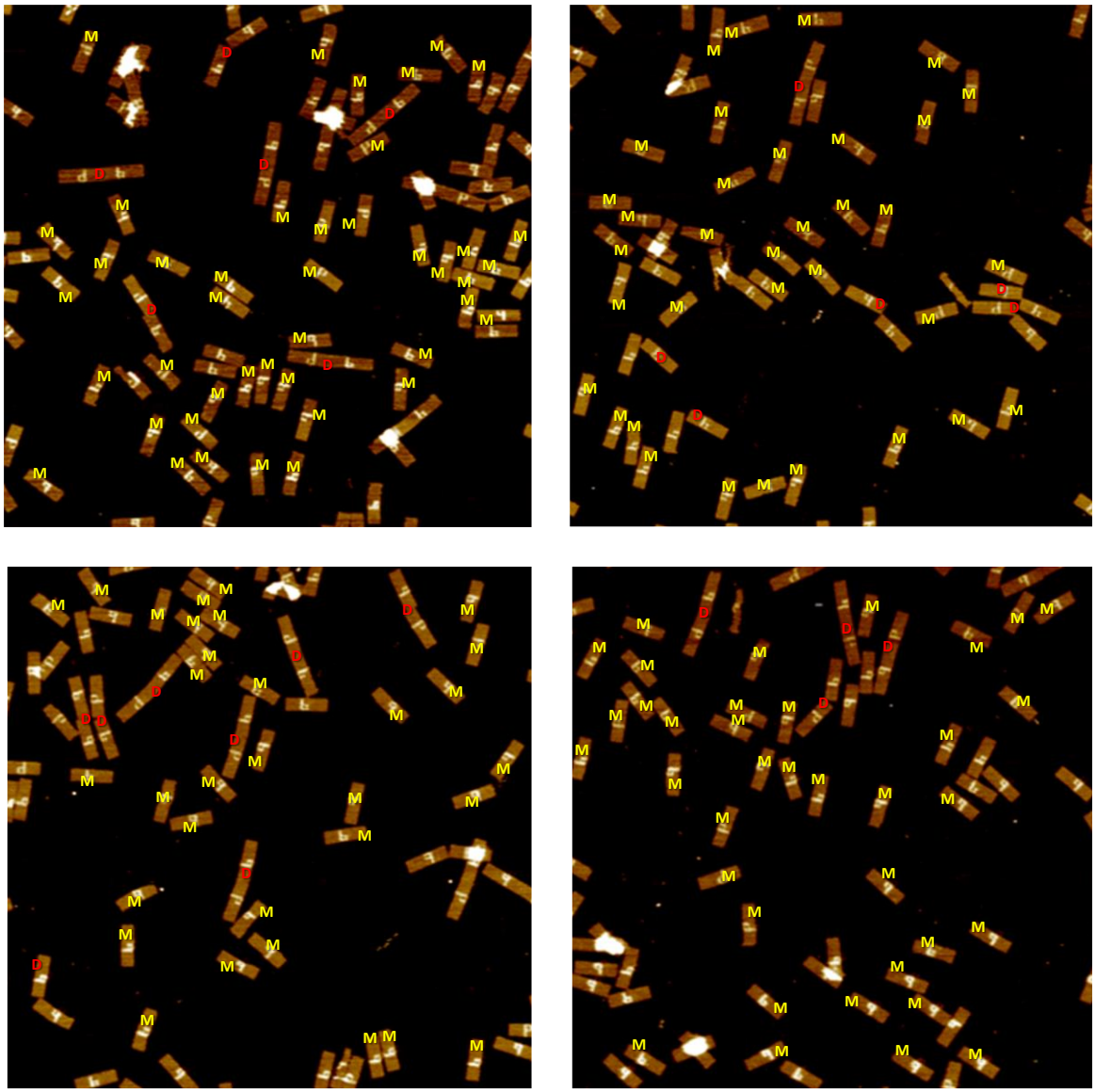

**Figure D.9: AFM images of B monomer after PEG purification.** Titration to 12mM $Mg^{2+}$, Narcos generated Sticky ends. The non-monomeric yield is 23.2% (units count is 189).

## D.3 Hexamer AFM

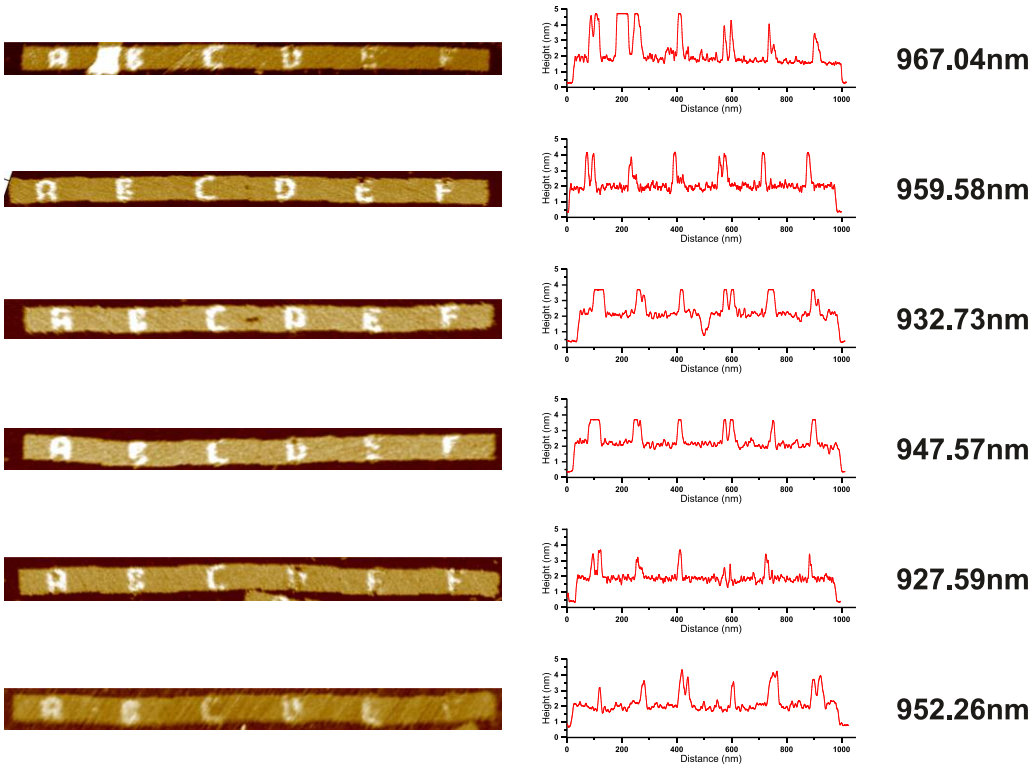


**Figure D.10:AFM images of selected hexamers.** That are laid straight on mica for measuring the stretched end-to-end distance.

## D.4 Hexamer AFM Counting – NuCraft SE

**Table D.2:** Summary of AFM hexamer for yield.

| Structure type | Count | Mass | Yield (mass %) |
|---|---|---|---|
| Monomer | 3 | 3 | 0.04% |
| Dimer | 58 | 116 | 1.46% |
| Trimer | 186 | 558 | 6.8% |
| Hexamer | 1251 | 7506 | 91.7% ± 0.9% |

Error is calculated by dividing the data to 3 sub data and standard deviation the 3-sets.

The counts were based of the following images:

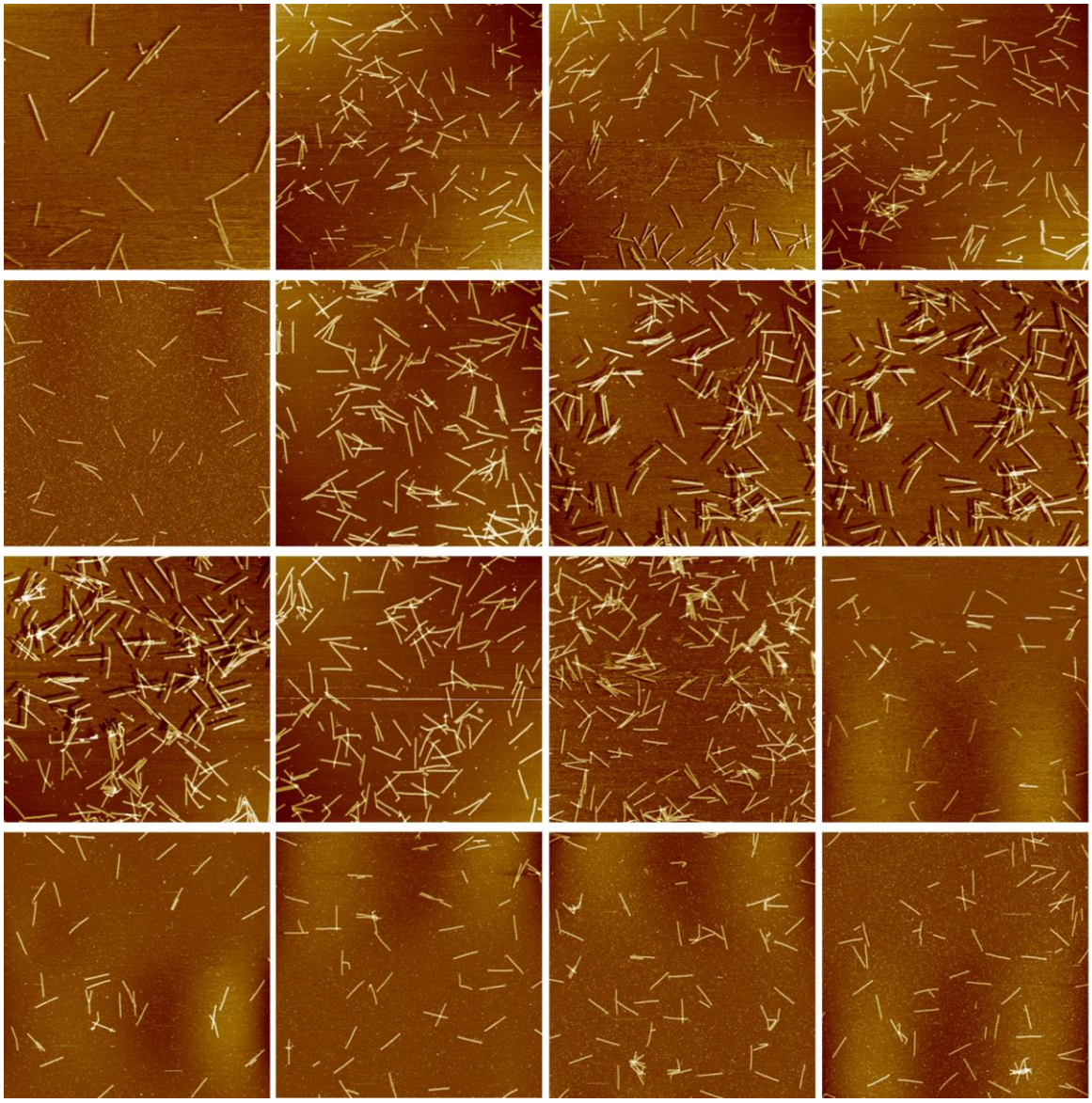

**Figure D.11:** AFM images of hexamer of Nucraft sticky ends, for yield calculations.

## D.5 Hexamers Buckling

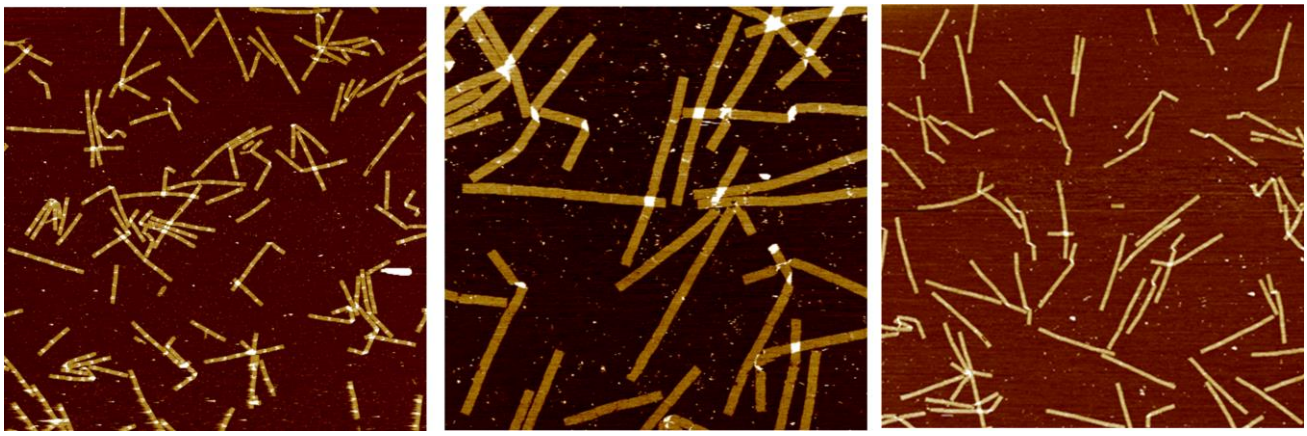

**Figure D.12:** AFM images of hexamers for buckling inspection.

# Appendix E: Sequences

## E.1 Tile

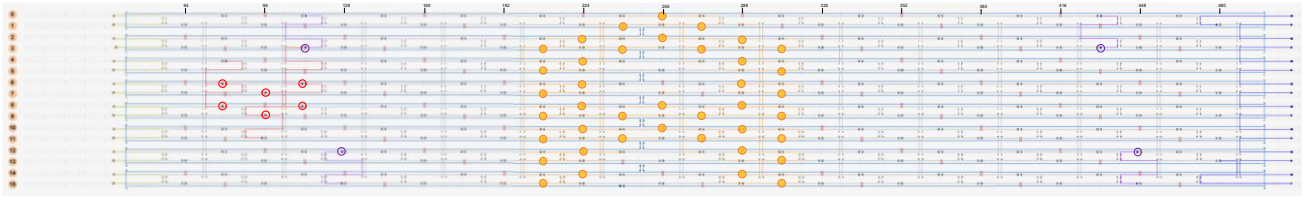

**Figure E.1: Example Tile cadnano, a A-origami.** Green staples represent passivation strands with 5T overhangs. Blue staples indicate SE staples. Red marks highlight possible extensions of staples that can hybridize with ATTO 647N-labeled strands. Purple marks show staples that can be replaced with biotinylated staples. Orange marks denote staples that can be replaced with staples containing dumbbell hairpins.

### Scaffold p7249

AAAATTATTATTCGCAATTCCTTTAGTTGTTCCTTTCTATTCTCACTCCGCTGAAACTGTTGAAAGTTGTTTAGCAAAATCCCATACAGAAAATTCATTTACTAACGTCTGGAAAGACGACAAAACTTTAGATCGTTACGCTAACTATGA
GGGCTGTCTGTGGAATGCTACAGGCGTTGTAGTTTGTACTGGTGACGAAACTCAGTGTTACGGTACATGGGTTCCTATTGGGCTTGCTATCCCTGAAAATGAGGGTGGTGGCTCTGAGGGTGGCGGTTCTGAGGGTGGCGGTTCTGAGGG
TGGCGGTACTAAACCTCCTGAGTACGGTGATACACCTATTCCGGGCTATACTTATATCAACCCTCTCGACGGCACTTATCCGCCTGGTACTGAGCAAAACCCCGCTAATCCTAATCCTTCTCTTGAGGAGTCTCAGCCTCTTAATACTTT
CATGTTTCAGAATAATAGGTTCCGAAATAGGCAGGGGGCATTAACTGTTTATACGGGCACTGTTACTCAAGGCACTGACCCCGTTAAAACTTATTACCAGTACACTCCTGTATCATCAAAAGCCATGTATGACGCTTACTGGAACGGTAA
ATTCAGAGACTGCGCTTTCCATTCTGGCTTTAATGAGGATTTATTTGTTTGTGAATATCAAGGCCAATCGTCTGACCTGCCTCAACCTCCTGTCAATGCTGGCGGCGGCTCTGGTGGTGGTTCTGGTGGCGGCTCTGAGGGTGGTGGCTC
TGAGGGTGGCGGTTCTGAGGGTGGCGGCTCTGAGGGAGGCGGTTCCGGTGGTGGCTCTGGTTCCGGTGATTTTGATTATGAAAAGATGGCAAACGCTAATAAGGGGGCTATGACCGAAAATGCCGATGAAAACGCGCTACAGTCTGACGC
TAAAGGCAAACTTGATTCTGTCGCTACTGATTACGGTGCTGCTATCGATGGTTTCATTGGTGACGTTTCCGGCCTTGCTAATGGTAATGGTGCTACTGGTGATTTTGCTGGCTCTAATTCCCAAATGGCTCAAGTCGGTGACGGTGATAA
TTCACCTTTAATGAATAATTTCCGTCAATATTTACCTTCCCTCCCTCAATCGGTTGAATGTCGCCCTTTTGTCTTTGGCGCTGGTAAACCATATGAATTTTCTATTGATTGTGACAAAATAAACTTATTCCGTGGTGTCTTTGCGTTTCT
TTTATATGTTGCCACCTTTATGTATGTATTTTCTACGTTTGCTAACATACTGCGTAATAAGGAGTCTTAATCATGCCAGTTCTTTTGGGTATTCCGTTATTATTGCGTTTCCTCGGTTTCCTTCTGGTAACTTTGTTCGGCTATCTGCTT
ACTTTTCTTAAAAAGGGCTTCGGTAAGATAGCTATTGCTATTTCATTGTTTCTTGCTCTTATTATTGGGCTTAACTCAATTCTTGTGGGTTATCTCTCTGATATTAGCGCTCAATTACCCTCTGACTTTGTTCAGGGTGTTCAGTTAATT
CTCCCGTCTAATGCGCTTCCCTGTTTTTATGTTATTCTCTCTGTAAAGGCTGCTATTTTCATTTTTGACGTTAAACAAAAAATCGTTTCTTATTTGGATTGGGATAAATAATATGGCTGTTTATTTTGTAACTGGCAAATTAGGCTCTGG
AAAGACGCTCGTTAGCGTTGGTAAGATTCAGGATAAAATTGTAGCTGGGTGCAAAATAGCAACTAATCTTGATTTAAGGCTTCAAAACCTCCCGCAAGTCGGGAGGTTCGCTAAAACGCCTCGCGTTCTTAGAATACCGGATAAGCCTTC
TATATCTGATTTGCTTGCTATTGGGCGCGGTAATGATTCCTACGATGAAAATAAAAACGGCTTGCTTGTTCTCGATGAGTGCGGTACTTGGTTTAATACCCGTTCTTGGAATGATAAGGAAAGACAGCCGATTATTGATTGGTTTCTACA
TGCTCGTAAATTAGGATGGGATATTATTTTTCTTGTTCAGGACTTATCTATTGTTGATAAACAGGCGCGTTCTGCATTAGCTGAACATGTTGTTTATTGTCGTCGTCTGGACAGAATTACTTTACCTTTTGTCGGTACTTTATATTCTCT
TATTACTGGCTCGAAAATGCCTCTGCCTAAATTACATGTTGGCGTTGTTAAATATGGCGATTCTCAATTAAGCCCTACTGTTGAGCGTTGGCTTTATACTGGTAAGAATTTGTATAACGCATATGATACTAAACAGGCTTTTTCTAGTAA
TTATGATTCCGGTGTTTATTCTTATTTAACGCCTTATTTATCACACGGTCGGTATTTCAAACCATTAAATTTAGGTCAGAAGATGAAATTAACTAAAATATATTTGAAAAAGTTTTCTCGCGTTCTTTGTCTTGCGATTGGATTTGCATC
AGCATTTACATATAGTTATATAACCCAACCTAAGCCGGAGGTTAAAAAGGTAGTCTCTCAGACCTATGATTTTGATAAATTCACTATTGACTCTTCTCAGCGTCTTAATCTAAGCTATCGCTATGTTTTCAAGGATTCTAAGGGAAAATT
AATTAATAGCGACGATTTACAGAAGCAAGGTTATTCACTCACATATATTGATTTATGTACTGTTTCCATTAAAAAAGGTAATTCAAATGAAATTGTTAAATGTAATTAATTTTGTTTTCTTGATGTTTGTTTCATCATCTTCTTTTGCTC
AGGTAATTGAAATGAATAATTCGCCTCTGCGCGATTTTGTAACTTGGTATTCAAAGCAATCAGGCGAATCCGTTATTGTTTCTCCCGATGTAAAAGGTACTGTTACTGTATATTCATCTGACGTTAAACCTGAAAATCTACGCAATTTCT
TTATTTCTGTTTTACGTGCAAATAATTTTGATATGGTAGGTTCTAACCCTTCCATTATTCAGAAGTATAATCCAAACAATCAGGATTATATTGATGAATTGCCATCATCTGATAATCAGGAATATGATGATAATTCCGCTCCTTCTGGTG
GTTTCTTTGTTCCGCAAAATGATAATGTTACTCAAACTTTTAAAATTAATAACGTTCGGGCAAAGGATTTAATACGAGTTGTCGAATTGTTTGTAAAGTCTAATACTTCTAAATCCTCAAATGTATTATCTATTGACGGCTCTAATCTAT
TAGTTGTTAGTGCTCCTAAAGATATTTTAGATAACCTTCCTCAATTCCTTTCAACTGTTGATTTGCCAACTGACCAGATATTGATTGAGGGTTTGATATTTGAGGTTCAGCAAGGTGATGCTTTAGATTTTTCATTTGCTGCTGGCTCTC
AGCGTGGCACTGTTGCAGGCGGTGTTAATACTGACCGCCTCACCTCTGTTTTATCTTCTGCTGGTGGTTCGTTCGGTATTTTTAATGGCGATGTTTTAGGGCTATCAGTTCGCGCATTAAAGACTAATAGCCATTCAAAAATATTGTCTG
TGCCACGTATTCTTACGCTTTCAGGTCAGAAGGGTTCTATCTCTGTTGGCCAGAATGTCCCTTTTATTACTGGTCGTGTGACTGGTGAATCTGCCAATGTAAATAATCCATTTCAGACGATTGAGCGTCAAAATGTAGGTATTTCCATGA
GCGTTTTTCCTGTTGCAATGGCTGGCGGTAATATTGTTCTGGATATTACCAGCAAGGCCGATAGTTTGAGTTCTTCTACTCAGGCAAGTGATGTTATTACTAATCAAAGAAGTATTGCTACAACGGTTAATTTGCGTGATGGACAGACTC
TTTTACTCGGTGGCCTCACTGATTATAAAAACACTTCTCAGGATTCTGGCGTACCGTTCCTGTCTAAAATCCCTTTAATCGGCCTCCTGTTTAGCTCCCCGCTCTGATTCTAACGAGGAAAGCACGTTATACGTGCTCGTCAAAGCAACCA
TAGTACGCGCCCTGTAGCGGCGCATTAAGCGCGGCGGGTGTGGTGGTTACGCGCAGCGTGACCGCTACACTTGCCAGCGCCCTAGCGCCCGCTCCTTTCGCTTTCTTCCCTTCCTTTCTCGCCACGTTCGCCGGCTTTCCCCGTCAAGCT
CTAAATCGGGGGCTCCCTTTAGGGTTCCGATTTAGTGCTTTACGGCACCTCGACCCCAAAAAACTTGATTTGGGTGATGGTTCACGTAGTGGGCCATCGCCCTGATAGACGGTTTTTCGCCCTTTGACGTTGGAGTCCACGTTCTTTAAT
AGTGGACTCTTGTTCCAAACTGGAACAACACTCAACCCTATCTCGGGCTATTCTTTTGATTTATAAGGGATTTTGCCGATTTCGGAACCACCATCAAACAGGATTTTCGCCTGCTGGGGCAAACCAGCGTGGACCGCTTGCTGCAACTCT
CTCAGGGCCAGGCGGTGAAGGGCAATCAGCTGTTGCCCGTCTCACTGGTGAAAAGAAAAACCACCCTGGCGCCCAATACGCAAACCGCCTCTCCCCGCGCGTTGGCCGATTCATTAATGCAGCTGGCACGACAGGTTTCCCGACTGGAAA


**Table E.1:** Tile's main staples.

| Name | Oligo Position<br>5' Helix[base]--> 3' Helix[base] | Sequence 5'→3' |
|---|---|---|
| LCO-2 | 0[79] --> 1[63] | AAGTATTAGACTTTACAAACAATTTTATTAAT |
| LCO-3 | 0[111] --> 1[95] | CCGTCAATAGATAATACATTTGAATTTTGCG |
| LCO-4 | 0[143] --> 1[127] | CTTTAGGAGCACTAACAACTAATAGCGGAATT |
| LCO-5 | 0[175] --> 1[159] | GAAAGGAATTGAGGAAGGTTATCTGATGGCA |
| LCO-6 | 0[207] --> 1[191] | TCAATATCTGGTCAGTTGGCAAATTTTGGATT |
| LCO-7 | 0[239] --> 1[223] | CCTTGCTGAACCTCAAATATCAAAGAACCTA |
| LCO-8 | 0[271] --> 0[240] | AGCCAGCAGCAAATGAAAAATCTAAAGCATCA |
| LCO-9 | 0[303] --> 1[287] | TTAACACCGCCTGCAACAGTGCCACGCAAAT |
| LCO-10 | 0[335] --> 1[319] | CAGAAGATAAAACAGAGGTGAGGCTGATTAGT |
| LCO-11 | 0[367] --> 1[351] | TCGCCATTAAAAATACCGAACGAAGAACTCA |
| LCO-12 | 0[399] --> 1[383] | TCTTTAATGCGCGAACTGATAGCCTCCAGAAC |
| LCO-13 | 0[431] --> 1[415] | GGCACAGACAATATTTTTGAATGAGGAAAAA |
| LCO-14 | 0[463] --> 1[447] | AACCCTTCTGACCTGAAAGCGTAATGACGCTC |
| LCO-15 | 0[487] --> 1[479] | GGACATTCTGGCCAACATTGGCAG |
| LCO-16 | 1[64] --> 3[63] | TTTAAAAGGATGATGAAACAAACTTTCATTT |
| LCO-17 | 1[96] --> 3[95] | GAACAAAGAATTATTCATTTCAATAGTACATA |
| LCO-18 | 1[128] --> 3[127] | ATCATCATGAATACCAAGTTACACTTGCTTC |
| LCO-19 | 1[160] --> 3[159] | ATTCATCAGAGAAACAATAACGGATTTTCCCT |
| LCO-20 | 1[192] --> 3[191] | ATACTTCTGAATATACAGTAACAAGCTTAGA |
| LCO-21 | 1[224] --> 3[223] | CCATATCAAATTGCGTAGATTTTCAGTGAATT |
| LCO-22 | 1[256] --> 2[240] | ACCGAGTAGTGTTTTTATAATCAAAAACAGA |
| LCO-23 | 1[288] --> 3[287] | TAACCGTTTAGACAGGAACGGTACAGTGTTGT |
| LCO-24 | 1[320] --> 3[319] | AATAACATGAGCTAAACAGGAGGATTAAAGA |
| LCO-25 | 1[352] --> 3[351] | AACTATCGATAACGTGCTTTCCTCCGAAAAAC |
| LCO-26 | 1[384] --> 3[383] | AATATTACGCGCGTACTATGGTTACGTGAAC |
| LCO-27 | 1[416] --> 3[415] | CGCTCATGCACACCCGCCGCGCTTGGGTCGAG |
| LCO-28 | 1[448] --> 3[447] | AATCGTCTCAAGTGTAGCGGTCACCCTAAAG |
| LCO-29 | 1[480] --> 3[479] | ATTCACCAGAAAGCGAAAGGAGCGCGGGGAAA |
| LCO-30 | 2[79] --> 0[80] | CAAAAGAATTTGAGTAACATTATCGGATTTAG |
| LCO-31 | 2[143] --> 0[144] | ATTGCTTTATTCCTGATTATCAGATAAAATAT |
| LCO-32 | 2[175] --> 0[176] | TACATCGGATATAATCCTGATTGCAACAGTT |
| LCO-33 | 2[207] --> 0[208] | CGTCAGATGAATAATGGAAGGGTTACCCTCAA |
| LCO-34 | 2[239] --> 1[255] | AATAAAGAAAATTATTTGCACGTGTGAGGCC |
| LCO-35 | 2[271] --> 0[272] | CCTGAGAAAAAGAGTCTGTCCATCACGCTGAG |
| LCO-36 | 2[303] --> 0[304] | AGGGATTTGTAGCAATACTTCTTGGTCAGTA |
| LCO-37 | 2[335] --> 0[336] | CAGAGCGGCACTTGCCTGAGTAGAACCACCAG |
| LCO-38 | 2[367] --> 0[368] | GAGCACGTGCCTTGCTGGTAATACTAAAACA |
| LCO-39 | 2[399] --> 0[400] | GCTACAGGCGCCAGCCATTGCAACGCTATTAG |
| LCO-40 | 2[463] --> 0[464] | GGCGCTGGGAAATGGATTATTTACAGAGATAG |
| LCO-41 | 3[64] --> 5[63] | GAATTACCGTTAAATAAGAATAAATTAGTATC |
| LCO-42 | 3[96] --> 5[95] | AATCAATATTTGAAATACCGACCAGTATAAA |
| LCO-43 | 3[112] --> 0[112] | TGAATAACAAATCGCGCAGAGGCGAAACCACCAGAAGGAGATTAGAG |
| LCO-44 | 3[128] --> 5[127] | TGTAAATCGTTAATTTCATCTTCTAATTGAGA |
| LCO-45 | 3[160] --> 5[159] | TAGAATCCAACGCGAGAAAACTTATGTAATT |
| LCO-46 | 3[192] --> 5[191] | TTAAGACGAATGCTGATGCAAATCGTAATAAG |
| LCO-47 | 3[224] --> 5[223] | TATCAAAACGGCTTAGGTTGGGTTAAAGTAA |
| LCO-48 | 3[256] --> 4[240] | AAGAATAGTCGGCAAAATCCCTTACTACCTTT |
| LCO-49 | 3[288] --> 5[287] | TCCAGTTTGCGAAAATCCTGTTTGTTGTAAA |
| LCO-50 | 3[320] --> 5[319] | ACGTGGACAGCAAGCGGTCCACGCATGCCTGC |
| LCO-51 | 3[352] --> 5[351] | CGTCTATCGCCCTTCACCGCCTGGTACCGAG |

| | | |
|---|---|---|
| LCO-52 | 3[384] --> 5[383] | CATCACCCCTTTTCACCAGTGAGAAGCTGTTT |
| LCO-53 | 3[416] --> 5[415] | GTGCCGTAGGTTTGCGTATTGGGACAATTCC |
| LCO-54 | 3[432] --> 0[432] | AATCGGAACGCTGCGCGTAACCACGAAATACCTACATTTGAATACGT |
| LCO-55 | 3[448] --> 5[447] | GGAGCCCCATTAATGAATCGGCCATAAAGTGT |
| LCO-56 | 3[480] --> 5[479] | GCCGGCGATTTCCAGTCGGGAAACAGCTAACT |
| LCO-57 | 4[79] --> 2[80] | AATAAGGCTTTTTTAATGGAAACTACCTGAG |
| LCO-58 | 4[143] --> 2[144] | ATATTTTAGTCGCTATTAATTAATTCGCCTG |
| LCO-59 | 4[175] --> 2[176] | AGACAAAGTTGAAAACATAGCGATGTACCTTT |
| LCO-60 | 4[207] --> 2[208] | TATATGTACTGAGAAGAGTCAATAGGTTTAA |
| LCO-61 | 4[239] --> 3[255] | TTAACCTCTCATAGGTCTGAGAGATAAATCAA |
| LCO-62 | 4[271] --> 2[272] | TTCCGAAACCCGAGATAGGGTTGGCCAGAAT |
| LCO-63 | 4[303] --> 2[304] | CCCAGCAGGGAACAAGAGTCCACTCCGATTAA |
| LCO-64 | 4[335] --> 2[336] | AGAGTTGCTCCAACGTCAAAGGGGTTAGAAT |
| LCO-65 | 4[367] --> 2[368] | AGCTGATTAGGGCGATGGCCCACTGCTTTGAC |
| LCO-66 | 4[399] --> 2[400] | TGGTTTTTAAATCAAGTTTTTTGAATGCGCC |
| LCO-67 | 4[463] --> 2[464] | CCAGCTGCCGATTTAGAGCTTGAGGCGCTAG |
| LCO-68 | 5[64] --> 7[63] | ATATGCGTCAAGCAAGCCGTTTTATAGCAAG |
| LCO-69 | 5[96] --> 7[95] | GCCAACGCGGTATTAAACCAAGTACCGGTATT |
| LCO-70 | 5[128] --> 7[127] | ATCGCCATTCGGCTGTCTTTCCTAACCTCCC |
| LCO-71 | 5[160] --> 7[159] | TAGGCAGATAATTTACGAGCATGTTTAAATCA |
| LCO-72 | 5[192] --> 7[191] | AGAATATAAGTCCTGAACAAGAAGCTACAAT |
| LCO-73 | 5[224] --> 7[223] | TTCTGTCCTGCAGAACGCGCCTGTTAACGAGC |
| LCO-74 | 5[256] --> 6[240] | CGCCAGGGTGCAAGGCGATTAAGCAACATGT |
| LCO-75 | 5[288] --> 7[287] | ACGACGGCCTATTACGCCAGCTGGATTGTATA |
| LCO-76 | 5[320] --> 7[319] | AGGTCGACTTGGGAAGGGCGATCTAATATTT |
| LCO-77 | 5[352] --> 7[351] | CTCGAATTAAGCGCCATTCGCCATTGTTAAAT |
| LCO-78 | 5[384] --> 7[383] | CCTGTGTGCGGCACCGCTTCTGGACGCCATC |
| LCO-79 | 5[416] --> 7[415] | ACACAACAGCCTCAGGAAGATCGCCCTGTAGC |
| LCO-80 | 5[448] --> 7[447] | AAAGCCTGCTGCCAGTTTGAGGGAGCGAGTA |
| LCO-81 | 5[480] --> 7[479] | CACATTAATTGGTGTAGATGGGCGGAACAAAC |
| LCO-82 | 6[79] --> 4[80] | ATCGAGAATATACAAATTCTTACCGTGTGATA |
| LCO-83 | 6[111] --> 3[111] | CAAGAACGTCAACAGTAGGGCTTGACCTAAATTTAATGGTATGTGAG |
| LCO-84 | 6[143] --> 4[144] | ATCAATAAATTTAACAACGCCAACTTTCAAAT |
| LCO-85 | 6[175] --> 4[176] | TCCCATCCGGCATTTTCGAGCCACAATCGCA |
| LCO-86 | 6[207] --> 4[208] | AATAGATAAAGTACCGACAAAAGGTATATAAC |
| LCO-87 | 6[239] --> 5[255] | TCAGCTAAAGACGACGACAATAAATTGGGTAA |
| LCO-88 | 6[271] --> 4[272] | GGATGTGCTTTTCCCAGTCACGACGATGGTGG |
| LCO-89 | 6[303] --> 4[304] | CCTCTTCGCAGTGCCAAGCTTGCTGGTTTGC |
| LCO-90 | 6[335] --> 4[336] | CGCAACTGTCTAGAGGATCCCCGGGCCCTGAG |
| LCO-91 | 6[367] --> 4[368] | ACCAGGCACGTAATCATGGTCATCGGGCAAC |
| LCO-92 | 6[399] --> 4[400] | CAGCTTTCAAATTGTTATCCGCTCCGCCAGGG |
| LCO-93 | 6[431] --> 3[431] | CAGTATCGTACGAGCCGGAAGCAACGCGCGGGGAGAGGCAAGCACTA |
| LCO-94 | 6[463] --> 4[464] | CCGTGCATGGGTGCCTAATGAGTGCTGTCGTG |
| LCO-95 | 7[64] --> 9[63] | CAAATCAGCGCTAATATCAGAGAGTAAGAGCA |
| LCO-96 | 7[96] --> 9[95] | CTAAGAACACACCCTGAACAAAGATCTTACC |
| LCO-97 | 7[128] --> 9[127] | GACTTGCGAGGGAAGCGCATTAGAGCAGATAG |
| LCO-98 | 7[160] --> 9[159] | AGATTAGTGCAGCCTTTACAGAGCCGAGGAA |
| LCO-99 | 7[192] --> 9[191] | TTTATCCTCGATTTTTTGTTTAACAAAGAACT |
| LCO-100 | 7[224] --> 9[223] | GTCTTTCCCCATATTATTTATCCGCAGTATG |
| LCO-101 | 7[256] --> 8[240] | AGAAAAGCTCATATGTACCCCGGTGTTACAAA |
| LCO-102 | 7[288] --> 10[288] | AGCAAATAATGAACGGTAATCGTGGGGCGCGAGCTGAAACTGCGAAC |
| LCO-103 | 7[320] --> 9[319] | TGTTAAAATGCCTGAGAGTCTGGATACTAATA |
| LCO-104 | 7[352] --> 9[351] | CAGCTCATTTTGAGAGATCTACATCATACAG |
| LCO-105 | 7[384] --> 9[383] | AAAAATAACTGATAAATTAATGCCTAAGCAAT |
| LCO-106 | 7[416] --> 9[415] | CAGCTTTCTCACCATCAATATGATCGGTTGT |
| LCO-107 | 7[448] --> 9[447] | ACAACCCGCAAAAGGGTGAGAAAGATACTTTT |
| LCO-108 | 7[480] --> 9[479] | GGCGGATTTGCAATGCCTGAGTAACAAGGATA |
| LCO-109 | 8[79] --> 6[80] | TAATTGAGATATAGAAGGCTTATCCGCACTC |
| LCO-110 | 8[111] --> 6[112] | TTAACTGAGCGAGGCGTTTTAGCGTATCATTC |
| LCO-111 | 8[143] --> 6[144] | ATAAAAACGGAGGTTTTGAAGCCAGAAACCA |
| LCO-112 | 8[175] --> 6[176] | TGAAAATATGCTATTTTGCACCCAAAATAATA |
| LCO-113 | 8[207] --> 6[208] | ATAAGAAAGAATCTTACCAACGCTTATCAAC |
| LCO-114 | 8[239] --> 7[255] | ATAAACAGAGAGCCTAATTTGCCATGATAATC |
| LCO-115 | 8[271] --> 6[272] | CATGTCAACCCAAAAACAGGAAGCGAAAGGG |
| LCO-116 | 8[303] --> 6[304] | GAGAATCGTTTAAATTGTAAACGTGGTGCGGG |
| LCO-117 | 8[335] --> 6[336] | CAGGTCATTTCGCATTAAATTTTTCAGGCTG |
| LCO-118 | 8[367] --> 6[368] | TAGCTATTTTTTTAACCAATAGGATGCCGGAA |

| | | |
|---|---|---|
| LCO-119 | 8[399] --> 6[400] | CGTTCTAGTTCGCGTCTGGCCTTACTCCAGC |
| LCO-120 | 8[431] --> 6[432] | CAGTCAAAATCAACATTAAATGTGGACGACGA |
| LCO-121 | 8[463] --> 6[464] | TAAAGATTTCGGATTCTCCGTGGCATCGTAA |
| LCO-122 | 9[64] --> 11[63] | AGAAACAAATCACCGTCACCGACCACCAGTA |
| LCO-123 | 9[96] --> 11[95] | GAAGCCCTTATTGACGGAAATTATGGAAACGT |
| LCO-124 | 9[128] --> 12[128] | CCGAACAAACATTCAACCGATTGCACCGTAATCAGTAGCCCAGCATT |
| LCO-125 | 9[160] --> 11[159] | ACGCAATATATGGTTTACCAGCGCGCCTTTAG |
| LCO-126 | 9[192] --> 11[191] | GGCATGATGTTTATTTTGTCACACGGCATTT |
| LCO-127 | 9[224] --> 11[223] | TTAGCAAATATAAAAGAAACGCAAGTTTGCCA |
| LCO-128 | 9[256] --> 10[240] | ACCTGTTTATACATTTCGCAAATCATAAAGG |
| LCO-129 | 9[320] --> 11[319] | GTAGTAGCTTTCATTCCATATAAATCGTCAT |
| LCO-130 | 9[352] --> 11[351] | GCAAGGCATAAATATGCAACTAAAAATGCTTT |
| LCO-131 | 9[384] --> 11[383] | AAAGCCTCGCTGAATATAATGCTCCATAAAT |
| LCO-132 | 9[416] --> 11[415] | ACCAAAAAGGTCATTTTTGCGGATCTATTATA |
| LCO-133 | 9[448] --> 12[448] | GCGGGAGAAGAGTACCTTTAATTAAAAAGATTAAGAGGAAAAAATCT |
| LCO-134 | 9[480] --> 11[479] | AAAATTTTACCGGAAGCAAACTCCAAATATCG |
| LCO-135 | 10[79] --> 8[80] | GGTGAATTTGAAATAGCAATAGCTTCAGAGGG |
| LCO-136 | 10[111] --> 8[112] | AAGGTAAATTTTAAGAAAAGTAACGGGAGAA |
| LCO-137 | 10[143] --> 8[144] | AAAGGGCGAGTTACCAGAAGGAAAAGAATAAC |
| LCO-138 | 10[175] --> 8[176] | AAAATTCAATAACGGAATACCCAGTCAAAAA |
| LCO-139 | 10[207] --> 8[208] | CGGAATAATAAGACTCCTTATTACCAATCCAA |
| LCO-140 | 10[239] --> 9[255] | TGGCAACACGTAGAAAATACATAGGTCAATA |
| LCO-141 | 10[271] --> 8[272] | ACCATTAGAGCTATATTTTCATTTAAAACTAG |
| LCO-142 | 10[287] --> 13[287] | GAGTAGATTGTTTAGACTGGATAGTTTACCAGACGACGAGGACAGAT |
| LCO-143 | 10[303] --> 8[304] | TCCCAATTAGGTGGCATCAATTCGCAAACAA |
| LCO-144 | 10[335] --> 8[336] | TCTGGAAGATTAACATCCAATAAAAAGGCTAT |
| LCO-145 | 10[367] --> 8[368] | ACATGTTTAAGAATTAGCAAAATGGAGAGGG |
| LCO-146 | 10[399] --> 8[400] | GCTTAATTAGAGCATAAAGCTAAATATTCAAC |
| LCO-147 | 10[431] --> 8[432] | TGATAAGACATTATGACCCTGTAGCCGGAGA |
| LCO-148 | 10[463] --> 8[464] | AGGATTAGAGCCTTTATTTCAACGTGTGTAGG |
| LCO-149 | 11[64] --> 13[63] | GCACCATTTCCTCATTAAAGCCAGCAGTAAGC |
| LCO-150 | 11[96] --> 13[95] | CACCAATGCGATTGGCCTTGATAAGGAGTGT |
| LCO-151 | 11[160] --> 13[159] | CGTCAGACGCCGCCACCAGAACCAGTTAATG |
| LCO-152 | 11[192] --> 13[191] | TCGGTCATGAACCGCCACCCTCAGTTATTCTG |
| LCO-153 | 11[224] --> 13[223] | TCTTTTCAGGAACCGCCTCCCTCAGACTCCT |
| LCO-154 | 11[256] --> 12[240] | TGCCAGAGGAGAGGCTTTTGCAAAAACCAGAG |
| LCO-155 | 11[320] --> 13[319] | AAATATTCGCATAGTAAGAGCAACTAGGCTGG |
| LCO-156 | 11[352] --> 13[351] | AAACAGTTGCAGATACATAACGCGACAAGAA |
| LCO-157 | 11[384] --> 13[383] | CAAAAATCGTTGAGATTTAGGAATACGTAACA |
| LCO-158 | 11[416] --> 13[415] | GTCAGAAGACAACATTATTACAGCTTGCCCT |
| LCO-159 | 11[480] --> 13[479] | CGTTTTAATGGCTCATTATACCAGTTTAATCA |
| LCO-160 | 12[79] --> 10[80] | CAAATAAAACCATTAGCAAGGCCTCATTAAA |
| LCO-161 | 12[111] --> 10[112] | AGGTCAGAAAACCATCGATAGCAGAGGGAGGG |
| LCO-162 | 12[127] --> 15[127] | GACAGGAGTCAGTGCCTTGAGTAACCGCCACCCTCAGAAGTCTTTCC |
| LCO-163 | 12[143] --> 10[144] | AGCCGCCGGACAGAATCAAGTTTCAAAGACA |
| LCO-164 | 12[175] --> 10[176] | CCCTCAGATGTAGCGCGTTTTCATATCAATAG |
| LCO-165 | 12[207] --> 10[208] | CACCCTCAAGCCCCCTTATTAGCAGACACCA |
| LCO-166 | 12[239] --> 11[255] | CCACCACCTAATCAAAATCACCGGAGAAGTTT |
| LCO-167 | 12[271] --> 10[272] | AAAATAGCGGGGTAATAGTAAAATTAGTTTG |
| LCO-168 | 12[303] --> 10[304] | AACCCTCGCGTCCAATACTGCGGACAGTTGAT |
| LCO-169 | 12[335] --> 10[336] | ATTACGAGATTGAATCCCCCTCAGTACGGTG |
| LCO-170 | 12[367] --> 10[368] | CAACTAATCAGAAAACGAGAATGAGTAGCTCA |
| LCO-171 | 12[399] --> 10[400] | ATTCATCAAGGTCTTTACCCTGAGGCTTAGA |
| LCO-172 | 12[431] --> 10[432] | CTAACGGACAAAGCGGATTGCATCGCTCCTTT |
| LCO-173 | 12[447] --> 15[447] | ACGTTAATGTAAATTGGGCTTGAGAAATACGTAATGCCACCCTCAGC |
| LCO-174 | 12[463] --> 10[464] | TTGGGAAGAGCCCGAAAGACTTCAACAGGTC |
| LCO-175 | 13[64] --> 15[63] | GTCATACAATAGGAACCCATGTATACAACGC |
| LCO-176 | 13[96] --> 15[95] | ACTGGTAACACCACCCTCATTTTCTCATAGTT |
| LCO-177 | 13[160] --> 15[159] | CCCCCTGCACTCAGGAGGTTTAGTGTATGGGA |
| LCO-178 | 13[192] --> 15[191] | AAACATGATAAGTATAGCCCGGATTCAGCGG |
| LCO-179 | 13[224] --> 15[223] | CAAGAGAACAGGCGGATAAGTGCCAAAGGAAT |
| LCO-180 | 13[256] --> 14[240] | ACCGAACTCGCAGACGGTCAATCGGGTTTTG |
| LCO-181 | 13[288] --> 15[287] | GAACGGTGGACCTGCTCCATGTTATTGTATCG |
| LCO-182 | 13[320] --> 15[319] | CTGACCTTTCATCGCCTGATAAAAATTTCTT |
| LCO-183 | 13[352] --> 15[351] | CCGGATATAAGCGCGAAACAAAGTCGCCGACA |
| LCO-184 | 13[384] --> 15[383] | AAGCTGCTACACTCATCTTTGACTAACCGAT |
| LCO-185 | 13[416] --> 15[415] | GACGAGAACTAAAACGAAAGAGGCGGGAGTTA |

| | | |
|---|---|---|
| LCO-186 | 13[480] --> 15[487] | TTGTGAATTTTTTCATGAGGAAGTGGGTAGCAACGGCTAC |
| LCO-187 | 14[79] --> 12[80] | CAAGCCCATGGCTTTTGATGATACTTCACAAA |
| LCO-188 | 14[111] --> 12[112] | CTCAGAGCTAAGTTTTAACGGGGGTTGAGGC |
| LCO-189 | 14[143] --> 12[144] | CCTCAGAACAGTGCCCGTATAAACACCACCAG |
| LCO-190 | 14[175] --> 12[176] | ATCACCGTCTATTTCGGAACCTAAGCCACCA |
| LCO-191 | 14[207] --> 12[208] | GGTTGATAAAGTATTAAGAGGCTGAGAGCCGC |
| LCO-192 | 14[239] --> 13[255] | CTCAGTACGGATTAGGATTAGCGATAAGGGA |
| LCO-193 | 14[271] --> 12[272] | GAACGAGGGACCAACTTTGAAAGATAAAAACC |
| LCO-194 | 14[303] --> 12[304] | AAATCCGCTACAGACCAGGCGCAACTATCAT |
| LCO-195 | 14[335] --> 12[336] | GATTTGTACATCAAGAGTAATCTTCAAAAGGA |
| LCO-196 | 14[367] --> 12[368] | ATTATACCTCATTACCCAAATCAACCACATT |
| LCO-197 | 14[399] --> 12[400] | ACACTAAACATTCAGTGAATAAGGGTAGAAAG |
| LCO-198 | 14[431] --> 12[432] | GCACCAACACACCAGAACGAGTAAAAACGAA |
| LCO-199 | 14[463] --> 12[464] | AACGGGTAATGGTTTAATTTCAACTCAGGACG |
| LCO-200 | 15[64] --> 14[80] | CTGTAGCATTCCACAGACAGCCCAGGGATAG |
| LCO-201 | 15[96] --> 14[112] | AGCGTAACGATCTAAAGTTTTGTCCCGCCACC |
| LCO-202 | 15[128] --> 14[144] | AGACGTTAGTAAATGAATTTTCTACCGCCAC |
| LCO-203 | 15[160] --> 14[176] | TTTTGCTAAACAACTTTCAACAGTATAGGTGT |
| LCO-204 | 15[192] --> 14[208] | AGTGAGAATAGAAAGGAACAACTGTCGAGAG |
| LCO-205 | 15[224] --> 15[255] | TGCGAATAATAATTTTGAAAATCTCCAAAAAA |
| LCO-206 | 15[256] --> 14[272] | AAGGCTCCAAAAGGAGCCTTTAACTTAGCCG |
| LCO-207 | 15[288] --> 14[304] | GTTTATCAGCTTGCTTTCGAGGTGTTGTGTCG |
| LCO-208 | 15[320] --> 14[336] | AAACAGCTTGATACCGATAGTTGACAACGGA |
| LCO-209 | 15[352] --> 14[368] | ATGACAACAACCATCGCCCACGCACCCCAGCG |
| LCO-210 | 15[384] --> 14[400] | ATATTCGGTCGCTGAGGCTTGCAAAAAGAAT |
| LCO-211 | 15[416] --> 14[432] | AAGGCCGCTTTTGCGGGATCGTCACTACGAAG |
| LCO-212 | 15[448] --> 14[464] | AGCGAAAGACAGCATCGGAACGATTCCATTA |

**Table E.2:** Poly-T passivation and random generated sticky ends strands.

| Name | Sequence 5'→3' |
|---|---|
| | Origami-A Poly-T-Loop Edge Staples (left side) [1] |
| L_T_U 0-1 | TTTTTATCCTTTGCCCGAACGCGACAACTCGTATTAATTTTT |
| L_T_U 2-3 | TTTTTTAATTACATTTAACAAATCAAGAAAACAAAATTTTTT |
| L_T_U 4-5 | TTTTTACTAGAAAAAGCCTGTCACCGGAATCATAATTTTTTT |
| L_T_U 6-7 | TTTTTATCATTACCGCGCCCATATTTTCATCGTAGGATTTTT |
| L_T_U 8-9 | TTTTTGAGTTAAGCCCAATAAATAACCCACAAGAATTTTTT |
| L_T_U 10-11 | TTTTTTTAGAGCCAGCAAAATTTGAGCCATTTGGGAATTTTT |
| L_T_U 12-13 | TTTTTTCTGAATTTACCGTTCAATGGAAAGCGCAGTCTTTTT |
| L_T_U 14-15 | TTTTTCGTCACCAGTACAAACCCGTAACACTGAGTTTTTTTT |
| | Origami-F Poly-T-Loop Edge Staples (right side) [1] |
| R_T_U 0 | TTTTTAGTAATAAAAGGGACATTCTGGCCAACATTGGCAG |
| R_T_U 1-2 | TTTTTAAGGAAGGGAAGTCACACGACCTTTTT |
| R_T_U 3-4 | TTTTTTCACTGCCCGCACGTGGCGAGATTTTT |
| R_T_U 5-6 | TTTTTGATAGGTCACGTTGCGTTGCGCTTTTT |
| R_T_U 7-8 | TTTTTTATATTTTAAAGACCGTAATGGTTTTT |
| R_T_U 9-10 | TTTTTAAGCGAACCAGTAGAACCCTCATTTTT |
| R_T_U 11-12 | TTTTTATTTTAAGAACTTCGAGCTTCATTTTT |
| R_T_U 13-14 | TTTTTGGACTAAAGACTACCTTATGCGTTTTT |
| R_T_U 15 | TTGTGAATTTTTTCATGAGGAAGTGGGTAGCAACGGCTACAGAGGCTTTGATTTTT |
| | SE1 Right origami Edge- 11-nt Bridging Strands [2] |
| 1_R_SE 0-5T | TTTTTAGTAATAAAAGGGACATTCTGGCCAACATTGGCAG |
| 1_R_SE 1-2 | AAGACCACGGGAAGGAAGGGAAGTCACACGACCTTGGCTAATCC |
| 1_R_SE 3-4 | GTTATAAACAATCACTGCCCGCACGTGGCGAGATCTGTGCTAGA |
| 1_R_SE 5-6 | CCATATATCAAGATAGGTCACGTTGCGTTGCGCTATTCAACGCG |
| 1_R_SE 7-8 | GGGTTCACGTGTATATTTTAAAGACCGTAATGGTCTGTCCTAAC |
| 1_R_SE 9-10 | TGACGCCGGAAAAGCGAACCAGTAGAACCCTCAGCGTTCAGGGT |
| 1_R_SE 11-12 | CGACTTCCGAGATTTTAAGAACTTCGAGCTTCATCCAAAGTGTC |
| 1_R_SE 13-14 | AAGGGCGAGAAGGACTAAAGACTACCTTATGCGTACGTAGCATG |
| 1_R_SE 15 | TTGTGAATTTTTTCATGAGGAAGTGGGTAGCAACGGCTACAGAGGCTTTGATGCCCGCGTTT |
| | SE1 Left origami Edge- 11-nt Bridging Strands [2] |
| 2_L_SE 0-1 | CCCGTGGTCTTATCCTTTGCCCGAACGCGACAACTCGTATTAAGGATTAGCCAA |
| 2_L_SE 2-3 | TTGTTTATAACTAATTACATTTAACAAATCAAGAAAACAAAATTCTAGCACAGA |
| 2_L_SE4-5 | TTGATATATGGACTAGAAAAAGCCTGTCACCGGAATCATAATTCGCGTTGAATA |
| 2_L_SE 6-7 | CACGTGAACCCATCATTACCGCGCCCATATTTTCATCGTAGGAGTTAGGACAGA |

| | |
|---|---|
| 2_L_SE 8-9 | TTCCGGCGTCAGAGTTAAGCCCAATAAATAACCCACAAGAATTACCCTGAACGC |
| 2_L_SE 10-11 | CTCGGAAGTCGTTAGAGCCAGCAAAATTTGAGCCATTTGGGAAGACACTTTGGA |
| 2_L_SE 12-13 | TTCTCGCCCTTTCTGAATTTACCGTTCAATGGAAAGCGCAGTCCATGCTACGTA |
| 2_L_SE 14-15 | TTTTTCGTCACCAGTACAAACCCGTAACACTGAGTTTAAACGCGGGCA |
| | SE2 Right origami Edge- 11-nt Bridging Strands [2] |
| 2_R_SE 0 | TCCATTTCGGTAGTAATAAAAGGGACATTCTGGCCAACATTGGCAG |
| 2_R_SE 1-2 | AGCTAGTTGTGAAGGAAGGGAAGTCACACGACCCATTCTCCGAG |
| 2_R_SE 3-4 | GGGTCCCATAATCACTGCCCGCACGTGGCGAGACCGTACTTGGA |
| 2_R_SE 5-6 | CGCACCTGATCGATAGGTCACGTTGCGTTGCGCCCGGACGAACC |
| 2_R_SE 7-8 | AGCTGCTTTACTATATTTTAAAGACCGTAATGGCGGGATGCTTT |
| 2_R_SE 9-10 | ATTCCTCAGGCAAGCGAACCAGTAGAACCCTCAGGGATCCATCG |
| 2_R_SE 11-12 | CATAGTGAGTTATTTTAAGAACTTCGAGCTTCACAGATCGTCTG |
| 2_R_SE 13-14 | CCCTCGAAACTGGACTAAAGACTACCTTATGCGTAAGTCAAGTC |
| 2_R_SE 15 | TTGTGAATTTTTTCATGAGGAAGTGGGTAGCAACGGCTACAGAGGCTTTGATTTTT |
| | SE2 Left origami Edge- 11-nt Bridging Strands [2] |
| 3_L_SE 0-1 | ACCGAAATGGAATCCTTTGCCCGAACGCGACAACTCGTATTAATTTTT |
| 3_L_SE 2-3 | CACAACTAGCTTAATTACATTTAACAAATCAAGAAAACAAAATCTCGGAGAATG |
| 3_L_SE4-5 | TTATGGGACCCACTAGAAAAAGCCTGTCACCGGAATCATAATTTCCAAGTACGG |
| 3_L_SE 6-7 | GATCAGGTGCGATCATTACCGCGCCCATATTTTCATCGTAGGAGGTTCGTCCGG |
| 3_L_SE 8-9 | GTAAAGCAGCTGAGTTAAGCCCAATAAATAACCCACAAGAATTAAAGCATCCCG |
| 3_L_SE 10-11 | GCCTGAGGAATTTAGAGCCAGCAAAATTTGAGCCATTTGGGAACGATGGATCCC |
| 3_L_SE 12-13 | AACTCACTATGTCTGAATTTACCGTTCAATGGAAAGCGCAGTCCAGACGATCTG |
| 3_L_SE 14-15 | AGTTTCGAGGGCGTCACCAGTACAAACCCGTAACACTGAGTTTGACTTGACTTA |
| | SE3 Right origami Edge- 11-nt Bridging Strands [2] |
| 3_R_SE 0 | TTTTTAGTAATAAAAGGGACATTCTGGCCAACATTGGCAG |
| 3_R_SE 1-2 | CTACTGAGTTGAAGGAAGGGAAGTCACACGACCTCCGAGCCTCA |
| 3_R_SE 3-4 | GCCGTGCGTAGTCACTGCCCGCACGTGGCGAGATCAAGCATGGC |
| 3_R_SE 5-6 | GATGCGACCATGATAGGTCACGTTGCGTTGCGCCGATCTCGCCC |
| 3_R_SE 7-8 | CTACGGGTTATTATATTTTAAAGACCGTAATGGCCGACTGCTCC |
| 3_R_SE 9-10 | TCTTCGTTCCGAAGCGAACCAGTAGAACCCTCACCGCGGACCAT |
| 3_R_SE 11-12 | GTTTCCGTTGTATTTTAAGAACTTCGAGCTTCAGCGCCATGATT |
| 3_R_SE 13-14 | TGTTCAGGGTGGGACTAAAGACTACCTTATGCGGATAGTGGGGA |
| 3_R_SE 15 | TTGTGAATTTTTTCATGAGGAAGTGGGTAGCAACGGCTACAGAGGCTTTGACTTGTCAGACC |
| | SE3 Left origami Edge- 11-nt Bridging Strands [2] |
| 4_L_SE 0-1 | CAACTCAGTAGATCCTTTGCCCGAACGCGACAACTCGTATTAATGAGGCTCGGA |
| 4_L_SE 2-3 | CTACGCACGGCTAATTACATTTAACAAATCAAGAAAACAAAATGCCATGCTTGA |
| 4_L_SE4-5 | ATGGTCGCATCACTAGAAAAAGCCTGTCACCGGAATCATAATTGGGCGAGATCG |
| 4_L_SE 6-7 | ATAACCCGTAGATCATTACCGCGCCCATATTTTCATCGTAGGAGGAGCAGTCGG |
| 4_L_SE 8-9 | CGGAACGAAGAGAGTTAAGCCCAATAAATAACCCACAAGAATTATGGTCCGCGG |
| 4_L_SE 10-11 | ACAACGGAAACTTAGAGCCAGCAAAATTTGAGCCATTTGGGAAAATCATGGCGC |
| 4_L_SE 12-13 | CACCCTGAACATCTGAATTTACCGTTCAATGGAAAGCGCAGTCTCCCCACTATC |
| 4_L_SE 14-15 | TTTTTCGTCACCAGTACAAACCCGTAACACTGAGTTTGGTCTGACAAG |

[1] green color indicates poly-T overhangs

[2] each color indicates a SE set

**Table E.3:** NuCraft generated sticky ends strands.

| Name | Sequence 5'→3' |
|---|---|
| | SE1 Right origami Edge- 11-nt Bridging Strands [2] |
| 1_R_SE 0-5T_op | TTTTTAGTAATAAAAGGGACATTCTGGCCAACATTGGCAG |
| 1_R_SE 1-2_op | CTGCACTACTAAAGGAAGGGAAGTCACACGACCCATTTCCCGGT |
| 1_R_SE 3-4_op | GGTGCTTGTCATCACTGCCCGCACGTGGCGAGAGGATGAGACAA |
| 1_R_SE 5-6_op | ACCTGGAATAGGATAGGTCACGTTGCGTTGCGCAGTCTTCGTAC |
| 1_R_SE 7-8_op | CCTCACGGTTATATATTTTAAAGACCGTAATGGACTGCTGCATT |
| 1_R_SE 9-10_op | ACGCACGAACAAAGCGAACCAGTAGAACCCTCAGTTATAGTCGC |
| 1_R_SE 11-12_op | GACCACAGTTCATTTTAAGAACTTCGAGCTTCAATGTCCGCGAT |
| 1_R_SE 13-14_op | TGGACGATCCTGGACTAAAGACTACCTTATGCGACCGCATCTAA |
| 1_R_SE 15_op | TTGTGAATTTTTTCATGAGGAAGTGGGTAGCAACGGCTACAGAGGCTTTGACTTGGCCTTAA |
| | SE1 Left origami Edge- 11-nt Bridging Strands [2] |
| 2_L_SE 0-1_op | TAGTAGTGCAGATCCTTTGCCCGAACGCGACAACTCGTATTAAACCGGGAAATG |
| 2_L_SE 2-3_op | TGACAAGCACCTAATTACATTTAACAAATCAAGAAAACAAAATTTGTCTCATCC |
| 2_L_SE4-5_op | CTATTCCAGGTACTAGAAAAAGCCTGTCACCGGAATCATAATTGTACGAAGACT |
| 2_L_SE 6-7_op | TAACCGTGAGGATCATTACCGCGCCCATATTTTCATCGTAGGAATGCAGCAGT |

| | |
|---|---|
| 2_L_SE 8-9_op | TGTTCGTGCGTGAGTTAAGCCCAATAAATAACCCACAAGAATTGCGACTATAAC |
| 2_L_SE 10-11_op | GAACTGTGGTCTTAGAGCCAGCAAAATTTGAGCCATTTGGGAAATCGCGGACAT |
| 2_L_SE 12-13_op | AGGATCGTCCATCTGAATTTACCGTTCAATGGAAAGCGCAGTCTTAGATGCGGT |
| 2_L_SE 14-15_op | TTTTTCGTCACCAGTACAAACCCGTAACACTGAGTTTTTAAGGCCAAG |
| | SE2 Right origami Edge- 11-nt Bridging Strands [2] |
| 2_R_SE 0_op | CCCACTCTTAGAGTAATAAAAGGGACATTCTGGCCAACATTGGCAG |
| 2_R_SE 1-2_op | TTGACTGACCCAAGGAAGGGAAGTCACACGACCCGCAGGTAAGT |
| 2_R_SE 3-4_op | GATTGGAGAGATCACTGCCCGCACGTGGCGAGAACTAGGGAGTC |
| 2_R_SE 5-6_op | CGAGCCTACATGATAGGTCACGTTGCGTTGCGCTTGTGCTACGG |
| 2_R_SE 7-8_op | CATATCGACCTTATATTTTAAAGACCGTAATGGACCGAGGCAAT |
| 2_R_SE 9-10_op | ATCCGTCATGTAAGCGAACCAGTAGAACCCTCACACCTTCATAC |
| 2_R_SE 11-12_op | AGATTAGCCGGATTTTAAGAACTTCGAGCTTCATCGGAACGTAT |
| 2_R_SE 13-14_op | ATAGCCCGTGTGGACTAAAGACTACCTTATGCGATACTCGGCGA |
| 2_R_SE 15_op | TTGTGAATTTTTTCATGAGGAAGTGGGTAGCAACGGCTACAGAGGCTTTGATTTTT |
| | SE2 Left origami Edge- 11-nt Bridging Strands [2] |
| 3_L_SE 0-1_op | CTAAGAGTGGGATCCTTTGCCCGAACGCGACAACTCGTATTAATTTTT |
| 3_L_SE 2-3_op | GGGTCAGTCAATAATTACATTTAACAAATCAAGAAAACAAAATACTTACCTGCG |
| 3_L_SE4-5_op | TCTCTCCAATCACTAGAAAAAGCCTGTCACCGGAATCATAATTGACTCCCTAGT |
| 3_L_SE 6-7_op | ATGTAGGCTCGATCATTACCGCGCCCATATTTTCATCGTAGGACCGTAGCACAA |
| 3_L_SE 8-9_op | AGGTCGATATGGAGTTAAGCCCAATAAATAACCCACAAGAATTATTGCCTCGGT |
| 3_L_SE 10-11_op | ACATGACGGATTTAGAGCCAGCAAAATTTGAGCCATTTGGGAAGTATGAAGGTG |
| 3_L_SE 12-13_op | CCGGCTAATCTTCTGAATTTACCGTTCAATGGAAAGCGCAGTCATACGTTCCGA |
| 3_L_SE 14-15_op | ACACGGGCTATCGTCACCAGTACAAACCCGTAACACTGAGTTTTCGCCGAGTAT |
| | SE3 Right origami Edge- 11-nt Bridging Strands [2] |
| 3_R_SE 0_op | TTTTTAGTAATAAAAGGGACATTCTGGCCAACATTGGCAG |
| 3_R_SE 1-2_op | CCATCCATCAAAAGGAAGGGAAGTCACACGACCGGGTACATCAT |
| 3_R_SE 3-4_op | ACGGACCAACTTCACTGCCCGCACGTGGCGAGAACCCTACCATT |
| 3_R_SE 5-6_op | GCGCTAGGTATGATAGGTCACGTTGCGTTGCGCGAGCGTCAACA |
| 3_R_SE 7-8_op | CTCCTTAGTGTTATATTTTAAAGACCGTAATGGACTTCACGCTT |
| 3_R_SE 9-10_op | TATTCTGGGCCAAGCGAACCAGTAGAACCCTCAGCTATGGACTG |
| 3_R_SE 11-12_op | ATGTGTCGGGTATTTTAAGAACTTCGAGCTTCAGTGCCCTTGAA |
| 3_R_SE 13-14_op | ATGCCGCCAAAGGACTAAAGACTACCTTATGCGACATTGGTGGG |
| 3_R_SE 15_op | TTGTGAATTTTTTCATGAGGAAGTGGGTAGCAACGGCTACAGAGGCTTTGATTCCTCTACCG |
| | SE3 Left origami Edge- 11-nt Bridging Strands [2] |
| 4_L_SE 0-1_op | TTGATGGATGGATCCTTTGCCCGAACGCGACAACTCGTATTAAATGATGTACCC |
| 4_L_SE 0-1_op | TTGATGGATGGATCCTTTGCCCGAACGCGACAACTCGTATTAAATGATGTACCC |
| 4_L_SE 0-1_op | TTGATGGATGGATCCTTTGCCCGAACGCGACAACTCGTATTAAATGATGTACCC |
| 4_L_SE 0-1_op | TTGATGGATGGATCCTTTGCCCGAACGCGACAACTCGTATTAAATGATGTACCC |
| 4_L_SE 0-1_op | TTGATGGATGGATCCTTTGCCCGAACGCGACAACTCGTATTAAATGATGTACCC |
| 4_L_SE 0-1_op | TTGATGGATGGATCCTTTGCCCGAACGCGACAACTCGTATTAAATGATGTACCC |
| 4_L_SE 0-1_op | TTGATGGATGGATCCTTTGCCCGAACGCGACAACTCGTATTAAATGATGTACCC |
| 4_L_SE 0-1_op | TTGATGGATGGATCCTTTGCCCGAACGCGACAACTCGTATTAAATGATGTACCC |

[1] green color indicates poly-T overhangs

[2] each color indicates a SE set

**Table E.4:** Labeling strands.

| Name | Exit Position Helix[base] | Sequence 5'→3' |
|---|---|---|
| | | Staples Extension out of origami-A [3,4] |
| LCO-96-EXT | 7[96] | ATATAGACGTTGTGGCTGCTTCTAAGAACACACCCTGAACAAAGATCTTACC |
| LCO-123-EXT | 9[96] | ATATAGACGTTGTGGCTGCTTGAAGCCCTTATTGACGGAAATTATGGAAACGT |
| LCO-83-EXT | 6[111] | ATATAGACGTTGTGGCTGCTTCAAGAACGTCAACAGTAGGGCTTGACCTAAATTTAATGGTATGTGAG |
| LCO-110-EXT | 8[111] | ATATAGACGTTGTGGCTGCTTTTAACTGAGCGAGGCGTTTTAGCGTATCATTC |
| LCO-109-EXT | 8[79] | ATATAGACGTTGTGGCTGCTTTAATTGAGATATAGAAGGCTTATCCGCACTC |
| LCO-135-EXT | 10[79] | ATATAGACGTTGTGGCTGCTTGGTGAATTTGAAATAGCAATAGCTTCAGAGGG |
| | | Staples Extension out of origami-F [3,4] |
| LCO-93-EXT | 6[431] | ATATAGACGTTGTGGCTGCTTCAGTATCGTACGAGCCGGAAGCAACGCGCGGGGAGAGGCAAGCACTA |
| LCO-120-EXT | 8[431] | ATATAGACGTTGTGGCTGCTTCAGTCAAAATCAACATTAAATGTGGACGACGA |
| LCO-237-EXT | 7[448] | ATATAGACGTTGTGGCTGCTTACAACCCGCAAAAGGGTGAGAAAGATACTTTT |
| LCO-133-EXT | 9[448] | ATATAGACGTTGTGGCTGCTTGCGGGAGAAGAGTACCTTTAATTAAAAAGATTAAGAGGAAAAAATCT |
| LCO-121-EXT | 8[463] | ATATAGACGTTGTGGCTGCTTTAAAGATTTCGGATTCTCCGTGGCATCGTAA |

| | | |
|---|---|---|
| LCO-148-EXT | 10[463] | ATATAGACGTTGTGGCTGCTTAGGATTAGAGCCTTTATTTCAACGTGTGTAGG |
| LCO-ATTO647 | | GCAGCCACAACGTCTATATCATATTO-647TGC |

(3) red indicates poly-T spacer
(4) green indicates elongation that hybridizes with labeled strands

**Table E.5:** Biotinylated strands.

| Name | Exit Position Helix[base] | Sequence 5'→3' |
|---|---|---|
| LCO-43-Biotin | 3[112] | /5Biosg/TTTTTGAATAACAAATCGCGCAGAGGCGAAACCACCAGAAGGAGATTAGAG |
| LCO-54-Biotin | 3[432] | /5Biosg/TTTTAATCGGAACGCTGCGCGTAACCACGAAATACCTACATTTGAATACGT |
| LCO-162-Biotin | 12[127] | /5Biosg/TTTTGACAGGAGTCAGTGCCTTGAGTAACCGCCACCCTCAGAAGTCTTTCC |
| LCO-173-Biotin | 12[447] | /5Biosg/TTTTACGTTAATGTAAATTGGGCTTGAGAAATACGTAATGCCACCCTCAGC |

(3) red indicates poly-T spacer

**Table E.6:** Dumbbell strands for AFM letters labeling.

| Name | Oligo Position 5' Helix[base]--> 3' Helix[base] | Sequence 5'→3' |
|---|---|---|
| LCO_DB_167 | 12[271] --> 10[272] | AAAATAGCGGGGTAATTCCTCTTTTGAGGAACAAGTTTTCTTGTAGTAAAATTAGTTTG |
| LCO_DB_101 | 7[256] --> 8[240] | AGAAAAGCTCATATGTTCCTCTTTTGAGGAACAAGTTTTCTTGTACCCCGGTGTTACAAA |
| LCO_DB_35 | 2[271] --> 0[272] | CCTGAGAAAAAGAGTCTCCTCTTTTGAGGAACAAGTTTTCTTGTTGTCCATCACGCTGAG |
| LCO_DB_139 | 10[207] --> 8[208] | CGGAATAATAAGACTCTCCTCTTTTGAGGAACAAGTTTTCTTGTCTTATTACCAATCCAA |
| LCO_DB_63 | 4[303] --> 2[304] | CCCAGCAGGGAACAAGTCCTCTTTTGAGGAACAAGTTTTCTTGTAGTCCACTCCGATTAA |
| LCO_DB_88 | 6[271] --> 4[272] | GGATGTGCTTTTCCCATCCTCTTTTGAGGAACAAGTTTTCTTGTGTCACGACGATGGTGG |
| LCO_DB_62 | 4[271] --> 2[272] | TTCCGAAACCCGAGATTCCTCTTTTGAGGAACAAGTTTTCTTGTAGGGTTGGCCAGAAT |
| LCO_DB_74 | 5[256] --> 6[240] | CGCCAGGGTGCAAGGTCCTCTTTTGAGGAACAAGTTTTCTTGTCGATTAAGCAACATGT |
| LCO_DB_153 | 11[224] --> 13[223] | TCTTTTCAGGAACCGTCCTCTTTTGAGGAACAAGTTTTCTTGTCCTCCCTCAGACTCCT |
| LCO_DB_114 | 8[239] --> 7[255] | ATAAACAGAGAGCCTATCCTCTTTTGAGGAACAAGTTTTCTTGTATTTGCCATGATAATC |
| LCO_DB_89 | 6[303] --> 4[304] | CCTCTTCGCAGTGCCATCCTCTTTTGAGGAACAAGTTTTCTTGTAGCTTGCTGGTTTGC |
| LCO_DB_173(f2/3) | 11[288] --> 13[287] | CTGGATAGTTTACCATCCTCTTTTGAGGAACAAGTTTTCTTGTGACGACGAGGACAGAT |
| LCO_DB_207 | 15[288] --> 14[304] | GTTTATCAGCTTGCTTTCCTCTTTTGAGGAACAAGTTTTCTTGTTCGAGGTGTTGTGTCG |
| LCO_DB_60 | 4[207] --> 2[208] | TATATGTACTGAGAAGTCCTCTTTTGAGGAACAAGTTTTCTTGTAGTCAATAGGTTTAA |
| LCO_DB_48 | 3[256] --> 4[240] | AAGAATAGTCGGCAAATCCTCTTTTGAGGAACAAGTTTTCTTGTATCCCTTACTACCTTT |
| LCO_DB_49 | 3[288] --> 5[287] | TCCAGTTTGCGAAAATCCTCTTTTGAGGAACAAGTTTTCTTGTTCCTGTTTGTTGTAAA |
| LCO_DB_166 | 12[239] --> 11[255] | CCACCACCTAATCAAATCCTCTTTTGAGGAACAAGTTTTCTTGTATCACCGGAGAAGTTT |
| LCO_DB_192 | 14[239] --> 13[255] | CTCAGTACGGATTAGGTCCTCTTTTGAGGAACAAGTTTTCTTGTATTAGCGATAAGGGA |
| LCO_DB_7 | 0[239] --> 1[223] | CCTTGCTGAACCTCATCCTCTTTTGAGGAACAAGTTTTCTTGTAATATCAAAGAACCTA |
| LCO_DB_87 | 6[239] --> 5[255] | TCAGCTAAAGACGACGTCCTCTTTTGAGGAACAAGTTTTCTTGTACAATAAATTGGGTAA |
| LCO_DB_34 | 2[239] --> 1[255] | AATAAAGAAAATTATTTCCTCTTTTGAGGAACAAGTTTTCTTGTTGCACGTGTGAGGCC |
| LCO_DB_116 | 8[303] --> 6[304] | GAGAATCGTTTAAATTTCCTCTTTTGAGGAACAAGTTTTCTTGTGTAAACGTGGTGCGGG |
| LCO_DB_61 | 4[239] --> 3[255] | TTAACCTCTCATAGGTTCCTCTTTTGAGGAACAAGTTTTCTTGTCTGAGAGATAAATCAA |
| LCO_DB_154 | 11[256] --> 12[240] | TGCCAGAGGAGAGGCTTCCTCTTTTGAGGAACAAGTTTTCTTGTTTTGCAAAAACCAGAG |
| LCO_DB_191 | 14[207] --> 12[208] | GGTTGATAAAGTATTATCCTCTTTTGAGGAACAAGTTTTCTTGTAGAGGCTGAGAGCCGC |
| LCO_DB_47 | 3[224] --> 5[223] | TATCAAAACGGCTTATCCTCTTTTGAGGAACAAGTTTTCTTGTGGTTGGGTTAAAGTAA |
| LCO_DB_8 | 0[271] --> 0[240] | AGCCAGCAGCAAATGATCCTCTTTTGAGGAACAAGTTTTCTTGTAAAATCTAAAGCATCA |
| LCO_DB_73 | 5[224] --> 7[223] | TTCTGTCCTGCAGAACTCCTCTTTTGAGGAACAAGTTTTCTTGTGCGCCTGTTAACGAGC |
| LCO_DB_100 | 7[224] --> 9[223] | GTCTTTCCCCATATTTCCTCTTTTGAGGAACAAGTTTTCTTGTATTTATCCGCAGTATG |
| LCO_DB_86 | 6[207] --> 4[208] | AATAGATAAAGTACCGTCCTCTTTTGAGGAACAAGTTTTCTTGTACAAAAGGTATATAAC |
| LCO_DB_133f1_173i1 | 9[288] --> 11[287] | AGCTGAAACTGCGAACTCCTCTTTTGAGGAACAAGTTTTCTTGTGAGTAGATTGTTTAGA |
| LCO_DB_165 | 12[207] --> 10[208] | CACCCTCAAGCCCCCTTCCTCTTTTGAGGAACAAGTTTTCTTGTTATTAGCAGACACCA |
| LCO_DB_206 | 15[256] --> 14[272] | AAGGCTCCAAAAGGAGTCCTCTTTTGAGGAACAAGTTTTCTTGTCCTTTAACTTAGCCG |
| LCO_DB_140 | 10[239] --> 9[255] | TGGCAACACGTAGAAATCCTCTTTTGAGGAACAAGTTTTCTTGTATACATAGGTCAATA |
| LCO_DB_9 | 0[303] --> 1[287] | TTAACACCGCCTGCATCCTCTTTTGAGGAACAAGTTTTCTTGTACAGTGCCACGCAAAT |
| LCO_DB_22 | 1[256] --> 2[240] | ACCGAGTAGTGTTTTTCCTCTTTTGAGGAACAAGTTTTCTTGTTATAATCAAAAACAGA |
| LCO_DB_127 | 9[224] --> 11[223] | TTAGCAAATATAAAAGTCCTCTTTTGAGGAACAAGTTTTCTTGTAAACGCAAGTTTGCCA |
| LCO_DB_168 | 12[303] --> 10[304] | AACCCTCGCGTCCAATTCCTCTTTTGAGGAACAAGTTTTCTTGTACTGCGGACAGTTGAT |
| LCO_DB_204 | 15[192] --> 14[208] | AGTGAGAATAGAAAGGTCCTCTTTTGAGGAACAAGTTTTCTTGTAACAACTGTCGAGAG |
| LCO_DB_33 | 2[207] --> 0[208] | CGTCAGATGAATAATGTCCTCTTTTGAGGAACAAGTTTTCTTGTGAAGGGTTACCCTCAA |

| | | |
|---|---|---|
| LCO_DB_143 | 10[303] --> 8[304] | TCCCAATTAGGTGGCATCCTCTTTTGAGGAACAAGTTTTCTTGTTCAATTCGCAAACAA |
| LCO_DB_181 | 13[288] --> 15[287] | GAACGGTGGACCTGCTTCCTCTTTTGAGGAACAAGTTTTCTTGTCCATGTTATTGTATCG |
| LCO_DB_36 | 2[303] --> 0[304] | AGGGATTTGTAGCAATTCCTCTTTTGAGGAACAAGTTTTCTTGTACTTCTTGGTCAGTA |
| LCO_DB_141 | 10[271] --> 8[272] | ACCATTAGAGCTATATTCCTCTTTTGAGGAACAAGTTTTCTTGTTTTCATTTAAAACTAG |
| LCO_DB_194 | 14[303] --> 12[304] | AAATCCGCTACAGACCTCCTCTTTTGAGGAACAAGTTTTCTTGTAGGCGCAACTATCAT |
| LCO_DB_180 | 13[256] --> 14[240] | ACCGAACTCGCAGACTCCTCTTTTGAGGAACAAGTTTTCTTGTGGTCAATCGGGTTTTG |
| LCO_DB_21 | 1[224] --> 3[223] | CCATATCAAATTGCGTTCCTCTTTTGAGGAACAAGTTTTCTTGTAGATTTTCAGTGAATT |
| LCO_DB_179 | 13[224] --> 15[223] | CAAGAGAACAGGCGGATCCTCTTTTGAGGAACAAGTTTTCTTGTTAAGTGCCAAAGGAAT |
| LCO_DB_75 | 5[288] --> 7[287] | ACGACGGCCTATTACGTCCTCTTTTGAGGAACAAGTTTTCTTGTCCAGCTGGATTGTATA |
| LCO_DB_115 | 8[271] --> 6[272] | CATGTCAACCCAAAAATCCTCTTTTGAGGAACAAGTTTTCTTGTCAGGAAGCGAAAGGG |
| LCO_DB_113 | 8[207] --> 6[208] | ATAAGAAAGAATCTTATCCTCTTTTGAGGAACAAGTTTTCTTGTCCAACGCTTATCAAC |
| LCO_DB_133(i2/3) | 7[288] --> 9[287] | AGCAAATAATGAACGTCCTCTTTTGAGGAACAAGTTTTCTTGTGTAATCGTGGGGCGCG |
| LCO_DB_205 | 15[224] --> 15[255] | TGCGAATAATAATTTTTCCTCTTTTGAGGAACAAGTTTTCTTGTGAAAATCTCCAAAAAA |
| LCO_DB_193 | 14[271] --> 12[272] | GAACGAGGGACCAACTTCCTCTTTTGAGGAACAAGTTTTCTTGTTTGAAAGATAAAAACC |
| LCO_DB_128 | 9[256] --> 10[240] | ACCTGTTTATACATTTCCTCTTTTGAGGAACAAGTTTTCTTGTTCGCAAATCATAAAGG |
| LCO_DB_23 | 1[288] --> 3[287] | TAACCGTTTAGACAGGTCCTCTTTTGAGGAACAAGTTTTCTTGTAACGGTACAGTGTTGT |

[5] orange indicates dumbbells

The DNA origami modification used to form letter is Dumbbell hairpins inserted into the midpoint of selected staples [36].

**Table E.7:** Letters configurations.

| Letter | Exit Position (strand number) |
|---|---|
| A | 60,86,113,139,165,191,204,21,47,73,100,127,153,179,34,61,140,166,22,101,128,167,141,62,35,23,49,75,133(i2/3),133(f1/3)173(i/3),173(f2/3),181,207,63,89,116,143,168,194 |
| B | 33,60,86,113,139,165,191,204,7,21,47,73,100,127,153,179,205,34,114,192,180,154,101,74,22,8,35,62,88,141,167,193,23,49,133(f1/3)173(i2/3) |
| C | 60,86,113,139,165,191,21,47,73,100,127,153,179,205,34,61,192,22,180,206,8,35,193,23,181,207,9,36,194 |
| D | 33,60,86,113,139,165,191,204,21,47,73,100,127,153,179,205,7,34,192,22,154,180,8,35,62,88,167,193,23,49, 75, 133(i2/3),133(f1/3)173(i/3),173(f2/3),89,116,143,168 |
| E | 33,60,86,113,139,165,191,204,21,47,73,100,127,153,179,205,7,34,114,192,22,74,101,154,180,206,8,35,193,23,173(f2/3),9 |
| F | 33,60,86,113,139,165,191,204,21,47,73,100,127,153,179,7,34,114,22,74,101,8,35,115,23,9 |
| P | 7,21,33,47,60,73,86,100,113,127,139,153,165,179,191,204,8,334,101,114,23,35,49,62,75,88,115 |

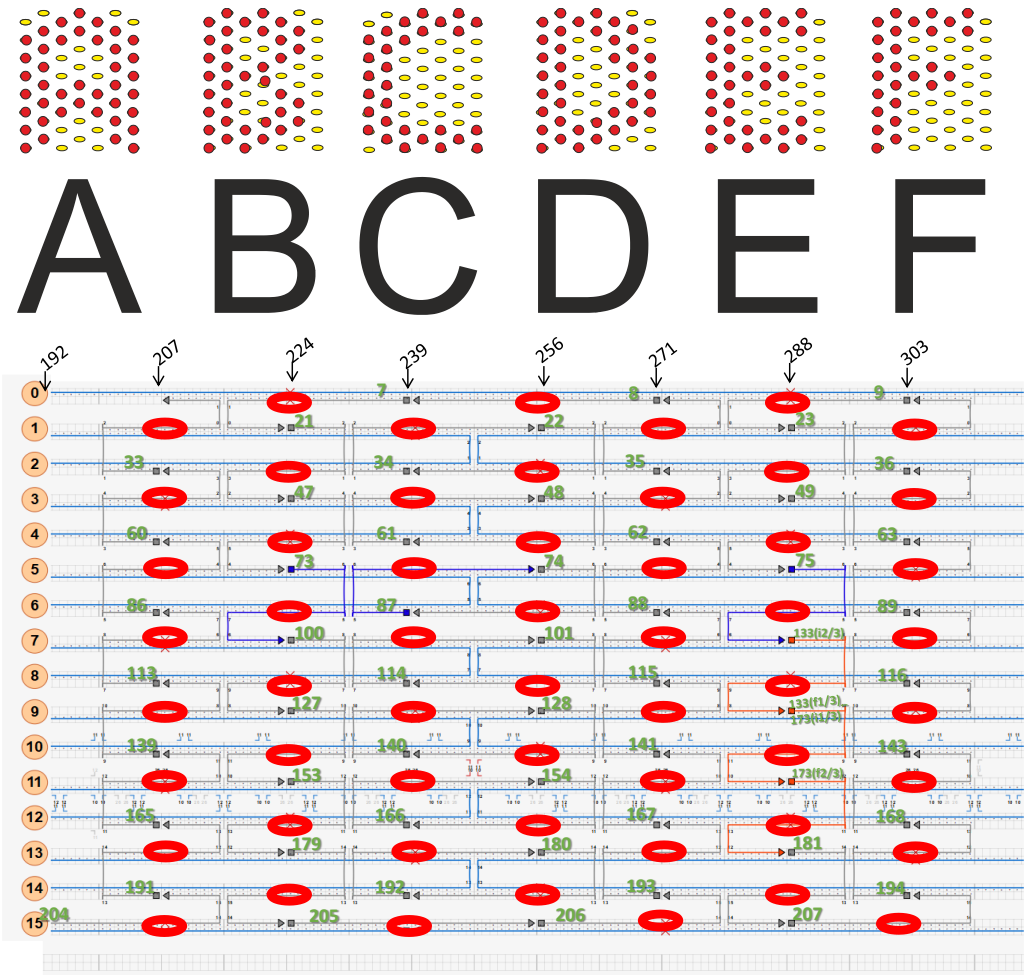


**Figure E.2:** Mapping of dumbbells for different letter designs.

## E.2 Rod

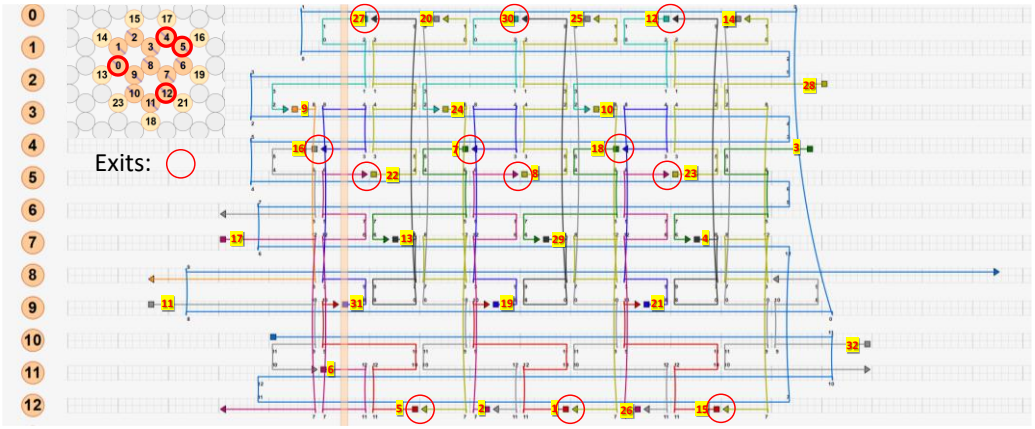


**Figure E.3: Cadnano file of the rod origami.** The red circle highlights the exit points for labeling, and the yellow highlights indicate the strand numbers.

IV_CS10_1033_v1, Dietz lab name 'Sam':

AGACTTCCGGCTTAAGCTCTGAAAGGGTTCTATATCTCCAGGTAGATCTGCTCCCAATGTAACATGCTCGGGACCTACAAGGTGTCAGGATCGAAGATTGCACGACGATGACTTACGGACAGCCGGACGTACTCCCTGAACAATGCGATT
CGATATACACGGTGGTGTTCTGTTTGGGCCTTCTGACTCAAAGCCAAGCCTGGATAACAGTGTCCTTCGGGTCCTCCGTGTTATGGAGCACGGCTGCTTAGAGCATTGCCACGGAGCCTTTGAAGGCAGCGAGGGCGTGGCCTCCCGACC

GCACTAGCACAACACAGGAGAGGACCGGCGACATACCTGGGTGGAAGTTTCATCGGAATACTCGTCAAACGACTAACCCATCAGCCATCGATCGTATGAATATGTATAATCCATCCGTACCTAGAGTCGCGGGCCAGCATCAACGCATGT
GGTAAATTGGTTGGATCCGCGAGCAGTAAGAACCCTTAAATCAAGCTTCCCGGCACAGCGTCAGTGGCGGATACGCGCGATGTCTGCCGTGCTGAAGTAGGGTAAGGGCCCTCCATGCGGACTTCTTGGTAGCTCCAAGAGTGGATTCCC
TCGTAAGTTCGGCTACGTCATTTACTGCAGCCTCTGCAAGCGGAGGAACTCCACTATGCACTTAGGGACTACTGATATCAAATTCGCCGCCGAAACCCGCAAGATGGTGCTCTTTAACTGGCCAATACATAGCCCAGTGAAACTGTTCGC
ATATGGCGAACCTTTCTGCGCCACTTGTTTCGCGCACGTTTAGGAGCTTATTAGCTAAATGAACCAGTTCTCTGGAGTGATACAGACTTGCGGCGTCCCGTAAACCGAGAGTAACTTAACCATAAAGCTGGTGGGTATAGAACATATAGC
GATCAGTACGGCCATTTGACGGCAAATACCGTCTGGCTGGCAAGTCGGGCTGATGAAATGCCTGACAGAACTTGAACTGACCAGAAGTGAGCAAAGGCGGTCTCAATTAACACTTTCCTATACGACACGTTGA

**Table E.8:** Rod origami staples.

| Name | Oligo Position<br>5' Helix[base]--> 3' Helix[base] | Sequence 5'→3' |
|---|---|---|
| RW_1 | 12[69] --> 9[58] | TCCAGGCGCTGTCCCCTGGAGATATAGAAGC |
| RW_2 | 12[58] --> 5[62] | CTTGCTGCCTCTTCCACGCGACTC |
| RW_3 | 4[103] --> 7[86] | **TTTTT**GCAGACATCGACGATCGGATGGGTTAGTCGTTCT |
| RW_4 | 7[87] --> 0[84] | AAGCTTGCTCAACGGGACCTGGTTC |
| RW_5 | 12[48] --> 9[37] | GAAGGCCATTGTTCCAGAGCTTAAGCCGGCT |
| RW_6 | 11[35] --> 5[41] | GAATCGCCAAACAGCGGTCGGGGTCCTCCACATGC |
| RW_7 | 4[55] --> 7[44] | GATTTAACTGGCCCCCAGGTATGTCGCCGAG |
| RW_8 | 5[63] --> 0[73] | TAGGTACGTGCCGGGAAGTCCCATAGTGTATTGGCCAGTTAATAAT |
| RW_9 | 3[31] --> 8[11] | CTTAAGCCAGACGGTATTTGCCG**TTTTT** |
| RW_10 | 3[73] --> 12[70] | TGGATCAGTTCCTCCGTGACTGTTA |
| RW_11 | 9[11] --> 11[34] | **TTTTT**TCAAATGGCCGTACTGATCGAAGTCTGTATATC |
| RW_12 | 0[83] --> 3[72] | ATTTAGCAGAGCACGTAGTCCCTAAGTGGCA |
| RW_13 | 7[45] --> 0[42] | GCCACAGCCCGGTTCTATAGTGGCG |
| RW_14 | 0[93] --> 11[111] | GAAGCCGCAACGAGCATTTCGATCCTGACACCT**TTTTT** |
| RW_15 | 12[90] --> 9[79] | AGGACCCTGCAATCGTTACATTGGGAGCTCG |
| RW_16 | 4[34] --> 6[21] | CGCGGATAATTTACTCCTGTGTT**TTTTT** |
| RW_17 | 7[21] --> 12[21] | **TTTTT**GTGCTAGTGAACACCACC**TTTTT** |
| RW_18 | 4[76] --> 7[65] | TGACGCTGGATGGAGTATTCCGATGAAATCA |
| RW_19 | 9[59] --> 4[56] | TTTAGTCAGGCCTACCAAGAAGCTT |
| RW_20 | 0[51] --> 12[59] | ACAACCCACCACCCTTTAGGGAGTACGTCCGTTGG |
| RW_21 | 9[80] --> 4[77] | GTTTCTTCTGGGGGCCCTCCGCCAC |
| RW_22 | 5[42] --> 0[52] | GTTGATGGGGTTCTATCCACTGCAGAGGGAACAGTTTCACTGCGAA |
| RW_23 | 5[84] --> 0[94] | TATTCATCGCGTATTACCCTAGATATCACATCTTGCGGGTTTCAGA |
| RW_24 | 3[52] --> 12[49] | GGAGATTTCATCGCCCTCTGAGTCA |
| RW_25 | 0[72] --> 12[80] | AAGGTTACTCAGATCTAGTAAGTCATCGTCGGAAG |
| RW_26 | 12[79] --> 5[83] | GACGCAATGCTTGACGATTATACA |
| RW_27 | 0[41] --> 3[30] | CAGAAAGCATATGCCTGCAGTAAATGACGAA |
| RW_28 | 2[105] --> 12[91] | **TTTTT**CGGCGAATTTCTTCAGCACCGCCTAGCCGTGAACACGG |
| RW_29 | 7[66] --> 0[63] | AAGGAAGTTCTTGGTTAACTCCTAA |
| RW_30 | 0[62] --> 3[51] | ACGTGCGGGCTATGGAGTTCCTCCGCTTCTT |
| RW_31 | 9[38] --> 4[35] | ATATACTTGCCCGAGGGATACTGCT |
| RW_32 | 10[111] --> 8[98] | **TTTTT**TGTAGGTCCGTCTGTAAATTGAG |

## E.3 Disc

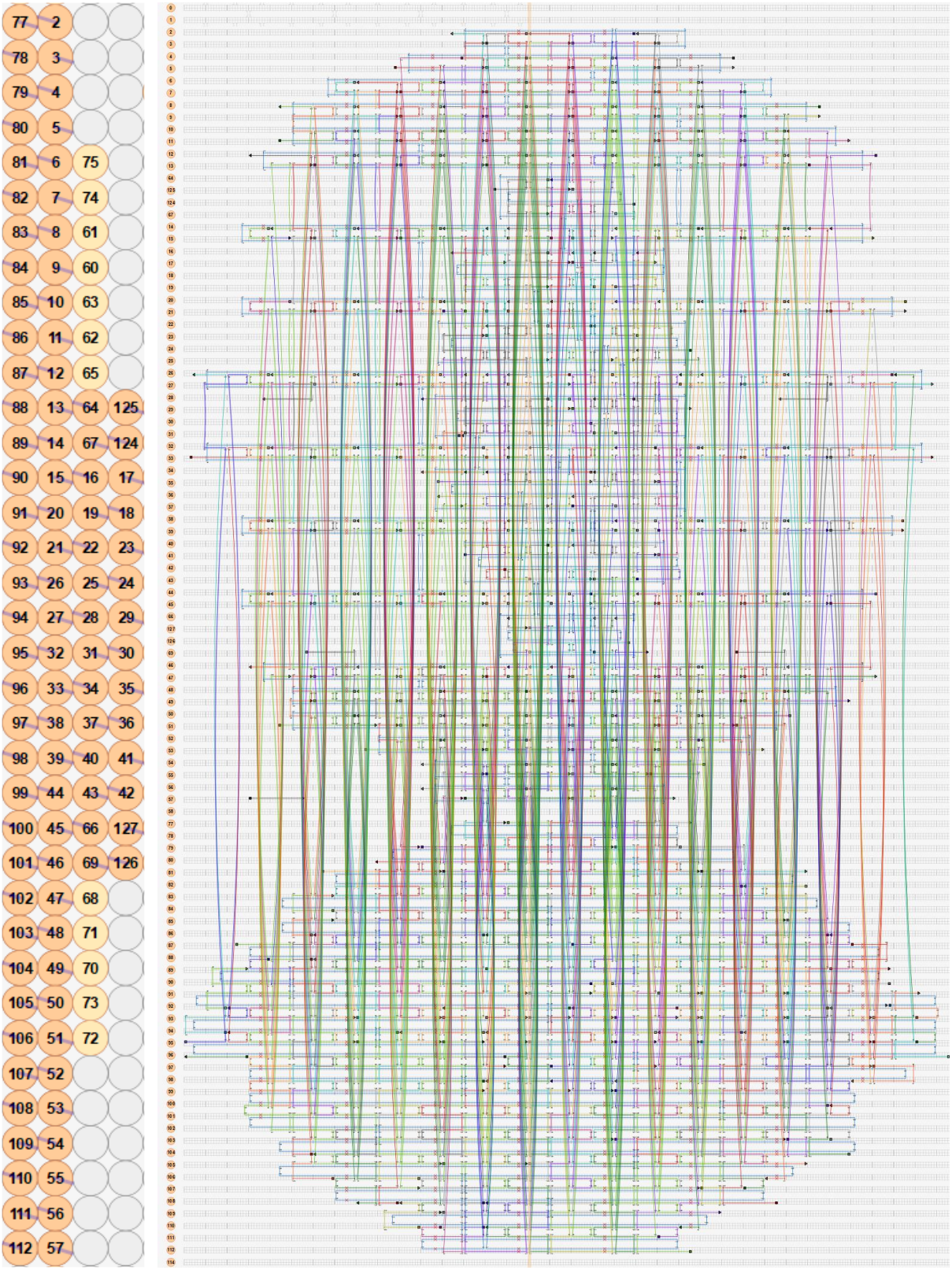


**Figure E.4:** Cadnano file of the disc origami.

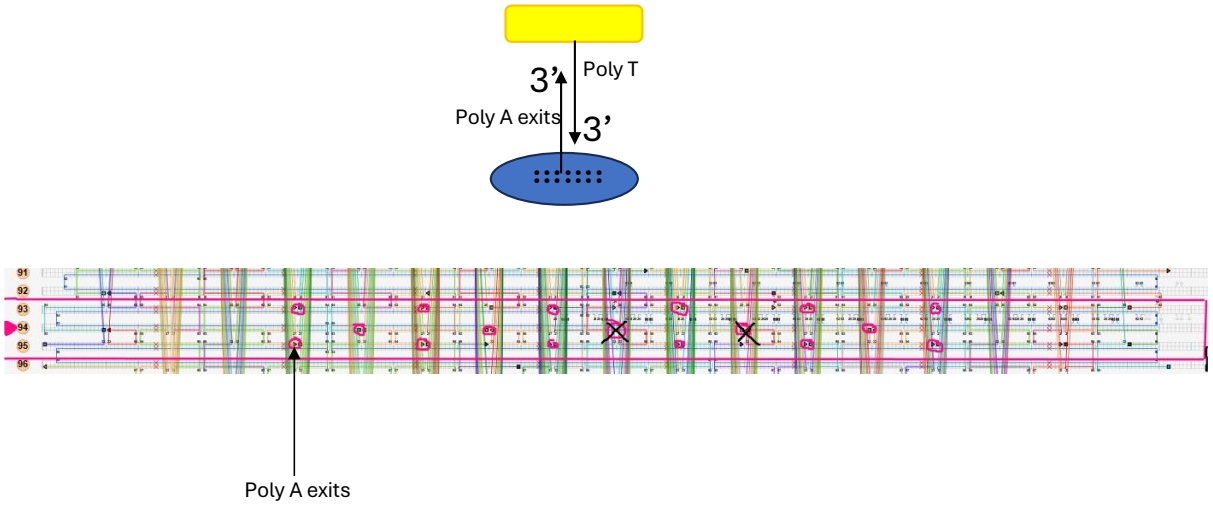


**Figure E.5:** Exact gold disc connectivity.

## Scaffold p8064:

GGCAATGACCTGATAGCCTTTGTAGATCTCTCAAAAATAGCTACCCTCTCCGGCATTAATTTATCAGCTAGAACGGTTGAATATCATATTGATGGTGATTTGACTGTCTCCGGCCTTTCTCACCCTTTTGAATCTTTACCTACACATTAC
TCAGGCATTGCATTTAAAATATATGAGGGTTCTAAAAATTTTTATCCTTGCGTTGAAATAAAGGCTTCTCCCGCAAAAGTATTACAGGGTCATAATGTTTTTGGTACAACCGATTTAGCTTTATGCTCTGAGGCTTTATTGCTTAATTTT
GCTAATTCTTTGCCTTGCCTGTATGATTTATTGGATGTTAATGCTACTACTATTAGTAGAATTGATGCCACCTTTTCAGCTCGCGCCCCAAATGAAAATATAGCTAAACAGGTTATTGACCATTTGCGAAATGTATCTAATGGTCAAACT
AAATCTACTCGTTCGCAGAATTGGGAATCAACTGTTATATGGAATGAAACTTCCAGACACCGTACTTTAGTTGCATATTTAAAACATGTTGAGCTACAGCATTATATTCAGCAATTAAGCTCTAAGCCATCCGCAAAAATGACCTCTTAT
CAAAAGGAGCAATTAAAGGTACTCTCTAATCCTGACCTGTTGGAGTTTGCTTCCGGTCTGGTTCGCTTTGAAGCTCGAATTAAAACGCGATATTTGAAGTCTTTCGGGCTTCCTCTTAATCTTTTTGATGCAATCCGCTTTGCTTCTGAC
TATAATAGTCAGGGTAAAGACCTGATTTTTGATTTATGGTCATTCTCGTTTTCTGAACTGTTTAAAGCATTTGAGGGGGATTCAATGAATATTTATGACGATTCGGAGCTGATCCGACTATTGGACGCTATCCAGTCTAAACATTTTACTATACCCCC
TCTGGCAAAACTTCTTTTGCAAAAGCCTCTCGCTATTTTGGTTTTTATCGTCGTCTGGTAAACGAGGGTTATGATAGTGTTGCTCTTACTATGCCTCGTAATTCCTTTTGGCGTTATGTATCTGCATTAGTTGAATGTGGTATTCCTAAA
TCTCAACTGATGAATCTTTCTACCTGTAATAATGTTGTTCCGTTAGTTCGTTTTATTAACGTAGATTTTTCTTCCCAACGTCCTGACTGGTATAATGAGCCAGTTCTTAAAATCGCATAAGGTAATTCACAATGATTAAAGTTGAAATTA
AACCATCTCAAGCCCAATTTACTACTCGTTCTGGTGTTTCTCGTCAGGGCAAGCCTTATTCACTGAATGAGCAGCTTTGTTACGTTGATTTGGGTAATGAATATCCGGTTCTTGTCAAGATTACTCTTGATGAAGGTCAGCCAGCCTATG
CGCCTGGTCTGTACACCGTTCATCTGTCCTCTTTCAAAGTTGGTCAGTTCGGTTCCCTTATGATTGACCGTCTGCGCCTCGTTCCGGCTAAGTAACATGGAGCAGGTCGCGGATTTCGACACAATTTATCAGGCGATGATACAAATCTCC
GTTGTACTTTGTTTCGCGCTTGGTATAATCGCTGGGGGTCAAAGATGAGTGTTTTAGTGTATTCTTTTGCCTCTTTCGTTTTAGGTTGGTGCCTTCGTAGTGGCATTACGTATTTTACCCGTTTAATGGAAACTTCCTCATGAAAAAGTC
TTTAGTCCTCAAAGCCTCTGTAGCCGTTGCTACCCTCGTTCCGATGCTGTCTTTCGCTGCTGAGGGTGACGATCCCGCAAAAGCGGCCTTTAACTCCCTGCAAGCCTCAGCGACCGAATATATCGGTTATGCGTGGGCGATGGTTGTTGT
CATTGTCGGCGCAACTATCGGTATCAAGCTGTTTAAGAAATTCACCTCGAAAGCAAGCTGATAAACCGATACAATTAAAGGCTCCTTTTGGAGCCTTTTTTTTGGAGATTTTCAACGTGAAAAAATTATTATTCGCAATTCCTTTAGTTG
TTCCTTTCTATTCTCACTCCGCTGAAACTGTTGAAAGTTGTTTAGCAAAATCCCATACAGAAAATTCATTTACTAACGTCTGGAAAGACGACAAAACTTTAGATCGTTACGCTAACTATGAGGGCTGTCTGTGGAATGCTACAGGCGTTG
TAGTTTGTACTGGTGACGAAACTCAGTGTTACGGTACATGGGTTCCTATTGGGCTTGCTATCCCTGAAAATGAGGGTGGTGGCTCTGAGGGTGGCGGTTCTGAGGGTGGCGGTTCTGAGGGTGGCGGTACTAAACCTCCTGAGTACGGTG
ATACACCTATTCCGGGCTATACTTATATCAACCCTCTCGACGGCACTTATCCGCCTGGTACTGAGCAAAACCCCGCTAATCCTAATCCTTCTCTTGAGGAGTCTCAGCCTCTTAATACTTTCATGTTTCAGAATAATAGGTTCCGAAATA
GGCAGGGGGCATTAACTGTTTATACGGGCACTGTTACTCAAGGCACTGACCCCGTTAAAACTTATTACCAGTACACTCCTGTATCATCAAAAGCCATGTATGACGCTTACTGGAACGGTAAATTCAGAGACTGCGCTTTCCATTCTGGCT
TTAATGAGGATTTATTTGTTTGTGAATATCAAGGCCAATCGTCTGACCTGCCTCAACCTCCTGTCAATGCTGGCGGCGGCTCTGGTGGTGGTTCTGGTGGCGGCTCTGAGGGTGGTGGCTCTGAGGGTGGCGGTTCTGAGGGTGGCGGCT
CTGAGGGAGGCGGTTCCGGTGGTGGCTCTGGTTCCGGTGATTTTGATTATGAAAAGATGGCAAACGCTAATAAGGGGGCTATGACCGAAAATGCCGATGAAAACGCGCTACAGTCTGACGCTAAAGGCAAACTTGATTCTGTCGCTACTG
ATTACGGTGCTGCTATCGATGGTTTCATTGGTGACGTTTCCGGCCTTGCTAATGGTAATGGTGCTACTGGTGATTTTGCTGGCTCTAATTCCCAAATGGCTCAAGTCGGTGACGGTGATAATTCACCTTTAATGAATAATTTCCGTCAAT
ATTTACCTTCCCTCCCTCAATCGGTTGAATGTCGCCCTTTGTCTTTGGCGCTGGTAAACCATATGAATTTTCTATTGATTGTGACAAAATAAACTTATTCCGTGGTGTCTTTGCGTTTCTTTTATATGTTGCCACCTTTATGTATGTAT
TTTCTACGTTTGCTAACATACTGCGTAATAAGGAGTCTTAATCATGCCAGTTCTTTTGGGTATTCCGTTATTATTGCGTTTCCTCGGTTTCCTTCTGGTAACTTTGTTCGGCTATCTGCTTACTTTTCTTAAAAAGGGCTTCGGTAAGAT
AGCTATTGCTATTTCATTGTTTCTTGCTCTTATTATTGGGCTTAACTCAATTCTTGTGGGTTATCTCTCTGATATTAGCGCTCAATTACCCTCTGACTTTGTTCAGGGTGTTCAGTTAATTCTCCCGTCTAATGCGCTTCCCTGTTTTTA
TGTTATTCTCTCTGTAAAGGCTGCTATTTTCATTTTTGACGTTAAACAAAAAATCGTTTCTTATTTGGATTGGGATAAATAATATGGCTGTTTATTTTGTAACTGGCAAATTAGGCTCTGGAAAGACGCTCGTTAGCGTTGGTAAGATTC
AGGATAAAATTGTAGCTGGGTGCAAAATAGCAACTAATCTTGATTTAAGGCTTCAAAACCTCCCGCAAGTCGGGAGGTTCGCTAAAACGCCTCGCGTTCTTAGAATACCGGATAAGCCTTCTATATCTGATTTGCTTGCTATTGGGCGCG
GTAATGATTCCTACGATGAAAATAAAAACGGCTTGCTTGTTCTCGATGAGTGCGGTACTTGGTTTAATACCCGTTCTTGGAATGATAAGGAAAGACAGCCGATTATTGATTGGTTTCTACATGCTCGTAAATTAGGATGGGATATTATTTT
TTCTTGTTCAGGACTTATCTATTGTTGATAAACAGGCGCGTTCTGCATTAGCTGAACATGTTGTTTATTGTCGTCGTCTGGACAGAATTACTTTACCTTTTGTCGGTACTTTATATTCTCTTATTACTGGCTCGAAAATGCCTCTGCCTA
AATTACATGTTGGCGTTGTTAAATATGGCGATTCTCAATTAAGCCCTACTGTTGAGCGTTGGCTTTATACTGGTAAGAATTTGTATAACGCATATGATACTAAACAGGCTTTTTCTAGTAATTATGATTCCGGTGTTTATTCTTATTTAA
CGCCTTATTTATCACACGGTCGGTATTTCAAACCATTAAATTTAGGTCAGAAGATGAAATTAACTAAAATATATTTGAAAAAGTTTTCTCGCGTTCTTTGTCTTGCGATTGGATTTGCATCAGCATTTACATATAGTTATATAACCCAAC
CTAAGCCGGAGGTTAAAAAGGTAGTCTCTCAGACCTATGATTTTGATAAATTCACTATTGACTCTTCTCAGCGTCTTAATCTAAGCTATCGCTATGTTTTCAAGGATTCTAAGGGAAAATTAATTAATAGCGACGATTTACAGAAGCAAG
GTTATTCACTCACATATATTGATTTATGTACTGTTTCCATTAAAAAAGGTAATTCAAATGAAATTGTTAAATGTAATTAATTTTGTTTTCTTGATGTTTGTTTCATCATCTTCTTTTGCTCAGGTAATTGAAATGAATAATTCGCCTCTG
CGCGATTTTGTAACTTGGTATTCAAAGCAATCAGGCGAATCCGTTATTGTTTCTCCCGATGTAAAAGGTACTGTTACTGTATATTCATCTGACGTTAAACCTGAAAATCTACGCAATTTCTTTATTTCTGTTTTACGTGCAAATAATTTT
GATATGGTAGGTTCTAACCCTTCCATTATTCAGAAGTATAATCCAAACAATCAGGATTATATTGATGAATTGCCATCATCTGATAATCAGGAATATGATGATAATTCCGCTCCTTCTGGTGGTTTCTTTGTTCCGCAAAATGATAATGTT
ACTCAAACTTTTAAAATTAATAACGTTCGGGCAAAGGATTTAATACGAGTTGTCGAATTGTTTGTAAAGTCTAATACTTCTAAATCCTCAAATGTATTATCTATTGACGGCTCTAATCTATTAGTTGTTAGTGCTCCTAAAGATATTTTA
GATAACCTTCCTCAATTCCTTTCAACTGTTGATTTGCCAACTGACCAGATATTGATTGAGGGTTTGATATTTGAGGTTCAGCAAGGTGATGCTTTAGATTTTTCATTTGCTGCTGGCTCTCAGCGTGGCACTGTTGCAGGCGGTGTTAAT
ACTGACCGCCTCACCTCTGTTTTATCTTCTGCTGGTGGTTCGTTCGGTATTTTTAATGGCGATGTTTTAGGGCTATCAGTTCGCGCATTAAAGACTAATAGCCATTCAAAAATATTGTCTGTGCCACGTATTCTTACGCTTTCAGGTCAG
AAGGGTTCTATCTCTGTTGGCCAGAATGTCCCTTTTATTACTGGTCGTGTGACTGGTGAATCTGCCAATGTAAATAATCCATTTCAGACGATTGAGCGTCAAAATGTAGGTATTTCCATGAGCGTTTTTCCTGTTGCAATGGCTGGCGGT
AATATTGTTCTGGATATTACCAGCAAGGCCGATAGTTTGAGTTCTTCTACTCAGGCAAGTGATGTTATTACTAATCAAAGAAGTATTGCTACAACGGTTAATTTGCGTGATGGACAGACTCTTTTACTCGGTGGCCTCACTGATTATAAA
AACACTTCTCAGGATTCTGGCGTACCGTTCCTGTCTAAAATCCCTTTAATCGGCCTCCTGTTTAGCTCCCGCTCTGATTCTAACGAGGAAAGCACGTTATACGTGCTCGTCAAAGCAACCATAGTACGCGCCCTGTAGCGGCGCATTAAG
CGCGGCGGGTGTGGTGGTTACGCGCAGCGTGACCGCTACACTTGCCAGCGCCCTAGCGCCCGCTCCTTTCGCTTTCTTCCCTTCCTTTCTCGCCACGTTCGCCGGCTTTCCCCGTCAAGCTCTAAATCGGGGGCTCCCTTTAGGGTTCCG
ATTTAGTGCTTTACGGCACCTCGACCCCAAAAAACTTGATTTGGGTGATGGTTCACGTAGTGGGCCATCGCCCTGATAGACGGTTTTTCGCCCTTTGACGTTGGAGTCCACGTTCTTTAATAGTGGACTCTTGTTCCAAACTGGAACAAC
ACTCAACCCTATCTCGGGCTATTCTTTTGATTTATAAGGGATTTTGCCGATTTCGGAACCACCATCAAACAGGATTTTCGCCTGCTGGGGCAAACCAGCGTGGACCGCTTGCTGCAACTCTCTCAGGGCCAGGCGGTGAAGGGCAATCAG
CTGTTGCCCGTCTCACTGGTGAAAAGAAAAACCACCCTGGCGCCCAATACGCAAACCGCCTCTCCCCGCGCGTTGGCCGATTCATTAATGCAGCTGGCACGACAGGTTTCCCGACTGGAAAGCGGGCAGTGAGCGCAACGCAATTAATGT
GAGTTAGCTCACTCATTAGGCACCCCAGGCTTTACACTTTATGCTTCCGGCTCGTATGTTGTGTGGAATTGTGAGCGGATAACAATTTCACACAGGAAACAGCTATGACCATGATTACGAATTCGAGCTCGGTACCCGGGGATCCTCAAC
TGTGAGGAGGCTCACGGACGCGAAGAACAGGCACGCGTGCTGGCAGAAACCCCCGGTATGACCGTGAAAACGGCCCGCCGCATTCTGGCCGCAGCACCACAGAGTGCACAGGCGCGCAGTGACACTGCGCTGGATCGTCTGATGCAGGGG
GCACCGGCACCGCTGGCTGCAGGTAACCCGGCATCTGATGCCGTTAACGATTTGCTGAACACACCAGTGTAAGGGATGTTTATGACGAGCAAAGAAACCTTTACCCATTACCAGCCGCAGGGCAACAGTGACCCGGCTCATACCGCAACC
GCGCCCGGCGGATTGAGTGCGAAAGCGCCTGCAATGACCCCGCTGATGCTGGACACCTCCAGCCGTAAGCTGGTTGCGTGGGATGGCACCACCGACGGTGCTGCCGTTGGCATTCTTGCGGTTGCTGCTGACCAGACCAGCACCACGCTG
ACGTTCTACAAGTCCGGCACGTTCCGTTATGAGGATGTGCTCTGGCCGGAGGCTGCCAGCGACGAGACGAAAAAACGGACCGCGTTTGCCGGAACGGCAATCAGCATCGTTTAACTTTACCCTTCATCACTAAAGGCCGCCTGTGCGGCT
TTTTTTACGGGATTTTTTTATGTCGATGTACACAACCGCCCAACTGCTGGCGGCAAATGAGCAGAAATTTAAGTTTGATCCGCTGTTTCTGCGTCTCTTTTTCCGTGAGAGCTATCCCTTCACCACGGAGAAAGTCTATCTCTCACAAAT
TCCGGGACTGGTAAACATGGCGCTGTACGTTTCGCCGATTGTTTCCGGTGAGGTTATCCGTTCCCGTGGCGGCTCCACCTCTGAAAGCTTGGCACTGGCCGTCGTTTTACAACGTCGTGACTGGGAAAACCCTGGCGTTACCCAACTTAA
TCGCCTTGCAGCACATCCCCCTTTCGCCAGCTGGCGTAATAGCGAAGAGGCCCGCACCGATCGCCCTTCCCAACAGTTGCGCAGCCTGAATGGCGAATGGCGCTTTGCCTGGTTTCCGGCACCAGAAGCGGTGCCGGAAAGCTGGCTGGA
GTGCGATCTTCCTGAGGCCGATACTGTCGTCGTCCCCTCAAACTGGCAGATGCACGGTTACGATGCGCCCATCTACACCAACGTGACCTATCCCATTACGGTCAATCCGCCGTTTGTTCCCACGGAGAATCCGACGGGTTGTTACTCGCT
CACATTTAATGTTGATGAAAGCTGGCTACAGGAAGGCCAGACGCGAATTATTTTTGATGGCGTTCCTATTGGTTAAAAAATGAGCTGATTTAACAAAAATTTAATGCGAATTTTAACAAAATATTAACGTTTACAATTTAAATATTTGCT
TATACAATCTTCCTGTTTTTGGGGCTTTTCTGATTATCAACCGGGGTACATATGATTGACATGCTAGTTTTACGATTACCGTTCATCGATTCTCTTGTTTGCTCCAGACTCTCA

## Scaffold CS4:

CATTGACCGGGAGCGCCCTGTAGCGGCGCATTAAGCGCGGCGGGTGTGGTGGTTACGCGCAGCGTGACCGCTACACTTGCCAGCGCCCTAGCGCCCGCTCCCGGGATCGGAATTCCGGCCATCGCCCTGATAGACGGTTTTTCGCCCTTT
GACGTTGGAGTCCACGTTCTTTAATAGTGGACTCTTGTTCCAAACTGGAACAACACTCAACCCTATCTCGGGCAAGCTTGTCACGCTGATATTCTACACGTAAGGCAAGATCATGTTCGCGGGTACAAACTACGTATGCTAAAATTTACA
TAGCCAATCATAGAGTCCGGAGAGTGAAAAGTACCGATTCGGCAGTCGCACGGCATTCTCAACTCGAAACGCCGTACACAAGGCGTGCACTGGTATTACAAGTTGGCGTCGAGCGCTTACCGTTACTTGCGAGGCCTCTC
GCGTCTAGACGAGGTCCTGAGAATCGTATAGAATGGCAACCGCGGGGGATACTGGGATCGTTGTCCGATCTGTAAGATCCTTTTCACGCTTGGCTCGTTCCTAGTCGTATCGTTAAGTGAGGAGGTACCAGGATGTCTTTTTTGACTCCA
AGGCACGGACACCCTGCATTTTGTCAGCAGTCCCCACTTTGTCCACTGACAGTATCATTGTTGGAGCGTCTGTGCTCTTATTACGATGCCATTATAGCGCTACTGTCTATTCAAGACGCTAGCGACCCGGTCCGCTGAAATCTATCGTCT
GGGCATTTCACACGCTATGCGAGTATCCGCGTAGCGTGCTACTTCCCCCGTGCAGCGATCAAGATTCCCTCGGGGAAGTCTTTCCGGGCAGGGACGCCACTAAGGACGATATGGCAGCCATGTATCCAAAGGATAACTACCCCTTCGTCA
CGTCATTCATCCGTGTTGCTGAGACCACCCCTCTACCGAATTATCCTGGGGGGTCAGTCTAGCCGATGGCTGCGTGATGCTACCCTACGCGTACCACAGCTTTTCGTGGTCCCGGGACGACCGCCCAAGGTTGGTATATCTTATACGGTG
AGGCAATTTCAGCTGCGCCTTAAAACACGAACGACTTGTAATGAATCTCGCAAGCGCCTGAGTTGGATTGTAGTAAGTACACGAGCCGAGTGAGATAGAACTCCCATCTGAGGTCGCCGAGATCCCATGGTTAGGGCGCCGATAGCCTTG
AATCATCTGTGGGTGCATACTTGAGGATCAGCATCCGCTATTACTTCGAATGACTTAAATATAAGACGATCGAGCCATATAATGGGATAAAGTGTATTGAACTAGAGTAAACAGTGTTAATTATTATTTGTTTGACAACTATCCCTCTGT
TTAGGAGAGCATGGCGTATATTCATTTTCGAGGAGTGTAGATCCGGCGAGGACACATACAAGGTCAATCACATTTGTAGGCCAACCCGAAGGCATAGCGTAGGGCCGAATAAAAGTCACCGCGTGAGACTGACCATTCCTAAGGCTCGCG
CGTCAACCTATAGTTGCTTAAGAGACTCCCTGACCCCTATTATGGCTCATGGTCCACAAGAATGATCGCTCTGGAAACGGCTGCACGGTTGCAACAAGACCAATTTGGCCAAATCTGATACGAGAAGTGGGGGAGACATGCCTGATCCT
ATTTCGTCTTACCCATAAATAAATTACCGACACGATGATCAGTGACGCAGTATTTACGAGTCCTGCTGAATCCGGAAGGTCGGACTCGTGTGCCACACCAGAACGCATACGTCAAACGGATATTAGACCGTTGCGTGGTGCAAGGATCCA

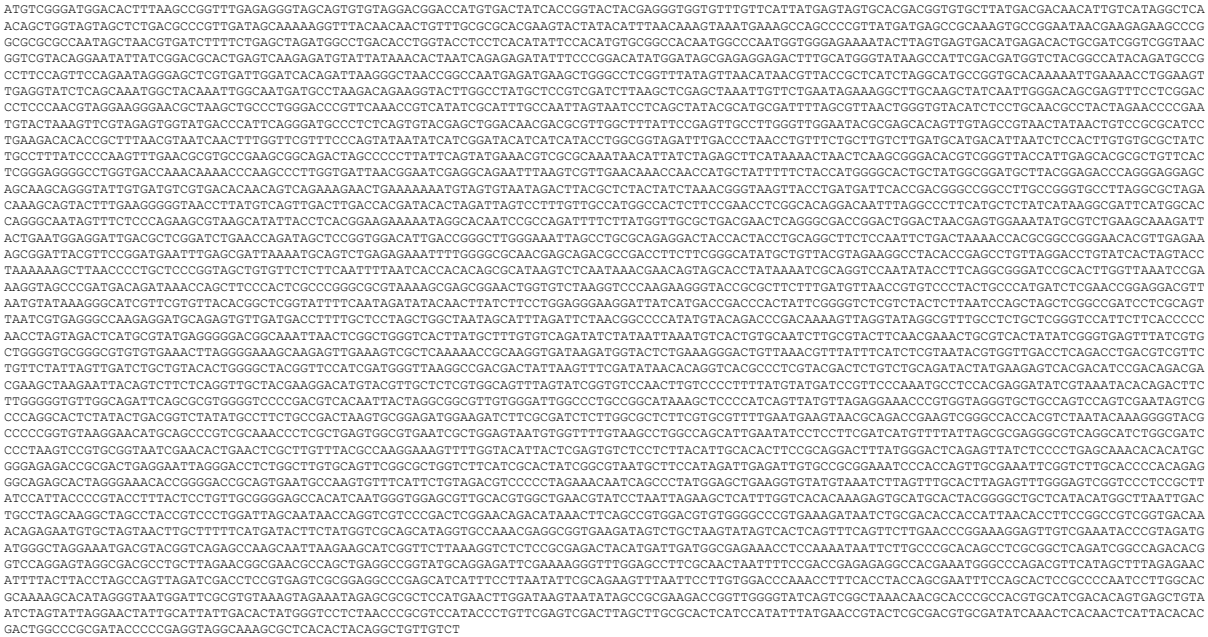


Table E.8: Disc origami staples

| Name | Oligo Position<br>5' Helix[base]--> 3' Helix[base] | Sequence 5'→3' |
|---|---|---|
| D_2 | 94[111] --> 26[104] | AAACTTCTAAATTAATAATAATAA |
| D_3 | 5[176] --> 2[168] | ATAGTCACAAACCGGCCATTCTTGTAGGATCAGGCATGTCTATGGGTATGATCATC |
| D_4 | 32[95] --> 44[96] | CTGCTTGACGAAGGATTATCAAGATAATACATTTGACATCACCTCCAAGCCCGTCCTCTG |
| D_8 | 98[111] --> 34[104] | ACGGCTGAGGATTTAGGTGCCAAGTAAAACGAAAGTCTGG |
| D_9 | 126[165] --> 45[151] | TTTTTAGCGAGTAACAACCCGTCGAGGAACGCAGCCAGCTGGCAGCCT |
| D_11 | 48[159] --> 52[160] | AAGTTGTCAGCGGTTGACGAGCAGGGCGCGTACTATTCAGCGAGGAAGAATGTAGATATC |
| D_13 | 8[127] --> 12[128] | ACGGGGCAGTAGCGATCCTAACTGAACAAGAAAAATCCTTTGGAGTCGAATGGCCGGTTA |
| D_16 | 56[127] --> 55[111] | TCTGAGGCGTGACCCTGCAGACAGAGTCGAAGCGGTCTACATAAAGATTGCCCTCACCAGT |
| D_22 | 38[175] --> 29[188] | GCAAGGCGCAGCTGGCCATTCGCCCGACCTGCTCATAAGGACATGTTTAGGCGCAGTTTTT |
| D_23 | 93[112] --> 16[99] | TACATTTAGAAACAGTACATAAATAACAAGAGCATCCCTGACATTCGGGGAGAAGCTTTTT |
| D_24 | 12[191] --> 20[192] | GATGAGCGCTCGAGCTCCTCAGAAAAGGATCTTACAATACCAGTCAAATGCGACGGCTAC |
| D_25 | 10[127] --> 67[135] | ACCAGAGGACCATCTACATGGCTCGCATAGCGTGTGCGGAATCAGTGCCTTGGAGAAGGATCGGTTGT |
| D_26 | 38[95] --> 46[96] | GGTGGAGTAATTTCTGCTGAAATGAAAAATCTAAAGGTCTTTAAGCTGATTGGTCAGCGT |
| D_29 | 90[159] --> 25[167] | AAATACGAAAAACCGTCTATCACGCGAGTACACAAGTGTTGGGGATTATAAAGT |
| D_32 | 23[168] --> 20[176] | GTCATTTTTGCGGATATAACTGTCATGCCTCGCGTA |
| D_33 | 39[160] --> 66[160] | TAATCTTTTTTCTCAATTGAGGGGCGTCTGGC |
| D_37 | 51[176] --> 47[175] | CAGAGGCATCCAGCGCGATCGCCATTCGATTACCGCACGGTCAGTCGCTTCCCTCCGTTCCGCT |
| D_38 | 42[119] --> 97[119] | TCATTGTGTTAATATTAAGCAAATTCCACCGGGACGGCCAAAGTATTA |
| D_40 | 35[128] --> 44[120] | AAACGAACCTTGACAAGAAAAGAAATTTTCCGGATTGTATTTGTTAAATGGAGAAG |
| D_41 | 49[48] --> 45[47] | GGCTGGTATGAGCCGGAGTAAAAGAGCAATACTTCTTTGAAACTCAAACCGTCGGTCGTAAAAA |
| D_42 | 125[115] --> 14[120] | TTTTTCGGATTGCAGCCTCAGAAGCTAAATTAGGATT |
| D_43 | 44[223] --> 48[224] | AATTTCTGGTGTAGGCTCCACGGTACGGGGTAATGGAACTAAGAGGGCTACCTAGCTGGA |
| D_45 | 95[224] --> 38[224] | TCAGCTGGTCTCGCCAAGTGGCCAGGGAGAAA |
| D_46 | 45[112] --> 98[112] | GCAAACGCCCTGCAGGTCTGTTCCACACGTCC |
| D_47 | 19[160] --> 28[152] | GTTTAGCTCCCAATTCGATAAGAGCTGAATATAATTTTACCCTCGGCTACCGTTCT |
| D_48 | 50[159] --> 54[160] | TGTGCACTGGGGGTGGTTTGCAAGAGCGCCAAGAGAACCCTACCCACACACGACTCTTGC |
| D_49 | 93[224] --> 32[224] | TACAGCTCGCTCTATTGTCACCAGCCTAAGGC |
| D_50 | 21[96] --> 28[88] | ACGTTAGTTTTTTTCAATGTGTAGAAAGGCTATCATTTTT |
| D_51 | 56[159] --> 55[143] | AGATCAACGTCGGCGTCTGTCGGATGTCGTGACTCTTCTAAACTGACAGAACGGAGATGAA |
| D_53 | 53[112] --> 49[111] | ACTGCCCGCCACACAAGCCCGACTTACCCCTTTGTATTAGTCACGCTGCGGTCATAGTGTTCAG |
| D_54 | 8[159] --> 12[160] | TCGTTATTCAGACTCTACAATTCGTTCGTGTTTTAACGGATGAATCTCGCTACTATAAAC |
| D_55 | 50[127] --> 54[128] | GGCGGGCCGTCCCCGGGGGCGTCGGTCTGCGTTACTTTGGAACAGTCGGGAACAACGCGC |
| D_56 | 39[120] --> 46[128] | AGCTATCTGGGCCCCGAGTCGGGACGACCTTGGCACAGTTTTCGTCCTCATAAC |
| D_58 | 39[176] --> 95[175] | CGCATATTGATGTGCTACCGTACGATGCTTCTTAATTGCTGGAAAATT |
| D_60 | 38[267] --> 98[248] | TTTTTTTCTTCCGTGAGGTAGGATTGTCGCCTCG |
| D_61 | 95[192] --> 38[192] | AAACCCTTGACCTTTAGCCTAAATGCCTTATG |
| D_62 | 62[15] --> 92[144] | CAACATTAAAAGATTCCCTGATAAAGCTGATAAAATAGCAAGCGGAGTAAGTCGACTAAATATG |
| D_64 | 16[135] --> 26[120] | TTATGACCATCAAAAATAAATATTCATTGAATGTTTAGACAGAACCCTGTGAGAAAAACTAAAG |
| D_67 | 106[87] --> 49[79] | TCGGAACCCTAAAGGGGCGGGCGCTGCCTGTTTTTGCTCG |

| | | |
|---|---|---|
| D_68 | 21[208] --> 13[207] | AGGGTCAAGCGGACAGGGGCGCTGTCGACGCCAACTTGTAGATCGGACGCCTTTCTCGACGGAG |
| D_69 | 28[135] --> 38[120] | CCGGAGAGTAGTAAGAAGATTTAGGAATACCACGTTAATACCCCAGCGAGCATGTCTGTAAAAC |
| D_75 | 15[48] --> 88[48] | CCTCAGAACCGGAATATAAATGCTTCAACAGT |
| D_77 | 93[160] --> 32[160] | GGGTATGGGGCGGAGTTTGTTCAAGTAGAGCG |
| D_78 | 21[104] --> 17[119] | AAATGAATTTAAATGCCTTTATTTAATGCTTTTTCAGAAAACGAGAAT |
| D_79 | 45[136] --> 66[120] | TCGTCGCTCGTTGGTGTAGATCGCATTAAATT |
| D_80 | 92[143] --> 20[136] | GATGAGTGCCAACGTCCGCGTCGT |
| D_81 | 9[80] --> 6[64] | AACGTCACGAATTATCCATTACCGGGCTTATCCGGTATTCCGACTTGCAGTTTATTTTGTCACA |
| D_83 | 49[112] --> 45[111] | CAAATCGTCGAACGATGATAGTGCGCTCTGCCCTCTGTGGGGAAAAACTGTAGAACCCGTTCCG |
| D_84 | 32[175] --> 24[168] | TTTAGATACGACTTAATAAATATGACGGTGTCCTTAATTG |
| D_87 | 57[104] --> 110[112] | GTTGCAGCTACGAGGGCAACAGCTAGGGGACAATTTGGGA |
| D_88 | 33[240] --> 21[239] | AAGGACTAACTGCTTTGTTCTAAGCAAGTTCATGGAGCGCACTGTGTCATAATGTTTGATGATG |
| D_91 | 13[48] --> 86[48] | ATTTACCGACAAATAATTAGGCAGTAAAGTAC |
| D_92 | 88[31] --> 15[39] | TCGCCATAGGTTGGGTTATATACATAGGTCCCCTCAGA |
| D_93 | 32[191] --> 44[192] | CAGGTAAATGAAGGAGAACCGTCATTTCCTAGCCCAACTAGCACGTTAGTCCATCGCTCA |
| D_94 | 10[191] --> 14[192] | GTATTTTATATCTCGTAGAGGAATAGACAGTAGCGCCCTGGTACCTTAAGATATTCAGAA |
| D_95 | 92[183] --> 16[168] | GTTTGATATCGCACGTGGGCGATGTTCCAACCTATAGCTGGGCGCGAG |
| D_97 | 43[128] --> 36[144] | ATTGGGCGCATCGTAAGAGATGGTTTACCCAAATCAACGTCTTCATCA |
| D_98 | 53[144] --> 49[143] | TGCCAGCTAAGCATAAAACGCACGGACGGGCTGCATGTTCGCTTAATGGCTGCGGCCCGGGTTA |
| D_100 | 15[144] --> 11[143] | CAGTTAACGGCTGAGAATGGTTTGAAATAAGAATAAACACAAATGCCCTCTCATTGGCTTATAC |
| D_102 | 95[64] --> 38[64] | TTTCAGGTCAGATGATACGGGTAATAACCTCA |
| D_103 | 10[159] --> 14[160] | TTGCCATAGTCTCCTGACGTGGATTTCAGCGGACCGGATAAATATTAATGCCCATGAAAG |
| D_107 | 13[176] --> 9[175] | ATTTCGGAGGTAACGTGCGTCTTGGGTGGTCTCAGCAACAGGCGCAGCGCCCCCTTTTTCATC |
| D_108 | 13[80] --> 9[79] | TTTTGATGCAGGTCAGTTGATCGCCGGAAAGACTTCCCCGTGTTCAGCGAACCGCCAGGCCGGA |
| D_109 | 15[80] --> 11[79] | CTCATTTTGTGCCGTCAAGAACGCATACAAATTCTTACCAAGGGAATCACGATTGGTGACAGGA |
| D_112 | 4[159] --> 8[160] | GACATTGACACCACCCAGAGCTACCAACGCTAACGACACTCCTCGCGCGCAAGCTTCTCT |
| D_113 | 10[223] --> 14[224] | ACCGATCTCTTGACATCGGCTTAAGAGCACAGACGCGGTGTCCGTTCTGTCTCTGTCCCA |
| D_114 | 39[208] --> 27[207] | CGCCCTGACCTGGTGCGGGTATTTTGTAGTCTCGCGGAGATTCGAATCCCCGTCGGACCAAGGG |
| D_115 | 21[48] --> 13[47] | GCCCTCATACCGTAACAATATCAGAACATGATCTTGCCTTACTATATGGGTGTATCGTCTCTGA |
| D_116 | 53[176] --> 49[175] | CCAGCACGCAGTGACAATCTTCCACAGCGATTCACGCCACACTTAGGGAGTGTCACCCCCTGCA |
| D_117 | 51[112] --> 47[111] | TCACAATTCGTTTTCACGCGTAACGAGCGGGAGCTAAACAATTACGCCGCCCTTTAGGCAGTAG |
| D_118 | 32[111] --> 23[111] | ACGACATCTCTCCGTAAGATCTACGTAAAGATAAAGAAGTTTTGCTTTTTTTTCAGAGGGGGTAAT |
| D_119 | 11[208] --> 7[207] | AATACATCGCAGTGTCCCTTGGGCATGGGATCTCGGCGACGCTGATCCAGCTCAGAGGCGTCAG |
| D_120 | 22[151] --> 91[151] | AGTAGATTACAGTTTCAAAGCCAAAAAGGGCG |
| D_121 | 90[151] --> 64[136] | GAGAATGCCGTGCGACTAAATTTACTCCTCAAAGTAACAGCAAAATTA |
| D_122 | 95[128] --> 37[135] | CTATGAACATCATTTTCACTAAAACACGACGTAATCATAT |
| D_123 | 52[95] --> 109[95] | ATAAAGTCTCACATCGTCAAAATAAATC |
| D_124 | 47[112] --> 99[111] | GGACACGGGCCGGACTGCTCATGGTTTTGAATGGCTATTAAGTTTATG |
| D_125 | 91[176] --> 13[175] | GCCGGAATTTGTGTACGGCGTTTCGGAACGAGTTCTGAAACCCTGCCT |
| D_127 | 4[127] --> 8[128] | AATATCCGCATGATCAGCCATTTGCACCCAGCTACATCCTAAACCATTTACTTCATCATA |
| D_128 | 9[144] --> 5[143] | CTTTAGCGTCCGGCACCCCATTATAATATACGCCATGCTCATTTTATCCGTAGAAACTTATTAC |
| D_128 | 9[144] --> 5[143] | CTTTAGCGTCCGGCACCCCATTATAATATACGCCATGCTCATTTTATCCGTAGAAACTTATTAC |
| D_130 | 93[192] --> 32[192] | GTCAATAAACCCTATGCGTTAATCTGAATCAT |
| D_131 | 52[159] --> 56[160] | TGACACATAAGTTTACGGGTTCGGCAGGGCCAATCCCAACACCCTCCCTTTCTGTACAGC |
| D_132 | 21[112] --> 13[111] | TTTCTGTATGAGAGGGTCCACTATTTTCACTCTCCGGACTAATATATTTTTGCTCAGGTAATAA |
| D_133 | 32[223] --> 44[224] | ACCCGGCTCGGAAGTCAATCACGACAACTCCTTTCCCGACCATAAGCGCAACCGCCCCAA |
| D_134 | 43[152] --> 48[160] | CTGCCAGTCGTGTTCCACAGCTACTGACCTGAAATGGATTATTTACGAATGAAAAGACACCAAGGAAGAT |
| D_135 | 45[48] --> 33[47] | AAGCCGCACTCATTTGCACCGCCTGTCAGTTGGCAAATCAAAAATATCGAAACGTATTTCATGA |
| D_136 | 9[176] --> 5[175] | GGCATTTTTATTGGCGAGTCATTCGTCCTCGCCGGATCTAGCGCGAGCCGTGCACTTACCGGTG |
| D_137 | 12[95] --> 20[96] | CTATTCTATACAGGATGCGTTGAGAAAACTTTTTCACTATGATTACTTTAGTAATGGGTC |
| D_138 | 38[191] --> 46[192] | ATAGAGCTCCACTCATTCTCTATTAAGCCATGTATGATAAAAGGAGTGATACTTTATTGA |
| D_139 | 45[176] --> 97[175] | GCTTTTTTCCGGAACGGGCAGTCAGTTTGTCACCGACGGCTGGCTCTG |
| D_142 | 47[80] --> 39[79] | GGCGCTTTGTCTGGTCTATTACCGACTGATAGCCCTAAAATGAGAGCCAGCGGATCTCACGGAA |
| D_144 | 52[127] --> 56[128] | AATTTGCCTTTCCAAGAGTCCGAGTGTTGTTCCAGTTATCCTCGCGTATTACACGTCAGG |
| D_146 | 6[159] --> 10[160] | TGAACAAACTTCGTGAAAATGATGGCTCGATCGTCTTGTACTTAGTAGCGCGATTAGCGT |
| D_147 | 26[31] --> 38[32] | TGCTTTCAGTTGCGTCGGGAGATTTGCACGTAAAACATTGTTTGAAAGACTTCAGCGCCA |
| D_149 | 32[63] --> 44[64] | TTGCGGGCCATTAAGGCAATTCACTAACAACTAATACTCAATCAGATAGCTCAAACTTAA |
| D_150 | 39[144] --> 27[143] | TCAATCCTCCAGGGTTTCGTATTAAAGTTTGAGTAACATTGTCTGGGCCATTTTTTTGGTAGAA |
| D_151 | 93[96] --> 34[88] | AGAAAACAGCGAATATTCCCTGGGACAATACCCATTGCCTAGCAAACAAGATTTTT |
| D_152 | 31[152] --> 98[160] | ATTGTGTCTAAGTCTACTCTTCGCATTTTAAAATCCTTTGCCCGAACGGAAGGT |
| D_154 | 48[63] --> 51[71] | TGCGGTAATGGGTACAGAATCAAGAAAGCGAAAGGAAGCCCCCGTTCGTAAT |
| D_156 | 97[136] --> 34[128] | TCGACAACTTCCCAGTCACGATCGAGGGCTCATCTTTGAC |
| D_157 | 43[168] --> 41[175] | ACGACGACAGTTTTTTTTCCCTGACGAGAAACACCAGTGAAT |
| D_158 | 79[88] --> 6[96] | AAAATAGCAGCCTTTCAAATAAGATAACGGAAAACGCAA |
| D_160 | 14[95] --> 92[96] | CGGATAATCTACGAGGCTATGGTTGTTCCAGTTTGGCAATATAT |
| D_161 | 87[144] --> 9[143] | AGACGATAACGAAGGGGTAGTTATCGAGATTCAATCAAAAAAGTTTGC |
| D_162 | 34[151] --> 93[143] | TGTTGGGAGTGCGGGCTTACACTACCATTTCGATTCGCTGGTAGGTGACGCAAGCT |

| | | |
|---|---|---|
| D_164 | 13[112] --> 86[112] | GTTTTAACATCTGTGACGCGGATACTGCCATA |
| D_165 | 48[191] --> 52[192] | CGGTCATGGAGCAATTCAGTGGATGCCTGACGCCCTAAAACCACATACCTAAGTACGCAA |
| D_166 | 7[176] --> 3[175] | TGTAAACCCACACCGTCTTAGGAACAACTATGAGGTTGACAGAGCGATTTAAAGTGATTCAGCA |
| D_168 | 35[94] --> 26[112] | TTTTTGACGTTGGGAAGAAAAATCTACATTCAACGAAACAAATTTTTGAGAGCATCCGGAATTGCG |
| D_170 | 10[95] --> 14[96] | GAGCCGCGGAACTGCCCTGCCTGCACGGGGGAAGTAAGTATCATAGTGTACTGTACCAGG |
| D_171 | 21[80] --> 13[79] | TTGTCGTCCAGGGATAGGTTGAGTTAAATTTTAGCATACGGCAAGACAGAGAGGGTTACATGGC |
| D_172 | 2[127] --> 6[128] | CAATAGCGTTTGACGGGAGAAAAAAACAGGGAAGCGAAAATAAATAAGACTCATACATAC |
| D_173 | 24[188] --> 26[184] | TTTTTGCTTAGAGTGGAAGTTTCATTTTTGCCGCTT |
| D_178 | 28[143] --> 16[144] | AATTAATGACAGTCAAGATAAAAAGTCCAATACTGAATTGCCTTTCGGAAATGGTCAATTCTAC |
| D_179 | 33[48] --> 21[47] | GGAAGTTTATCGTCACAGAAATTGTATACAGTAACAGTACGCGAATTATATCGGTTCACAGACA |
| D_183 | 54[127] --> 57[143] | GGGGAGATCAACCATGGAGGCAGTTGGACACCGATACATAGTATTGTGTTATATCGAAAC |
| D_185 | 44[191] --> 48[192] | AATTCATAGGTACTGACATTCGTCACACGACCAGTAAGGGCTGAGGGCGAGTTAGTGGGT |
| D_187 | 67[160] --> 22[152] | CAATAAATCTGAAAAGCGAACCAGTCAGGATTAGAGAGTACTCCTTTTTGCGAACG |
| D_189 | 95[96] --> 37[103] | ACTGGCTAGGAGCGGACACCAACCCTTTCAGATCGATGAA |
| D_191 | 57[144] --> 53[143] | TTAATAGTCTAATAGACCACGAGAGTCTGTGTATTTACGAATGGGGAGGAATCGGCACCTGTCG |
| D_192 | 6[95] --> 10[96] | AGACACCGGCGACATATAGAACGCCCAATAGCAAGCAACCAATCACCATCGACTCCCTCA |
| D_193 | 110[111] --> 53[111] | ACGGATCAAGCCCGAGGCGTATTGTTGCGCTC |
| D_194 | 108[111] --> 51[111] | AGAACGTGACGTGGTGCATACGAGTTATCCGC |
| D_195 | 69[128] --> 43[151] | TCATTTTTTAACCAATGATTCTCCATAGGTCATTCATCAATTGGGCTTCCGTGCAT |
| D_196 | 55[112] --> 108[112] | GAGACGGGGGCGGTTTATAGGGTTACTATTAA |
| D_197 | 21[240] --> 14[232] | TATCCGATATTACGTTCGTAACCACGCGAGAGGCCTCGCATTGCCATTGAAACTCG |
| D_198 | 44[63] --> 48[64] | ATTTCTGCAGGCGGTTAAAAACTTGCTGGTAATATCCAAATTAACAGCGGGGGGCGCGGT |
| D_200 | 14[63] --> 26[64] | GTATAGCCCGCCACACCCGCGCGTGACAAGCTTGCCTAAATCGTGTAACGATGCTCCAAA |
| D_202 | 23[112] --> 14[112] | AGTAAAATCCCCCTCACAACGCAACTTTTGCGGGTTCTAGAGCGGGGT |
| D_204 | 28[167] --> 34[152] | CAACTTCAGTAGCTCAGAACCGAACTGGGTAGTTACAACCTGCGCAAC |
| D_205 | 15[176] --> 11[175] | AGGATTACACCTATTACCAAGCGTCTTAACGATACGACTAGGTCGCTATATGTTAATCCATATG |
| D_206 | 79[160] --> 6[160] | CCGTTTCCGCGTCTTTCCTCGTAGACTCATAA |
| D_210 | 2[167] --> 79[159] | GTGTCGGTCCAATAAAGTCCGATTCTCGTCGTGCAG |
| D_211 | 95[160] --> 38[160] | TCTCGGTCCGTTATTATATTACGCATTAAGTT |
| D_212 | 127[128] --> 46[120] | GTAATGGGGTGGGAACAAACGGATCAGCGGAACGT |
| D_215 | 49[144] --> 46[136] | CCTGCAGCATATCTATACAAGCCACATTCACTGCGGTCCCGACGCTCAAGCACATC |
| D_217 | 3[144] --> 4[160] | GGCACACGTAAGAGCAAGAATTGAGTTAAGCAATTTATTTCCCCCACCCTTCCGGTCCATCCC |
| D_219 | 12[127] --> 19[135] | GCCCTTAGGGGTCATAATTACTTTCATCTTCTGACCTGCCGAATGCAGGAGATGTCCAGCATTAGATA |
| D_221 | 11[112] --> 7[111] | TGGCCGTACCACCACCGATAAGTCTTTACGAGCATGTAGAAATAATTAGACGGAAAATTGAGGG |
| D_222 | 11[80] --> 7[79] | GGTTGAGGCACCCTCATAATGCAGGGCTGTCTTTCCTTATGTAGGAATACCGTCACGCGCCAAA |
| D_224 | 37[144] --> 99[159] | GTTGATAACCAGCTTTGGGTAACGCCATTCAGGTTAATGGGGACGG |
| D_225 | 32[31] --> 44[32] | CAGCATCGAGGACTGATTATATGAGGAAGGTTATCTACAGTTGATGTGAGAGAGTTGGGC |
| D_226 | 13[208] --> 9[207] | CATAGGCCAATTTTTGCATCGTAAAGACTGACCCCCCAGGTATACCAATCATGTCACATTGTGG |
| D_227 | 44[95] --> 48[96] | CGCAGGCAAACGATTGCGCGACCAGCCATTGCAACAGGTGCAAGAGATCATGTACATTAA |
| D_229 | 37[160] --> 66[152] | CCGGCACCGAAGATCGTGCTCATTCAGAACGAGTAGTAAACATTAAATCTTCCTGT |
| D_230 | 47[144] --> 99[143] | CCTTCTTGCCGGCCAGATCGTCTGAAAGCGTAAGAATACGGGTTATTG |
| D_231 | 96[119] --> 95[111] | AAAGAAACCACCAGAAGGTAAGTA |
| D_233 | 49[176] --> 45[175] | TCAGACGAGATAATCCGGTCTCTCTAGGGGGACGTCTACAATTGGCAGTGGTGATTGGGGTTAA |
| D_234 | 51[80] --> 47[79] | TAGCTGTTAGCACGCGTAGGGCGCGGATTTTAGACAGGAATTTCCGCGATCCGCCGTCATTGCA |
| D_235 | 15[120] --> 91[127] | TAGGCGTTCGGTACTTAAAGAA |
| D_237 | 47[176] --> 44[168] | CGCTTTTAGCGCTGTGATTCACCATGGCCAACAGAGATAGCCTTGCTATAATCCGC |
| D_244 | 12[159] --> 20[160] | CGAGGCCTAAACAGAGGCGTTAAATACCGACCGTGTGAGTTGAGCGCATGCGCAAGGCAA |
| D_245 | 15[208] --> 11[207] | GTTTGAACGCTTGCAAAACGATCCGAGTCAAAAAAGACATTATAATGGTGCACCGGGTGTTTAT |
| D_246 | 40[135] --> 127[127] | AACAGGAAGATATTCATTAATTTCAACTTTAAGATTGACC |
| D_247 | 33[120] --> 44[128] | AAAGAATAGCGGAACGACTTTACAAACAATTCTTTCACGGTTCAGAGTCAGAAT |
| D_248 | 31[160] --> 40[144] | GAAATCCGATTCAGGCAACTTTGAGCATAGGCTGGCTGACAACAAAGCCACTCCAGTCAGAAAA |
| D_250 | 77[120] --> 4[128] | TAATATCAGAGAGATCATTAGACGTATGCGTAACGGTCT |
| D_251 | 100[239] --> 39[239] | TTCAGCCAGACCAAATGCTCGTTGCATAAGAA |
| D_253 | 26[143] --> 17[143] | GAGAATAGAACTTTCATAGTTTGACATTTCGCAATCGTCATCAGGTCT |
| D_254 | 22[135] --> 32[120] | CCATTTTTTGGATAGCCCAAAATAGCGAGAGGACGAGGCAGGTAGCTAGTACAACGTTCTGACT |
| D_255 | 44[111] --> 36[94] | TAGTGGTAGGTCAATGATTTAAATCGGTAATCTTATACCAGTCAGTTTTT |
| D_256 | 15[136] --> 125[143] | TGTACACCTAAAAACAACCAATAGTGACTATTGATTAAGA |
| D_257 | 91[128] --> 25[135] | CGTGGACTTTACCTTTTGCTAAACAAAGGAACGGCCGGAG |
| D_259 | 10[63] --> 14[64] | AGCCACCAGCCGCCGAGAATAAGGCATTTTCGAGCCGTATAAAGAAGCGTCATGATATAA |
| D_260 | 9[208] --> 82[208] | CCGCACATGGCCATCTTCAAGTATTTGGCCTA |
| D_262 | 48[127] --> 105[127] | TGTAACATAACGGCAGAATCACACCACA |
| D_263 | 6[127] --> 10[128] | ATAAAGGTGGCTTTAGAGGGATACTCTAGTTCAATAAATATCCCACAGAATCTCACCGGA |
| D_265 | 39[80] --> 27[79] | AAAGAGACCCGCCACGCCGTCAATTCATATTCCTGATTATCGCGACTCGAGTTAAATATTCGGT |
| D_267 | 89[112] --> 11[111] | TTAGTTAATAGAAAAAGCCTGTTTGCACGCTATCCAATCACATCTGTA |
| D_269 | 41[104] --> 34[112] | TTTTTTACCTTATGCGCTGGCTCAGTAAAACTATTATACC |
| D_271 | 47[120] --> 50[128] | TTAACATCCCTAGTGATGAAGACCAGCGCTCCTCGTTATCAGATGCAGAATGC |
| D_272 | 14[191] --> 91[191] | CAATTTATAATTGGGCACGCCTCCGATC |

| | | |
|---|---|---|
| D_273 | 3[112] --> 77[119] | AAAAGTAATATCTTACTTGAGCGC |
| D_275 | 47[208] --> 39[207] | GGTTTATCTAGGTGCTGGAGTAAACCATTGATGTGGCTCCAGCAGCCCGCATTTTAAGTCCGGT |
| D_278 | 48[95] --> 105[95] | CGTCCTCATCCCTTATTAAAGTGGCAAG |
| D_279 | 91[192] --> 26[192] | CCGGGAGCTGTAATGACAAGCAGAGCTAGTCT |
| D_280 | 27[208] --> 15[207] | CTTGGGTTCATACTGATTCCTAATTCGCGGGCCAGTCGTGGGGCGCTATTATAGTTATATGACG |
| D_284 | 93[64] --> 32[64] | TGAGCAAATTAACGTCAACCGATAGGCCGCTT |
| D_285 | 91[224] --> 26[224] | TAGCGGTCCCTACCTCGCCAGGTAATTTGCGC |
| D_286 | 49[208] --> 45[207] | TGCATCCTTAGACGAGAGATAACTACACCTTCAGCTCCATCCGCAACAACTGTTCGAGGTCCTA |
| D_287 | 99[160] --> 69[172] | TAGGCTAGAACCCTTCCGGGAGCAAAAATTGAATAATTCGTTTTT |
| D_288 | 49[80] --> 45[79] | TCATAAACCGCACTCAGCACAATCTTCGCAACTGGTGGGACAGAACAAAGCAGCAAGATGAAGG |
| D_290 | 9[112] --> 5[111] | CCGTAATCTAAATATTACACTGTTTAGTTGTCAAACAAATAAGATTAGTATAAAAGATACCCAA |
| D_291 | 14[223] --> 91[223] | ATTGATAGGGTCCCTAAGCGCGCAAGTG |
| D_292 | 39[168] --> 35[175] | GCTTCAGAGGCCTCAGGCTTCTGGGACCAGGCAAGAGGAC |
| D_293 | 45[120] --> 48[128] | GGTCCGTTACAATATAAATACCTACATTTTCGGTGTTTCAAAGAAGCCGAGCCG |
| D_294 | 47[48] --> 39[47] | GGAGGTGTCGGCAGCACTATCGGCTACCGAACGAACCACCAGTATTAACCGCCAGCATAGACTT |
| D_295 | 65[45] --> 20[64] | TTCACAATTCCAGTCCAACGCGATGCAAATCCAATCTAGTTTGTCCTCAGAGAATAGGAA |
| D_296 | 35[176] --> 93[183] | AGATGAACACGGTCAATCCATGTTCCGGAACGATTCTGCCCGGCACGCTAGAGGAC |
| D_297 | 17[144] --> 12[144] | TTATCGAGTTAATCCCTAGTAGCAAGAATTAGTGCCCGTACAGCTTCA |
| D_298 | 5[144] --> 2[128] | GCAGTATGGATCCTTGGTTGCAACATCAGATTTGGCCAAAAACCCACAAGAAACAATGAAATAG |
| D_299 | 11[176] --> 7[175] | TCCGGGAACGGTCATATGAAATTGTATCTCACTCGGCTCGTATATTTACGCGCCGGACAGTTGT |
| D_300 | 44[143] --> 35[151] | TGGTTTTATCCGAGCGGCCCCAAAGTACCCCGAGAGTAATTAACGGAA |
| D_301 | 26[263] --> 95[255] | GAGTTAGTTTTATGACAGCGCGACTTATCCAGGCGT |
| D_302 | 45[208] --> 33[207] | ACAGGCTCCTCAGACTCGTAGTGCCATGAAAAAGCAAGTTTCATCTACCATGAATCTGTCCTGT |
| D_305 | 94[175] --> 17[175] | AGGATTGGACGCGGGTGTTCAAACGAGATTAAAGTTGATTATATTTTCCCAACAGGACCGGAAG |
| D_308 | 44[151] --> 98[136] | CGGCCGCGCTAATCCAGTGGTGTCGCAGATTA |
| D_309 | 45[80] --> 33[79] | GTAAAGTTGCAGAAACAGCAGCAACCTCAAATATCAAACCGATTAGAGGGAACGGAAATACGTA |
| D_311 | 93[256] --> 97[255] | TGCGTTGTGCTATATTTGCTCAATTACCCCCTTCAAAGTATCTAGTGGGCAAGACTGAGT |
| D_313 | 64[135] --> 20[120] | AGCAATAAATCAAAAAATAGTCAGAAGCAAAGGACCATAACTGTAATAGGATAAAATCGTACAC |
| D_314 | 81[96] --> 61[114] | CTTAAATCAAATCAGATTCAACCGTTATTCAT |
| D_315 | 125[144] --> 15[159] | GGAAGCCCGAAAGACTCAAGGCAATTAACATCTATTAAGAGCTAAAAT |
| D_316 | 6[191] --> 10[192] | TCATAAGTTTTTGCTGTATGTGAAGTAATAGCGGATCTCAGATGCATTGGGCCTCACTAA |
| D_317 | 41[176] --> 94[176] | AAGGCTTGGGTGTACATGCCGGAACAAAGCGCGAAAGGGGCTTACCCGAGTTGCGAGCGTGCCA |
| D_319 | 124[167] --> 16[152] | TTTTTAATATCGCGTTCTTCAAAGGTGGCATC |
| D_322 | 69[152] --> 103[159] | CATCAAAAAGAGAACGGACCTTCACTTGGGAGGTCC |
| D_324 | 27[80] --> 15[79] | CGCTGAGGAATCTCCAATGAAACAAATAACCTTGCTTCTGCGAGATAGGCAAGCCCCCACCACC |

**Table E.9:** Poly-C edge staples.

| | | |
|---|---|---|
| D_15_C | 8[236] --> 85[223] | **cccc**AGGTACCAGGTGTCAGTGGAATCCTAACCGGTCGTC |
| D_d_p2_20_C | 95[272] --> 26[264] | **cccc**CCAACCGGTCTTCGCGTTAGCCGATCCCGCTT |
| D_31_C | 53[67] --> 107[87] | **cccc**CTAATGAGTGAGCTAAGTAAAGCCTCAAGTTT |
| D_34_C | 90[262] --> 21[268] | **cccc**CTCGTCTAGACCACACCCGCCGCGCTGAGACAATACTGGGA**cccc** |
| D_35_C | 3[176] --> 77[188] | GGACTCGTTGCGTCACAGACGAAA**cccc** |
| D_36_C | 89[240] --> 11[247] | CTATACGATGCTGACAAAATGCAGTCCAACAAGATACCTCTCCGATAATAT**cccc** |
| D_39_C | 7[80] --> 80[71] | GACAAAAGACGGAATAGGGAGGTTTTTTGTTTAA**cccc** |
| D_44_C | 82[231] --> 9[236] | **cccc**TGCCTTCGGGGCACCCACAGATGATATCGGCGCATGTGAGG**cccc** |
| D_57_C | 38[31] --> 46[24] | TGTTTACCGGAATTAAGGAATAGAGGTGAGGCGGTCAGCAGAAGAAAAATCCGGTGCCATCCC**cccc** |
| D_66_C | 50[95] --> 54[88] | TTCTGCCTCCTGTGCACTAAATTTGGGGTCGAGGTGGACTCCAATAATTGCGGGCGCCAGGGT**cccc** |
| D_70_C | 54[193] --> 51[175] | **cccc**GCGGTTTTGAGCCGCCTAGTCGACTGGACTGGCAGCTCGCGAAGTTTAATTAGACCCGAG |
| D_71_C | 48[223] --> 105[231] | TTAAGAGCTTGGCCACCAAAAGATCGAAGGA**cccc** |
| D_85_C | 81[51] --> 8[64] | **cccc**TTTAGCGAACCTCCTAAGAACGGTTTACCACGACTTGA |
| D_89_C | 44[257] --> 33[239] | **cccc**AAGGTCGGCGTCTGAGCTTCTTTTGGCACCTATGCTGGGGTTCAAACGCTTCTTGGCAACA |
| D_96_C | 84[55] --> 8[35] | TATTAAACCAAGTACCCGAGAACAGAGCCAGC**cccc** |
| D_99_C | 88[47] --> 12[24] | AGGGCTTACATGTAATATCCTCATTAAAGCCAGAA**cccc** |
| D_110_C | 96[23] --> 96[0] | CTTCTGAATAATGGAAGGGTT**cccc** |
| D_111_C | 94[15] --> 26[3] | ACGGATTCGCCTG**cccccccc**ATTGCTTTGAATATTTCTTAA**cccc** |
| D_140_C | 11[35] --> 85[55] | **cccc**CCAGAACCACCACCAGACCCTCAGCCAGACGA |
| D_141_C | 54[159] --> 57[182] | TTTCCCCTTAACAGCCAAGAAGCAACGTACATGTCCGCTTCGTCCTTAACCCATCGATGGAAC**cccc** |
| D_143_C | 33[2] --> 94[16] | **cccc**CGGCTACAGAGGCTTTGGAACGAGTCAAAATTAAACAATA |
| D_148_C | 112[188] --> 55[172] | **cccc**AAGACTGTAATTCTTATTCGTAGCAGCCCCAGAGAGT |
| D_153_C | 103[224] --> 49[247] | CCATAAAGAGTAATGTCTCACGATTAACTGCGAGG**cccc** |
| D_159_C | 107[192] --> 53[215] | ACTTAGTCGCCTGGGCCACCCGATATAGTGACGCA**cccc** |
| D_163_C | 4[204] --> 81[191] | **cccc**CACTGCTACCCTCTCATGGTCCTCTTAAGTGGTCAG |
| D_167_C | 92[239] --> 15[256] | GCGCTTTGACGCTGCGAAAGCGGTTTAGCGTTCCCTTCCTACGTT**cccc** |
| D_174_C | 12[257] --> 86[240] | **cccc**AGCCATTTGCTGATGATACTGCGCGTAGG |
| D_175_C | 87[19] --> 14[32] | **cccc**ATTTAACAACGCCAAATTGAGAAAAAGCGCAACCGTACT |
| D_176_C | 44[31] --> 47[39] | GGTTGTGGACATAAATAAAAC**cccc**TTGCCTGAGTAGAAGTTAGTAATCAACCAGC |

| | | |
|---|---|---|
| D_177_C | 45[240] --> 100[240] | CATATGCCCGAAGCCCCCCCCGATCCCGCCTGAAAGGGACCGAGGATACG |
| D_181_C | 7[208] --> 81[231] | AGCTACTAGTTGAGCCTTATTCGGCCCTACGCTACCCC |
| D_182_C | 50[225] --> 47[207] | CCCCTGGGGCCGTTAGATAAAACATCTTTCCTTGGCGTAAACTCAGGGGACCCCGAAGGGAAGCT |
| D_199_C | 5[112] --> 2[99] | AAGAACTGGCAGATAGAATAACATTTAACTGAACACCCTGGAGGGTAACGAAGCCCCCCC |
| D_208_C | 51[35] --> 104[48] | CCCCGATCCCCGGGTACCGACCTCCTCAAGGAAGGGCTGAGAAG |
| D_209_C | 5[78] --> 81[95] | CCCCGGAAACGCAATAAAACGATTTGAAGC |
| D_213_C | 52[191] --> 109[199] | GATTGCAATAAACTGACTATTAATTGTGACGCCCC |
| D_220_C | 92[15] --> 89[23] | GCTTAGATTGAGAAGAGTCAATAGCTACCTTTTTACCCCCCCCACCTCCGGCTT |
| D_236_C | 104[247] --> 47[257] | TAAGAGGAGACACTCGTCCTGCGGGGCCGAGCTTTCGGATTTAACCAAGTGCGCCCC |
| D_239_C | 96[284] --> 27[278] | CCCCCCGATCTGAGCCGCGACCTGGACCCATAAGGTGGTAACCCGACCCCC |
| D_241_C | 95[256] --> 33[278] | CGCCTACTGGCTGTGCGTATCGTGGTCAAGTCAACCCCC |
| D_243_C | 108[220] --> 51[204] | CCCCACCGTCAGTATAGAGTGGCAGAAGTCGTTGAACTTTT |
| D_252_C | 95[0] --> 92[16] | CCCCAGAACCTACCATAGGTAGCAATTACAGCTTGATACCGATGAGGTGAACCAAGTTATAGCGATA |
| D_d_p2_270 _C | 93[272] --> 91[273] | CCCCTTGGGCGCTCCCGGTCAATTAATGCGCC |
| D_274_C | 13[232] --> 14[240] | TAGGCATCATTGCCAATTTGTTTTTTGGGAGGGTCCGAG |
| D_d_p2_277_C | 97[256] --> 39[267] | CCCCAGACTATCTTCACGCCTATTTCCCC |
| D_289_C | 110[87] --> 108[80] | TCCGAAATCGGCCCCCCCCCAAAATCCCTTGGGCGAAA |
| D_304_C | 87[248] --> 89[262] | TCAGTGGACACCCCCCCCAAGTGGGGACTTCTCAGGACCCCC |
| D_312_C | 79[184] --> 5[204] | TGGACCATGAGCCATAATAGCCCCCCCCGGGTCAGGGAGTCGTCCTACACCCC |
| D_320_C | 20[268] --> 93[255] | CCCCAACGAACCAAAGTTGGATATTACAGCCTGTGGCGGG |
| D_323_C | 109[96] --> 56[88] | AAAAGAATCTGTTTGATTTTCTTTTTCACCGCCTGCCCC |

**Table E.10:** Swivel staples.

| | | |
|---|---|---|
| D72_S_top | --118[175] --> 25[159] | GTATCCGGTCAAGTAAGGCCTAGAGGGAGGTTTTATCATAACCAGACGACATCACCATCAATATGA |
| D129_S_bottom | 31[128] --> 118[112]-- | GAGATTTGTATCATCGATCAGTTGGCAACACTTTTTCCTCCCTCTAGGCCTTACTTGACCGGATACACTGTCCTTG |
| Anti-Swivel | | CAAGGACAGTGTATCCGGTCAAGTAAGGCCTAGAGGGAGG |

**Table E.11:** Gold capture site strands.

| | | |
|---|---|---|
| D_5_Au_A | 33[80] --> 137[89] | ATGCCACTCTTGCAGGACGGAGGTATGATGCTCCAAAAAAAAAA |
| D_6_Au_A | 26[159] --> 134[150] | AAAGGCAGTGGTTGGTGCTGGAATGGCCTCCCAAAAAAAAAA |
| D_18_Au_A | 26[223] --> 134[214] | GACGTTTTTGTTTGTCTACTTACCGGCCCCAAAAAAAAAA |
| D_27_Au_A | 33[208] --> 137[217] | GCCGAGGTAAGGCCGGTCCTGCATTACACGCGCCAAAAAAAAAA |
| D_28_Au_A | 20[95] --> 132[86] | ATACCACTTTCCAGGTGAGTGAACATCACCAAAAAAAAAA |
| D_30_Au_A | 19[152] --> 132[150] | AATAACCTCTCGGAATATAGCGCACGGTTCATCGAACACCAAAAAAAAAA |
| D_86_Au_A | 26[63] --> 134[54] | AGGAGCCCACGCATAGATGAACGTAGATCCAAAAAAAAAA |
| D_106_Au_A | 20[63] --> 132[54] | CCCATGTAGTTAGCCGCTATTAATTACCCCAAAAAAAAAA |
| D_184_Au_A | 26[95] --> 134[86] | CGTTGAACTGCTCCTAAGGAACGATCTACCAAAAAAAAAA |
| D_190_Au_A | 21[120] --> 132[117] | TGGGATTTTTTAATGACAATTTCCAAAAAAAAAA |
| D_201_Au_A | 27[184] --> 134[182] | TCGATTCTGCTTTTAGGCTCCCCAAAAAAAAAA |
| D_207_Au_A | 27[120] --> 134[118] | CCATAGCAGGTCCACTCTAAAGCCAAAAAAAAAA |
| D_240_Au_A | 33[112] --> 137[121] | AAGAGGCAGTTGTGTCAAATGTTCAAGGAATTCCAAAAAAAAAA |
| D_266_Au_A | 20[191] --> 132[182] | AACTGTGATCAAGAGTTGTGACCATAGTCCAAAAAAAAAA |
| D_276_Au_A | 20[223] --> 132[214] | AGGATGCATCTACCGGGGGTAACTAGATCCAAAAAAAAAA |
| thiol-5'-21T | | /5ThioMC6-D/TTTTTTTTTTTTTTTTTTTT |

**Table E.12:** Legs strands.

| | | |
|---|---|---|
| D232_Leg_L_3' | First-L1P9 | TCTCCGTGCAATCGGCTTTAGGAGCATCAATATAATCCTGAGAAATAACCTCAGCAGACAACAATTTTTGAGGTGCAATCTCCTATC |
| D126c_Leg_L_5' | Second-L2P9 | CGATGGTGTCTAGATCACTTTTTCCATCGCCTTTAATTGTTCATTTCAATTAATTTTCCCTTA |
| D59_Leg_R_3' | First-L1P3 | AATCTGGCATATGCTTGAACTGAAAATTATTTTGGAGGTTCGTTCGCCGTCTAGCGGCCCCTCCTTTTTGAGGTGCAATCTCCTATC |
| D321e_Leg_R_5' | Second-L2P3 | CGATGGTGTCTAGATCACTTTTTCGAGTGAAAGCTCTAGGATGCACGTAGTGTGA*GCGCTTTG* |

**Table E.13:** Strands for biotin.

| | |
|---|---|
| D281_biocomp5 | AAACTATCACAAACTTAATTTGTAGCGGCCGTAAAGTGAAATTGCCGGAAGC |
| D268_biocomp6 | AAACTATCACAAACTTAATTCCCGCCGCCTTACACCCTCATACGGCCGAGTT |
| D261_biocomp7 | AAACTATCACAAACTTAATTCATTTGAAAAGGTTTGGTGCCCCATCAGTTCT |
| D216_biocomp8 | AAACTATCACAAACTTAATTCAAATGTGGGTGACTTTATGACAATGTTGTCG |
| D73_biocomp2 | AAACTATCACAAACTTAATTAATCCATTTGCAATAGATAAGGGGAACAGGTT |
| D82_biocomp4 | AAACTATCACAAACTTAATTCGGGCCTCAGAAGATGAAAAAAAGCTAAAGTT |
| D101_biocomp1 | AAACTATCACAAACTTAATTTCGTCCTTCAACAATAGGAACCGCTAGCAGCA |
| D283_biocomp3 | AAACTATCACAAACTTAATTCTAATTCCGGTTGCTTGCCGGTGCTGCGCGCC |
| biotin hook | /5Biosg/TTTTTTAAGTTTGTGATAGTTTATTGAGTGGC |
| anti-bio-hook | GCCACTCAATAAACTATCACAAACTTAA |

**Table E.14:** Foothold strands.

| | |
|---|---|
| D303_FH1_V2 | GCTGTACTTTGGTTACT**TTTT**CGTTAGCCTCCCACGGAGTTCCCTCACCGTATAAGAATAATTCGTCTGATTACATGCCTA |
| D105_FH2_V2 | CCGGGACCACGCAGCCTCAGTGCGAACTTCCA**TTTT**TGTATGGGCAGTAGCGT |
| D321_FH3_V2 | TCCACATCGGACTCTGT**TTTT**CGAGTGAAAGCTCTAGGATGCACGTAGTGTGA*GCGCTTTG* |
| D145_FH4_V2 | CTATTGCGTTCGTCGAAGTATATGCACTCTTTGTGTCGTGCAACGCCTTCTAGGACCTGC**TTTT**CAGCATTGTCGTCAGGT |
| D307_FH5_V2 | AGCTCATGCGCAACTTG**TTTT**CCAGCTAAACGCCTATTACTCTCTCCGC*ACTTAGTC* |
| D10_FH6_V2 | ATAAACGTGCATTAATCTTTATGCTCCTCTAACATAACTGTCATTCAAGTGACCCACATGAGTC**TTTT**AGAGTCGGCACATTACT |
| D66_FH7_V2 | GCTGTACTTTGGTTACT**TTTT**TTCTGCCTCCTGTGCACTAAATTTGGGGTCGAGGTG |
| D214_FH8_V2 | CCGGAAAGTGAAGGATATCTGGCAACAGTGCCACGCCATCGCCACCTTTAGTCCGCAAGA**TTTT**TGTATGGGCAGTAGCGT |
| D126_FH9_V2 | TCCACATCGGACTCTGT**TTTT**CCATCGCCTTTAATTGTTCATTTCAATTAATTTTCCCTTA |
| D228_FH10_V2 | GCCATTTCCATTACGAACGGGCGACAATAAACAACAAGTAATAAGCCAGCATCCTTGATA**TTTT**CAGCATTGTCGTCAGGT |
| D282_FH11_V2 | AGCTCATGCGCAACTTG**TTTT**TAAAGGTCAATGAAAATAATCAACGCGCCTGTTTATAGTGGCGTGAAGGCGGCGAGCTCC |
| D249_FH12_V2 | CCATGCAACTTTTCATATTACAAGCCAACTCAGGCGCTTGCACTTTATTTTGCGGCTTGTTAAA**TTTT**AGAGTCGGCACATTACT |

**Table E.15:** Fuel strands.

| | |
|---|---|
| F1 | CAATTTACCCAGTAACCAAAGTACAGC**ACTGC**GATAGGAGATTGCACC |
| F2 | GATCTAGACACCATCG**TTGAA**ACGCTACTGCCCATACAGACTGTTACG |
| F3 | ATCATTGTCGACAGAGTCCGATGTGGA**AGTCA**GATAGGAGATTGCACC |
| F4 | GATCTAGACACCATCG**CTCAG**ACCTGACGACAATGCTGGGATCAGTTA |
| F5 | TTGCGTGTATCAAGTTGCGCATGAGCT**CCAGT**GATAGGAGATTGCACC |
| F6 | GATCTAGACACCATCG**CTGCT**AGTAATGTGCCGACTCTAGTCTGTCAA |

**Table E.16:** Anti-fuel strands.

| | |
|---|---|
| AF1 | CTCCTATC**GCAGT**GCTGTACTTTGGTTACTGGGTAAATTG |
| AF2 | CGTAACAGTCTGTATGGGCAGTAGCGT**TTCAA**CGATGGTG |
| AF3 | CTCCTATC**TGACT**TCCACATCGGACTCTGTCGACAATGAT |
| AF4 | TAACTGATCCCAGCATTGTCGTCAGGT**CTGAG**CGATGGTG |
| AF5 | CTCCTATC**ACTGG**AGCTCATGCGCAACTTG ATACACGCAA |
| AF6 | TTGACAGACTAGAGTCGGCACATTACT**AGCAG**CGATGGTG |

# Bibliography

[1] E. Toprak, A. Yildiz, M. T. Hoffman, S. S. Rosenfeld and P. R. Selvin, "Why kinesin is so processive," *Proceedings of the National Academy of Sciences,* vol. 106, *(31),* pp. 12717–12722, 2009.

[2] Y. Sowa and R. M. Berry, "Bacterial flagellar motor," *Q. Rev. Biophys.,* vol. 41, *(2),* pp. 103–132, 2008.

[3] S. Enoki, R. Iino, Y. Niitani, Y. Minagawa, M. Tomishige and H. Noji, "High-speed angle-resolved imaging of a single gold nanorod with microsecond temporal resolution and one-degree angle precision," *Anal. Chem.,* vol. 87, *(4),* pp. 2079–2086, 2015.

[4] J. L. Martin, R. Ishmukhametov, T. Hornung, Z. Ahmad and W. D. Frasch, "Anatomy of F1-ATPase powered rotation," *Proceedings of the National Academy of Sciences,* vol. 111, *(10),* pp. 3715–3720, 2014.

[5] J. Bath, S. Green and A. Turberfield, "A free-running DNA motor powered by a nicking enzyme." *Angewandte Chemie (International Ed.in English),* vol. 44, *(28),* 2005.

[6] J. Mai, I. M. Sokolov and A. Blumen, "Directed particle diffusion under “burnt bridges” conditions," *Physical Review E,* vol. 64, *(1),* pp. 011102, 2001.

[7] J. Shin and N. A. Pierce, "A synthetic DNA walker for molecular transport," *J. Am. Chem. Soc.,* vol. 126, *(35),* pp. 10834–10835, 2004.

[8] W. B. Sherman and N. C. Seeman, "A precisely controlled DNA biped walking device," *Nano Letters,* vol. 4, *(7),* pp. 1203–1207, 2004.

[9] T. E. Tomov, R. Tsukanov, Y. Glick, Y. Berger, M. Liber, D. Avrahami, D. Gerber and E. Nir, "DNA bipedal motor achieves a large number of steps due to operation using microfluidics-based interface," *ACS Nano,* vol. 11, *(4),* pp. 4002–4008, 2017.

[10] P. Yin, H. Yan, X. G. Daniell, A. J. Turberfield and J. H. Reif, "A unidirectional DNA walker that moves autonomously along a track," *Angewandte Chemie International Edition,* vol. 43, *(37),* pp. 4906–4911, 2004.

[11] Y. Tian, Y. He, Y. Chen, P. Yin and C. Mao, "A DNAzyme that walks processively and autonomously along a one-dimensional track," *Angewandte Chemie-German Edition,* vol. 117, *(28),* pp. 4429–4431, 2005.

[12] T. Omabegho, R. Sha and N. C. Seeman, "A bipedal DNA Brownian motor with coordinated legs," *Science,* vol. 324, *(5923),* pp. 67–71, 2009.

[13] R. E. Franklin and R. G. Gosling, "Molecular configuration in sodium thymonucleate," *Nature,* vol. 171, *(4356),* pp. 740–741, 1953.

[14] N. VOL, "Molecular structure of deoxypentose nucleic acids," *Nature,* vol. 171, 1953.

[15] J. D. Watson and F. H. Crick, "Molecular structure of nucleic acids: a structure for deoxyribose nucleic acid," *Nature,* vol. 171, *(4356),* pp. 737–738, 1953.

[16] W. Jd and C. Fh, "Genetical implications of the structure of deoxyribonucleic acid." *Nature,* vol. 171, *(4361),* pp. 964–967, 1953.

[17] N. C. Seeman, "Nucleic acid junctions and lattices," *J. Theor. Biol.,* vol. 99, *(2),* pp. 237–247, 1982.

[18] R. Holliday, "A mechanism for gene conversion in fungi," *Genetics Research,* vol. 5, *(2),* pp. 282–304, 1964.

[19] J. Chen and N. C. Seeman, "Synthesis from DNA of a molecule with the connectivity of a cube," *Nature,* vol. 350, *(6319),* pp. 631–633, 1991.

[20] T. J. Fu and N. C. Seeman, "DNA double-crossover molecules," *Biochemistry (N. Y. ),* vol. 32, *(13),* pp. 3211–3220, 1993.

[21] Y. Zhang and N. C. Seeman, "Construction of a DNA-truncated octahedron," *J. Am. Chem. Soc.,* vol. 116, *(5),* pp. 1661–1669, 1994.

[22] Y. Ke, Y. Liu, J. Zhang and H. Yan, "A study of DNA tube formation mechanisms using 4-, 8-, and 12-helix DNA nanostructures," *J. Am. Chem. Soc.,* vol. 128, *(13),* pp. 4414–4421, 2006.

[23] S. H. Park, C. Pistol, S. J. Ahn, J. H. Reif, A. R. Lebeck, C. Dwyer and T. H. LaBean, "Finite-size, fully addressable DNA tile lattices formed by hierarchical assembly procedures," *Angewandte Chemie,* vol. 118, *(5),* pp. 749–753, 2006.

[24] K. Lund, Y. Liu and H. Yan, "Combinatorial self-assembly of DNA nanostructures," *Organic & Biomolecular Chemistry,* vol. 4, *(18),* pp. 3402–3403, 2006.

[25] H. Yan, T. H. LaBean, L. Feng and J. H. Reif, "Directed nucleation assembly of DNA tile complexes for barcode-patterned lattices," *Proceedings of the National Academy of Sciences,* vol. 100, *(14),* pp. 8103–8108, 2003.

[26] C. Lin, Y. Liu, S. Rinker and H. Yan, "DNA tile based self-assembly: building complex nanoarchitectures," *ChemPhysChem,* vol. 7, *(8),* pp. 1641–1647, 2006. .

[27] D. Liu, M. Wang, Z. Deng, R. Walulu and C. Mao, "Tensegrity: construction of rigid DNA triangles with flexible four-arm DNA junctions," *J. Am. Chem. Soc.,* vol. 126, *(8),* pp. 2324–2325, 2004.

[28] C. M. Erben, R. P. Goodman and A. J. Turberfield, "A self-assembled DNA bipyramid," *J. Am. Chem. Soc.,* vol. 129, *(22),* pp. 6992–6993, 2007.

[29] F. A. Aldaye and H. F. Sleiman, "Modular access to structurally switchable 3D discrete DNA assemblies," *J. Am. Chem. Soc.,* vol. 129, *(44),* pp. 13376–13377, 2007.

[30] R. P. Goodman, I. A. Schaap, C. F. Tardin, C. M. Erben, R. M. Berry, C. F. Schmidt and A. J. Turberfield, "Rapid chiral assembly of rigid DNA building blocks for molecular nanofabrication," *Science,* vol. 310, *(5754),* pp. 1661–1665, 2005.

[31] Y. He, T. Ye, M. Su, C. Zhang, A. E. Ribbe, W. Jiang and C. Mao, "Hierarchical self-assembly of DNA into symmetric supramolecular polyhedra," *Nature,* vol. 452, *(7184),* pp. 198–201, 2008.

[32] H. Yan, S. H. Park, G. Finkelstein, J. H. Reif and T. H. LaBean, "DNA-templated self-assembly of protein arrays and highly conductive nanowires," *Science,* vol. 301, *(5641),* pp. 1882–1884, 2003.

[33] C. M. Erben, R. P. Goodman and A. J. Turberfield, "Single-molecule protein encapsulation in a rigid DNA cage," *Angewandte Chemie International Edition,* vol. 45, *(44),* pp. 7414–7417, 2006.

[34] C. Lin, Y. Liu and H. Yan, "Self-assembled combinatorial encoding nanoarrays for multiplexed biosensing," *Nano Letters,* vol. 7, *(2),* pp. 507–512, 2007.

[35] E. Winfree, F. Liu, L. A. Wenzler and N. C. Seeman, "Design and self-assembly of two-dimensional DNA crystals," *Nature,* vol. 394, *(6693),* pp. 539–544, 1998.

[36] P. W. Rothemund, "Folding DNA to create nanoscale shapes and patterns," *Nature,* vol. 440, *(7082),* pp. 297–302, 2006.

[37] W. M. Shih, J. D. Quispe and G. F. Joyce, "A 1.7-kilobase single-stranded DNA that folds into a nanoscale octahedron," *Nature,* vol. 427, *(6975),* pp. 618–621, 2004.

[38] S. M. Douglas, H. Dietz, T. Liedl, B. Högberg, F. Graf and W. M. Shih, "Self-assembly of DNA into nanoscale three-dimensional shapes," *Nature,* vol. 459, *(7245),* pp. 414–418, 2009.

[39] Y. Ke, S. M. Douglas, M. Liu, J. Sharma, A. Cheng, A. Leung, Y. Liu, W. M. Shih and H. Yan, "Multilayer DNA origami packed on a square lattice," *J. Am. Chem. Soc.,* vol. 131, *(43),* pp. 15903–15908, 2009.

[40] D. Han, S. Pal, J. Nangreave, Z. Deng, Y. Liu and H. Yan, "DNA origami with complex curvatures in three-dimensional space," *Science,* vol. 332, *(6027),* pp. 342–346, 2011.

[41] A. Kuzuya and M. Komiyama, "Design and construction of a box-shaped 3D-DNA origami," *Chemical Communications, (28),* pp. 4182–4184, 2009.

[42] H. Dietz, S. M. Douglas and W. M. Shih, "Folding DNA into twisted and curved nanoscale shapes," *Science,* vol. 325, *(5941),* pp. 725–730, 2009.

[43] S. M. Douglas, A. H. Marblestone, S. Teerapittayanon, A. Vazquez, G. M. Church and W. M. Shih, "Rapid prototyping of 3D DNA-origami shapes with caDNAno," *Nucleic Acids Res.,* vol. 37, *(15),* pp. 5001–5006, 2009.

[44] T. E. Ouldridge, A. A. Louis and J. P. Doye, "Structural, mechanical, and thermodynamic properties of a coarse-grained DNA model," *J. Chem. Phys.,* vol. 134, *(8),* 2011.

[45] C. Maffeo and A. Aksimentiev, "MrDNA: a multi-resolution model for predicting the structure and dynamics of DNA systems," *Nucleic Acids Res.,* vol. 48, *(9),* pp. 5135–5146, 2020.

[46] E. S. Andersen, M. Dong, M. M. Nielsen, K. Jahn, R. Subramani, W. Mamdouh, M. M. Golas, B. Sander, H. Stark and C. L. Oliveira, "Self-assembly of a nanoscale DNA box with a controllable lid," *Nature,* vol. 459, *(7243),* pp. 73–76, 2009.

[47] M. Marini, L. Piantanida, R. Musetti, A. Bek, M. Dong, F. Besenbacher, M. Lazzarino and G. Firrao, "A revertible, autonomous, self-assembled DNA-origami nanoactuator," *Nano Letters,* vol. 11, *(12),* pp. 5449–5454, 2011.

[48] F. Zhang, J. Nangreave, Y. Liu and H. Yan, "Reconfigurable DNA origami to generate quasifractal patterns," *Nano Letters,* vol. 12, *(6),* pp. 3290–3295, 2012.

[49] T. Gerling, K. F. Wagenbauer, A. M. Neuner and H. Dietz, "Dynamic DNA devices and assemblies formed by shape-complementary, non–base pairing 3D components," *Science,* vol. 347, *(6229),* pp. 1446–1452, 2015.

[50] H. Zhang, J. Chao, D. Pan, H. Liu, Q. Huang and C. Fan, "Folding super-sized DNA origami with scaffold strands from long-range PCR," *Chemical Communications,* vol. 48, *(51),* pp. 6405–6407, 2012.

[51] X. Chen, Q. Wang, J. Peng, Q. Long, H. Yu and Z. Li, "Self-assembly of large DNA origami with custom-designed scaffolds," *ACS Applied Materials & Interfaces,* vol. 10, *(29),* pp. 24344–24348, 2018.

[52] A. N. Marchi, I. Saaem, B. N. Vogen, S. Brown and T. H. LaBean, "Toward larger DNA origami," *Nano Letters,* vol. 14, *(10),* pp. 5740–5747, 2014.

[53] W. Liu, H. Zhong, R. Wang and N. C. Seeman, "Crystalline two-dimensional DNA origami arrays," *Angewandte Chemie (International Ed.in English),* vol. 50, *(1),* pp. 264, 2011.

[54] R. Jungmann, M. Scheible, A. Kuzyk, G. Pardatscher, C. E. Castro and F. C. Simmel, "DNA origami-based nanoribbons: assembly, length distribution, and twist," *Nanotechnology,* vol. 22, *(27),* pp. 275301, 2011.

[55] Z. Li, L. Wang, H. Yan and Y. Liu, "Effect of DNA hairpin loops on the twist of planar DNA origami tiles," *Langmuir,* vol. 28, *(4),* pp. 1959–1965, 2012.

[56] Z. Li, M. Liu, L. Wang, J. Nangreave, H. Yan and Y. Liu, "Molecular behavior of DNA origami in higher-order self-assembly," *J. Am. Chem. Soc.,* vol. 132, *(38),* pp. 13545–13552, 2010.

[57] K. F. Wagenbauer, C. Sigl and H. Dietz, "Gigadalton-scale shape-programmable DNA assemblies," *Nature,* vol. 552, *(7683),* pp. 78–83, 2017.

[58] R. Schreiber, S. Kempter, S. Holler, V. Schüller, D. Schiffels, S. S. Simmel, P. C. Nickels and T. Liedl, "DNA origami-templated growth of arbitrarily shaped metal nanoparticles," *Small,* vol. 7, *(13),* pp. 1795–1799, 2011.

[59] J. Fern, J. Lu and R. Schulman, "The energy landscape for the self-assembly of a two-dimensional DNA origami complex," *ACS Nano,* vol. 10, *(2),* pp. 1836–1844, 2016.

[60] M. Liber, T. E. Tomov, R. Tsukanov, Y. Berger and E. Nir, "A bipedal DNA motor that travels back and forth between two DNA origami tiles," *Small,* vol. 11, *(5),* pp. 568–575, 2015.

[61] M. Liber, T. E. Tomov, R. Tsukanov, Y. Berger, M. Popov, D. C. Khara and E. Nir, "Study of DNA origami dimerization and dimer dissociation dynamics and of the factors that limit dimerization," *Small,* vol. 14, *(23),* pp. 1800218, 2018.

[62] T. C. Wu, M. Rahman and M. L. Norton, "From nonfinite to finite 1D arrays of origami tiles," *Acc. Chem. Res.,* vol. 47, *(6),* pp. 1750–1758, 2014.

[63] R. Wang, K. Gorday, C. Nuckolls and S. J. Wind, "Control of DNA origami inter-tile connection with vertical linkers," *Chemical Communications,* vol. 52, *(8),* pp. 1610–1613, 2016.

[64] S. Woo and P. W. Rothemund, "Programmable molecular recognition based on the geometry of DNA nanostructures," *Nature Chemistry,* vol. 3, *(8),* pp. 620–627, 2011.

[65] T. Gerling, K. F. Wagenbauer, A. M. Neuner and H. Dietz, "Dynamic DNA devices and assemblies formed by shape-complementary, non–base pairing 3D components," *Science,* vol. 347, *(6229),* pp. 1446–1452, 2015.

[66] P. Ketterer, E. M. Willner and H. Dietz, "Nanoscale rotary apparatus formed from tight-fitting 3D DNA components," *Science Advances,* vol. 2, *(2),* pp. e1501209, 2016.

[67] J. Ye, S. Helmi, J. Teske and R. Seidel, "Fabrication of metal nanostructures with programmable length and patterns using a modular DNA platform," *Nano Letters,* vol. 19, *(4),* pp. 2707–2714, 2019.

[68] A. Rajendran, M. Endo, Y. Katsuda, K. Hidaka and H. Sugiyama, "Programmed two-dimensional self-assembly of multiple DNA origami jigsaw pieces," *ACS Nano,* vol. 5, *(1),* pp. 665–671, 2011.

[69] M. Endo, T. Sugita, Y. Katsuda, K. Hidaka and H. Sugiyama, "Programmed-assembly system using DNA jigsaw pieces," *Chemistry–A European Journal,* vol. 16, *(18),* pp. 5362–5368, 2010.

[70] M. Endo, T. Sugita, A. Rajendran, Y. Katsuda, T. Emura, K. Hidaka and H. Sugiyama, "Two-dimensional DNA origami assemblies using a four-way connector," *Chemical Communications,* vol. 47, *(11),* pp. 3213–3215, 2011.

[71] G. Tikhomirov, P. Petersen and L. Qian, "Programmable disorder in random DNA tilings," *Nature Nanotechnology,* vol. 12, *(3),* pp. 251–259, 2017.

[72] G. Tikhomirov, P. Petersen and L. Qian, "Fractal assembly of micrometre-scale DNA origami arrays with arbitrary patterns," *Nature,* vol. 552, *(7683),* pp. 67–71, 2017.

[73] Z. Zhao, Y. Liu and H. Yan, "Organizing DNA origami tiles into larger structures using preformed scaffold frames," *Nano Letters,* vol. 11, *(7),* pp. 2997–3002, 2011.

[74] J. Zenk, C. Tuntivate and R. Schulman, "Kinetics and thermodynamics of Watson–Crick base pairing driven DNA origami dimerization," *J. Am. Chem. Soc.,* vol. 138, *(10),* pp. 3346–3354, 2016.

[75] B. Sheheade, M. Liber, M. Popov, Y. Berger, D. C. Khara, J. Jopp and E. Nir, "Self-Assembly of DNA Origami Heterodimers in High Yields and Analysis of the Involved Mechanisms," *Small,* vol. 15, *(51),* pp. 1902979, 2019.

[76] F. A. Engelhardt, F. Praetorius, C. H. Wachauf, G. Brüggenthies, F. Kohler, B. Kick, K. L. Kadletz, P. N. Pham, K. L. Behler and T. Gerling, "Custom-size, functional, and durable DNA origami with design-specific scaffolds," *ACS Nano,* vol. 13, *(5),* pp. 5015–5027, 2019.

[77] J. SantaLucia Jr, "A unified view of polymer, dumbbell, and oligonucleotide DNA nearest-neighbor thermodynamics," *Proceedings of the National Academy of Sciences,* vol. 95, *(4),* pp. 1460–1465, 1998.

[78] R. Owczarzy, P. M. Vallone, F. J. Gallo, T. M. Paner, M. J. Lane and A. S. Benight, "Predicting sequence-dependent melting stability of short duplex DNA oligomers," *Biopolymers: Original Research on Biomolecules,* vol. 44, *(3),* pp. 217–239, 1997.

[79] O. Gotoh and Y. Tagashira, "Stabilities of nearest-neighbor doublets in double-helical DNA determined by fitting calculated melting profiles to observed profiles," *Biopolymers: Original Research on Biomolecules,* vol. 20, *(5),* pp. 1033–1042, 1981.

[80] A. V. Vologodskii, B. R. Amirikyan, Y. L. Lyubchenko and M. D. Frank-Kamenetskii, "Allowance for heterogeneous stacking in the DNA helix-coil transition theory," *Journal of Biomolecular Structure and Dynamics,* vol. 2, *(1),* pp. 131–148, 1984.

[81] K. J. Breslauer, R. Frank, H. Blöcker and L. A. Marky, "Predicting DNA duplex stability from the base sequence." *Proceedings of the National Academy of Sciences,* vol. 83, *(11),* pp. 3746–3750, 1986.

[82] S. G. Delcourt and R. D. Blake, "Stacking energies in DNA," *J. Biol. Chem.,* vol. 266, *(23),* pp. 15160–15169, 1991.

[83] J. SantaLucia, H. T. Allawi and P. A. Seneviratne, "Improved nearest-neighbor parameters for predicting DNA duplex stability," *Biochemistry (N. Y. ),* vol. 35, *(11),* pp. 3555–3562, 1996.

[84] N. Sugimoto, S. Nakano, M. Yoneyama and K. Honda, "Improved thermodynamic parameters and helix initiation factor to predict stability of DNA duplexes," *Nucleic Acids Res.,* vol. 24, *(22),* pp. 4501–4505, 1996.

[85] S. Ghosh, S. Takahashi, T. Ohyama, T. Endoh, H. Tateishi-Karimata and N. Sugimoto, "Nearest-neighbor parameters for predicting DNA duplex stability in diverse molecular crowding conditions," *Proceedings of the National Academy of Sciences,* vol. 117, *(25),* pp. 14194–14201, 2020.

[86] D. Banerjee, H. Tateishi-Karimata, T. Ohyama, S. Ghosh, T. Endoh, S. Takahashi and N. Sugimoto, "Improved nearest-neighbor parameters for the stability of RNA/DNA hybrids under a physiological condition," *Nucleic Acids Res.,* vol. 48, *(21),* pp. 12042–12054, 2020.

[87] M. Schickinger, M. Zacharias and H. Dietz, "Tethered multifluorophore motion reveals equilibrium transition kinetics of single DNA double helices," *Proceedings of the National Academy of Sciences,* vol. 115, *(32),* pp. E7512–E7521, 2018.

[88] H. Hata, T. Kitajima and A. Suyama, "Influence of thermodynamically unfavorable secondary structures on DNA hybridization kinetics," *Nucleic Acids Res.,* vol. 46, *(2),* pp. 782–791, 2018.

[89] D. Pörschke, O. C. Uhlenbeck and F. H. Martin, "Thermodynamics and kinetics of the helix-coil transition of oligomers containing GC base pairs," *Biopolymers: Original Research on Biomolecules,* vol. 12, *(6),* pp. 1313–1335, 1973.

[90] D. Y. Zhang and E. Winfree, "Control of DNA strand displacement kinetics using toehold exchange," *J. Am. Chem. Soc.,* vol. 131, *(47),* pp. 17303–17314, 2009.

[91] D. Pörschke and M. Eigen, "Co-operative non-enzymatic base recognition III. Kinetics of the helix—coil transition of the oligoribouridylic· oligoriboadenylic acid system and of oligoriboadenylic acid alone at acidic pH," *J. Mol. Biol.,* vol. 62, *(2),* pp. 361–381, 1971.

[92] D. Pörschke, "Cooperative nonenzymic base recognition II. thermodynamics of the helix-coil transition of oligoadenylic oligouridylic acids," *Biopolymers: Original Research on Biomolecules,* vol. 10, *(10),* pp. 1989–2013, 1971.

[93] M. Eigen and D. Pörschke, "Co-operative non-enzymic base recognition: I. Thermodynamics of the helix-coil transition of oligoriboadenylic acids at acidic pH," *J. Mol. Biol.,* vol. 53, *(1),* pp. 123–141, 1970.

[94] T. E. Ouldridge, P. Šulc, F. Romano, J. P. Doye and A. A. Louis, "DNA hybridization kinetics: zippering, internal displacement and sequence dependence," *Nucleic Acids Res.,* vol. 41, *(19),* pp. 8886–8895, 2013.

[95] E. J. Sambriski, D. C. Schwartz and J. J. De Pablo, "Uncovering pathways in DNA oligonucleotide hybridization via transition state analysis," *Proceedings of the National Academy of Sciences,* vol. 106, *(43),* pp. 18125–18130, 2009.

[96] C. B. Markegard, C. P. Gallivan, D. D. Cheng and H. D. Nguyen, "Effects of concentration and temperature on DNA hybridization by two closely related sequences via large-scale coarse-grained simulations," *The Journal of Physical Chemistry B,* vol. 120, *(32),* pp. 7795–7806, 2016.

[97] Y. Gao, L. K. Wolf and R. M. Georgiadis, "Secondary structure effects on DNA hybridization kinetics: a solution versus surface comparison," *Nucleic Acids Res.,* vol. 34, *(11),* pp. 3370–3377, 2006.

[98] C. Chen, W. Wang, Z. Wang, F. Wei and X. S. Zhao, "Influence of secondary structure on kinetics and reaction mechanism of DNA hybridization," *Nucleic Acids Res.,* vol. 35, *(9),* pp. 2875–2884, 2007.

[99] J. S. Schreck, T. E. Ouldridge, F. Romano, P. Šulc, L. P. Shaw, A. A. Louis and J. P. Doye, "DNA hairpins destabilize duplexes primarily by promoting melting rather than by inhibiting hybridization," *Nucleic Acids Res.,* vol. 43, *(13),* pp. 6181–6190, 2015.

[100] J. X. Zhang, J. Z. Fang, W. Duan, L. R. Wu, A. W. Zhang, N. Dalchau, B. Yordanov, R. Petersen, A. Phillips and D. Y. Zhang, "Predicting DNA hybridization kinetics from sequence," *Nature Chemistry,* vol. 10, *(1),* pp. 91–98, 2018.

[101] S. Hertel, R. E. Spinney, S. Y. Xu, T. E. Ouldridge, R. G. Morris and L. K. Lee, "The stability and number of nucleating interactions determine DNA hybridization rates in the absence of secondary structure," *Nucleic Acids Res.,* vol. 50, *(14),* pp. 7829–7841, 2022.

[102] B. Yurke and A. P. Mills, "Using DNA to power nanostructures," *Genetic Programming and Evolvable Machines,* vol. 4, pp. 111–122, 2003.

[103] D. Y. Zhang and E. Winfree, "Control of DNA strand displacement kinetics using toehold exchange," *J. Am. Chem. Soc.,* vol. 131, *(47),* pp. 17303–17314, 2009.

[104] A. J. Genot, D. Y. Zhang, J. Bath and A. J. Turberfield, "Remote toehold: a mechanism for flexible control of DNA hybridization kinetics," *J. Am. Chem. Soc.,* vol. 133, *(7),* pp. 2177–2182, 2011.

[105] X. Chen, "Expanding the rule set of DNA circuitry with associative toehold activation," *J. Am. Chem. Soc.,* vol. 134, *(1),* pp. 263–271, 2012.

[106] R. R. Machinek, T. E. Ouldridge, N. E. Haley, J. Bath and A. J. Turberfield, "Programmable energy landscapes for kinetic control of DNA strand displacement," *Nature Communications,* vol. 5, *(1),* pp. 5324, 2014.

[107] N. E. Haley, T. E. Ouldridge, I. Mullor Ruiz, A. Geraldini, A. A. Louis, J. Bath and A. J. Turberfield, "Design of hidden thermodynamic driving for non-equilibrium systems via mismatch elimination during DNA strand displacement," *Nature Communications,* vol. 11, *(1),* pp. 2562, 2020.

[108] A. J. Turberfield, J. C. Mitchell, B. Yurke, A. P. Mills Jr, M. I. Blakey and F. C. Simmel, "DNA fuel for free-running nanomachines," *Phys. Rev. Lett.,* vol. 90, *(11),* pp. 118102, 2003.

[109] G. Seelig, B. Yurke and E. Winfree, "Catalyzed relaxation of a metastable DNA fuel," *J. Am. Chem. Soc.,* vol. 128, *(37),* pp. 12211–12220, 2006.

[110] B. Li, A. D. Ellington and X. Chen, "Rational, modular adaptation of enzyme-free DNA circuits to multiple detection methods," *Nucleic Acids Res.,* vol. 39, *(16),* pp. e110, 2011.

[111] T. E. Tomov, R. Tsukanov, M. Liber, R. Masoud, N. Plavner and E. Nir, "Rational design of DNA motors: fuel optimization through single-molecule fluorescence," *J. Am. Chem. Soc.,* vol. 135, *(32),* pp. 11935–11941, 2013.

[112] S. J. Green, D. Lubrich and A. J. Turberfield, "DNA hairpins: fuel for autonomous DNA devices," *Biophys. J.,* vol. 91, *(8),* pp. 2966–2975, 2006.

[113] S. J. Green, J. Bath and A. J. Turberfield, "Coordinated chemomechanical cycles: a mechanism for autonomous molecular motion," *Phys. Rev. Lett.,* vol. 101, *(23),* pp. 238101, 2008.

[114] R. M. Dirks and N. A. Pierce, "Triggered amplification by hybridization chain reaction," *Proceedings of the National Academy of Sciences,* vol. 101, *(43),* pp. 15275–15278, 2004.

[115] S. Venkataraman, R. M. Dirks, P. W. Rothemund, E. Winfree and N. A. Pierce, "An autonomous polymerization motor powered by DNA hybridization," *Nature Nanotechnology,* vol. 2, *(8),* pp. 490–494, 2007.

[116] X. Olson, S. Kotani, J. E. Padilla, N. Hallstrom, S. Goltry, J. Lee, B. Yurke, W. L. Hughes and E. Graugnard, "Availability: a metric for nucleic acid strand displacement systems," *ACS Synthetic Biology,* vol. 6, *(1),* pp. 84–93, 2017.

[117] X. Chen, N. Briggs, J. R. McLain and A. D. Ellington, "Stacking nonenzymatic circuits for high signal gain," *Proceedings of the National Academy of Sciences,* vol. 110, *(14),* pp. 5386–5391, 2013.

[118] C. Ducani, C. Kaul, M. Moche, W. M. Shih and B. Högberg, "Enzymatic production of'monoclonal stoichiometric'single-stranded DNA oligonucleotides," *Nature Methods,* vol. 10, *(7),* pp. 647–652, 2013.

[119] D. Y. Zhang, A. J. Turberfield, B. Yurke and E. Winfree, "Engineering entropy-driven reactions and networks catalyzed by DNA," *Science,* vol. 318, *(5853),* pp. 1121–1125, 2007.

[120] B. Li, Y. Jiang, X. Chen and A. D. Ellington, "Probing spatial organization of DNA strands using enzyme-free hairpin assembly circuits," *J. Am. Chem. Soc.,* vol. 134, *(34),* pp. 13918–13921, 2012.

[121] L. Qian and E. Winfree, "Scaling up digital circuit computation with DNA strand displacement cascades," *Science,* vol. 332, *(6034),* pp. 1196–1201, 2011.

[122] P. Yin, H. M. Choi, C. R. Calvert and N. A. Pierce, "Programming biomolecular self-assembly pathways," *Nature,* vol. 451, *(7176),* pp. 318–322, 2008.

[123] Y. S. Jiang, S. Bhadra, B. Li and A. D. Ellington, "Mismatches improve the performance of strand-displacement nucleic acid circuits," *Angewandte Chemie,* vol. 126, *(7),* pp. 1876–1879, 2014.

[124] C. Thachuk, E. Winfree and D. Soloveichik, "Leakless DNA strand displacement systems," in *DNA Computing and Molecular Programming: 21st International Conference, DNA 21, Boston and Cambridge, MA, USA, August 17-21, 2015. Proceedings 21,* 2015, pp. 133–153.

[125] H. Gu, J. Chao, S. Xiao and N. C. Seeman, "A proximity-based programmable DNA nanoscale assembly line," *Nature,* vol. 465, *(7295),* pp. 202–205, 2010.

[126] S. Basak, "Computer-controlled Fast and Processive Bipedal DNA Motor that Travels Long Distances," PhD Thesis, 2023.

[127] Y. Glick, D. Avrahami, E. Michaely and D. Gerber, "High-throughput protein expression generator using a microfluidic platform," *JoVE (Journal of Visualized Experiments), (66),* pp. e3849, 2012.

[128] T. Thorsen, S. J. Maerkl and S. R. Quake, "Microfluidic large-scale integration," *Science,* vol. 298, *(5593),* pp. 580–584, 2002.

[129] J. Valero, N. Pal, S. Dhakal, N. G. Walter and M. Famulok, "A bio-hybrid DNA rotor–stator nanoengine that moves along predefined tracks," *Nature Nanotechnology,* vol. 13, *(6),* pp. 496–503, 2018.

[130] N. E. C. Haley, "Structures and Mechanisms for Synthetic DNA Motors," PhD thesis, 2017.

[131] R. Tsukanov, T. E. Tomov, M. Liber, Y. Berger and E. Nir, "Developing DNA nanotechnology using single-molecule fluorescence," *Acc. Chem. Res.,* vol. 47, *(6),* pp. 1789–1798, 2014.

[132] J. K. Bhattacharjee, D. Thirumalai and J. D. Bryngelson, "Distribution function of the end-to-end distance of semiflexible polymers," *arXiv Preprint Cond-Mat/9709345,* 1997.

[133] M. Karymov, D. Daniel, O. F. Sankey and Y. L. Lyubchenko, "Holliday junction dynamics and branch migration: single-molecule analysis," *Proceedings of the National Academy of Sciences,* vol. 102, *(23),* pp. 8186–8191, 2005.

[134] K. Hübner, M. Raab, J. Bohlen, J. Bauer and P. Tinnefeld, "Salt-induced conformational switching of a flat rectangular DNA origami structure," *Nanoscale,* vol. 14, *(21),* pp. 7898–7905, 2022. .

[135] E. Kopperger, J. List, S. Madhira, F. Rothfischer, D. C. Lamb and F. C. Simmel, "A self-assembled nanoscale robotic arm controlled by electric fields," *Science,* vol. 359, *(6373),* pp. 296–301, 2018.

[136] A. J. Thubagere, W. Li, R. F. Johnson, Z. Chen, S. Doroudi, Y. L. Lee, G. Izatt, S. Wittman, N. Srinivas and D. Woods, "A cargo-sorting DNA robot," *Science,* vol. 357, *(6356),* pp. eaan6558, 2017.

[137] Y. Ke, G. Bellot, N. V. Voigt, E. Fradkov and W. M. Shih, "Two design strategies for enhancement of multilayer–DNA-origami folding: underwinding for specific intercalator rescue and staple-break positioning," *Chemical Science,* vol. 3, *(8),* pp. 2587–2597, 2012.

[138] T. G. Martin and H. Dietz, "Magnesium-free self-assembly of multi-layer DNA objects," *Nature Communications,* vol. 3, *(1),* pp. 1103, 2012.

[139] Pazdernik, N., Youtsey, A.Johnson, A, "Getting enough full-length oiligo," 2017. Available: https://eu.idtdna.com/pages/education/decoded/article/getting-enough-fulllength-oligo.

[140] K. F. Wagenbauer, F. A. Engelhardt, E. Stahl, V. K. Hechtl, P. Stömmer, F. Seebacher, L. Meregalli, P. Ketterer, T. Gerling and H. Dietz, "How we make DNA origami," *ChemBioChem,* vol. 18, *(19),* pp. 1873–1885, 2017.

[141] D. C. Khara, J. S. Schreck, T. E. Tomov, Y. Berger, T. E. Ouldridge, J. P. Doye and E. Nir, "DNA bipedal motor walking dynamics: an experimental and theoretical study of the dependency on step size," *Nucleic Acids Res.,* vol. 46, *(3),* pp. 1553–1561, 2018.

[142] A. Kuzyk, Y. Yang, X. Duan, S. Stoll, A. O. Govorov, H. Sugiyama, M. Endo and N. Liu, "A light-driven three-dimensional plasmonic nanosystem that translates molecular motion into reversible chiroptical function," *Nature Communications,* vol. 7, *(1),* pp. 10591, 2016.

[143] P. Zhan, P. K. Dutta, P. Wang, G. Song, M. Dai, S. Zhao, Z. Wang, P. Yin, W. Zhang and B. Ding, "Reconfigurable three-dimensional gold nanorod plasmonic nanostructures organized on DNA origami tripod," *ACS Nano,* vol. 11, *(2),* pp. 1172–1179, 2017.

[144] K. Park, S. Biswas, S. Kanel, D. Nepal and R. A. Vaia, "Engineering the optical properties of gold nanorods: independent tuning of surface plasmon energy, extinction coefficient, and scattering cross section," *The Journal of Physical Chemistry C,* vol. 118, *(11),* pp. 5918–5926, 2014.

[145] X. Ye, Y. Gao, J. Chen, D. C. Reifsnyder, C. Zheng and C. B. Murray, "Seeded growth of monodisperse gold nanorods using bromide-free surfactant mixtures," *Nano Letters,* vol. 13, *(5),* pp. 2163–2171, 2013.

[146] S. J. Hurst, A. K. Lytton-Jean and C. A. Mirkin, "Maximizing DNA loading on a range of gold nanoparticle sizes," *Anal. Chem.,* vol. 78, *(24),* pp. 8313–8318, 2006.

[147] SHELLEY WICKHAM, "DNA ORIGAMI A SUBSTRATE FOR THE STUDY OF MOLECULAR MOTORS ," PhD Thesis, 2011.

[148] J. Bath, S. Green, K. e. Allen and A. Turberfield, "Mechanism for a directional, processive, and reversible DNA motor." *Small (Weinheim an Der Bergstrasse, Germany),* vol. 5, *(13),* 2009.

[149] Z. Wang, R. Hou and I. Y. Loh, "Track-walking molecular motors: a new generation beyond bridge-burning designs," *Nanoscale,* vol. 11, *(19),* pp. 9240–9263, 2019.

[150] M. Liu, J. Cheng, S. R. Tee, S. Sreelatha, I. Y. Loh and Z. Wang, "Biomimetic autonomous enzymatic nanowalker of high fuel efficiency," *Acs Nano,* vol. 10, *(6),* pp. 5882–5890, 2016.

[151] Nadine L. Dabb, "Synthetic Molecular Machines for Active Self-Assembly: Prototype Algorithms, Designs, and Experimental Study," PhD Thesis, February 4 , 2013.

[152] C. Li, Y. Li, Y. Chen, R. Lin, T. Li, F. Liu and N. Li, "Modulating the DNA strand-displacement kinetics with the one-sided remote toehold design for differentiation of single-base mismatched DNA," *RSC Advances,* vol. 6, *(78),* pp. 74913–74916, 2016.

[153] Y. S. Ang, R. Tong and L. L. Yung, "Engineering a robust DNA split proximity circuit with minimized circuit leakage," *Nucleic Acids Res.,* vol. 44, *(14),* pp. e121, 2016.

[154] S. Hoops, S. Sahle, R. Gauges, C. Lee, J. Pahle, N. Simus, M. Singhal, L. Xu, P. Mendes and U. Kummer, "COPASI—a complex pathway simulator," *Bioinformatics,* vol. 22, *(24),* pp. 3067–3074, 2006.

[155] F. T. Bergmann, "BASICO: A simplified Python interface to COPASI," *Journal of Open Source Software,* vol. 8, *(90),* pp. 5553, 2023.

[156] S. Li, P. Li, M. Ge, H. Wang, Y. Cheng, G. Li, Q. Huang, H. He, C. Cao and D. Lin, "Elucidation of leak-resistance DNA hybridization chain reaction with universality and extensibility," *Nucleic Acids Res.,* vol. 48, *(5),* pp. 2220–2231, 2020.

[157] J. Cabello-Garcia, W. Bae, G. V. Stan and T. E. Ouldridge, "Handhold-mediated strand displacement: a nucleic acid based mechanism for generating far-from-equilibrium assemblies through templated reactions," *ACS Nano,* vol. 15, *(2),* pp. 3272–3283, 2021.

[158] M. E. Fornace, J. Huang, C. T. Newman, N. J. Porubsky, M. B. Pierce and N. A. Pierce, "NUPACK: analysis and design of nucleic acid structures, devices, and systems," 2022.

[159] R. Jungmann, C. Steinhauer, M. Scheible, A. Kuzyk, P. Tinnefeld and F. C. Simmel, "Single-molecule kinetics and super-resolution microscopy by fluorescence imaging of transient binding on DNA origami," *Nano Letters,* vol. 10, *(11),* pp. 4756–4761, 2010.

[160] D. B. Broadwater, A. W. Cook and H. D. Kim, "First passage time study of DNA strand displacement," *Biophys. J.,* vol. 120, *(12),* pp. 2400–2412, 2021.

תקציר

מימוש של מנועים מולקולריים סינתטיים מהירים ובעלי יכולת פעולה גבוהה, הצורכים אנרגיה ומבצעים פעולות היא משימה קשה. המנועיים הקיימים, גרועים מכל הבחינות ביחס למנועים ביולוגים. במחקרי כאן, פיתחתי מנועים מולקולריים ליניאריים וסיבוביים מבוססי דנ"א ,הנשלטים חיצונית או אוטונומים, על ידי עיצוב חדשני ואופטימיזציה. התזה מחולקת לשלושה חלקים: ייצור מסלול ארוך הבוסס על דנ"א אוריגמי המיועד למנועים ליניאריים דו-רגליים, תיכנון וייצור מנועים סיבוביים מבוססי אוריגמי, והצעה מפורטת למנגנון פעולה אוטונומי דו-רגלי שניתן ליישם במנוע הסיבובי.

ראשית, הנדסתי ויצרתי מסילת דנ"א אוריגמי באורך 955 ננומטר, העשוי משש יחדות אוריגמי מלבניות, המחוברות זו לזו, בשיטת הקצוות הדביקים (sticky ends), העבודה כללה פיתוח של תוכנה מחשב חדשנית, שמייצרת את הרצף של הקצוות ובנוסף בוצעה אופטימיזציה של תנאי היונים והסביבה כדי למנוע אגרגציה.

שנית, תיכננתי ויצרתי מנוע סיבובי מבוסס דנ"א אוריגמי המאפשר מסילה "אינסופית", המורכב משני דיסקים המחוברים באמצעות אלמנטים של דנ"א חד-גדילי המאפשרים סיבוביות חופשית ומונעים פירוק. הרוטור מונע על ידי שתי מערכות הליכה דו-רגליות הנשלטות חיצונית, המנוע מנוטר באמצעות פיזור אור מננו חלקיק מוארך של זהב שמחובר למנוע, דבר המאפשר אפיון זוויתי מדויק. הדגמנו ביצוע של שמונה סיבובים מלאים, בסה"כ, 96 צעדים הנשלטים חיצונית.

לבסוף, הצעתי עיצוב מפורט למנגנון הנעה אוטונומי המונע כימית, המסוגל לפעולה מתמשכת ומהירה ללא "שריפת הגשר". המנגנון החדשני הזה משתמש באטבי דנ"א (hairpin) כדלק ועושה שימוש בגדיל קטליטי למתן כיווניות סיבוב ותיאום בין הרגליים. באמצעות אופטימיזציה ועיצוב קפדניים, הראנו בסימולציות מחשב שהמערכת מסוגלת לבצע צעדים אוטונומיים ביעילות כימית של 99% וזמן צעידה מתחת ל-3 דקות. ניתן ליישם את המנגנון הנ"ל על המנוע הסיבובי שלנו.

העבודה נעשתה בהדרכת פרופסור אייל ניר

במחלקה לכימיה

בפקולטה למדעי הטבע

# ממנועי דנ"א מולקולריים
# הנשלטים חיצונית למנועים אוטונומיים

**מחקר לשם מילוי חלקי של הדרישות**

**לקבלת תואר "דוקטור לפילוסופיה"**

**מאת**


## בריוריוס שחאדה

**הוגש לסינאט אוניברסיטת בן גוריון בנגב**


**נובמבר ,תשפ״ה**

**באר שבע**